In vivo confocal microscopy

expanding horizons in corneal imaging

TOINE HILLENAAR

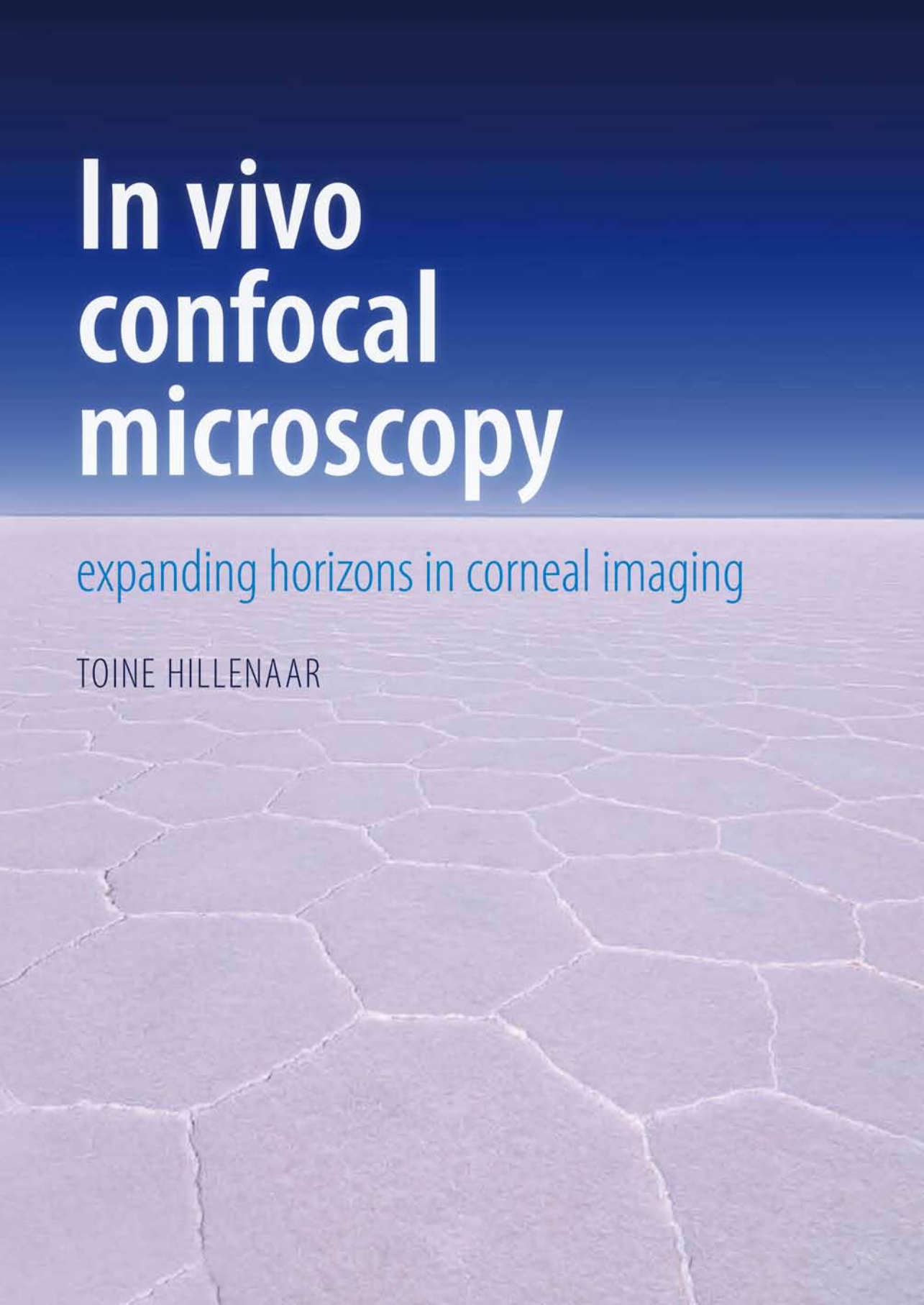

In vivo confocal microscopy

Expanding horizons in corneal imaging

Toine Hillenaar

ACKNOWLEDGEMENTS

The studies presented in this thesis were supported by the Research Foundation SWOO Flieringa, Rotterdam; The Dutch Cornea Foundation, Rotterdam; and the OOG Foundation 's Gravenzande, The Netherlands.

The publication of this thesis was financially supported by Alcon Nederland BV; AMO Netherlands BV; Bausch & Lomb; D.O.R.C. International BV; Ergra Low Vision; Landelijke Stichting voor Blinden en Slechtzienden; Merck Sharp & Dohme BV; NIDEK Medical Srl, Italy; Oculenti Contactlenspraktijken; Rotterdamse Stichting Blindenbelangen; Stichting Blindenhulp; Stichting Cornea Bank Rotterdam; SWOO-Prof.dr. H.J. Flieringa; Théa Pharma; Ursapharm Benelux BV

ISBN: 978-94-6169-306-8

Layout and printing: Optima Grafische Communicatie, Rotterdam, The Netherlands

In vivo confocal microscopy

Expanding horizons in corneal imaging

In vivo confocale microscopie

Blikverruimend in corneale beeldvorming

Proefschrift

ter verkrijging van de graad van doctor
aan de Erasmus Universiteit Rotterdam
op gezag van de rector magnificus

Prof.dr. H.G. Schmidt

en volgens besluit van het College voor Promoties.

De openbare verdediging zal plaatsvinden op
donderdag 15 november 2012 om 9.30 uur

door

Toine Hillenaar

geboren te Dirksland

PROMOTIECOMMISSIE

Promotor:	Prof.dr. J.C. van Meurs
Overige leden:	Prof.dr. G. van Rij Prof.dr. A.D.M.E. Osterhaus Dr. R.M.M.A. Nuijts
Copromotor:	Dr. L. Remeijer

CONTENTS

Voor Sas en Jord

1

Introduction

INTRODUCTION

Confocal microscopy is an emerging optical technique that allows the living human cornea to be imaged on a cellular level. As such, confocal microscopy enables morphologic and quantitative analysis of corneal resident cells in health and disease and provides an exciting bridge between *in vivo* diagnosis and *ex vivo* histological confirmation of pathologic processes.[1]

1.1 HISTORY OF CONFOCAL MICROSCOPY

The development of *in vivo* confocal microscopy is not a new paradigm or a paradigm shift, but a continuous series of interlinked technical advances.[2] An excellent historical overview from Masters and Böhnke[3] served as guidance to describe the developments since the invention of the compound microscope via the ophthalmoscope, slit-lamp, and specular microscope to today's confocal microscopes.

Compound microscope

In a rural town situated on one of the beautiful peninsulas along the Dutch North Sea coast, only 25 miles as the crow flies from the birth town of this thesis' author, history of *in vivo* confocal microscopy had its origin. Around 1595, a spectacle maker from Middelburg combined multiple glass lenses in a metal tube and found that the objects in front of the tube appeared to be greatly enlarged.[4] Until today it is unclear if Zaccharias Janssen or his neighbor Johannes Lipperhey discovered what is currently known as the first compound microscope. What is sure is that they could not have guessed that their design underlied the greatest discoveries in nature science. Yet, without their invention Galileo Galilei (1611) would not have made his telescopic journey through space, Robert Hooke (1655) would not have observed the small honeycomb structures or "cells" in cork, and Antoni van Leeuwenhoek (1683) would not have discovered the animalcules that populated the plaque between his own teeth. By mastering the art of grinding lenses, Antoni van Leeuwenhoek made many more discoveries which he documented in his letters to the Royal Society of London. In one of these letters, he described the structure of the human cornea, lens, retina, and optic nerve with microscopic precision, laying the foundations of modern ophthalmology.[5]

Ophthalmoscope

It took more than a century (1823) before the physiologist Jan Evangelista Purkinje observed the living retina. Purkinje placed a candle behind a subject and used his myopic

spectacles to reflect light from the candle into the subject's eye.[6] Because the detailed findings of this first ophthalmoscopy were published in Latin and tucked away among other important discoveries in his thesis, Purkinje's contribution to ophthalmoscopy remained unrecognised for many years.[7] In 1846, the mathematician Charles Babbage, known for his work on the computer, invented the direct view ophthalmoscope based on a glass mirror with a central hole.[8] Unfortunately, his instrument failed to display the retina when he showed it to the renowned ophthalmologist Wharton Jones.[9] Discouraged, Babbage ignored the instrument. Five years later (1851), unaware of Babbage's design, Hermann von Helmholtz reinvented the ophthalmoscope. Recognising the clinical usefulness of his invention, von Helmholtz published his findings and began to manufacture the ophthalmoscope.[10] Because of his awareness, von Helmholtz is generally credited with the invention of the ophthalmoscope. In the following years many technical variations were introduced to improve illumination and reflection of the ophthalmoscope and to correct for refractive errors of both patients and physicians.[11] In 1949, Sir Harold Ridley, who was the first to implant an intraocular lens, introduced the television ophthalmoscope.[12] Ridley's concept of scanning point illumination of the retina is considered a milestone in the modern development of the scanning laser ophthalmoscope.[3]

Slit-lamp biomicroscope

In 1911, Alvar Gullstrand was awarded with the Nobel Prize in Physiology or Medicine for his work on the dioptrics of the eye[13] and became, up until today, the only ophthalmologist honoured with this prize. In the same year, ophthalmology made a giant leap forward when Gullstrand presented his "large reflection-free ophthalmoscope" at the Versammlung der deutschen Ophthalmologischen Gesellschaft in Heidelberg.[14] Gullstrand's first concept of the slit-lamp allowed ophthalmologists to observe the ocular structures *in vivo* with a magnification that was previously unattainable. The slit-lamp biomicroscope subsequently led to identification of numerous new morphological phenomena and ocular disorders[15] and is, at present, still the gold standard for patient examination by ophthalmologists.

Specular microscope

In 1939, Hans Goldmann equipped Gullstrand's slit-lamp with a photographic system. The instrument continuously maintained its focus, as the slit beam moved forward conjugate with the camera, capturing the entire optical section sharply onto film.[16] The concept of this confocal instrument was further refined by David Maurice, who focused at the specular reflection of the interface from endothelium to aqueous humor. With the

angle of incidence equalling the angle of reflection, the specular reflection provided high magnification images of the corneal endothelial cells. In 1968, Maurice used the specular microscope to image the corneal endothelium of a rabbit eye, *ex vivo*.[17] After modifying Maurice's specular microscope, Ronald Laing was the first to photograph human corneal endothelium *in vivo*, with a magnification of 100X.[18]

Confocal microscope

In parallel with the specular microscope, the confocal microscope was developed. In 1955 Marvin Minsky constructed an instrument which he called the 'double focusing stage scanning microscope'. The instrument was patented in 1957 and used a symmetrical design comprising a condenser lens to focus the light source on a small area of tissue and an objective lens with the same focal point.[19] Because the illumination and observation pathways have a common focal point, this principle is termed "confocal".[20] To further enhance the spatial resolution, Minsky placed two conjugate apertures in the illumination and observation pathways to block the scattered light coming from above and below the focal plane. Compared to conventional microscopes that use the same wavelength and objective, this confocal design results in enhanced lateral and axial resolution and improved image contrast.[21]

Besides his original prototype, Minsky also proposed the single-lens reflected light scheme that is used in today's confocal microscopes (Figure 1). As the use of a beam splitter would elicit a brightness loss and consequently needed a longer exposure time,

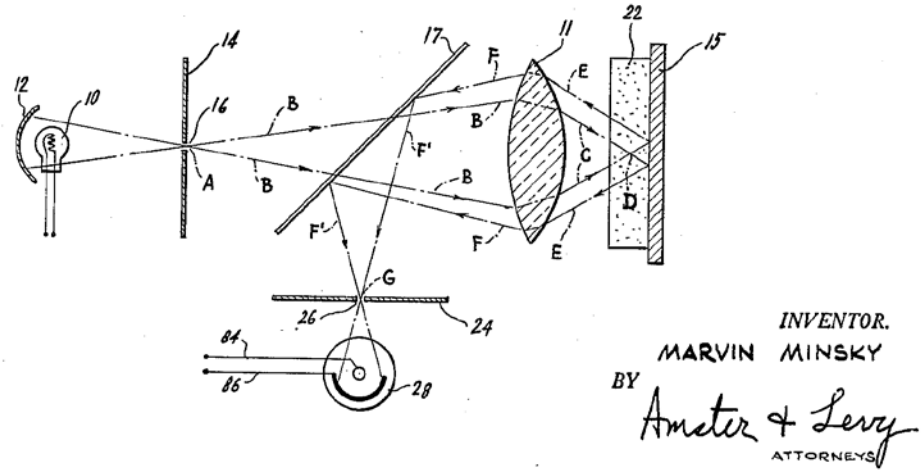

Figure 1. Original drawing of the optical path in the reflection confocal microscope, as patented by Marvin Minsky in 1957. Retrieved from:
http://patimg2.uspto.gov/.piw?Docid=03013467&PageNum=1&Rtype=&SectionNum=&idkey=NONE
United States Patent and Trademark Office, Patent Number: US003013467.

Minsky was reluctant to employ this scheme into a working prototype. Hence, another ten years passed before Minsky's scheme was implemented in two real-time confocal microscope types: tandem scanning and slit scanning confocal microscopes. These microscopes differ in their technique to scan a larger area, which is necessary as the major disadvantage of confocal microscopy is the restricted field of view.

Tandem scanning confocal microscope

The tandem scanning confocal microscope (TSCM) was introduced in 1968 by Petran and co-workers.[22] This instrument is based on a Nipkow disc comprising 64000 conjugate pinholes arranged in Archimedean spirals. By rapidly spinning the Nipkow disc, real-time scanning of the focal plane is achieved. Because the focal plane is moved through the entire cornea at a high constant speed while x-y images at the focal plane are digitized, the cornea is optically sectioned.[23] TSCM was first used for *ex vivo* imaging of unstained brain and ganglion cells of salamanders and frogs[24] and later for *ex vivo* imaging of animal corneas.[25] The first human cornea was imaged *ex vivo* by Lemp et al.[26] in 1985 and *in vivo* by Cavanagh et al.[20] in 1989.

Slit scanning confocal microscope

Contemporary with TSCM, slit scanning confocal microscopy (SSCM) was introduced by Svishchev in 1967.[27] Instead of a Nipkow disc, the SSCM uses a slit aperture to eliminate out of focus light. Because a slit aperture is used instead of a pinhole, the SSCM is truly confocal only in the axis perpendicular to the slit height.[28] To extent the imaging area, SSCM uses an oscillating two-sided mirror for scanning and descanning the focal plane.[29] Compared to tandem scanning, a slit-scanning design attains lower transverse and axial resolution. For practical purposes however, the decrease in resolution does not outweigh the gain in image contrast, as a slit scanning design has superior light throughput.[30] This great advantage of slit scanning systems has led to the extinction of commercially available TSCM.[31] The SSCM was initially developed to study neural tissue,[32] but only after further modifications by Thaer, the SSCM enabled real time imaging of corneal tissue *in vivo*.[33] We used a SSCM (Confocan 4, Nidek Technologies, Albignasego, Padova, Italy) (Figure 2) for the studies presented in this thesis.

Laser scanning confocal microscope

Based on Sir Ridley's concept of scanning point illumination and Minsky's design for confocal microscopy, Robert Webb developed the laser scanning ophthalmoscope for real-time imaging of the human retina.[36–38] To enable scanning in x and y directions, a

Figure 2. For the studies presented in this thesis, we used a slit scanning confocal microscope (Confoscan 4, NIDEK Technologies, Albignasego, Padova, Italy; reprinted with permission) equipped with a 100 watt halogen light source. Using a 40X Zeiss Acroplan objective lens with a high numerical aperture of 0.75, this instrument achieves a lateral resolution of 0.6 µm[1] and an axial resolution of 10 to 26 µm.[34,35] An optical coupling agent is applied to the objective lens to provide high-resolution images of 425x320 µm, after reducing the blink reflex with topical anesthetics. A *z*-ring adapter can be used to further reduce the motion artifacts induced by involuntary eye movements, pulse, and respiration during the 12 seconds of image acquisition. (*See also Color figures, p. 203.*)

laser beam is scanned over the microscope's focal plane using a set of galvanometer scanning mirrors.[3] Webb's concept is implemented in the Heidelberg retina tomograph (Heidelberg Engineering, Heidelberg, Germany), one of the well-established *in vivo* confocal imaging systems in ophthalmology.[21] In ophthalmic practice, this confocal scanning device is used to detect glaucomatous damage of the optic nerve head. In 2002, Joachim Stave introduced the 'Rostock cornea module', which is mounted onto the Heidelberg retina tomograph to enable visualization of the ocular anterior segment.[39] By using a coherent 670 µm laser source instead of white-light, this laser scanning confocal microscope (LSCM) is able to image not only the cornea, but also other non-transparent tissues of the ocular surface such as: the corneoscleral limbus, the bulbar and tarsal conjunctiva, and the lid margin.[40,41] Compared to white-light SSCM, LSCM performed better imaging the corneal epithelial layers due to greater image contrast.[42,43] The posterior stroma and the corneal endothelium however, are better visualized by white-light SSCM, because folds are induced in the posterior stroma by applanation of the cornea, which is necessary using LSCM.[42,44] Another advantage of white-light SSCM

is the automatic volume scan of the total cornea, whereas the volume scan with LSCM is currently limited to a section of 85 µm.[42]

1.2 *IN VIVO* IMAGING OF THE HUMAN CORNEA

The cornea represents the transparent part of the tissues that constitute the fibrous tunic of the ocular globe. Its main function is equivocal, as the cornea serves as a protective barrier against mechanic trauma, intruding pathogens, and dehydration, but is also responsible for approximately two-thirds of the total refractive power of the eye.[45] Because its purpose is to transmit the incoming light, the cornea is completely avascular.[46] Instead, oxygen and nutrients reach the corneal resident cells via diffusion from the surrounding environment: tear fluid, aqueous humor and limbal circulation. The total thickness of the central cornea measures, on average 534 µm, but increases towards the periphery.[47] This highly curved transparent tissue is elliptically shaped with an average diameter of 11.5 mm in the vertical and 12.0 mm in the horizontal axis.

The normal human cornea comprises five layers: epithelium, Bowman's layer, stroma, Descemet's membrane, and endothelium (Figure 3). The microscopic anatomy of each layer can be studied, *in vivo*, using several corneal imaging techniques. For the purpose of this thesis only slit-lamp biomicroscopy, specular microscopy, and *in vivo* confocal microscopy are highlighted.

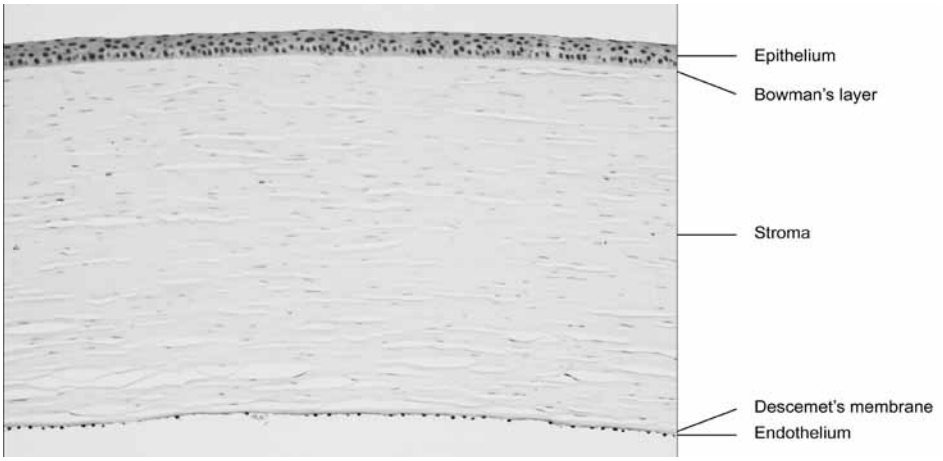

Figure 3. Histological cross section of the normal human cornea. (Courtesy of C.M. Mooy, PhD)

Slit-lamp biomicroscopy

Using slit-lamp biomicroscopy, ocular structures can be observed up to 40X magnification with a lateral resolution of 30 µm.[31] The various settings of this microscope allow the cornea to be appreciated in several ways: direct diffuse illumination, optical section, scattering sclero-corneal illumination, specular reflection, retro-illumination, and fluorescence observation.[48]

Direct illumination of the cornea with diffuse light can be used to detect gross abnormalities. A ground glass called a diffuser is placed in the optical path of a perpendicularly directed slit beam, opened at maximum wide. At a glance, this method facilitates a complete overview of the eye and its adnexa.

An optical section of the cornea is obtained by an obliquely directed slit-beam using narrow wide and maximum height. With illuminating and viewing axes both focused in the cornea, depth of a stromal lesion can be determined.

To achieve scattering sclero-corneal illumination, a wide slit beam is directed onto the limbal region of the cornea at a low angle of incidence, allowing the light to be transmitted by total internal reflection. With the microscope focused at the central cornea, even the faintest stromal lesions become brightly illuminated.

With retro-illumination a 2 to 4-mm slit beam is directed at the iris or at the fundus after pupil dilation. By dissociating the focal points of the illuminating and viewing pathways, abnormalities are highlighted against a comparatively dark background or against the red fundus reflex.

The specular reflection of the endothelium can be seen alongside the bright specular reflex of the epithelium when the angle of incidence equals the angle of observation and both axes are focused in the cornea at a 45 degree angle.

A cobalt blue filter can be placed in front of the tungsten light source to detect fluorescent epithelial defects after staining of the tear film with fluorescein.

Because of this wide variety of observation methods slit-lamp biomicroscopy remains unequalled in clinical assessment of the human cornea. The transparent nature of the healthy cornea, however, limits illustration of these observation methods. Therefore they are demonstrated in corneas affected by different manifestations of the herpes simplex virus (HSV) (Figure 4).

Specular microscopy

As the first specular microscope designed by Maurice used two conjugate (confocal) slits, this device can be regarded as a variant of the confocal microscope.[2] Although the specular microscope has been used to image all corneal layers,[49] the currently available specular microscopes solely image the corneal endothelium with magnifications around

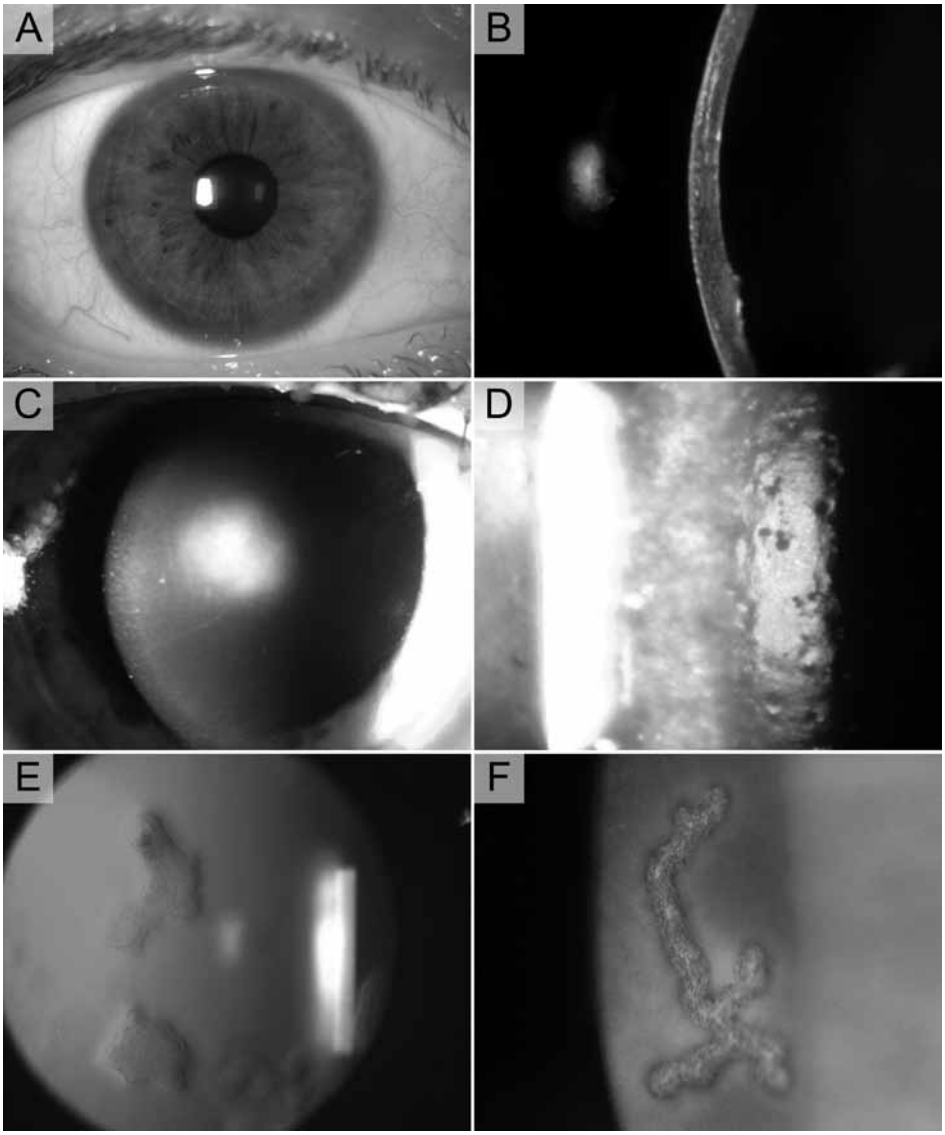

Figure 4. Standard observation techniques for clinical slit-lamp biomicroscopy illustrated by photography of different manifestations of HSV keratitis. **A.** Direct diffuse illumination showing mild conjunctival hyperemia. **B.** Optical section showing sheet-like corneal opacifications, stromal edema, and keratic precipitates in herpetic endotheliitis. **C.** Scattering sclero-corneal illumination showing spherical immune stromal keratitis. **D.** Specular illumination showing pseudoguttae. **E.** Retro-illumination showing thinned corneal areas after necrotizing stromal keratitis. **F.** Fluorescence illumination showing dendritic ulceration of the corneal epithelium. (*See also Color figures, p. 204.*)

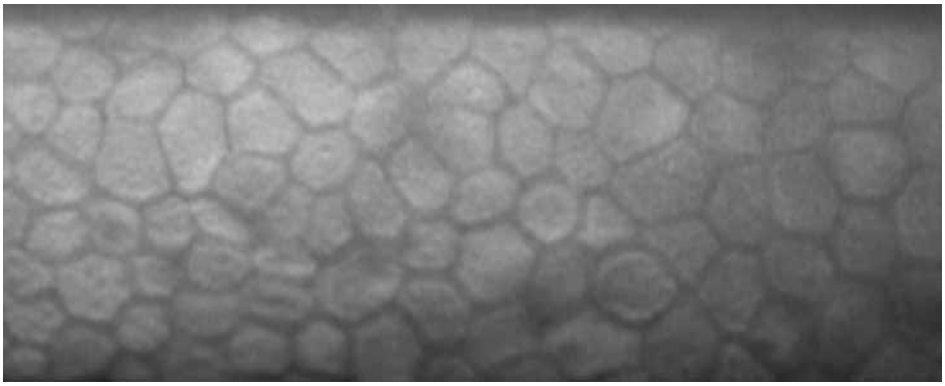

Figure 5. Specular microscopy (Topcon SP-2000P; Topcon Corp., Tokyo, Japan) of corneal endothelium showing polymegatism and pleomorphism.

200X (Figure 5). These endothelial images are relatively unaffected by patient movements due to the short acquisition time and can be obtained without physical contact between the objective and the cornea. In ophthalmic clinic, specular microscopy is primarily used for preoperative assessment of the corneal decompensation risk by determining the endothelial cell density. A major limitation of the specular microscope, however, is the inability to obtain clear images through edematous or inflamed corneal tissue.

In vivo confocal microscopy

Without fixing, processing, or sectioning tissue prior to observation, IVCM allows microstructural analysis of each corneal layer with a magnification up to 500X.[20] By providing "en face" images, orientation of IVCM images is very different from the typical sections obtained in histopathology in which tissue is cut along the thickness of the cornea (Figure 3). The plane of IVCM images is orthogonal to these sagittal sections, resembling histological whole mounts (Figure 6).[30]

Using IVCM, the corneal epithelium can be subdivided into three layers: superficial epithelial cells, intermediate wing cells, and basal epithelial cells. The polygonal superficial epithelial cells have dark cell bodies and a bright nucleus, surrounded by a dark halo.[50] Their cell size is about 20-30 µm in diameter and they are 5 µm thick.[51] The smaller wing cells represent the transition from basal to superficial epithelial cells. They are characterized by bright cellular borders, dark cell bodies and a bright nucleus without a dark halo.[51] The nucleus is indistinguishable in the 10-15 µm wide basal epithelial cells, which form a regular mosaic of dark cell bodies and bright borders.[52] The mean cell density of the basal epithelial cells appears to be constant with age.[50]

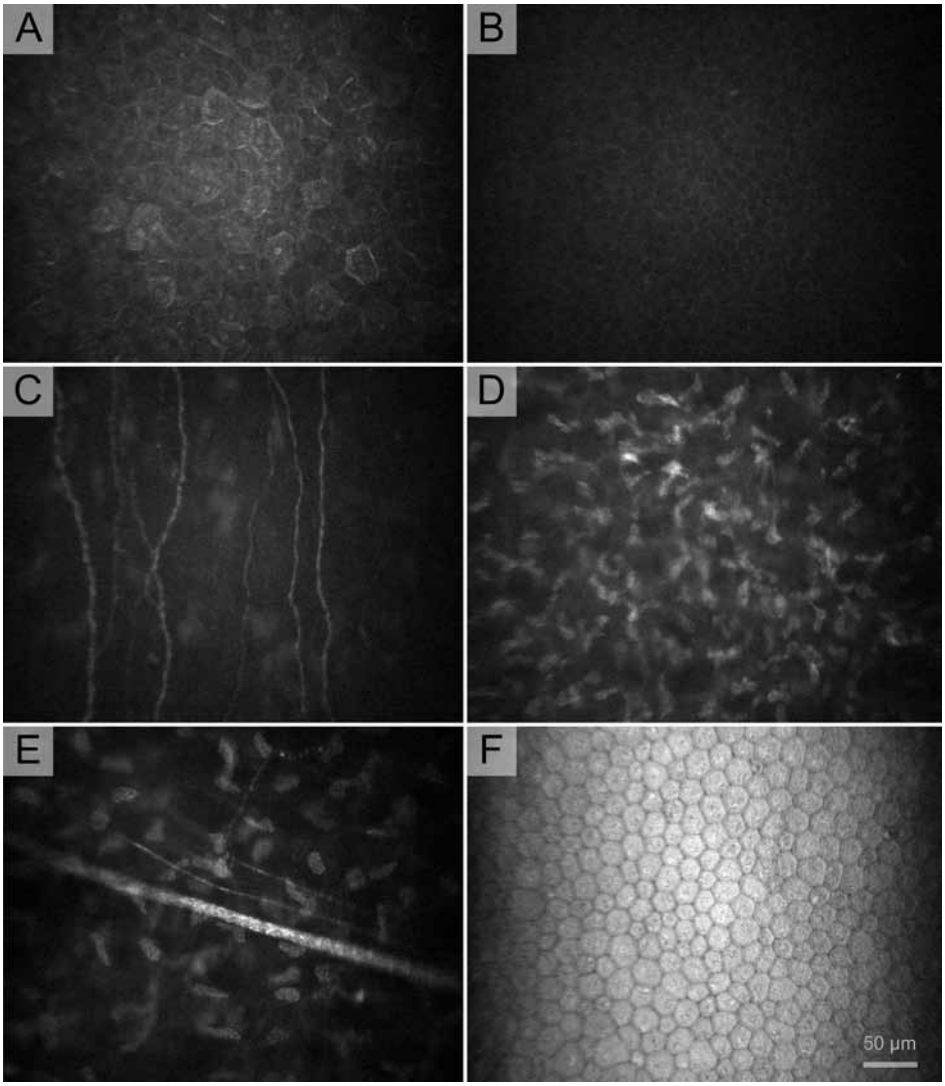

Figure 6. Characteristic layers of the normal corneal as observed by *in vivo* confocal microscopy. **A.** Superficial epithelial cells. **B.** Basal epithelial cells. **C.** Subbasal nerve plexus. **D**. Anterior stroma, characterized by a higher keratocyte density compared to middle and posterior thirds of the stroma. **E.** Mid-stroma showing a straight stromal nerve. **F.** Endothelial cells. This figure is adapted from Hillenaar, 2011.[66]

Interspersed between the epithelial basal cells and their basement membrane lies the subbasal nerve plexus.[53] On IVCM, the subbasal nerve plexus comprises parallel running beaded nerve fibers showing numerous branches and anastomoses. Upon mapping, the subbasal nerve plexus displays a vortex pattern,[54] which migrates in a centripetal fashion, converging 1-2 mm inferior to the corneal apex.[55]

The underlying amorphous Bowman's layer can only be differentiated from the surrounding layers when abnormalities are present.[56] By scanning the cornea in an oblique fashion, extensions of Bowman's membrane have been identified, the so-called K-structures.[57] These K-structures are thought to be responsible for the formation of the anterior corneal mosaic.[58]

On IVCM, the corneal stroma is characterized by hyperreflective keratocyte nuclei without showing the cell processes. The nuclei appear as well-defined, bright, oval to round objects with varying orientation against a dark background.[43] This dark background is elicited by the stromal collagen fibrils which, because of their specific lamellar orientation, are highly transparent and invisible at IVCM.[59] The keratocyte density declines with age and is highest in the anterior 10% of the stroma.[60] In the anterior and mid-stroma, straight hyperreflective nerves are observed. These nerves display a dichotomous branching pattern.[53]

Like Bowman's layer, Descemet's membrane is usually indistinguishable from the surrounding layers.[56] This 6-10 µm-thick acellular layer is made up of an anterior banded layer that is produced in the prenatal period and a posterior non-banded layer that is deposited by the endothelial cells during life.[61,62]

The endothelium forms the inner border of the cornea and consists of a monolayer of hexagonal cells arranged in a regular mosaic. Only sometimes can the nuclei be distinguished from the brightly reflecting endothelial cell bodies, which are separated by dark cell borders.[31] The endothelial cell density decreases with age, at a rate of 0.2% to 2.8% per year.[63–65]

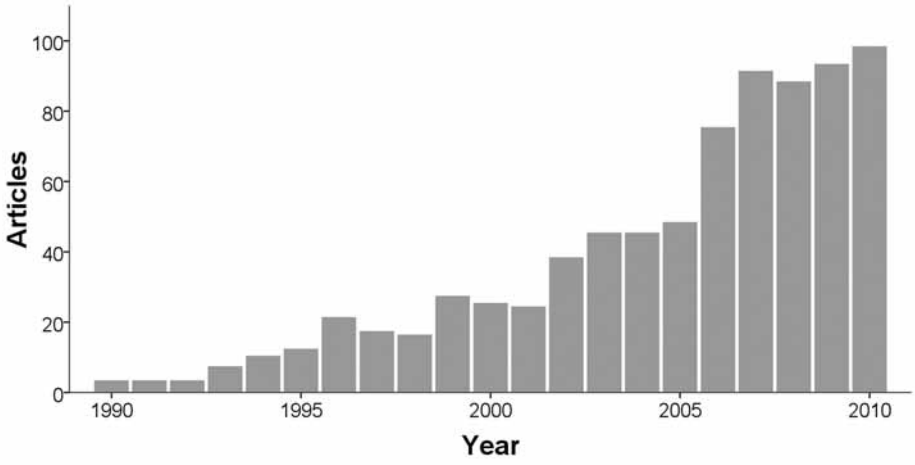

Figure 7. Twenty-year publication trends for *in vivo* confocal microscopy of the human cornea. The annual number of articles on this topic was identified by an electronic search in Pubmed using individual keywords: confocal, microscopy, and cornea. The identified articles were then reviewed if they covered *in vivo* confocal microscopy of the human cornea. Since 1990 the annual number of articles on IVCM of the human cornea has shown a gradual increase.

1.3 CLINICAL APPLICATIONS OF *IN VIVO* CONFOCAL MICROSCOPY

Since the introduction of IVCM of the cornea, twenty years ago, interest for this technique has increased continuously (Figure 7). In the first decade, many isolated case-reports appeared, documenting on cellular morphology in rare corneal disorders, whereas, in the second decade, the main focus shifted to larger case-series with quantitative assessment in normal and diseased corneas.[1] Because IVCM has already proven its value as a research tool, the logical next step would be to implement this technique in daily ophthalmic practice. In the past few years, IVCM has clearly made this step "from bench to bedside" by combining morphologic and quantitative assessment techniques.[67]

Morphologic assessment

In microbial keratitis, early diagnosis is of major importance as delay in appropriate treatment has detrimental effects on the best visual outcome.[68,69] To ascertain the causative agent, culture of corneal scrape specimens remains the gold standard.[70] Culture however, often takes three or more days before definite results become available. For the most prevalent corneal pathogens, the diagnostic interval has substantially reduced since the introduction of polymerase chain reaction (PCR) tests.[71] These PCR tests take only one day before results become available. IVCM, on the other hand, has the potential to identify *Acanthamoeba* and fungal keratitis, immediately.[72] Also, differentiation between bacterial and viral keratitis has been suggested, based on a pathogen specific immune response.[21,73] However, more research on these immunological reactions is needed, before IVCM can be used to distinguish bacterial from viral keratitis in a clinical setting.

For diagnosis of *Acanthamoeba* keratitis, IVCM has clearly proven its additional value.[74] *Acanthamoeba* is a ubiquitous protozoan living in soil and fresh water. As causative agent of keratitis, *Acanthamoeba* is associated with contact lens wear, especially in unhygienic circumstances like the use of nonsterile lens solutions, swimming while wearing contact lenses, and inadequate desinfection practices.[75,76] Because clinical presentation of *Acanthamoeba* keratitis resembles herpetic keratitis and rates of positive cultures rarely exceed 60%,[77] initial misdiagnosis is common. *Acanthamoeba* keratitis is often suspected at later stages when a ring infiltrate and radial perineuritis have developed and patients complain typically of intense pain.[70] *Acanthamoeba* cysts and, to a lesser extent, trophozoites can be distinguished from the corneal cellular structures using IVCM.[78–81] Double-walled *Acanthamoeba* cysts appear as coffee bean-shaped hyperreflective structures 15-28 µm in diameter (Figure 8), whereas the trophozoites are larger measuring 25-40 µm.[82] In literature, some controversy consists concerning the diagnostic accuracy of IVCM in *Acanthamoeba* keratitis. Using white light confocal microscopy, several authors have found a high sensitivity of >88%,[74,83,84] whereas Hau

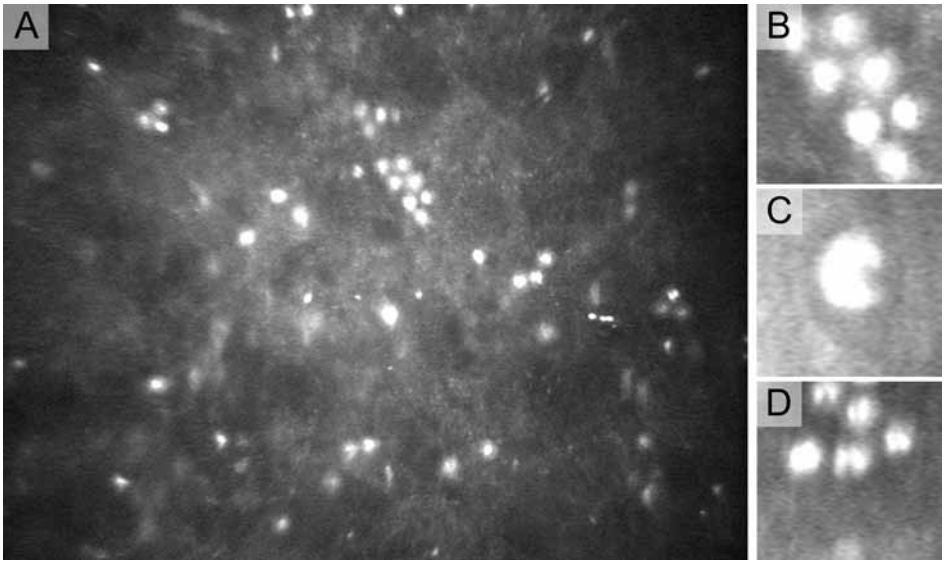

Figure 8. *In vivo* confocal microscopy of *Acanthamoeba* keratitis **A.** *Acanthamoeba* cysts observed in the mid-stroma. **B.** The encapsulated *Acanthamoeba* cyst typically appears as a hyperreflective structure (15-28 µm) surrounded by a halo. **C.** Depending on the cross-section the cyst may also appear coffee bean-shaped, **D**. or may display two parallel lines.

et al,[85] found a much lower sensitivity of <56% using LSCM. This large discrepancy is unlikely to be caused by the different light sources, as the lateral resolution of the microscope types does not differ much. Alternatively, the sensitivity in the studies that used white light may be overestimated because of observer and selection bias, the absence of masking the observers from the microbiological diagnosis, and lack of appropriate controls.[85] In our experience, *Acanthamoeba* can be diagnosed with a sensitivity of 58% and a specificity of 93%.[86]

Although fungal keratitis may present with classical signs such as grayish-white or yellowish-white infiltrates with feathery edges and satellite lesions, early manifestations are often atypical and frequently misdiagnosed as bacterial or viral keratitis. Worldwide the prevalence of fungal keratitis varies considerably,[87] with proportions as high as 67% of all corneal infections in agriculture-based regions with warm, humid climates,[88] to as low as 1.8% in temperate climates such as The Netherlands.[89] This corresponds with our IVCM experience, comprising over 9000 examinations of more than 2000 patients. Approximately 800 of these patients had microbial keratitis, but only one patient was diagnosed with filamentous fungal keratitis. The gold standard for diagnosis is corneal smear or culture. Because both have a varying sensitivity[90] and approximately one-fourth of fungal cultures take 2 or more weeks to become positive,[91] IVCM has an important role in early detection of fungal keratitis.[92] At IVCM, hyphae of filamentous fungi appear as hyperreflective, interlocking white lines of 5-10 µm in diameter and 200-400 µm in length,

which branch dichotomously at a 45 degree angle (*Aspergillus*) or at a 90 degree angle (*Fusarium*).[92–94] Filamentous fungi can be identified with a sensitivity of 89%-94% and a specificity of 78%-93% using white light confocal microscopy.[74,83] These studies were performed in regions where fungal keratitis is flourishing and filamentous fungi such as *Fusarium* and *Aspergillus* species are the major etiologic agents.[90] In temperate climates, yeast, in particular *Candida* species, are the most common cause of fungal keratitis.[94,95] *Candida* species however, are much harder to detect than filamentous fungi, because the pseudohyphae appear as hyperreflective elongated particles measuring only 10-40 µm which are hard to distinguish from the surrounding inflammatory cells.[94] Therefore, sensitivity and specificity of detection of fungal elements by IVCM may be lower in ophthalmic centers in temperate climates. Besides detection of fungal keratitis, IVCM has also been used to monitor and guide antifungal therapy[93,96,97] and to support the decision to perform a penetrating keratoplasty.[98] Moreover, IVCM is the only method to determine the depth of invasion, which is an important prognostic factor in fungal keratitis.[70]

Another clinical application of IVCM is early detection of corneal dystrophies and degenerations (Figure 9). Most of these corneal diseases, however, can also be detected by slit-lamp biomicroscopy. IVCM has been found truly valuable in the differentiation of endothelial disorders such as Fuchs' endothelial dystrophy, posterior polymorphous dystrophy and the iridocorneal endothelial syndrome.[99,100] In these cases, endothelial detail at slit-lamp or specular microscopy is often obscured by corneal edema, whereas IVCM provides at least a glimpse of the endothelial morphology. The microscopic characteristics and distinguishing features of these endothelial disorders are thoroughly described in chapters 2 and 7 of this thesis.

Quantitative assessment

Besides morphological evaluation of the cornea at a cellular level, IVCM also allows objective assessment of several quantitative parameters. One such parameter which is commonly used in ophthalmic practice is the endothelial cell density (ECD). Because IVCM eliminates most out of focus light, the ECD can be assessed even in the presence of corneal edema or haze. Although ECD is not directly correlated with the pumping function of the endothelial cells, a critical ECD of 300 to 500 cells/mm^2 seems needed to prevent corneal decompensation.[101,102] For this reason, ECD measurement is often used to assess the risk of corneal decompensation prior to intraocular surgery.

Like endothelial cells, other corneal resident cells and related structures such as superficial and basal epithelial cells, subbasal nerve plexus, dendriform cells, and keratocytes can be quantified using IVCM. Densities of these corneal elements have recently been summarized in an excellent review article by Niederer and McGhee.[1] Of these parameters, quantification of the subbasal nerve plexus seems the most promising as it may

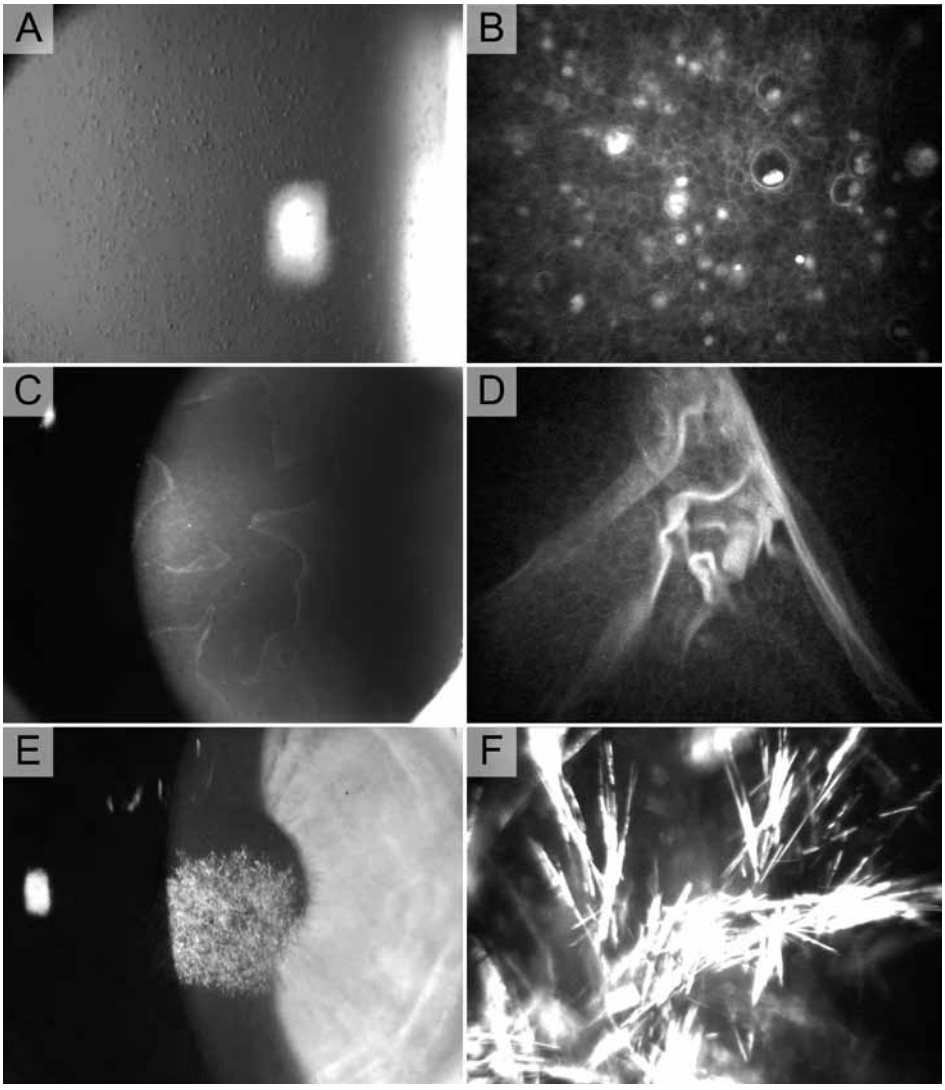

Figure 9. *In vivo* confocal microscopy (IVCM) allows early detection of corneal dystrophies and degenerations. **A.** Meesmann corneal dystrophy. **B.** Confocal microscopy showed intraepithelial cysts filled with peculiar substance. **C.** Epithelial basement membrane dystrophy (EBMD). Unlike the term suggests, EBMD is generally regarded an age-related corneal degeneration. **D.** Confocal microscopy showed extensive folding of Bowman's layer. **E.** Schnyder crystalline corneal dystrophy. **F.** Confocal microscopy showed crystalline deposits in the anterior stroma. (*See also Color figures, p. 205.*)

indicate the stage of peripheral neuropathy in diabetes mellitus.[103,104] Nevertheless, the clinical relevance of quantification of the subbasal nerve plexus and of the other parameters remains to be confirmed.

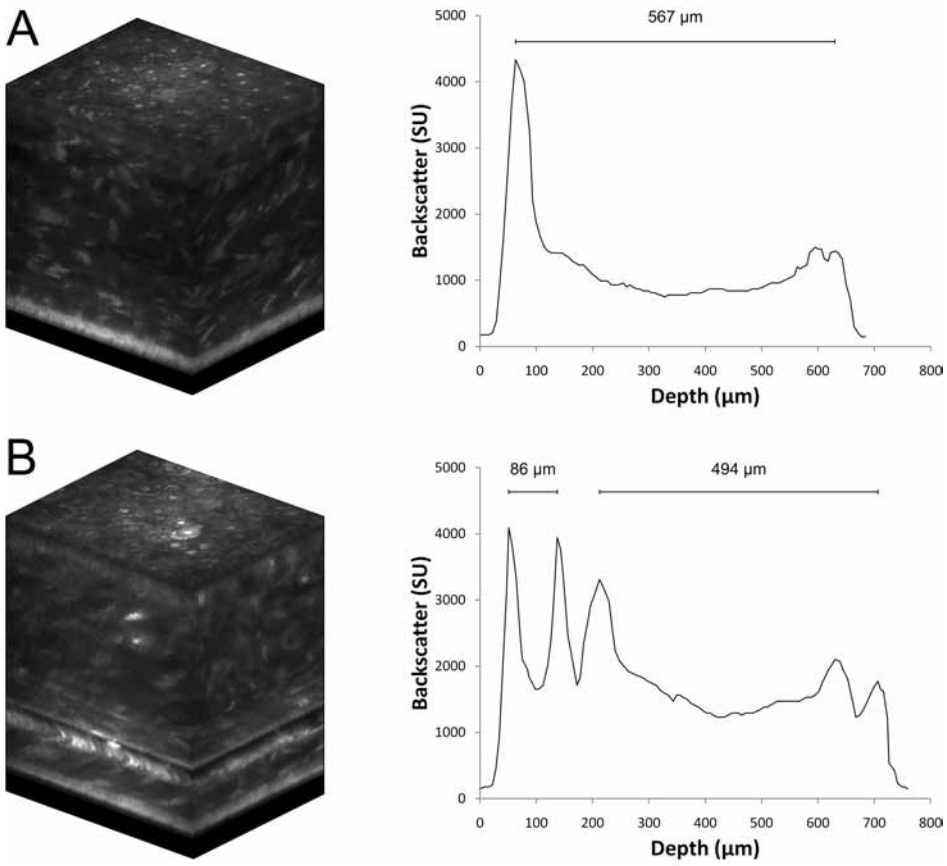

Figure 10. 3-D image reconstructions and corresponding *z*-scan curves of full-thickness corneal scans by *in vivo* confocal microscopy (IVCM). **A.** In a normal cornea, the pachymetry (567 µm) can be measured based on the z-scan curve by calculating the distance from the first intensity peak (endothelium) to the last intensity peak (epithelium). **B.** Interface fluid syndrome after Descemet's stripping automated endothelial keratoplasty (DSAEK). Compared with a normal cornea the *z*-scan curve in interface fluid syndrome shows two additional intensity peaks. These peaks can be used to calculate the lamellar thickness (86 µm) and the thickness of the remaining host cornea (494 µm).

Two other important quantitative IVCM parameters are pachymetry and sublayer pachymetry. These parameters can be computed based on a so-called *z*-scan curve (Figure 10) which is generated by plotting depth of each frame in the IVCM image series against the mean pixel intensity in the central 285 x 285 µm of that frame. Because image intensity peaks at sudden transitions of refractive index,[23] the interfaces from viscoelastic gel to epithelium and from endothelium to aqueous humor can easily be identified. Consequently, the distance between these interface peaks defines the corneal pachymetry,[105] which can be measured with high intrainstrument and interobserver repeatability.[106] The precision of IVCM pachymetry, however, is almost 4 times lower

compared to ultrasonic pachymetry because of antero-posterior eye movements during the scan. Its accuracy on the other hand, is better than ultrasonic pachymetry.[107] Because each point on the *z*-scan curve is directly correlated with high-resolution images, the distance between two separate corneal layers can be computed. Similar to measuring the epithelial or stromal thickness in the normal cornea, this sublayer pachymetry has also been used to determine the lamellar thickness based on the artificially induced interface after laser-assisted in situ keratomilieusis[108] or lamellar keratoplasty.[109] Likewise, the depth of stromal deposits can be measured to determine the treatment depth before phototherapeutic keratectomy or lamellar keratoplasty.[110]

Besides thickness measurements the *z*-scan curve can also be used to estimate the amount of backscattered light from healthy and diseased corneas. This corneal backscatter, which comprises scatter as well as specular reflection originating at the focal plane when measured by IVCM, correlates with clinical haze grading by slit-lamp biomicroscopy, but is more sensitive to small changes in corneal opacity.[111] Because of its sensitivity and objectivity, this haze grading technique becomes increasingly popular in the evaluation of the wound healing process after corneal surgery.[109,111–113] Moreover, other applications of corneal backscatter measurement such as quantification of edema[114] and staging diabetic retinopathy[115] seem even more promising. Nevertheless, despite its great potential, corneal backscatter analysis has not yet been implemented in ophthalmic practice.

1.4 THESIS OUTLINE

The aim of this thesis is to investigate the role of *in vivo* confocal microscopy for the corneal specialist. As described above, the role of IVCM at the start of this work was confined to diagnosing specific causes of microbial keratitis, early detection of corneal dystrophies and degenerations, assessing the ECD in opacified corneas and determining the depth of these opacities. To expand the clinical applications of IVCM, we focused on the combination of morphologic assessment and corneal backscatter measurement to detect and monitor corneal pathology. However, before this powerful combination can be used in a clinical setting, several basic studies had to be performed. The results of these studies are documented in Part I: Basic research (Chapters 2 to 4).

PART I

Chapter 2 describes the effects of aging on corneal morphology as seen by IVCM. The eight most common features that illustrate the morphologic diversity of the normal cornea are studied for their age-relatedness. To further emphasize this morphologic diversity a novel phenotype of corneal endothelium is introduced.

Chapter 3 presents two methods for intra- and interinstrument calibration of backscatter measurement by IVCM, covering normal and opaque corneas. These calibration methods are necessary as backscatter measurement is subject to large interinstrument differences.

Chapter 4 describes the effects of sex, age, and diurnal variation on corneal backscatter as measured by IVCM. Based on these influencing factors and the repeatability of backscatter measurements, a generalized normal range and minimum detectable change is proposed for seven backscatter variants. In ophthalmic practice, each of these backscatter variants may serve different purposes.

Simultaneously with gaining essential knowledge on morphology and corneal backscatter in the normal cornea, a large IVCM database was constructed that included more than 2000 individuals comprising over one-hundred corneal disorders and surgical techniques.[116] Of the many diagnoses in this database, we studied herpetic keratitis in detail. The results of the studies on this recrudescent disease, which is generally regarded as the number one cause of unilateral infectious blindness in developed countries,[117] are outlined in Part II: Herpetic keratitis (Chapters 5 to 7).

PART II

Chapter 5 reports on the appearance, frequency, and clinical consequences of transient endothelial alterations in HSV keratitis as observed by IVCM. These endotheliitis specific alterations often precede formation of keratic precipitates and may be used to indicate disease activity in HSV keratitis.

Chapter 6 demonstrates the role of IVCM in the follow-up of herpetic stromal keratitis (HSK). The multifactorial characteristics of HSK pose diagnostic difficulties in detection and monitoring inflammatory activity. In the follow-up of HSK, IVCM may be advantageous to slit-lamp examination, by combining objective backscatter measurement and morphologic assessment at a cellular level. On the other hand, slit-lamp biomicroscopy has the advantage of viewing the whole cornea.

Chapter 7 presents a new subset of idiopathic corneal edema: zipper cell endotheliopathy. The unique endothelial alterations were detected *in vivo*, using confocal microscopy in a presumed herpes affected cornea. After excision, the corneal button was subjected to real-time polymerase chain reaction, immunohistochemistry and electron microscopy to exclude a herpetic origin of the endothelial alterations and to confirm their morphological distinctiveness.

REFERENCES

1. Niederer RL, McGhee CN. Clinical in vivo confocal microscopy of the human cornea in health and disease. Prog Retin Eye Res 2010;29:30-58.
2. Masters BR. David Maurice's contributions to optical ophthalmic instrumentation: roots of the scanning slit clinical confocal microscope. Exp Eye Res 2004;78:315-26.
3. Masters BR, Bohnke M. Three-dimensional confocal microscopy of the living human eye. Annu Rev Biomed Eng 2002;4:69-91.
4. van der Laan J. Holland claims the microscope. J Am Med Assoc 2012;XIII:720.
5. Hoole S. The select works of Antony van Leeuwenhoek. London: G. Sidney, 1798, Vol.1; 1807, Vol.2.
6. Keeler C.R. A brief history of the Ophthalmoscope. Optometry In Practice 2003;4:137-45.
7. Reese PD. The neglect of Purkinje's technique of ophthalmoscopy prior to Helmholtz's invention of the ophthalmoscope. Ophthalmology 1986;93:1457-60.
8. Duke-Elder S. System of Ophthalmology. London: Kimpton, 1962;233-7.
9. Jones T.W. Report on the ophthalmoscope. Br Foreign Med-Chir Rev 1854;24:425-32.
10. von Helmholtz H. Helmholtz's treatise on physiological optics. Translated from the Third German Edition. Vol. 1. New York: Optical Society of America, 1924;261-482.
11. Pearce JM. The ophthalmoscope: Helmholtz's Augenspiegel. Eur Neurol 2009;61:244-9.
12. Ridley H. Recent methods of fundus examination including electronic ophthalmoscopy. Trans Ophthalmol Soc UK 1952;72:497-509.
13. Nobel Lectures, Physiology or Medcine 1901-1921. Amsterdam: Elsevier Publishing Company, 1967.
14. Gullstrand A. Demonstration der Nerstspaltlampe. Heidelberg: Heidelberger Bericht, 1911.
15. Vogt A. Lehrbuch und Atlas der Spaltlampenmikroskopie des lebenden Auges. Berlin: Julius Springer, 1930.
16. Goldmann H. Spaltlampenphotographie und photometrie. Ophthalmologica 1939;98:257-70.
17. Maurice DM. Cellular membrane activity in the corneal endothelium of the intact eye. Experientia 1968;24:1094-5.
18. Laing RA, Sandstrom MM, Leibowitz HM. In vivo photomicrography of the corneal endothelium. Arch Ophthalmol 1975;93:143-5.
19. Minski M. Memoir on inventing the confocal scanning microscope. Scanning 1988;10:128-38.
20. Cavanagh HD, Jester JV, Essepian J, et al. Confocal microscopy of the living eye. CLAO J 1990;16: 65-73.
21. Guthoff RF, Zhivov A, Stachs O. In vivo confocal microscopy, an inner vision of the cornea - a major review. Clin Experiment Ophthalmol 2009;37:100-17.
22. Petran M, Hadravsky M, Egger MD, Galambos R. Tandem scanning reflected light microscope. J Opt Soc Am 1968;58:661-4.
23. Cavanagh HD, El Agha MS, Petroll WM, Jester JV. Specular microscopy, confocal microscopy, and ultrasound biomicroscopy: diagnostic tools of the past quarter century. Cornea 2000;19:712-22.
24. Egger MD, Petran M. New reflected-light microscope for viewing unstained brain and ganglion cells. Science 1967;157:305-7.
25. Egger MD, Gezari W, Davidovits P, et al. Observation of nerve fibers in incident light. Experientia 1969;25:1225-6.
26. Lemp MA, Dilly PN, Boyde A. Tandem-scanning (confocal) microscopy of the full-thickness cornea. Cornea 1985;4:205-9.

27. Svishchev GM. Methods of correcting for errors in luminescence measurements on thick microscopic objects. Zh Prikl Spektrosk 1967;7:887-909.
28. Masters BR, Bohnke M. Confocal microscopy of the human cornea in vivo. Int Ophthalmol 2001; 23:199-206.
29. Svishchev GM. Microscope for the study of transparent light-scattering objects in incident light. Opt Spectrosc 1969;30:188-91.
30. Bohnke M, Masters BR. Confocal microscopy of the cornea. Prog Retin Eye Res 1999;18:553-628.
31. Efron N. Contact lens-induced changes in the anterior eye as observed in vivo with the confocal microscope. Prog Retin Eye Res 2007;26:398-436.
32. Masters BR. Selected Papers on Confocal Microscopy (SPIE milestone series: v. MS131). Bellingham: SPIE-The International Society for Optical Engineering, 1996.
33. Masters BR, Thaer AA. Real-time scanning slit confocal microscopy of the in vivo human cornea. Appl Opt 1994;33:695-701.
34. Kaufman SC, Musch DC, Belin MW, et al. Confocal microscopy: a report by the American Academy of Ophthalmology. Ophthalmology 2004;111:396-406.
35. McLaren JW, Nau CB, Kitzmann AS, Bourne WM. Keratocyte density: comparison of two confocal microscopes. Eye Contact Lens 2005;31:28-33.
36. Webb RH, Hughes GW, Pomerantzeff O. Flying spot TV ophthalmoscope. Appl Opt 1980;19: 2991-7.
37. Webb RH, Hughes GW, Delori FC. Confocal scanning laser ophthalmoscope. Appl Opt 1987;26: 1492-9.
38. Webb RH. Scanning laser ophthalmoscope. In: Masters BR, ed. Noninvasive Techniques in Ophthalmology. New York: Springer-Verlag, 1990.
39. Stave J, Zinser G, Grummer G, Guthoff R. [Modified Heidelberg Retinal Tomograph HRT. Initial results of in vivo presentation of corneal structures]. Ophthalmologe 2002;99:276-80.
40. Zhivov A, Stachs O, Kraak R, et al. In vivo confocal microscopy of the ocular surface. Ocul Surf 2006;4:81-93.
41. Nubile M, Mastropasqua L. In vivo confocal microscopy of the ocular surface: where are we now? Br J Ophthalmol 2009;93:850-2.
42. Szaflik JP. Comparison of in vivo confocal microscopy of human cornea by white light scanning slit and laser scanning systems. Cornea 2007;26:438-45.
43. Patel DV, McGhee CN. Contemporary in vivo confocal microscopy of the living human cornea using white light and laser scanning techniques: a major review. Clin Experiment Ophthalmol 2007;35:71-88.
44. Auran JD, Koester CJ, Rapaport R, Florakis GJ. Wide field scanning slit in vivo confocal microscopy of flattening-induced corneal bands and ridges. Scanning 1994;16:182-6.
45. Pavan-Langston D. Manual of Ocular Diagnosis and Therapy. Hagerstown, MD: Lippincott Williams & Wilkins, 2007;405.
46. Cursiefen C, Chen L, Saint-Geniez M, et al. Nonvascular VEGF receptor 3 expression by corneal epithelium maintains avascularity and vision. Proc Natl Acad Sci U S A 2006;103:11405-10.
47. Doughty MJ, Zaman ML. Human corneal thickness and its impact on intraocular pressure measures: a review and meta-analysis approach. Surv Ophthalmol 2000;44:367-408.
48. Eye examination with the slit lamp. Brochure of Carl Zeiss Meditec AG . 2012. Electronic Citation
49. Maurice DM. A scanning slit optical microscope. Invest Ophthalmol 1974;13:1033-7.
50. Mustonen RK, McDonald MB, Srivannaboon S, et al. Normal human corneal cell populations evaluated by in vivo scanning slit confocal microscopy. Cornea 1998;17:485-92.

51. Masters BR, Thaer AA. In vivo real-time confocal microscopy of wing cells in the human cornea: a new benchmark for in vivo corneal microscopy. Bioimages 1995;3:7-11.
52. Tomii S, Kinoshita S. Observations of human corneal epithelium by tandem scanning confocal microscope. Scanning 1994;16:305-6.
53. Oliveira-Soto L, Efron N. Morphology of corneal nerves using confocal microscopy. Cornea 2001; 20:374-84.
54. Patel DV, McGhee CN. Mapping of the normal human corneal sub-Basal nerve plexus by in vivo laser scanning confocal microscopy. Invest Ophthalmol Vis Sci 2005;46:4485-8.
55. Patel DV, McGhee CN. In vivo laser scanning confocal microscopy confirms that the human corneal sub-basal nerve plexus is a highly dynamic structure. Invest Ophthalmol Vis Sci 2008;49: 3409-12.
56. Efron N, Perez-Gomes I, Mutalib HA, Hollingsworth J. Confocal microscopy of the normal human cornea. Contact Lens Anterior Eye 2001;24:16-23.
57. Kobayashi A, Yokogawa H, Sugiyama K. In vivo laser confocal microscopy of Bowman's layer of the cornea. Ophthalmology 2006;113:2203-8.
58. Bron AJ. Anterior corneal mosaic. Br J Ophthalmol 1968;52:659-69.
59. Maurice DM. The structure and transparency of the cornea. J Physiol 1957;136:263-86.
60. Patel S, McLaren J, Hodge D, Bourne W. Normal human keratocyte density and corneal thickness measurement by using confocal microscopy in vivo. Invest Ophthalmol Vis Sci 2001;42:333-9.
61. Jakus MA. Studies on the cornea. II. The fine structure of Descement's membrane. J Biophys Biochem Cytol 1956;2:243-52.
62. Johnson DH, Bourne WM, Campbell RJ. The ultrastructure of Descemet's membrane. I. Changes with age in normal corneas. Arch Ophthalmol 1982;100:1942-7.
63. Bourne WM, Nelson LR, Hodge DO. Central corneal endothelial cell changes over a ten-year period. Invest Ophthalmol Vis Sci 1997;38:779-82.
64. Yee RW, Matsuda M, Schultz RO, Edelhauser HF. Changes in the normal corneal endothelial cellular pattern as a function of age. Curr Eye Res 1985;4:671-8.
65. Doughty MJ, Muller A, Zaman ML. Assessment of the reliability of human corneal endothelial cell-density estimates using a noncontact specular microscope. Cornea 2000;19:148-58.
66. Hillenaar T, Cals RH, Eilers PH, et al. Normative database for corneal backscatter analysis by in vivo confocal microscopy. Invest Ophthalmol Vis Sci 2011;52:7274-81.
67. Zhivov A, Guthoff RF, Stachs O. In vivo confocal microscopy of the ocular surface: from bench to bedside and back again. Br J Ophthalmol 2010;94:1557-8.
68. Thomas PA, Geraldine P. Infectious keratitis. Curr Opin Infect Dis 2007;20:129-41.
69. McLeod SD, LaBree LD, Tayyanipour R, et al. The importance of initial management in the treatment of severe infectious corneal ulcers. Ophthalmology 1995;102:1943-8.
70. Kumar RL, Cruzat A, Hamrah P. Current state of in vivo confocal microscopy in management of microbial keratitis. Semin Ophthalmol 2010;25:166-70.
71. Van Gelder RN. Applications of the polymerase chain reaction to diagnosis of ophthalmic disease. Surv Ophthalmol 2001;46:248-58.
72. Chew SJ, Beuerman RW, Assouline M, et al. Early diagnosis of infectious keratitis with in vivo real time confocal microscopy. CLAO J 1992;18:197-201.
73. Zhivov A, Stachs O, Kraak R, Guthoff R. [Cellular laser microscopy of corneal ulcer and infiltrate]. Klin Monbl Augenheilkd 2008;225:86-90.
74. Vaddavalli PK, Garg P, Sharma S, et al. Role of confocal microscopy in the diagnosis of fungal and acanthamoeba keratitis. Ophthalmology 2011;118:29-35.

75. Radford CF, Lehmann OJ, Dart JK. Acanthamoeba keratitis: multicentre survey in England 1992-6. National Acanthamoeba Keratitis Study Group. Br J Ophthalmol 1998;82:1387-92.
76. Stehr-Green JK, Bailey TM, Visvesvara GS. The epidemiology of Acanthamoeba keratitis in the United States. Am J Ophthalmol 1989;107:331-6.
77. Yeh DL, Stinnett SS, Afshari NA. Analysis of bacterial cultures in infectious keratitis, 1997 to 2004. Am J Ophthalmol 2006;142:1066-8.
78. Pfister DR, Cameron JD, Krachmer JH, Holland EJ. Confocal microscopy findings of Acanthamoeba keratitis. Am J Ophthalmol 1996;121:119-28.
79. Mathers WD, Nelson SE, Lane JL, et al. Confirmation of confocal microscopy diagnosis of Acanthamoeba keratitis using polymerase chain reaction analysis. Arch Ophthalmol 2000;118:178-83.
80. Bourcier T, Dupas B, Borderie V, et al. Heidelberg retina tomograph II findings of Acanthamoeba keratitis. Ocul Immunol Inflamm 2005;13:487-92.
81. Kobayashi A, Ishibashi Y, Oikawa Y, et al. In vivo and ex vivo laser confocal microscopy findings in patients with early-stage acanthamoeba keratitis. Cornea 2008;27:439-45.
82. Illingworth CD, Cook SD. Acanthamoeba keratitis. Surv Ophthalmol 1998;42:493-508.
83. Kanavi MR, Javadi M, Yazdani S, Mirdehghanm S. Sensitivity and specificity of confocal scan in the diagnosis of infectious keratitis. Cornea 2007;26:782-6.
84. Tu EY, Joslin CE, Sugar J, et al. The relative value of confocal microscopy and superficial corneal scrapings in the diagnosis of Acanthamoeba keratitis. Cornea 2008;27:764-72.
85. Hau SC, Dart JK, Vesaluoma M, et al. Diagnostic accuracy of microbial keratitis with in vivo scanning laser confocal microscopy. Br J Ophthalmol 2010;94:982-7.
86. Weenen C, Hillenaar T, van Cleynenbreugel H, Remeijer L. De plaats van in vivo confocale microscopie in de diagnose van acanthamoeba keratitis. vergadering Nederlands Oogheelkundig Gezelschap . 2011. Abstract
87. Shah A, Sachdev A, Coggon D, Hossain P. Geographic variations in microbial keratitis: an analysis of the peer-reviewed literature. Br J Ophthalmol 2011;95:762-7.
88. Basak SK, Basak S, Mohanta A, Bhowmick A. Epidemiological and microbiological diagnosis of suppurative keratitis in Gangetic West Bengal, eastern India. Indian J Ophthalmol 2005;53:17-22.
89. van der Meulen I, van Rooij J, Nieuwendaal CP, et al. Age-related risk factors, culture outcomes, and prognosis in patients admitted with infectious keratitis to two Dutch tertiary referral centers. Cornea 2008;27:539-44.
90. Srinivasan M. Fungal keratitis. Curr Opin Ophthalmol 2004;15:321-7.
91. O'Day DM, Akrabawi PL, Head WS, Ratner HB. Laboratory isolation techniques in human and experimental fungal infections. Am J Ophthalmol 1979;87:688-93.
92. Labbe A, Khammari C, Dupas B, et al. Contribution of in vivo confocal microscopy to the diagnosis and management of infectious keratitis. Ocul Surf 2009;7:41-52.
93. Winchester K, Mathers WD, Sutphin JE. Diagnosis of Aspergillus keratitis in vivo with confocal microscopy. Cornea 1997;16:27-31.
94. Brasnu E, Bourcier T, Dupas B, et al. In vivo confocal microscopy in fungal keratitis. Br J Ophthalmol 2007;91:588-91.
95. Tanure MA, Cohen EJ, Sudesh S, et al. Spectrum of fungal keratitis at Wills Eye Hospital, Philadelphia, Pennsylvania. Cornea 2000;19:307-12.
96. Shi W, Li S, Liu M, et al. Antifungal chemotherapy for fungal keratitis guided by in vivo confocal microscopy. Graefes Arch Clin Exp Ophthalmol 2008;246:581-6.
97. Takezawa Y, Shiraishi A, Noda E, et al. Effectiveness of in vivo confocal microscopy in detecting filamentous fungi during clinical course of fungal keratitis. Cornea 2010;29:1346-52.

98. Florakis GJ, Moazami G, Schubert H, et al. Scanning slit confocal microscopy of fungal keratitis. Arch Ophthalmol 1997;115:1461-3.
99. Grupcheva CN, Craig JP, Sherwin T, McGhee CN. Differential diagnosis of corneal oedema assisted by in vivo confocal microscopy. Clin Experiment Ophthalmol 2001;29:133-7.
100. Hara M, Morishige N, Chikama T, Nishida T. Comparison of confocal biomicroscopy and noncontact specular microscopy for evaluation of the corneal endothelium. Cornea 2003;22:512-5.
101. Waring GO, III, Bourne WM, Edelhauser HF, Kenyon KR. The corneal endothelium. Normal and pathologic structure and function. Ophthalmology 1982;89:531-90.
102. van Dooren BT. The corneal endothelium reflected. 2006. Erasmus University Rotterdam. Thesis/ Dissertation
103. Rosenberg ME, Tervo TM, Immonen IJ, et al. Corneal structure and sensitivity in type 1 diabetes mellitus. Invest Ophthalmol Vis Sci 2000;41:2915-21.
104. Hossain P, Sachdev A, Malik RA. Early detection of diabetic peripheral neuropathy with corneal confocal microscopy. Lancet 2005;366:1340-3.
105. Li HF, Petroll WM, Moller-Pedersen T, et al. Epithelial and corneal thickness measurements by in vivo confocal microscopy through focusing (CMTF). Curr Eye Res 1997;16:214-21.
106. Brugin E, Ghirlando A, Gambato C, Midena E. Central corneal thickness: z-ring corneal confocal microscopy versus ultrasound pachymetry. Cornea 2007;26:303-7.
107. McLaren JW, Nau CB, Patel SV, Bourne WM. Measuring corneal thickness with the ConfoScan 4 and z-ring adapter. Eye Contact Lens 2007;33:185-90.
108. Gokmen F, Jester JV, Petroll WM, et al. In vivo confocal microscopy through-focusing to measure corneal flap thickness after laser in situ keratomileusis. J Cataract Refract Surg 2002;28:962-70.
109. Marchini G, Mastropasqua L, Pedrotti E, et al. Deep lamellar keratoplasty by intracorneal dissection: a prospective clinical and confocal microscopic study. Ophthalmology 2006;113:1289-300.
110. Erie JC, McLaren JW, Patel SV. Confocal microscopy in ophthalmology. Am J Ophthalmol 2009; 148:639-46.
111. Moller-Pedersen T, Vogel M, Li HF, et al. Quantification of stromal thinning, epithelial thickness, and corneal haze after photorefractive keratectomy using in vivo confocal microscopy. Ophthalmology 1997;104:360-8.
112. McCulley JP, Petroll WM. Quantitative assessment of corneal wound healing following IntraLASIK using in vivo confocal microscopy. Trans Am Ophthalmol Soc 2008;106:84-90.
113. Kobayashi A, Mawatari Y, Yokogawa H, Sugiyama K. In vivo laser confocal microscopy after descemet stripping with automated endothelial keratoplasty. Am J Ophthalmol 2008;145:977-85.
114. Morishige N, Takahashi N, Chikamoto N, Nishida T. Quantitative evaluation of corneal epithelial oedema by confocal microscopy. Clin Experiment Ophthalmol 2009;37:249-53.
115. Morishige N, Chikama TI, Sassa Y, Nishida T. Abnormal light scattering detected by confocal biomicroscopy at the corneal epithelial basement membrane of subjects with type II diabetes. Diabetologia 2001;44:340-5.
116. Hillenaar T, Remeijer L. Endothelial involvement indicates disease activity in Herpes simplex virus keratitis. Acta Ophthalmologica 2010;88:0.
117. Dawson CR, Togni B. Herpes simplex eye infections: clinical manifestations, pathogenesis and management. Surv Ophthalmol 1976;21:121-35.

Part I

Basic research

2

How normal is the transparent cornea? Effects of aging on corneal morphology

Toine Hillenaar
Hugo van Cleynenbreugel
Lies Remeijer

Ophthalmology 2012;119:241-248

ABSTRACT

Purpose: To ascertain the effects of aging on corneal morphology and to illustrate the morphologic diversity of the different layers in the normal cornea as seen by in vivo confocal microscopy (IVCM).

Design: Observational cross-sectional study.

Participants: A total of 150 healthy subjects, evenly distributed over 5 age categories, comprising 75 men and 75 women.

Methods: Both transparent corneas (n = 300) of all subjects were examined in duplicate by white light IVCM (Confoscan 4, NIDEK Technologies, Albignasego, Padova, Italy). After reviewing the IVCM examinations for morphologic variations of the corneal layers, we selected the 8 most common features to illustrate the morphologic diversity. Subsequently, all 600 IVCM examinations were assessed for the presence of these features. We used binary logistic regression analyses to assess the age-relatedness of each feature.

Main outcome measures: Age distribution of bright superficial epithelial cells, dendriform cells, alterations characteristic of epithelial basement membrane dystrophy (EBMD), tortuous stromal nerves, stromal microdots in the anterior stroma, folds in the posterior stroma, opacification of Descemet's membrane, and corneal guttae.

Results: Four features were found characteristic of the aging cornea: stromal microdots in the anterior stroma ($P<0.0001$), folds in the posterior stroma ($P<0.0001$), opacification of Descemet's membrane ($P<0.0001$), and corneal guttae ($P<0.0001$). Alterations characteristic of EBMD were found in 3% of all eyes and only detected in subjects aged ≥40 years, suggesting age-relatedness ($P = 0.09$). Other features, such as bright superficial epithelial cells (n = 38, 13%), dendriform cells (n = 42, 14%), and tortuous stromal nerves (n = 115, 38%), were age-independent. We also found a novel phenotype of corneal endothelium in 4 normal eyes of 2 subjects, which we coined "salt and pepper endothelium." We could not establish whether this novel phenotype represented a morphologic variant of normal endothelium, an early stage of a known corneal endothelial disorder, or a completely new disease entity.

Conclusions: Knowledge of the common morphologic variations of the corneal layers and the effects of aging on corneal morphology as seen by IVCM increases our understanding of corneal degenerative disorders and is essential to detect corneal pathology. Our finding of a novel phenotype of corneal endothelium emphasizes the morphologic diversity of this optically transparent tissue.

INTRODUCTION

The ever advancing technique of in vivo confocal microscopy (IVCM) allows the cornea to be imaged with continually improving quality. By using a lateral resolution that bridges slit-lamp and ultrastructural examination, the different layers of the cornea can be observed, in vivo, on a cellular level. Many reports have addressed the morphologic aspects of the transparent cornea.[1–8] Also, the effects of aging on the density of different corneal cell populations, such as basal epithelial cells, subbasal nerve plexus, keratocytes, and endothelial cells, have been studied extensively.[9–12] However, the diversity of normal corneal layers and the effects of aging on corneal morphology remain largely undiscussed. Knowledge of the normal appearance of the corneal layers and their common morphologic variants is essential when IVCM is applied in ophthalmic practice to identify corneal pathology. The aim of this report is to ascertain the effects of aging on normal corneal morphology as observed by IVCM and to emphasize morphologic diversity of the corneal layers, illustrated by a novel phenotype of corneal endothelium.

MATERIALS AND METHODS

To assess the effects of aging on the morphology of the different corneal layers, both corneas (n = 300) of 150 healthy subjects were examined by IVCM. Our study population comprised 75 men and 75 women who were evenly distributed over 5 age categories: 20–29, 30–39, 40–49, 50–59, and 60–79 years. Before IVCM examination, the corneas were subjected to standard slit-lamp examination to ensure only subjects with transparent corneas without signs of ocular inflammation were enrolled. Other exclusion criteria were previous ocular trauma or surgery; previous inflammation, infection, or allergic reaction of the eye; or a history of contact lens wear. This study was part of a larger project that was conducted to generate a normative database for IVCM backscatter measurements. Further details concerning this project are described in a separate article.[13] The study protocol was approved by our institutional review board and the local medical ethical committee and adhered to the tenets of the Declaration of Helsinki. All subjects gave their informed consent after explanation of the study protocol.

All corneal layers were imaged using a white light scanning slit confocal microscope (Confoscan 4, NIDEK Technologies, Albignasego, Padova, Italy), according to a previously described method.[14] Briefly, both corneas in each subject were anesthetized using 1 drop of oxybuprocaine 0.4% (Ceban BV, Breda, The Netherlands). As an optical coupling medium, a viscous gel (Vidisic, Dr. Mann Pharma, Berlin, Germany) was applied to the microscope's 40X objective lens, after which a *z*-ring adapter was placed in front to stabilize the eye during image acquisition. The central cornea was then imaged with 500X

magnification, virtually sectioning the cornea into tangential slices with a scan step of 6 µm. The IVCM examinations were repeated until 2 high-quality scans were recorded for each cornea. During the study, light intensity was kept constant at 72% and regular reference scans were performed to ensure long-term stability of the light source.[15]

For the current study, we focused on the morphologic variations of the different corneal layers. The general appearance of these layers and the effects of aging on the density of different corneal cell populations were left unexplored, because these topics have been covered by several excellent review articles.[5,6,8] After exploration of our normative IVCM database, we selected the 8 most common features that represent the morphologic diversity of the cornea: bright superficial epithelial cells, dendriform cells, alterations characteristic of epithelial basement membrane dystrophy (EBMD), microdots in the anterior stroma, tortuous stromal nerves, folds in the posterior stroma, opacification of Descemet's membrane, and corneal guttae. Subsequently, all 600 IVCM scans were assessed for the presence of these 8 morphologic features. A feature was scored positive when at least 1 of the duplicate scans of a cornea contained 1 frame showing this feature. Dendriform cells and microdots in the anterior stroma were scored positive only when ≥5 of these structures were counted in a single frame. Because Descemet's membrane is usually indiscernible using IVCM, opacification of Descemet's membrane was scored positive when Descemet's membrane was clearly recognizable between the keratocyte nuclei of the posterior stroma and the endothelial cells. When other unusual changes in the morphology of the various corneal layers were observed, these were noted.

We used binary logistic regression analysis to assess the effects of aging on all 8 morphologic features. Odds ratios and 95% confidence intervals were determined. Two-sided *P* values less than 0.05 were considered statistically significant. Statistical analysis was conducted using SPSS for Windows (version 17.0, SPSS, Inc., Chicago, IL).

RESULTS

Morphologic assessment of all corneal layers was possible in all 600 IVCM examinations. Figure 1 shows the morphologic features that were scored to assess the effects of corneal aging. With aging of the cornea, we found a statistically significant increase of microdots in the anterior stroma, folds in the posterior stroma, opacification of Descemet's membrane, and corneal guttae (Table 1). Bright superficial epithelial cells (n = 38, 13%), dendriform cells (n = 42, 14%), and tortuous stromal nerves (n = 115, 38%) were evenly distributed over the age categories. Five subjects (3%) showed, all bilaterally, similar alterations as those that can be seen in EBMD. Although these subjects were aged ≥40 years, a statistically significant age-relatedness of the EBMD characteristic alterations was not found ($P = 0.09$).

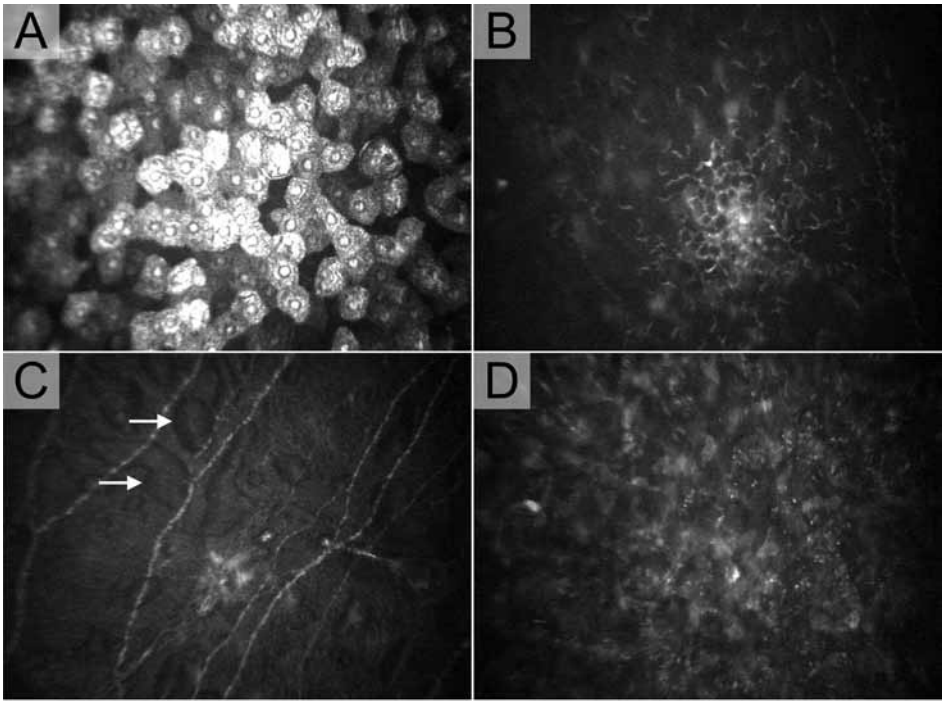

Figure 1. Morphologic diversity of the corneal layers. These images represent clear examples of the 8 features scored to assess the effects of aging on corneal morphology. In ophthalmic practice, these alterations are often more subtle. Images are 425x320 µm. **A,** On IVCM, punctate epithelial spots appeared as bright superficial epithelial cells with a hyperreflective nucleus surrounded by a dark halo. **B,** Small dendriform cells (<25 µm) crowded around a hyperreflective possible antigen at subbasal nerve plexus level. **C,** Five subjects showed bleb formations (*arrows*) or other alterations of the epithelial basement membrane, characteristic of EBMD. **D,** Microdots (1–2 µm) were detected in the stroma of nearly all corneas but were assessed for age-relatedness only in the anterior stroma.

In addition to the 8 common morphologic variations that were assessed for age-relatedness, we also discovered a novel phenotype of corneal endothelium in 2 male participants aged 57 and 70 years (Fig 2). We coined these alterations "salt and pepper endothelium." Some cells had a light cell body and dark cell borders, as do normal endothelial cells. Other cells, however, displayed a reversed pattern showing dark cell bodies and light cell borders. Except for pigmented granules precipitated on the endothelial layer of 1 of the 2 subjects, and subtle alterations of the endothelium in specular view, slit-lamp examination did not show any alterations of the other corneal layers. Best-corrected visual acuity was 20/16 or better in the eyes of both subjects. The intraocular pressures (<14 mmHg) and corneal thicknesses (<588 µm) of all 4 eyes were within normal range. Both subjects' eyes revealed open angles on gonioscopy without peripheral anterior synechiae. One year after the initial visit, the morphologic appearance of the endothelium and the endothelial cell density were unchanged in all 4 eyes on IVCM.

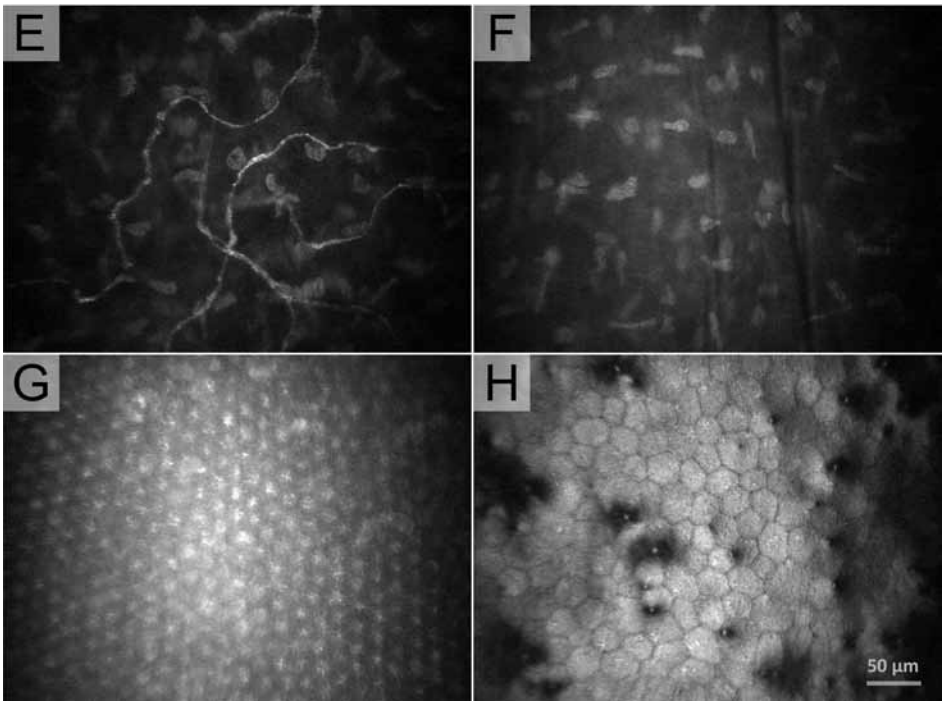

Figure 1. E, Tortuous stromal nerves were detected in the anterior and mid-stroma. **F,** Folds in the posterior stroma. **G,** In 4 eyes of 3 subjects, increased backscatter of Descemet's membrane enabled visualization of its hexagonal lattice structure. This regular pattern did not correspond with the underlying endothelial cells. **H,** Corneal guttae appeared as dark bulges in between the endothelial cells, with a hyperreflective dot in the center. EBMD = epithelial basement membrane dystrophy; IVCM = in vivo confocal microscopy.

DISCUSSION

The current study illustrates the morphologic diversity of the transparent cornea as observed by IVCM. This diversity is enhanced by 4 characteristic manifestations of corneal aging: stromal microdots, folds in the posterior stroma, opacification of Descemet's membrane, and corneal guttae. These common degenerative processes were studied in clinically normal corneas and may, in a minority of cases, progress into cornea farinata, posterior crocodile shagreen, or Fuchs' endothelial dystrophy. We discuss, from epithelium to endothelium, the 8 most common morphologic variants of the different corneal layers that were observed in our study, complemented by a novel phenotype of corneal endothelium.

In apparently normal corneas, fluorescent punctate staining can occur.[16] Only recently has punctate staining been linked to enhanced fluorescence of the cytoplasm of superficial epithelial cells.[17] With the use of IVCM, these fluorescent cells appear as bright

Table 1. Effects of aging on the normal corneal morphology as observed by *in vivo* confocal microscopy

Age category, years	20-29	30-39	40-49	50-59	60-69	70-79		
Eyes, n	60	60	60	60	42	18	P	OR (95% CI)
Bright superficial epithelial cells	9 (15)	6 (10)	6 (10)	4 (7)	10 (24)	3 (17)	0.46	1.01 (0.99-1.03)
Dendriform cells	7 (12)	12 (20)	5 (8)	9 (15)	7 (17)	2 (11)	0.78	1.00 (0.98-1.03)
Alterations characteristic of EBMD	0 (0)	0 (0)	4 (7)	2 (3)	4 (10)	0 (0)	0.09	1.04 (0.99-1.08)
Microdots anterior stroma	0 (0)	2 (3)	3 (5)	20 (33)	22 (52)	14 (80)	<0.0001	1.15 (1.11-1.19)
Tortuous stromal nerves	24 (40)	23 (38)	25 (42)	17 (28)	18 (43)	8 (44)	0.97	1.00 (0.98-1.02)
Folds posterior stroma	1 (2)	1 (2)	3 (5)	15 (25)	16 (38)	11 (61)	<0.0001	1.12 (1.08-1.15)
Opacification of DM	0 (0)	0 (0)	4 (7)	5 (8)	8 (19)	7 (39)	<0.0001	1.10 (1.05-1.14)
Corneal guttae	0 (0)	0 (0)	5 (8)	9 (15)	11 (26)	6 (33)	<0.0001	1.10 (1.06-1.14)

CI = confidence interval; DM = Descemet's membrane; EBMD = epithelial basement membrane dystrophy; OR = odds ratio. Values shown as n (%) unless otherwise indicated.

superficial epithelial cells in 36% of normal corneas, but have been found absent without fluorescein staining.[18] The age-independent presence of bright superficial epithelial cells in our study may be artificially induced. These bright cells have been suggested to indicate a loss of contact in the process of desquamation.[1] In our study desquamation may be enhanced, because all IVCM examinations were performed in duplicate and preceded by ultrasonic pachymetry. Furthermore, preservatives in the anesthetic eye drops and the coupling gel used for IVCM may have accelerated desquamation of the epithelial cells.[19] In our experience, IVCM is often preceded by other ophthalmic tests or performed after corneal fluorescein staining in a clinical setting. Therefore, appearance of bright superficial epithelial cells is a phenomenon often encountered in ophthalmic practice.

An important advantage of IVCM over slit-lamp examination is the possibility to visualize dendritic cells in the cornea. Dendritic cells serve as a major link between the innate and adaptive immune systems by capturing and processing antigens and presenting them to lymphocytes.[20] In the cornea, dendritic cells have been observed in close vicinity of the subbasal nerve plexus and postulated to represent Langerhans' cells or dendritic cells.[21–23] However, defining Langerhans' cells on the basis of IVCM appearance alone may erroneously include other cell phenotypes.[24] With the use of laser-scanning IVCM, dendriform cells have been reported in the central cornea in 20% to 30% of normal eyes, whereas their density has been demonstrated to increase toward the corneal periphery.[23,24] Zhivov et al[23] could not decide on the effects of aging on dendriform cell prevalence, because their results showed some disproportion between male and female

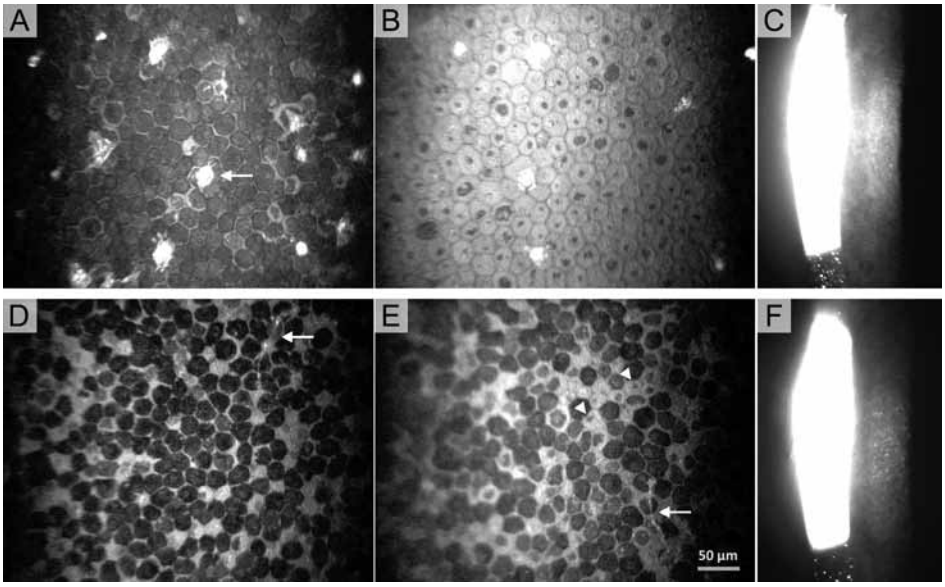

Figure 2. Salt and pepper endothelium. Two subjects with transparent corneas showed unique morphologic alterations of the corneal endothelial cells. The IVCM images are 425x320 µm. **A–C**, The first subject was a 70-year-old man. **A**, His right eye showed a dark-light reversal of the endothelial cells and precipitated granules (*arrow*) on a flat endothelial layer. Endothelial cell density (ECD): 2373 cells/mm^2. **B**, The left eye showed an early stage of the same endothelial alterations. The center of nearly all endothelial cells showed a variable-sized black discoloration. This eye also showed pigmented material on the endothelium. ECD: 2054 cells/mm^2. **C**, At slit-lamp examination, the endothelial specular reflection had a somewhat grayish aspect in the right eye, whereas the left eye displayed no evident alterations in specular view (not shown). **D–F**, The second subject was a 57-year-old man. **D**, Salt and pepper endothelium (black and white cell bodies) was seen in the right eye. A small dendritiform structure was precipitated on the endothelial layer (*arrow*). ECD: 2442 cells/mm^2. **E**, The left eye also showed salt and pepper endothelium. Some of the endothelial cells displayed early-stage alterations, as were seen in the left eye of the first subject (*arrowheads*). Again, a dendritiform precipitate (*arrow*) was observed. ECD: 2529 cells/mm^2. **F**, Endothelium in specular view with the slit-lamp showed a gravel tile aspect in both eyes. IVCM = in vivo confocal microscopy. (*See also Color figures, p. 206.*)

subjects. By using white light IVCM, we found dendriform cells were sometimes hard to distinguish from anastomoses of nerve fibers in the subbasal nerve plexus. Nevertheless, we demonstrated that dendriform cell prevalence was constant over age. Because changes in the density and morphology of dendriform cells may reflect the immune status of the cornea,[5,7] future research should focus on the appearance of dendriform cells during follow-up of chronic inflammatory processes, such as herpetic stromal keratitis. The appearance of dendriform cells on IVCM may prove an important parameter for therapy guidance in inflammatory processes of the cornea.

Epithelial basement membrane dystrophy is characterized by maps, dots, fingerprint lines, and blebs as observed by slit-lamp examination,[25–27] whereas the same alterations

appear as hyperreflective streaks, microcysts, microfolds, and circular hyporeflective areas on IVCM.[28–31] We found similar alterations in 3% of our study population, which completely agrees with histopathologic findings of EBMD in normal corneas.[32] Because we examined only a small area (0.14%) of the central cornea, our results cannot be compared with slit-lamp– based reports on the prevalence of EBMD, which range from 5% to 43%.[33,34] Although autosomal-dominant inheritance has been documented in a subset of patients,[35] EBMD is generally regarded as an age-related degeneration.[36] Our results correspond with the age distribution of EBMD, as has been reported in a clinical setting.[33,34] However, because of the low number of cases in our study, we could not statistically confirm the age-relatedness of EBMD.

Nerves in the mid-stroma have been reported as thick, straight nerves with a mainly dichotomous branching pattern.[21,37] In corneal pathologic processes[38–42] or after corneal surgery,[43–46] the stroma has been found to contain tortuous structures, which were suggested to represent aberrant regenerated stromal nerves. However, similar tortuous stromal nerves with a beaded appearance have been identified in the normal corneas of 43% of healthy subjects.[47] Our results confirmed the findings of Visser et al,[47] but we also found these tortuous nerves to be age independent. By using immunohistochemical staining, tortuous nerves have been shown to originate from the straight mid-stromal nerves to form the mid-stromal and subepithelial nerve plexus, which both display a patchy distribution in the central cornea and increase in density toward the periphery.[48] In contrast with the straight mid-stromal nerves, the tortuous nerve fibers supply less than 5% of the epithelial innervation. Therefore, the tortuous nerves are thought to represent a functionally distinct nerve population that may provide epithelial reinnervation after corneal injury or possess specific sensory or trophic functions.[47,48]

Small, highly reflective microdots (~1–2 μm in diameter) should be considered a normal feature of human corneal morphology.[4,49] However, not all reports endorse this statement.[50] Our findings confirm the results of Efron et al,[4] who observed microdots throughout the stroma in nearly all corneas. These small particles have been postulated to represent dysgenic or apoptotic cellular remnants, such as lipofuscin granules, which constitute a degenerative process also known as "cornea farinata."[4,51] This degenerative process may be enhanced by contact lens wear, as indicated by the higher density and size of the microdots,[52] increasing with the duration of the contact lens wear.[50] By assessing the anterior stroma for the presence of microdots, we demonstrated that these particles increased with aging of the cornea. This increase of microdots probably caused backscatter in the stroma to increase in subjects aged ≥50 years, as we found in a parallel study.[13] This increase in backscatter was most prominent in the anterior stroma.

Folds in the posterior stroma have been reported in 10%, 18%, and 29% of the population in the sixth, seventh, and eighth decades of life, respectively.[11] We statistically confirmed the age-relatedness of posterior stromal folds, but we found a considerably

higher prevalence in elderly subjects than did Hollingsworth et al.[11] This increased number of folds may be associated with the use of a *z*-ring, which may have slightly flattened the cornea in our study. Applanation of the cornea has been shown to induce the normally invisible anterior corneal mosaic, posterior stromal bands, and posterior surface ridges.[53–55] These reproducible flattening-induced effects are likely to become more apparent as the cornea stiffens with age,[56] which is thought to be due to increased collagen cross-linking and an increase in diameter of the collagen fibrils as a result of the continuous deposition of collagen molecules.[57,58] These 2 biochemical effects of the aging cornea may also underlie the irregular collagen arrangement that forms sawtooth-like configurations in posterior crocodile shagreen.[59] In this degenerative corneal disorder, increased backscatter of the extracellular stromal matrix due to the irregular collagen arrangement enhances visibility of the posterior stromal folds, which we consider part of a normally invisible posterior corneal mosaic. Posterior crocodile shagreen should be distinguished from the presence of stromal edema, which also increases the visibility and severity of the folds[60] of the posterior corneal mosaic.

In normal corneas, Descemet's membrane comprises an anterior banded layer and a posterior nonbanded layer.[61] During life, the anterior banded layer remains approximately 3-µm thick, whereas the posterior nonbanded layer increases 5-fold in thickness to approximately 10 µm at 80 years of age.[62] The increase in thickness with age may explain the increased visibility of Descemet's membrane in elderly subjects, as observed by IVCM.[11] We confirmed the increased visibility with age, but we also found Descemet's membrane to display a hexagonal lattice structure. Ultrastructural examination of normal human corneas has shown a similar hexagonal lattice structure of the anterior banded layer, which contained type VIII collagen fibers arranged into a meshwork of nodes and rods, with an internodal distance of 100 to 110 nm.[61,63,64] By using en face images instead of corneal cross-sections, we found a larger internodal distance of 20 µm. The nodes we observed by IVCM may correspond with vertically arranged type VIII collagen fibers spanning Descemet's membrane,[65] suggesting a highly ordered structure of Descemet's membrane in *x*-, *y*-, and *z*-directions.

Aging of Descemet's membrane also manifests as corneal guttae. Corneal guttae are focal excrescences of Descemet's membrane that represent abnormal collagen deposition by distressed endothelial cells.[66] Only in a minority of cases will corneal guttae progress to Fuchs' endothelial dystrophy, which involves formation of stromal edema and eventually bullous epithelial edema. This degenerative process is more commonly observed in women[67] and has a lower prevalence in Asians.[68] Also, a climactic influence has been suggested.[69] The prevalence of corneal guttae in non-Asians aged ≥50 years greatly differs among reports: 9% to 76%.[70,71] With the use of IVCM, corneal guttae have been shown in 6%, 12%, and 29% of the population in the sixth, seventh, and eighth decades of life, respectively.[11] We found a higher prevalence of corneal guttae for these

decades, confirming, in vivo, the results of Kaufman et al,[72] who reported corneal guttae in 20% of all donor corneas aged ≥50 years.

The novel phenotype of corneal endothelium, which was observed in both eyes of 2 healthy subjects, perfectly illustrates the morphologic diversity of the transparent cornea. To our knowledge, we are the first to describe a salt and pepper appearance of the corneal endothelium, which may represent a morphologic variant of normal endothelium, an early stage of a known corneal endothelial disorder, or a completely new disease entity. The differential diagnosis of salt and pepper endothelium comprises Fuchs' endothelial dystrophy,[73] posterior polymorphous dystrophy,[74] iridocorneal endothelial (ICE) syndrome,[75] and corneal endotheliitis (Fig 3), all of which seem improbable

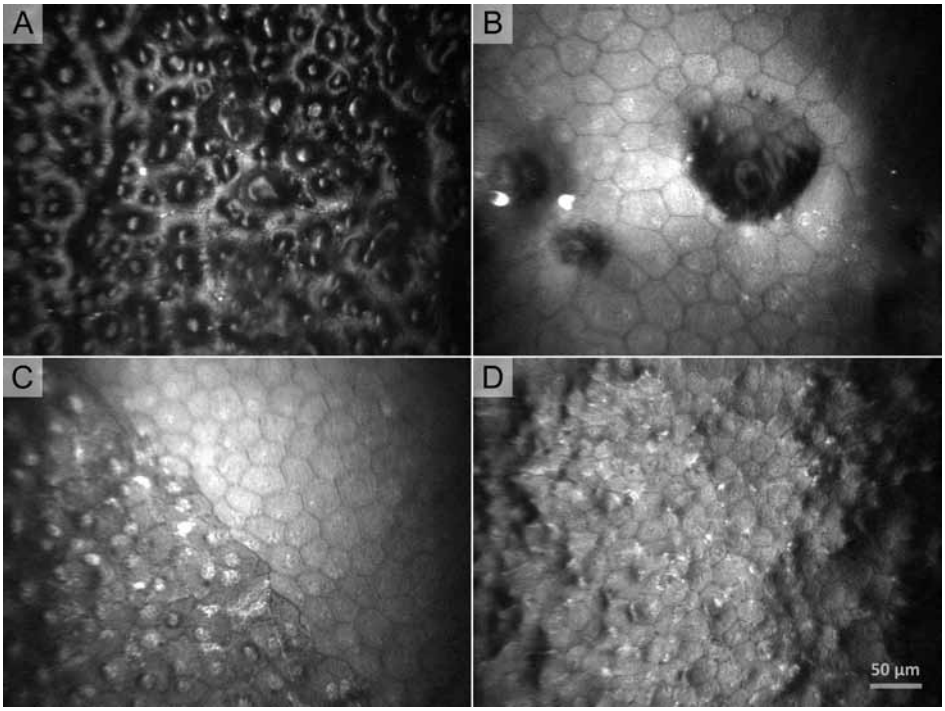

Figure 3. The IVCM appearance of 4 corneal endothelial disorders in the differential diagnosis of salt and pepper endothelium. Images are 425x320 µm. **A**, Fuchs' endothelial dystrophy is characterized by corneal guttae, observed as bright spots surrounded by a dark halo interspersed between enlarged endothelial cells.[73] The appearance may best be described as being like the surface of a strawberry.[6] **B**, Posterior polymorphous dystrophy is characterized by vesicles and band formations in the endothelial layer.[74] **C**, Like salt and pepper endothelium, the iridocorneal endothelial (ICE) syndrome is characterized by a dark-light reversal of the endothelial cells, the so-called ICE cells.[75] These ICE cells, however, display hyperreflective nuclei and form a cobblestone-shaped endothelial layer because of multilayering. Sometimes a boundary can be visualized between normal endothelial cells and ICE cells in this mainly unilateral disorder. **D**, Corneal endotheliitis in herpetic keratitis is characterized by pseudoguttae, which completely resolve within a few weeks after initiation of appropriate therapy.[14] IVCM = in vivo confocal microscopy.

because corneal guttae, vesicles or band formations, ICE cells, and pseudoguttae were not observed. Long-term follow-up of these 2 subjects is needed to ascertain the significance of these unique endothelial alterations.

In conclusion, our study emphasizes the inherent morphologic diversity of the transparent cornea as observed by IVCM. We demonstrated the 8 most common morphologic variants of the different layers complemented by salt and pepper endothelium, a novel phenotype of corneal endothelium. Of the 8 common morphologic variants, stromal microdots in the anterior stroma, folds in the posterior stroma, opacification of Descemet's membrane, and corneal guttae were enhanced with aging of the cornea. Knowledge of these common morphologic variants and the effects of aging on corneal morphology is essential to differentiate between normal aging effects and degenerative disorders or pathologic processes in the cornea.

REFERENCES

1. Bohnke M, Masters BR. Confocal microscopy of the cornea. Prog Retin Eye Res 1999;18:553– 628.
2. Jalbert I, Stapleton F, Papas E, et al. In vivo confocal microscopy of the human cornea. Br J Ophthalmol 2003; 87:225–36.
3. Mustonen RK, McDonald MB, Srivannaboon S, et al. Normal human corneal cell populations evaluated by in vivo scanning slit confocal microscopy. Cornea 1998;17:485–92.
4. Efron N, Perez-Gomez I, Mutalib HA, Hollingsworth J. Confocal microscopy of the normal human cornea. Cont Lens Anterior Eye 2001;24:16 –24.
5. Efron N. Contact lens-induced changes in the anterior eye as observed in vivo with the confocal microscope. Prog Retin Eye Res 2007;26:398–436.
6. Patel DV, McGhee CN. Contemporary in vivo confocal microscopy of the living human cornea using white light and laser scanning techniques: a major review. Clin Experiment Ophthalmol 2007;35:71– 88.
7. Guthoff RF, Zhivov A, Stachs O. In vivo confocal microscopy, an inner vision of the cornea - a major review. Clin Experiment Ophthalmol 2009;37:100 –17.
8. Niederer RL, McGhee CN. Clinical in vivo confocal microscopy of the human cornea in health and disease. Prog Retin Eye Res 2010;29:30 –58.
9. Bourne WM, Nelson LR, Hodge DO. Central corneal endothelial cell changes over a ten-year period. Invest Ophthalmol Vis Sci 1997;38:779–82.
10. Moller-Pedersen T. A comparative study of human corneal keratocyte and endothelial cell density during aging. Cornea 1997;16:333– 8.
11. Hollingsworth J, Perez-Gomez I, Mutalib HA, Efron N. A population study of the normal cornea using an in vivo, slit-scanning confocal microscope. Optom Vis Sci 2001;78: 706–11.
12. Niederer RL, Perumal D, Sherwin T, McGhee CN. Agerelated differences in the normal human cornea: a laser scanning in vivo confocal microscopy study. Br J Ophthalmol 2007;91:1165–9.
13. Hillenaar T, Cals RH, Eilers PH, et al. Normative database for corneal backscatter analysis by in vivo confocal microscopy. Invest Ophthalmol Vis Sci 2011;52:7274–81.
14. Hillenaar T, Weenen C, Wubbels RJ, Remeijer L. Endothelial involvement in herpes simplex virus keratitis: an in vivo confocal microscopy study. Ophthalmology 2009;116: 2077– 86.
15. Hillenaar T, Sicam VA, Vermeer KA, et al. Wide-range calibration of corneal backscatter analysis by in vivo confocal microscopy. Invest Ophthalmol Vis Sci 2011;52: 2136 – 46.
16. Korb DR, Korb JM. Corneal staining prior to contact lens wearing. J Am Optom Assoc 1970;41:228 –32.
17. Mokhtarzadeh M, Casey R, Glasgow BJ. Fluorescein punctate staining traced to superficial corneal epithelial cells by impression cytology and confocal microscopy. Invest Ophthalmol Vis Sci 2011; 52:2127–35.
18. Mocan MC, Irkec M. Fluorescein enhanced confocal microscopy in vivo for the evaluation of corneal epithelium. Clin Experiment Ophthalmol 2007;35:38–43.
19. Masters BR, Bohnke M. Confocal microscopy of the human cornea in vivo. Int Ophthalmol 2001; 23:199 –206.
20. Banchereau J, Steinman RM. Dendritic cells and the control of immunity. Nature 1998;392:245–52.
21. Auran JD, Koester CJ, Kleiman NJ, et al. Scanning slit confocal microscopic observation of cell morphology and movement within the normal human anterior cornea. Ophthalmology 1995; 102:33– 41.

22. Rosenberg ME, Tervo TM, Muller LJ, et al. In vivo confocal microscopy after herpes keratitis. Cornea 2002;21:265–9.
23. Zhivov A, Stave J, Vollmar B, Guthoff R. In vivo confocal microscopic evaluation of Langerhans cell density and distribution in the normal human corneal epithelium. Graefes Arch Clin Exp Ophthalmol 2005;243:1056–61.
24. Mastropasqua L, Nubile M, Lanzini M, et al. Epithelial dendritic cell distribution in normal and inflamed human cornea: in vivo confocal microscopy study. Am J Ophthalmol 2006;142:736–44.
25. Cogan DG, Donaldson DD, Kuwabara T, Marshall D. Microcystic dystrophy of the corneal epithelium. Trans Am Ophthalmol Soc 1964;62:213–25.
26. Guerry D III. Observations on Cogan's microcystic dystrophy of the corneal epithelium. Trans Am Ophthalmol Soc 1965; 63:320 –34.
27. Bron AJ, Brown NA. Some superficial corneal disorders. Trans Ophthalmol Soc U K 1971;91:XII, 13–29.
28. Hernandez-Quintela E, Mayer F, Dighiero P, et al. Confocal microscopy of cystic disorders of the corneal epithelium. Ophthalmology 1998;105:631– 6.
29. Rosenberg ME, Tervo TM, Petroll WM, Vesaluoma MH. In vivo confocal microscopy of patients with corneal recurrent erosion syndrome or epithelial basement membrane dystrophy. Ophthalmology 2000;107:565–73.
30. Labbe A, Nicola RD, Dupas B, et al. Epithelial basement membrane dystrophy: evaluation with the HRT II Rostock Cornea Module. Ophthalmology 2006;113:1301– 8.
31. Bozkurt B, Irkec M. In vivo laser confocal microscopic findings in patients with epithelial basement membrane dystrophy. Eur J Ophthalmol 2009;19:348 –54.
32. Ehlers N, Heegaard S, Hjortdal J, et al. Morphological evaluation of normal human corneal epithelium. Acta Ophthalmol 2010;88:858–61.
33. Laibson PR. Microcystic corneal dystrophy. Trans Am Ophthalmol Soc 1976;74:488 –531.
34. Werblin TP, Hirst LW, Stark WJ, Maumenee IH. Prevalence of map-dot-fingerprint changes in the cornea. Br J Ophthalmol 1981;65:401–9.
35. Boutboul S, Black GC, Moore JE, et al. A subset of patients with epithelial basement membrane corneal dystrophy have mutations in *TGFBI*/*BIGH3*. Hum Mutat 2006;27:553–7.
36. Weiss JS, Moller HU, Lisch W, et al. The IC3D classification of the corneal dystrophies. Cornea 2008; 27(Suppl):S1– 83.
37. Oliveira-Soto L, Efron N. Morphology of corneal nerves using confocal microscopy. Cornea 2001; 20:374–84.
38. Rosenberg ME, Tervo TM, Gallar J, et al. Corneal morphology and sensitivity in lattice dystrophy type II (familial amyloidosis, Finnish type). Invest Ophthalmol Vis Sci 2001;42: 634–41.
39. Ciancaglini M, Carpineto P, Zuppardi E, et al. In vivo confocal microscopy of patients with amiodarone-induced keratopathy. Cornea 2001;20:368 –73.
40. Ciancaglini M, Carpineto P, Doronzo E, et al. Morphological evaluation of Schnyder's central crystalline dystrophy by confocal microscopy before and after phototherapeutic keratectomy. J Cataract Refract Surg 2001;27:1892–5.
41. Mocan MC, Durukan I, Irkec M, Orhan M. Morphologic alterations of both the stromal and subbasal nerves in the corneas of patients with diabetes. Cornea 2006;25:769 –73.
42. Zhao C, Lu S, Tajouri N, et al. In vivo confocal laser scanning microscopy of corneal nerves in leprosy [letter]. Arch Ophthalmol 2008;126:282– 4.
43. Richter A, Slowik C, Somodi S, et al. Corneal reinnervation following penetrating keratoplasty—correlation of esthesiometry and confocal microscopy. Ger J Ophthalmol 1996;5: 513–7.

44. Patel SV, Erie JC. Aberrant regeneration of corneal nerves after laser in situ keratomileusis. J Cataract Refract Surg 2003;29:387–9.
45. Erie JC, Patel SV, Bourne WM. Aberrant corneal nerve regeneration after PRK. Cornea 2003;22: 684–6.
46. Hollingsworth JG, Efron N, Tullo AB. A longitudinal case series investigating cellular changes to the transplanted cornea using confocal microscopy. Cont Lens Anterior Eye 2006;29:135– 41.
47. Visser N, McGhee CN, Patel DV. Laser-scanning in vivo confocal microscopy reveals two morphologically distinct populations of stromal nerves in normal human corneas. Br J Ophthalmol 2009; 93:506 –9.
48. Marfurt CF, Cox J, Deek S, Dvorscak L. Anatomy of the human corneal innervation. Exp Eye Res 2010;90:478 –92.
49. Efron N. Microdot stromal degenerations [letter]. Eye Contact Lens 2005;31:46.
50. Trittibach P, Cadez R, Eschmann R, et al. Determination of microdot stromal degenerations within corneas of long-term contact lens wearers by confocal microscopy. Eye Contact Lens 2004;30: 127–31.
51. Faragher RG, Mulholland B, Tuft SJ, et al. Aging and the cornea. Br J Ophthalmol 1997;81:814 –7.
52. Bohnke M, Masters BR. Long-term contact lens wear induces a corneal degeneration with microdot deposits in the corneal stroma. Ophthalmology 1997;104:1887–96.
53. Bron AJ. Anterior corneal mosaic. Br J Ophthalmol 1968;52: 659–69.
54. Sherrard ES, Buckley RJ. Relocation of specific endothelial features with the clinical specular microscope. Br J Ophthalmol 1981;65:820–7.
55. Auran JD, Koester CJ, Rapaport R, Florakis GJ. Wide field scanning slit in vivo confocal microscopy of flatteninginduced corneal bands and ridges. Scanning 1994;16:182– 6.
56. Elsheikh A, Wang D, Brown M, et al. Assessment of corneal biomechanical properties and their variation with age. Curr Eye Res 2007;32:11–9.
57. Malik NS, Moss SJ, Ahmed N, et al. Ageing of the human corneal stroma: structural and biochemical changes. Biochim Biophys Acta 1992;1138:222– 8.
58. Daxer A, Misof K, Grabner B, et al. Collagen fibrils in the human corneal stroma: structure and aging. Invest Ophthalmol Vis Sci 1998;39:644–8.
59. Krachmer JH, Dubord PJ, Rodrigues MM, Mannis MJ. Corneal posterior crocodile shagreen and polymorphic amyloid degeneration. Arch Ophthalmol 1983;101:54 –9.
60. Efron N, Mutalib HA, Perez-Gomez I, Koh HH. Confocal microscopic observations of the human cornea following overnight contact lens wear. Clin Exp Optom 2002;85:149 –55.
61. Jakus MA. Studies on the cornea. II. The fine structure of Descemet's membrane. J Biophys Biochem Cytol 1956; 2(Suppl):243–52.
62. Johnson DH, Bourne WM, Campbell RJ. The ultrastructure of Descemet's membrane. I. Changes with age in normal corneas. Arch Ophthalmol 1982;100:1942–7.
63. Sawada H, Konomi H, Hirosawa K. Characterization of the collagen in the hexagonal lattice of Descemet's membrane: its relation to type VIII collagen. J Cell Biol 1990;110:219 –27.
64. Levy SG, Moss J, Sawada H, et al. The composition of wide-spaced collagen in normal and diseased Descemet's membrane. Curr Eye Res 1996;15:45–52.
65. Zhang C, Bell WR, Sundin OH, et al. Immunohistochemistry and electron microscopy of early-onset Fuchs corneal dystrophy in three cases with the same L450W *COL8A2* mutation. Trans Am Ophthalmol Soc 2006;104:85–97.
66. Hogan MJ, Wood I, Fine M. Fuchs' endothelial dystrophy of the cornea. 29th Sanford Gifford Memorial Lecture. Am J Ophthalmol 1974;78:363– 83.

67. Krachmer JH, Purcell JJ Jr, Young CW, Bucher KD. Corneal endothelial dystrophy: a study of 64 families. Arch Ophthalmol 1978;96:2036 –9.
68. Nagaki Y, Hayasaka S, Kitagawa K, Yamamoto S. Primary cornea guttata in Japanese patients with cataract: specular microscopic observations. Jpn J Ophthalmol 1996;40:520 –5.
69. Kitagawa K, Kojima M, Sasaki H, et al. Prevalence of primary cornea guttata and morphology of corneal endothelium in aging Japanese and Singaporean subjects. Ophthalmic Res 2002;34: 135– 8.
70. Zoega GM, Fujisawa A, Sasaki H, et al. Prevalence and risk factors for cornea guttata in the Reykjavik Eye Study. Ophthalmology 2006;113:565–9.
71. Lorenzetti DW, Uotila MH, Parikh N, Kaufman HE. Central cornea guttata: incidence in the general population. Am J Ophthalmol 1967;64:1155– 8.
72. Kaufman HE, Capella JA, Robbins JE. The human corneal endothelium. Am J Ophthalmol 1966;61: 835– 41.
73. Chiou AG, Kaufman SC, Beuerman RW, et al. Confocal microscopy in cornea guttata and Fuchs' endothelial dystrophy. Br J Ophthalmol 1999;83:185–9.
74. Patel DV, Grupcheva CN, McGhee CN. In vivo confocal microscopy of posterior polymorphous dystrophy. Cornea 2005;24:550–4.
75. Grupcheva CN, McGhee CN, Dean S, Craig JP. In vivo confocal microscopic characteristics of iridocorneal endothelial syndrome. Clin Experiment Ophthalmol 2004;32:275– 83.

3

Wide-range calibration of corneal backscatter analysis by in vivo confocal microscopy

Toine Hillenaar
Victor Arni D. P. Sicam
Koenraad A. Vermeer
Boy Braaf
Lies Remeijer
Roger H. H. Cals
Johannes F. de Boer

Invest Ophthalmol Vis Sci. 2011;52:2136-2146

ABSTRACT

Purpose: To report intra- and interinstrument calibration methods for corneal backscatter analysis by in vivo confocal microscopy.

Methods: Applicability of two reference standards was evaluated for corneal backscatter calibration. Repeated measurements of four concentrations of AMCO Clear (GFS Chemicals, Inc., Powell, OH) suspension and three transparencies (26%, 49%, and 65%) of polymethylmethacrylate (PMMA) slabs were performed to assess image intensity acquisition in a wide backscatter range. Intra- and intersession repeatability and lot-to-lot variation were determined for both standards. The effect of light intensity (LI) variation on image intensity acquisition was evaluated by examination of PMMA slabs with nonreference (60% and 80%) and reference (72%) LIs. Both reference standards were implemented in the protocol. Intrainstrument calibration was verified by measuring three normal corneas with 60%, 72%, and 80% LIs. Interinstrument calibration was tested by measuring PMMA slabs on a second, similar confocal microscope.

Results: AMCO Clear was used to express image intensity in absolute scatter units (SU), whereas the 49% transparent PMMA slab showed best repeatability, without image saturation, to adjust for LI variation. Intrainstrument calibration for LI variation reduced mean differences from –38.3% to 1.7% (60% LI) and from 33.9% to –0.6% (80% LI). The mean difference between similar microscopes decreased from 18.4% to 1.2%, after calibration of the second microscope.

Conclusions: Large interinstrument differences necessitate calibration of corneal backscatter measurements. With AMCO Clear suspension and PMMA slabs, standardization was achieved in a wide backscatter range corresponding to normal and opaque corneas. These methods can easily be applied in ophthalmic practice.

INTRODUCTION

In vivo confocal microscopy (IVCM) is an optical technique in which minute structures on the order of micrometers can be visualized. In ophthalmic practice, IVCM can be used for measurement of endothelial cell density, analysis of corneal and intracorneal thicknesses, and assessment of cellular morphology and histopathologic changes in corneal sublayers.[1] Another important feature of IVCM is objective quantification of corneal backscatter. Currently, this feature is not widely used. Corneal backscatter determined by IVCM is based on image intensity measurements, composed of backscatter and reflectance,[2,3] at different corneal depths. Corneal backscatter analysis by IVCM has been used primarily to define objective haze grading in refractive and lamellar corneal surgery.[1,4–6] These reports however, lack a universal calibration method. Therefore, comparison between machines or over time is unreliable. Only recently, a calibration method has been described that expresses corneal backscatter measured by IVCM in absolute scatter units (SU).[7] This method has proven sufficient for measuring backscatter of normal corneas. Opaque corneas require a larger backscatter range and may need a different approach. For this study, two general methods for intra- and interinstrument calibration of corneal backscatter analysis by IVCM were developed. The performances of both methods were verified for a wide backscatter range corresponding to both normal and opaque corneas.

METHODS

Device Settings

Backscatter was measured with a confocal microscope (Confoscan 4; Nidek Technologies, Padova, Italy). At full-thickness setting, this device captures 350 images of 425 x 320 µm within 12 seconds at a focal plane along the *z*-axis. Scan depth can be adjusted manually in a range of 100 to 1500 µm and scan step in a range of 1.5 to 100 µm. The Confoscan 4 has a 100-W halogen light source (Xenophot HLX 64625; Osram Sylvania, Munich, Germany). A 360° rotary knob allowed analog adjustment of the light intensity (LI) between 0% and 100%. As in a previous study,[8] a reference LI of 72% was used, because at this setting the corneal endothelium was visualized optimally, without image saturation. The backscattered and reflected light at the focal plane was captured by a charge-coupled device (CCD) camera. As an immersion substance, one drop of viscous gel (Vidisic Carbomer, 2.0 mg/g; Dr. Mann Pharma, Berlin, Germany) was applied to the 40X objective lens before each examination.

Setup and Reference Standards

We devised a setup (Fig. 1) to standardize corneal backscatter analysis. A customized holder was used to fix a reference standard at any appropriate angle. To position the reference standard perpendicular to the objective, we centered the specular reflection at the immersion gel to the reference standard interface in the confocal image. Two potential reference standards were compared: AMCO Clear (GFS Chemicals Inc., Powell, OH) and polymethylmethacrylate (PMMA, Perspex GS; Lucite International Ltd., Southampton, UK).

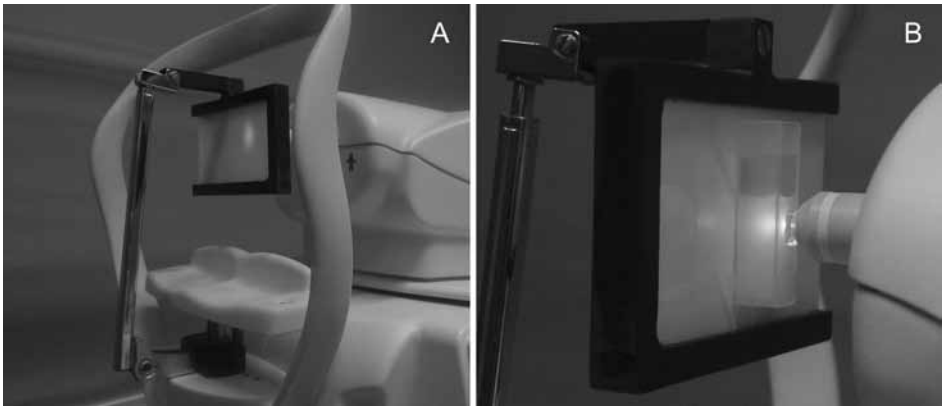

FIGURE 1. Calibration setup. (**A**) A customized holder was fixed to the chin rest of the confocal microscope (Confoscan 4; Nidek Technologies, Padova, Italy), so that PMMA slabs could be measured perpendicularly. (**B**) A rectangular sample cell was attached to a PMMA slab so that a standard turbidity suspension could be measured.

AMCO Clear is a stable suspension of styrene-di-vinylbenzene copolymer beads that is commercially available as a calibration standard for measuring turbidity. This suspension was examined through a transparent rectangular 10-mm sample cell (LPZ045; Hach Lange, Tiel, The Netherlands). First, the intensity profile of the sample cell with distilled water was measured, to correct for specular reflection at the glass–liquid interface. Next, this setup was measured with AC-4000 (AMCO Clear in a maximum concentration that accounts for 4000 nephelometric turbidity units [NTU]) and, after gradual dilution, with AC-2000, AC-1000, and AC-500.

The PMMA examinations were performed with three 3-mm-thick slabs with different light transmittances: 26%, 49%, and 65% (opal/white 028, 040, and 030). According to the manufacturer, the light transmittances of the slabs vary by ±3%.

To determine intra- and intersession repeatability and lot-to-lot variation, we examined three samples from different lots of AC-4000 and PMMA at all three transparencies in triplicate on three different dates.

Fixed device settings were used for all examinations on reference standards: semi-automatic mode; 72% LI; scan depth, 1500 µm; scan step, 10 µm; and autoalignment function, off. The examination was started after the focal plane had been positioned at a depth of approximately 1400 µm in the reference standard.

Influence of LI Variation

The PMMA slabs with 26%, 49%, and 65% transparency covered the whole range (gray-scale) of image intensities, but AMCO Clear did not. Therefore, the slabs were used to assess the effect of LI variation on the image intensity acquisition. In addition to the 72% LI measurements, the three slabs were measured with 60% and 80% LIs. On the basis of the results, two functions were calculated for adjusting the image intensities measured with 60% and 80% LIs to reference values.

Subsequently, three eyes randomly selected from three healthy volunteers were examined to verify the performance of these functions. The clear corneas were measured with 60%, 72%, and 80% LIs. To adjust image intensities acquired with 60% and 80% LIs, the corresponding functions (determined by the PMMA slabs) were applied to the image intensity data (measured in vivo on the three normal corneas). After determining mean corneal backscatter for each scan (Appendix A), backscatter values with and without adjustment for LI variation were compared with backscatter values acquired with reference LI.

All examinations on subjects were performed according to a previously described method.[8] The present study was approved by the local Institutional Review Board and adhered to the tenets of the Declaration of Helsinki. Informed consent was obtained from each subject.

Interinstrument Calibration

To assess the interinstrument difference in image intensity acquisition, we re-examined the PMMA slabs with 72% LI on a second, similar confocal microscope (Confoscan 4; Nidek) and the resulting image intensities were compared with the reference values measured with the first microscope. The mean absolute and relative differences between the two microscopes were determined by using the function that adjusts for LI variation.

By measuring AMCO Clear on microscope 2 with gradually increasing LIs, we found the LI for microscope 2 that corresponded to the reference LI (72%) of microscope 1. Using this corresponding LI, we re-examined all three PMMA slabs on microscope 2. The results were compared with the 72% LI measurements on microscope 1.

Data Processing

The *z*-scan curve is an image intensity–depth profile generated by plotting average pixel intensities of consecutive high-resolution images as a function of depth in the *z*-axis.[9] Exporting raw data from the *z*-scan curve yielded four main parameters per image: Z MotPos, W MotPos, intensity, and pressure. Only W MotPos and intensity were used to calibrate corneal backscatter measurements. W MotPos is measured by Hall sensors and expresses the distance in micrometers from the measurement starting point to the focal plane where the image was taken. Intensity, in this article expressed as image intensity, accounts for the mean gray level from 0 to 255 of an image pixel sample, sampling 1190 pixels from the image center. These pixels were obtained by sampling, respectively, 34 with 16-pixel spacing, and 35 with 15-pixel spacing in the *X* and *Y* directions. For analysis of the AMCO Clear measurements, different *z*-scan curves were aligned in depth with respect to the specular reflection at the sample cell–AMCO Clear interface. The center of this reflectance peak was set at a depth of 0 µm. Appendix B illustrates the alignment process. The *z*-scan curves of the PMMA slabs were aligned on the basis of the immersion gel–PMMA interface and the normal corneas were aligned on the basis of the specular reflection of the endothelium.

With a scan depth of 1500 µm and a scan step of 10 µm, one *z*-scan curve always contained two complete passes through the reference specimen. Every reference specimen was examined in triplicate, so each one had six complete passes. After alignment, the raw image intensity data of these six passes were plotted against depth, whereupon a smoothing interpolation was applied. A smoothing spline was fitted by visually estimating the smoothing parameter (0.0001), by using a curve-fitting toolbox (MatLab R2009b; The MathWorks. Inc., Natick, MA).

As the 49% transparent PMMA slab covered a large part of the image intensity range without image saturation, the smoothing spline corresponding to this slab was used to predict image intensities for every micrometer in a 1000-µm depth range (200–1200 µm). This method yielded 1000 image intensity pairs when two LIs or two microscopes were compared. These image intensity pairs were then plotted, and linear regression analysis was performed. The goodness of fit of the linear model was expressed as the coefficient of determination (R^2). This linear model was regarded as the function for adjusting image intensities measured with a different LI or another microscope to values measured with our reference LI.

Statistical Analysis

Intra- and intersession repeatability and lot-to-lot variation were expressed as the mean coefficient of variation (COV) and as the mean coefficient of repeatability (COR). The COV was defined as the standard deviation divided by the mean image intensity. Because

the set of depth values was not consistent between different passes in a *z*-scan curve, image intensity predictions per scan (obtained by smoothing interpolation) were used to calculate a COV for every micrometer in a 200- to 1200-µm depth range. The COR was derived by multiplying the SD by a *t*-value of 1.96.

The three normal corneas were examined to verify intrainstrument calibration for LI variation. Before and after correction for LI variation, differences in mean corneal backscatter were compared with the SD of the mean corneal backscatter for repeated measurements in a normal population. In a pilot study in which the eyes of 19 healthy volunteers were measured eight times a day, the SD of the mean corneal backscatter for repeated measurements was 40 SU (data not shown).

RESULTS

Specular reflection at the sample cell–distilled water interface affected image intensity up to a depth of 173 µm. Hence, all image intensity data acquired up to a 200-µm depth in the AMCO Clear and PMMA measurements were excluded. AMCO Clear showed less inhomogeneities at the focal plane than did PMMA (Fig. 2). Image intensity in AMCO Clear appeared inversely proportional with depth (Fig. 3A). On closer consideration, however, image intensity profiles of all concentrations behaved as negative exponential functions. Higher concentrations of AMCO Clear showed more image intensity decrease per unit depth than did lower concentrations. Accordingly, the relation between image intensity and turbidity depended on the imaging depth (Fig. 3B). Only at a 200-µm depth did image intensity show a linear relationship with turbidity ($R^2 = 0.99995$). This relationship was nonlinear at deeper levels in the suspension.

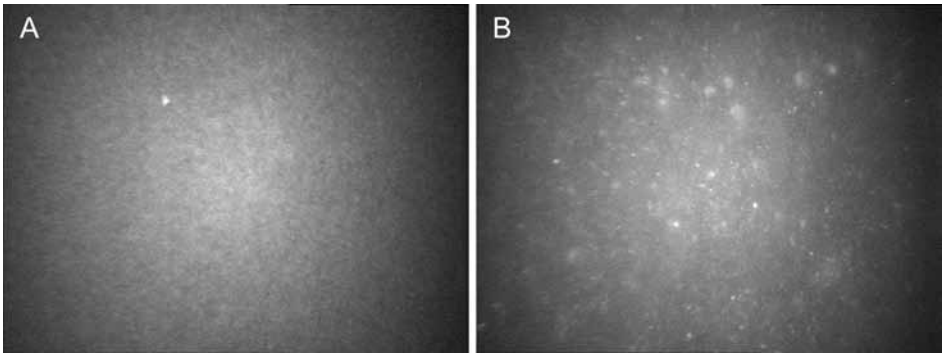

FIGURE 2. Confocal microscopy images of two different reference standards. (**A**) AMCO Clear in a concentration of 4000 NTU (GFS Chemicals, Inc., Howell, OH). (**B**) PMMA slab with 49% transparency. AMCO Clear showed less inhomogeneity than did PMMA.

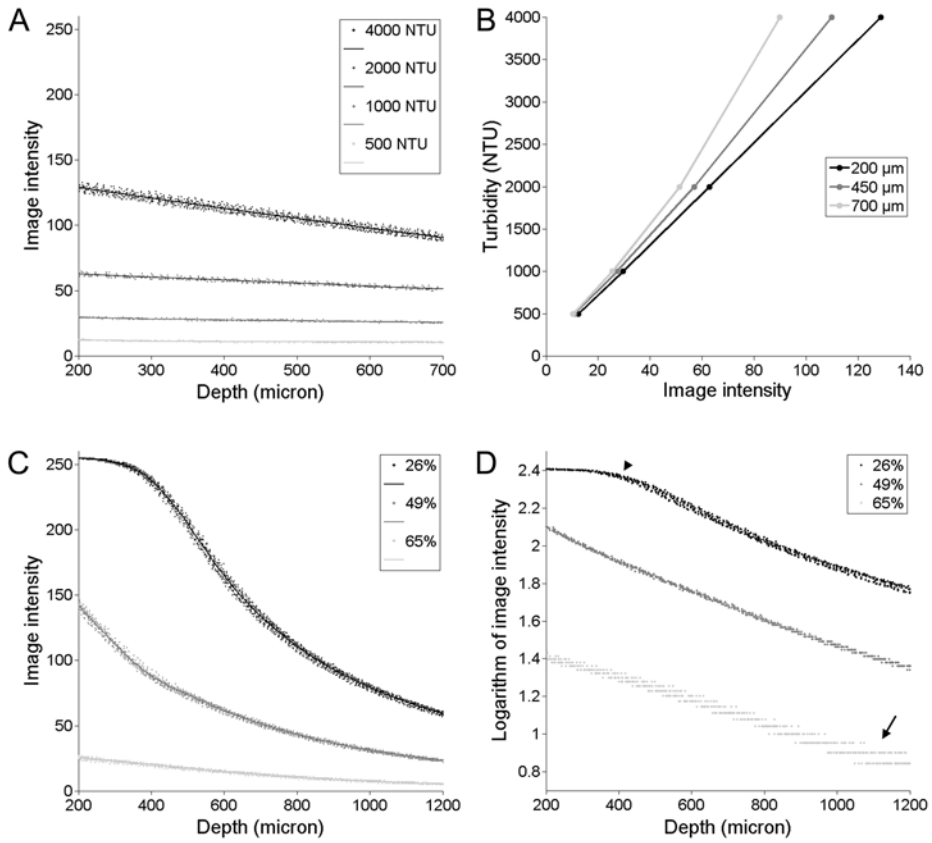

FIGURE 3. Characteristics of two different reference standards. (**A**) AMCO Clear (GFS Chemicals, Inc., Howell, OH) in four concentrations. The AMCO Clear concentrations covered only the lower half of the image intensity spectrum. (**B**) Effect of imaging depth on the relationship between image intensity and turbidity. Only at 200-µm depth was a linear relationship found. When the focal plane was chosen deeper in the suspension, the relation between image intensity and turbidity was nonlinear. (**C**) Image intensity profiles of PMMA slabs in three different transparencies. The PMMA slabs covered the whole range of image intensities. (**D**) Logarithm of the raw image intensity data of the three PMMA slabs showed artificial bending at the higher end of the gray level spectrum, due to image saturation (*arrowhead*). The lower end of this image intensity spectrum displayed enlarged distribution of the data due to quantization error (*arrow*). (▪) Individual measurements; (—) smooth interpolation (smoothing spline).

Whereas AMCO Clear in different concentrations covered only part of the range of image intensities, the whole 8-bit range was covered by the three PMMA slabs (Fig. 3C). Similar to AMCO Clear, the image intensity profiles of the PMMA slabs consisted of negative exponential functions, except for the slab with 26% transparency. At the higher end of the image intensity range, the image intensity profile of this slab showed artificial bending toward maximum gray level (255). This phenomenon was attributed to image saturation and was clearly noticeable when image intensity was displayed in logarithmic scale (Fig. 3D).

Table 1. Intrasession, intersession, and lot-to-lot variation in a depth range of 200 to 700 µm

	Intrasession		Intersession		Lot-to-lot	
	COV	COR	COV	COR	COV	COR
AMCO Clear (4000 NTU)	0.014	2.9	0.016	3.4	0.062	13.8
PMMA (26% transparency)	0.012	4.5	0.004	1.5	0.057	20.7
PMMA (49% transparency)	0.020	3.3	0.006	1.1	0.065	10.3
PMMA (65% transparency)	0.030	1.1	0.029	1.1	0.033	1.2

When repeatability was compared between the two reference standards, only minor differences were observed (Table 1). PMMA with 26% transparency showed highest intrasession and intersession repeatability. Lot-to-lot variation was comparable between reference standards, with the 65% transparent PMMA slab showing the least variation. Repeated measurements on the PMMA slabs with different transparencies showed a negative correlation between repeatability and the degree of transparency.

Varying the LI of the confocal microscope (Fig. 4) resulted in a corresponding linear change in measured image intensity. However, image intensity was affected by saturation from gray levels of 200 and higher. Only below this saturation point did the function to adjust image intensities to reference values show a linear relation. Most of the image intensity range below the saturation point was covered by the 49% transparent PMMA slab. Therefore, this slab was used to calculate the two functions that adjust image intensities measured with 60% and 80% LIs to reference values. Linear regression showed excellent coefficients of determination for the 60% LI ($R^2 = 0.99995$) and the 80% LI ($R^2 = 0.99989$) functions (Fig. 4E).

In accordance with the slab measurements, backscatter in the normal corneas increased with a higher LI setting (Table 2, Fig. 5). After correction for LI variation, mean differences reduced from –38.3% to 1.7% (60% LI) and from 33.9% to –0.6% (80% LI).

Table 2. Mean corneal backscatter of three normal eyes measured with different light intensities

		Nonadjusted			Adjusted		
Light intensity	72%	60%	difference	(%)	60%	difference	(%)
Eye 1	1226	799	-428	(-34.9)	1296	70	(5.7)
Eye 2	1155	695	-460	(-39.9)	1177	21	(1.8)
Eye 3	1197	715	-482	(-40.3)	1167	-30	(-2.5)
		Nonadjusted			**Adjusted**		
Light intensity	72%	80%	difference	(%)	80%	difference	(%)
Eye 1	1226	1621	394	(32.1)	1203	-23	(-1.9)
Eye 2	1155	1569	414	(35.8)	1164	8	(0.7)
Eye 3	1197	1601	403	(33.7)	1188	-9	(-0.8)

(Non-) adjusted: Without or with correction for measurement with nonreference light intensity. Data are expressed in scatter units.

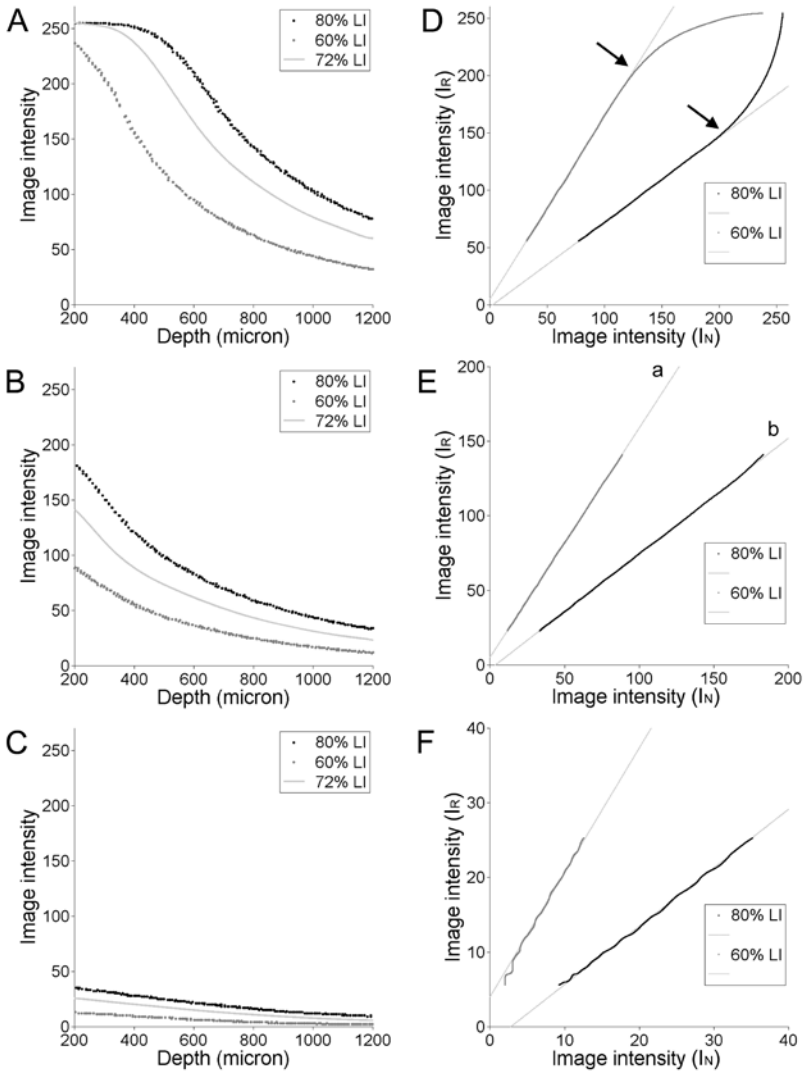

FIGURE 4. Intrainstrument LI variation. (**A–C**) PMMA slabs with different transparencies measured with different LIs. Markers represent individual data points measured with 80% and 60% LIs. The reference image intensity profile measured with 72% LI is based on Figure 3C. (**A**) PMMA slab with 26% transparency. (**B**) PMMA slab with 49% transparency. (**C**) PMMA slab with 65% transparency. (**D–F**) Scatterplots of 60% and 80% versus 72% LI data. (**D**) PMMA slab with 26% transparency. Robust linear fits (*gray lines*) showed image saturation (*arrows*) occurred from an image intensity of approximately 200 gray levels. (**E**) PMMA slab with 49% transparency. *Gray lines*: standard linear fittings that represent the functions used to adjust image intensities measured with 60% ($I_{60\%}$) or 80% ($I_{80\%}$) to reference LI (I_R) values. (a) $I_R = 1.537 \times I_{60\%} + 5.070$; $R^2 = 0.99995$. (b) $I_R = 0.7738 \times I_{80\%} - 2.890$; $R^2 = 0.99989$. (**F**) PMMA slab with 65% transparency. Below an image intensity of approximately 10 gray levels, readings became increasingly unreliable as was shown by robust linear fits (*gray lines*); I_R, image intensity acquired with reference LI; I_N, image intensity acquired with nonreference LI.

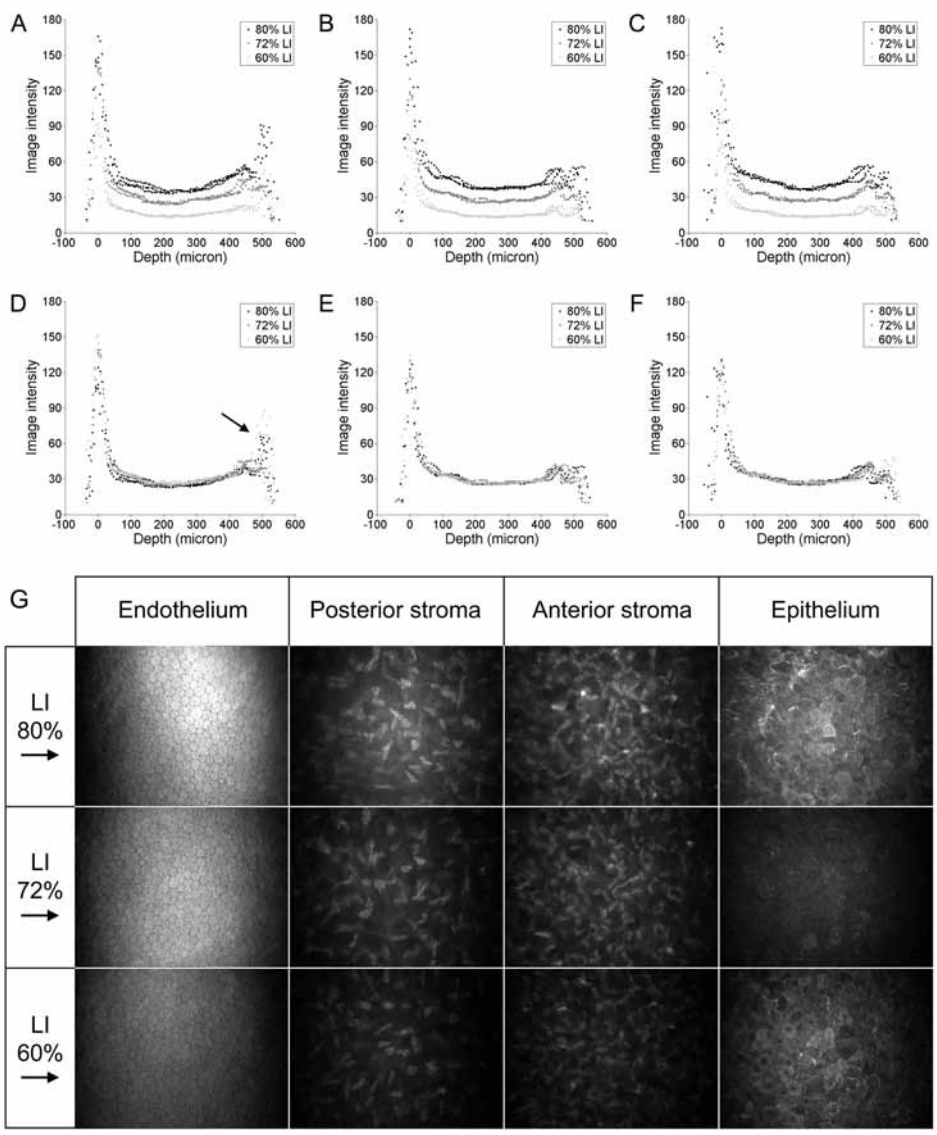

FIGURE 5. Adjustment of image intensity acquired with nonreference LI to reference values. (**A–C**) Image intensity profiles before adjustment. (**A**) Eye 1, (**B**) eye 2, and (**C**) eye 3. (**D–F**) Image intensity profiles after adjustment. (**D**) Eye 1. A small part of the *z*-scan curve corresponding with the superficial epithelial layers showed disagreement (*arrow*) between the reference 72% LI values and the adjusted values. (**E**) Eye 2 and (**F**) eye 3. (**G**) Four characteristic corneal layers of eye 1 measured with different LIs. The endothelium and stroma showing increasing image intensity with increasing LI. Images of the epithelium depicted the disagreement in the *z*-scan curve of (**D**), showing higher image intensity with 60% than with 72% LI.

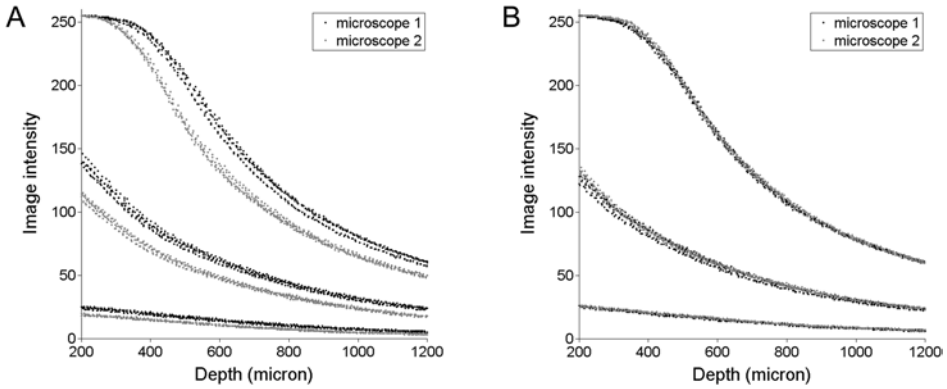

FIGURE 6. Interinstrument calibration. (**A**) Image intensity data of three PMMA slabs measured with 72% LI by two similar confocal microscopes. (**B**) Image intensity of three PMMA slabs after LI adjustment of microscope 2 to 78%.

Measurement of the PMMA slabs with similar device settings on both machines showed a large interinstrument difference in image intensity acquisition (Fig. 6A). On the basis of the AMCO Clear measurements, we found 78% LI on microscope 2 to correspond with 72% LI on microscope 1. After LI adjustment of microscope 2, the mean absolute difference decreased from 21.5 to 1.2 gray levels. The mean relative difference decreased from 18.4% to 1.2%.

DISCUSSION

Calibration of corneal backscatter measurement is mandatory, as manufacturer settings show large differences between microscopes. AMCO Clear and PMMA, two possible reference standards for calibration of corneal backscatter measurement, were assessed. AMCO Clear had one main advantage over PMMA. This turbidity standard, developed for reference purposes, enabled expression of image intensity in scatter units. In contrast with AMCO Clear, the inhomogeneous structure of PMMA made standardization to absolute values impossible. Nevertheless, this solid reference standard performed better than AMCO Clear on the correction for LI variation. After considering the pros and cons of these potential reference standards, we implemented both in our calibration methods.

Repeatability

A sample cell was used to determine the image intensity profile of AMCO Clear. Contrary to PMMA measurements, the AMCO Clear setup displayed two interfaces: one from

immersion gel to glass and one from glass to AMCO Clear. Part of the incoming light was reflected at the first interface, depending on the shape and regularity of the front surface of the sample cell. Furthermore, part of the incoming light was scattered by the sample cell itself, depending on the cell's transparency. These sample cell characteristics have a large effect on the standardization measurements.[7] For standardization of the AMCO Clear calibration setup, a commercially available sample cell should be used, as this improved repeatability.

Repeated measurements on the three PMMA slabs indicated that the degree of transparency influenced repeatability. A lower COV (better repeatability) was found when transparency of the reference standard decreased. This reduction can be explained by a quantization error due to rounding off to stationary image intensity increments (Fig. 3D). For example, a difference of two gray levels in image intensity will have a larger effect, in terms of percentage, on a mean image intensity of 20 than on a mean of 200 gray levels. The negative correlation between the degree of transparency and repeatability is enhanced by image saturation above image intensity of 200 gray levels, artificially creating a lower COV of the 26% transparent PMMA slab. When comparing COVs of two different reference standards, one should take the effect of transparency on the repeatability into account. In a depth range of 200 to 700 µm, mean image intensity of AC-4000 showed best agreement with PMMA of 49% transparency. Comparison of these two materials showed a slightly better intrasession repeatability of the reference standard with least inhomogeneities (AC- 4000). Because the sample cell affected repeatability in the AC-4000 setup, intersession repeatability was clearly in favor of the 49% transparent PMMA slab. Lot-to-lot variation was equal for both materials, despite the fact that only AMCO Clear was developed for reference purposes.

When reporting corneal backscatter measurements in long-term follow-up studies, care should be taken to correct for small changes in detector sensitivity and illumination intensity.[1] Although a previous IVCM study has indicated long-term stability of the backscatter detection system,[10] potential changes have to be quantified. In the authors' opinion PMMA with 49% transparency is first choice to detect changes over time, as this solid reference standard showed the lowest intersession repeatability without image saturation and was most practical in use. Unfortunately, backscatter changes of the PMMA slab over time are largely unknown. These changes however, probably do not outweigh the relatively large lot-to-lot variation for AMCO Clear (Table 1), which is important, as stability of the suspension is guaranteed for only 1 year. Moreover, the PMMA slab can be recalibrated against AMCO Clear to monitor and correct for aging of the PMMA.

Limited information is available on the repeatability of corneal backscatter techniques.[11] A daily reference scan of 2.5% hydroxypropyl methylcellulose with a tandem scanning confocal microscope showed a COV of 6%.[10] With a slit scanning confocal microscope, the present study showed better intersession repeatability (COV, 0.4%–2.9%)

for solid as well as for liquid reference standards. Considering corneal backscatter measurement in humans, best intersession repeatability has been reported for slit lamp-based haze measurements (COV, 3%–7%).[12,13] With IVCM, involuntary movements due to pulse, respiration, and ocular microsaccades, negatively affect repeatability of backscatter measurements.[11] These motion artifacts in the *z*-axis can be reduced by using a *z*-ring adapter. However, this contact method has a low infection hazard. Without a *z*-ring adapter, tandem scanning and slit scanning confocal microscopes showed moderate repeatability, with a COV of 35%[1] and a COR of 15.5 gray levels (Jalbert I, et al. *IOVS* 2002;43:ARVO E-abstract 1713), respectively.

Expressing Image Intensity in SUs

Without calibration, a direct relation between image intensity expressed in gray levels and backscatter is lacking. For turbidity measurements the degree of haze has been standardized, defined by the turbidity of a reference suspension in NTU. The relation between turbidity and image intensity can be used to express image intensity in SUs, provided that 1 SU is equal to the image intensity measured in a 1-NTU suspension.[2,7] To determine this relation in a turbidity range corresponding to normal corneas (200–1500 NTU), McLaren et al.[7] used a mean image intensity in a 400-µm depth range. By extending the turbidity range to concentrations that account for more opaque corneas (2000–4000 NTU), we showed that this relation was dependent on the imaging depth (Fig. 3B). Therefore, image intensity should not be averaged over a depth range. Only at a depth of 200 µm can the following linear model[7] be used to express image intensity in scatter units (I_{SU})

$$I_{SU} = a \cdot I_R + b \tag{1}$$

where image intensity (I_R) acquired with our reference LI setting (72%) was characterized by $a = 30.13$ and $b = 116.2$.

Influence of LI Variation

The image intensity profiles of the PMMA slabs (Fig. 3C) showed that decreased light propagation and image saturation affected backscatter measurements in the range corresponding to more opaque corneas. A complex analytical model would be needed to describe these image intensity profiles. Instead, smoothing interpolation was used to obtain smooth image intensity profiles and to assess the influence of LI variation. LI variation was found to affect image intensity (Figs. 4A–C). This subsequently led to a change in model 1 for determining corneal backscatter. Therefore, every time a nonref-

erence LI is used, it is mandatory to determine a new model that describes the relation between turbidity and image intensity specific for this LI. One way to derive this model is by re-examination of different concentrations of AMCO Clear and subsequent determination of a ratio that compensates for LI variations.[7] In ophthalmic practice, however, repetition of a reference scan every time a nonreference LI is used is undesirable. Single determination of functions for every relevant nonreference LI is more feasible. After the image saturation point was determined with the 26% transparent PMMA slab, we found these functions by measuring the 49% transparent PMMA slab with different LIs. In accordance with McLaren et al.,[7] a ratio was found that adjusts for changes in the LI setting. However, an offset had to be included to complete this linear model

$$I_R = a \cdot I_N + b \tag{2}$$

where I_R is image intensity adjusted to reference LI, and I_N is image intensity acquired with nonreference LI. Linear regression analysis of a scatterplot with I_N on the *x*-axis and I_R on the *y*-axis (Fig. 4E) rendered the parameters *a* and *b*.

First Method

Considering all observations of the two potential reference standards, the following method for intra- and interinstrument calibration is proposed:

1. Choose a reference LI.
2. On the basis of different concentrations of AMCO Clear, find the standardization function (model 1) that characterizes the reference LI and enables expression of image intensity in SU.
3. On the basis of the 49% transparent PMMA slab, determine functions (model 2) for every relevant nonreference LI, that adjust for LI variation.
4. Reduce LI when image saturation occurs (>200 gray levels) and adjust image intensity to reference values afterward.
5. Every week, re-examine the 49% transparent PMMA slab with reference LI to detect degradation of the backscatter detection system.
6. Once a year re-examine a new lot of AMCO Clear (4000 NTU) to detect changes in the transparency of the PMMA slab.

Verification of this calibration method indicated agreement between mean backscatter values after calibration for all three corneas. Differences after standardization were less than ±2 SD (±80 SU) for repeated measurements found in a normal population (data not shown). On closer examination, the first eye showed, after standardization, disagree-

ment in a small part of the *z*-scan curve (Fig. 5D). This can be explained by morphologic changes in the corneal epithelial layer. Images of the superficial epithelial cells of the first eye (Fig. 5G) showed brightening, when acquired with 80% and, to a greater extent, 60% LI. As image acquisition took place in a fixed order ([1], 72% LI; [2], 80% LI; [3], 60% LI), and other corneal layers appeared unaffected, these changes are probably caused by development of punctate lesions during the repeated measurements on this eye in combination with epithelial exposure to preservatives in the corneal anesthetic eye drop and the immersion gel.

Second Method

As shown in Figure 5G, LI variation influenced assessment of cell morphology. To enable interinstrument comparison of cell morphology assessment, LI should be matched between two microscopes. For this purpose, the method is as follows:

1. After examination of AC-4000 with reference LI on microscope 1, determine the image intensity measured at 200 µm depth.
2. Find the corresponding LI on microscope 2 by measuring AC-4000 by gradually varying the LI until similar image intensity is measured at a 200-µm depth.
3. If necessary, verification is obtained by measuring the 49% PMMA slab with reference LI on microscope 1 and with corresponding LI on microscope 2.

This second method can be used as an alternative one for interinstrument calibration of corneal backscatter analysis. However, matching LI between microscopes is coarser than the first calibration method. Eventually, only 6% LI change was needed to correct for 18.4% difference in mean image intensity. Because LI was adjusted by a small 360° rotary knob, fine tuning was fairly difficult. Despite this coarse LI setting, a minor difference of 1.2% in mean image intensity after calibration was found.

With the availability of IVCM the number of reports describing corneal backscatter has increased in the past few years. Nevertheless, this feature is still not widely used in a clinical setting. Reports have been primarily focused on the evaluation of surgical techniques including photorefractive keratectomy,[1,10,14–16] laser in situ keratomileusis,[4,7,17–23] deep lamellar keratoplasty,[5] and Descemet's stripping (automated) endothelial keratoplasty.[6,24,25] However, other interesting potential applications for corneal backscatter analysis, such as assessment of corneal hydration[26] and quantification of the effects on corneal backscatter of diabetes,[27,28] contact lens wear,[29,30] and fluorescein drops,[31] have been suggested. Although our results point out the necessity of calibration of corneal backscatter analysis, most IVCM reports lack this standardization. Nonstandardized backscatter measurements can be used to compare relative values within one study.

However, these studies cannot be reproduced by other researchers. Application of our calibration methods enables comparison of standardized absolute backscatter values between studies on a similar subject and allows introduction of backscatter measurements into prospective multicenter trails.

Besides motion artifacts due to involuntary eye movements, two other major limiting factors in corneal backscatter analysis by IVCM remain. First, with a magnification up to 500 times, only a small portion of the cornea is imaged, 0.14% of the corneal surface.[8] In combination with a moderate positional repeatability in the paracentral and peripheral corneal regions, backscatter analysis by IVCM is limited to a miniscule area of the central cornea and therefore seems less suited for follow-up of nonhomogenous corneal opacities. Second, backscatter, as measured by IVCM, is affected by interface reflection of two layers with different refractive indices, such as the endothelium-to-anterior chamber interface. Only with polarizing filters can backscatter be separated from reflectance.[2,32] However, no commercially available device that measures corneal backscatter is equipped with these filters.

Several other imaging techniques, including Scheimpflug photography,[33–40] slit lamp photometry,[2,13,41–49] CCD camera systems,[12,32,50–55] opacity lensometers,[56] high-frequency ultrasound, [57,58] and anterior segment optical coherence tomography (AS-OCT),[59,60] have been used to measure corneal backscatter. Only some of these studies have standardized their measurements, using liquid (formazin,[61] sodium fluorescein,[13] latex microspheres,[28,37] styrene-di-vinylbenzene copolymer beads[2,7,45–48]) or solid (neutral-density filters,[32,51,52,54] fluorescent glass,[30] and thermoplastic resin [Spectralon; Labsphere, Vinkeveen, The Netherlands][43,44,49]) reference standards. This diversity indicates the lack of a universal reference standard for calibration of backscatter measurement. A complicating factor in finding such a universal reference standard is the use of different measurement angles and wavelengths by the different imaging techniques. Because backscatter shows dependency on these factors,[62,63] these techniques are noninterchangeable. Currently, the best option for a universal reference standard is a turbidity standard solution. Yet, a solid homogenous material that is stable over time and has a low lot-to-lot variation would be more practical.

Of the noncontact imaging techniques, AS-OCT shows the greatest potential for objective backscatter measurement, whereas this technique allows high depth penetration and high-resolution imaging in opaque corneas, when compared to other techniques. Repeatability will be even further enhanced when AS-OCT is equipped with an eye-tracking system. Despite its great potential for measuring corneal backscatter, AS-OCT is still surpassed by IVCM in terms of lateral resolution. Especially the unique combination of objective backscatter quantification and assessment of cellular morphology is essential for monitoring corneal diseases and consequent therapeutic actions. Supplementary to slit lamp examination, IVCM serves this purpose best.

In summary, we have demonstrated with large interinstrument differences the necessity of standardized corneal backscatter analysis. Combination of two reference standards enabled intra- and interinstrument calibration of backscatter measurement in a wide range of corneal opacities. With standardization, IVCM combines objective backscatter measurement with assessment of corneal morphology, thus allowing clinical evaluation of treatment modalities for prevention of haze formation.

REFERENCES

1. Møller-Pedersen T, Vogel M, Li HF, Petroll WM, Cavanagh HD, Jester JV. Quantification of stromal thinning, epithelial thickness, and corneal haze after photorefractive keratectomy using in vivo confocal microscopy. *Ophthalmology*. 1997;104:360–368.
2. Patel SV, Winter EJ, McLaren JW, Bourne WM. Objective measurement of backscattered light from the anterior and posterior cornea in vivo. *Invest Ophthalmol Vis Sci*. 2007;48:166–172.
3. Erie JC, McLaren JW, Patel SV. Confocal microscopy in ophthalmology. *Am J Ophthalmol*. 2009;148: 639–646.
4. McCulley JP, Petroll WM. Quantitative assessment of corneal wound healing following IntraLASIK using in vivo confocal microscopy. *Trans Am Ophthalmol Soc*. 2008;106:84–90.
5. Marchini G, Mastropasqua L, Pedrotti E, Nubile M, Ciancaglini M, Sbabo A. Deep lamellar keratoplasty by intracorneal dissection: a prospective clinical and confocal microscopic study. *Ophthalmology*. 2006;113:1289–1300.
6. Prasher P, Muftuoglu O, Bowman RW, et al. Tandem scanning confocal microscopy of cornea after descemet stripping automated endothelial keratoplasty. *Eye Contact Lens*. 2009;35:196–202.
7. McLaren JW, Bourne WM, Patel SV. Standardization of Corneal Haze Measurement in Confocal Microscopy. *Invest Ophthalmol Vis Sci*. 2010;51:5610–5616.
8. Hillenaar T, Weenen C, Wubbels RJ, Remeijer L. Endothelial involvement in herpes simplex virus keratitis: an in vivo confocal microscopy study. *Ophthalmology*. 2009;116:2077–2086.
9. Brugin E, Ghirlando A, Gambato C, Midena E. Central corneal thickness: z-ring corneal confocal microscopy versus ultrasound pachymetry. *Cornea*. 2007;26:303–307.
10. Møller-Pedersen T, Li HF, Petroll WM, Cavanagh HD, Jester JV. Confocal microscopic characterization of wound repair after photorefractive keratectomy. *Invest Ophthalmol Vis Sci*. 1998;39: 487–501.
11. Jalbert I, Stapleton F, Papas E, Sweeney DF, Coroneo M. In vivo confocal microscopy of the human cornea. *Br J Ophthalmol*. 2003;87:225–236.
12. Maldonado MJ, Arnau V, Martinez-Costa R, et al. Reproducibility of digital image analysis for measuring corneal haze after myopic photorefractive keratectomy. *Am J Ophthalmol*. 1997;123: 31–41.
13. Olsen T. Light scattering from the human cornea. *Invest Ophthalmol Vis Sci*. 1982;23:81–86.
14. Jester JV, Møller-Pedersen T, Huang J, et al. The cellular basis of corneal transparency: evidence for 'corneal crystallins'. *J Cell Sci*. 1999;112:613–622.
15. Møller-Pedersen T, Cavanagh HD, Petroll WM, Jester JV. Corneal haze development after PRK is regulated by volume of stromal tissue removal. *Cornea*. 1998;17:627–639.
16. Møller-Pedersen T, Cavanagh HD, Petroll WM, Jester JV. Stromal wound healing explains refractive instability and haze development after photorefractive keratectomy: a 1-year confocal microscopic study. *Ophthalmology*. 2000;107:1235–1245.
17. Auzerie O, Pisella PJ, Bokobza Y, Baudouin C. Corneal stromal changes after LASIK (in French). *J Fr Ophtalmol*. 2002;25:9 –14.
18. Hu MY, McCulley JP, Cavanagh HD, et al. Comparison of the corneal response to laser in situ keratomileusis with flap creation using the FS15 and FS30 femtosecond lasers: clinical and confocal microscopy findings. *J Cataract Refract Surg*. 2007;33:673–681.
19. Morishige N, Kesler-Diaz A, Wahlert AJ, et al. Corneal response to femtosecond laser photodisruption in the rabbit. *Exp Eye Res*. 2008;86:835–843.

20. Petroll WM, Bowman RW, Cavanagh HD, Verity SM, Mootha VV, McCulley JP. Assessment of keratocyte activation following LASIK with flap creation using the IntraLase FS60 laser. *J Refract Surg*. 2008;24:847–849.
21. Pisella PJ, Auzerie O, Bokobza Y, Debbasch C, Baudouin C. Evaluation of corneal stromal changes in vivo after laser in situ keratomileusis with confocal microscopy. *Ophthalmology*. 2001;108: 1744–1750.
22. Slowik C, Somodi S, Richter A, Guthoff R. Assessment of corneal alterations following laser in situ keratomileusis by confocal slit scanning microscopy. *Ger J Ophthalmol*. 1996;5:526 –531.
23. Vesaluoma M, Perez-Santonja J, Petroll WM, Linna T, Alio J, Tervo T. Corneal stromal changes induced by myopic LASIK. *Invest Ophthalmol Vis Sci*. 2000;41:369–376.
24. Espana EM, Huang B. Confocal microscopy study of donor-recipient interface after Descemet's stripping with endothelial keratoplasty. *Br J Ophthalmol*. 2010;94:903–908.
25. Kobayashi A, Mawatari Y, Yokogawa H, Sugiyama K. In vivo laser confocal microscopy after descemet stripping with automated endothelial keratoplasty. *Am J Ophthalmol*. 2008;145:977–985.
26. Morishige N, Takahashi N, Chikamoto N, Nishida T. Quantitative evaluation of corneal epithelial oedema by confocal microscopy. *Clin Experiment Ophthalmol*. 2009;37:249–253.
27. Morishige N, Chikama TI, Sassa Y, Nishida T. Abnormal light scattering detected by confocal biomicroscopy at the corneal epithelial basement membrane of subjects with type II diabetes. *Diabetologia*. 2001;44:340–345.
28. Takahashi N, Wakuta M, Morishige N, Chikama T, Nishida T, Sumii Y. Development of an instrument for measurement of light scattering at the corneal epithelial basement membrane in diabetic patients. *Jpn J Ophthalmol*. 2007;51:185–190.
29. Nagel S, Wiegand W, Thaer AA, Geyer OC. Light scattering study of the cornea in contact lens patients. In vivo studies using confocal slit scanning microscopy (in German). *Ophthalmologe*. 1996;93:252–256.
30. Patel SV, McLaren JW, Hodge DO, Bourne WM. Confocal microscopy in vivo in corneas of long-term contact lens wearers. *Invest Ophthalmol Vis Sci*. 2002;43:995–1003.
31. Mocan MC, Irkec M. Fluorescein enhanced confocal microscopy in vivo for the evaluation of corneal epithelium. *Clin Experiment Ophthalmol*. 2007;35:38–43.
32. Lohmann CP, Timberlake GT, Fitzke FW, Gartry DS, Muir MK, Marshall J. Corneal light scattering after excimer laser photorefractive keratectomy: the objective measurements of haze. *Refract Corneal Surg*. 1992;8:114 –121.
33. Binder PS, Bosem M, Weinreb RN. Scheimpflug anterior segment photography assessment of wound healing after myopic excimer laser photorefractive keratectomy. *J Cataract Refract Surg*. 1996;22:205–212.
34. Busin M, Spitznas M, Laser H, Leyendecker M, Hockwin O. In vivo evaluation of epikeratophakia lenses by means of Scheimpflug photography. *Refract Corneal Surg*. 1989;5:155–160.
35. Holden R, Shun-Shin GA, Brown NA. Central corneal light scatter in long-term diabetics. *Eye* (*Lond*). 1994;8:44–45.
36. Smith GT, Brown NA, Shun-Shin GA. Light scatter from the central human cornea. *Eye* (*Lond*). 1990;4:584 –588.
37. Soya K, Amano S, Oshika T. Quantification of simulated corneal haze by measuring back-scattered light. *Ophthalmic Res*. 2002;34:380–388.
38. Huebscher HJ, Schmidt H. On-line scheimpflug imaging and its potential for in vivo examination of cornea and lens. *Ophthalmic Res*. 1994;26(suppl):33–38.

39. Cherny M, Stasiuk R, Kelly P, Lee P, Golembo G, Taylor H. Computerised scheimpflug densitometry as a measure of corneal opacification following excimer laser surgery. *Ophthalmic Res*. 1994; 26(suppl):48 –54.
40. van de Pol C, Soya K, Hwang DG. Objective assessment of transient corneal haze and its relation to visual performance after photorefractive keratectomy. *Am J Ophthalmol*. 2001;132:204–210.
41. Braunstein RE, Jain S, McCally RL, Stark WJ, Connolly PJ, Azar DT. Objective measurement of corneal light scattering after excimer laser keratectomy. *Ophthalmology*. 1996;103:439–443.
42. Jain S, Khoury JM, Chamon W, Azar DT. Corneal light scattering after laser in situ keratomileusis and photorefractive keratectomy. *Am J Ophthalmol*. 1995;120:532–534.
43. Jain S, Hahn TW, McCally RL, Azar DT. Antioxidants reduce corneal light scattering after excimer keratectomy in rabbits. *Lasers Surg Med*. 1995;17:160–165.
44. Jain S, McCally RL, Connolly PJ, Azar DT. Mitomycin C reduces corneal light scattering after excimer keratectomy. *Cornea*. 2001;20:45–49.
45. Patel SV, Maguire LJ, McLaren JW, Hodge DO, Bourne WM. Femtosecond laser versus mechanical microkeratome for LASIK: a randomized controlled study. *Ophthalmology*. 2007;114:1482–1490.
46. Patel SV, McLaren JW, Hodge DO, Baratz KH. Scattered light and visual function in a randomized trial of deep lamellar endothelial keratoplasty and penetrating keratoplasty. *Am J Ophthalmol*. 2008;145:97–105.
47. Patel SV, McLaren JW, Hodge DO, Bourne WM. The effect of corneal light scatter on vision after penetrating keratoplasty. *Am J Ophthalmol*. 2008;146:913–919.
48. Patel SV, Baratz KH, Hodge DO, Maguire LJ, McLaren JW. The effect of corneal light scatter on vision after descemet stripping with endothelial keratoplasty. *Arch Ophthalmol*. 2009;127:153–160.
49. McCally RL, Hochheimer BF, Chamon W, Azar DT. A simple device for objective measurements of haze following excimer laser ablation of cornea. *SPIE*. 1993;1877:20–25.
50. Chang SS, Maurice DM, Ramirez-Florez S. Quantitative measurement of corneal haze after myopic PRK. *J Refract Surg*. 1996;12:412–416.
51. Lohmann CP, Fitzke F, O'Brart D, Muir MK, Timberlake G, Marshall J. Corneal light scattering and visual performance in myopic individuals with spectacles, contact lenses, or excimer laser photorefractive keratectomy. *Am J Ophthalmol*. 1993;115:444–453.
52. Lohmann CP, Gartry DS, Muir MK, Timberlake GT, Fitzke FW, Marshall J. Corneal haze after excimer laser refractive surgery: objective measurements and functional implications. *Eur J Ophthalmol*. 1991;1:173–180.
53. Maldonado MJ, Arnau V, Navea A, et al. Direct objective quantification of corneal haze after excimer laser photorefractive keratectomy for high myopia. *Ophthalmology*. 1996;103:1970–1978.
54. Rajan MS, Shafiei S, Mohrenfels CV, et al. Effect of exogenous keratinocyte growth factor on corneal epithelial migration after photorefractive keratectomy. *J Cataract Refract Surg*. 2004;30: 2200–2206.
55. Ramirez-Florez S, Maurice DM. Inflammatory cells, refractive regression, and haze after excimer laser PRK. *J Refract Surg*. 1996; 12:370–381.
56. Andrade HA, McDonald MB, Liu JC, Abdelmegeed M, Varnell R, Sunderland G. Evaluation of an opacity lensometer for determining corneal clarity following excimer laser photoablation. *Refract Corneal Surg*. 1990;6:346 –351.
57. Allemann N, Chamon W, Silverman RH, et al. High-frequency ultrasound quantitative analyses of corneal scarring following excimer laser keratectomy. *Arch Ophthalmol*. 1993;111:968–973.
58. Silverman RH, Patel MS, Gal O, et al. Effect of corneal hydration on ultrasound velocity and backscatter. *Ultrasound Med Biol*. 2009; 35:839–846.

59. Hosseini K, Kholodnykh AI, Petrova IY, Esenaliev RO, Hendrikse F, Motamedi M. Monitoring of rabbit cornea response to dehydration stress by optical coherence tomography. *Invest Ophthalmol Vis Sci*. 2004;45:2555–2562.
60. Wang J, Simpson TL, Fonn D. Objective measurements of corneal light-backscatter during corneal swelling, by optical coherence tomography. *Invest Ophthalmol Vis Sci*. 2004;45:3493–3498.
61. Jester JV, Budge A, Fisher S, Huang J. Corneal keratocytes: phenotypic and species differences in abundant protein expression and in vitro light-scattering. *Invest Ophthalmol Vis Sci*. 2005;46: 2369–2378.
62. Feuk T, McQueen D. The angular dependence of light scattered from rabbit corneas. *Invest Ophthalmol*. 1971;10:294–299.
63. Feuk T. The wavelength dependence of scattered light intensity in rabbit corneas. *IEEE Trans Biomed Eng*. 1971;18:92–96.

APPENDIX A

Mean corneal backscatter

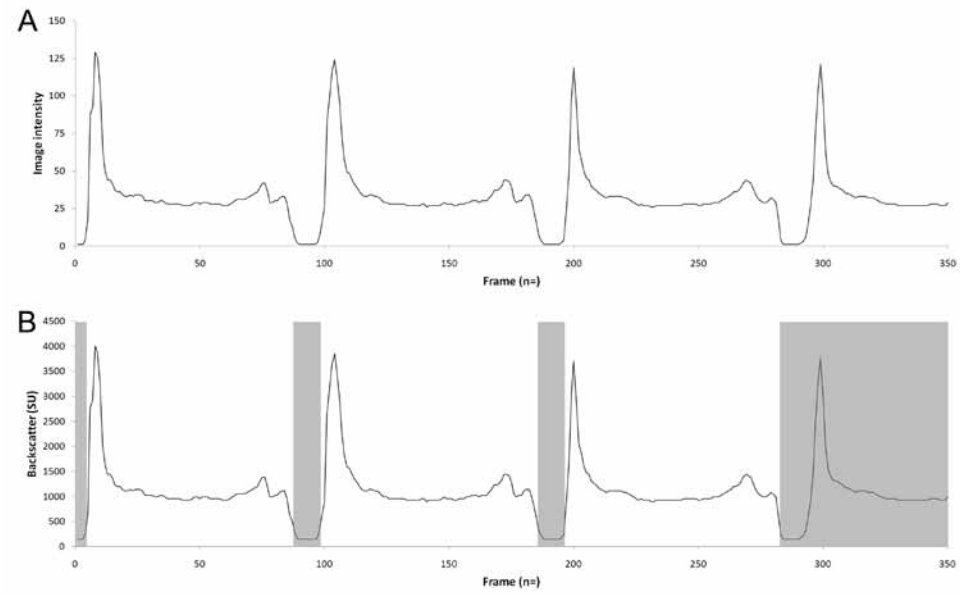

Figure A1 (A) With a scan step of 6 µm, a full-thickness scan of an average cornea (550-µm-thick) always contained three complete passes. When a scan was performed with a nonreference LI, image intensities were adjusted to reference values. (**B**) After adjustment for LI variation, image intensities were standardized to SUs, on the basis of the standardization function derived from the AMCO Clear measurements (model 1) (GFS Chemicals, Inc., Howell, OH). All backscatter values lower than 400 SU and also the incomplete fourth pass were discarded (*shaded areas*). A mean backscatter value was determined for each pass by summing all the backscatter values in that pass and dividing them by the number of frames. Mean corneal backscatter was the average of the three passes. This example: pass 1, 99730/83 = 1202; pass 2, 106789/87 = 1227; and pass 3, 100018/86 = 1163. Mean corneal backscatter: (1202 + 1227 + 1163)/3 = 1197 SU.

APPENDIX B

Alignment process

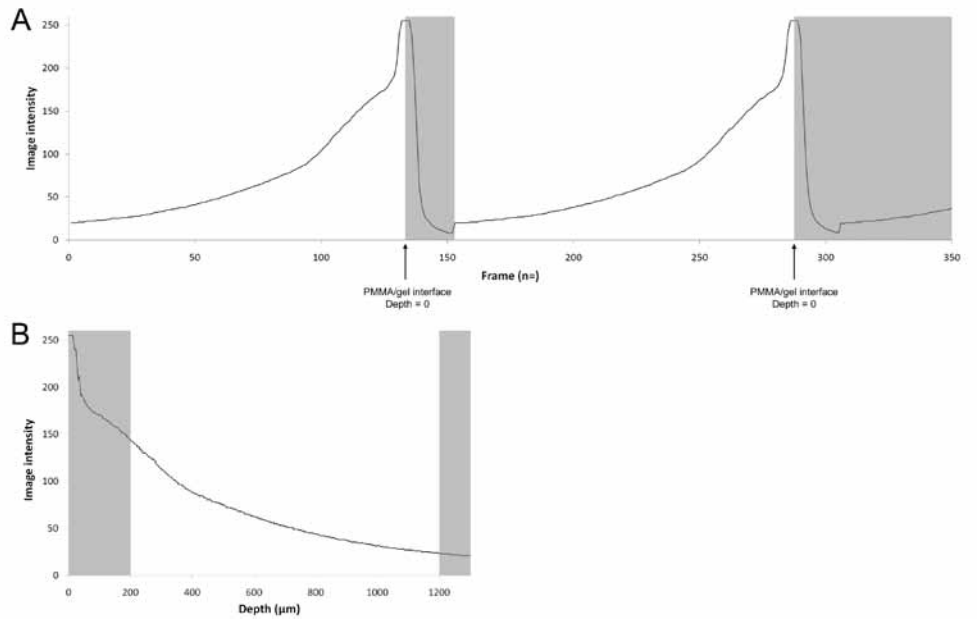

Figure A2 (**A**) The *z*-scan curve of the PMMA slab with 49% transparency measured on microscope 1. At fixed settings (semiautomatic mode; 72% light intensity; scan depth, 1500 µm; scan step, 10 µm; and autoalignment function, off) the *z*-scan curve of all reference standards always contained two complete passes. Alignment was based on the PMMA–coupling gel interface (*arrow*). The center of this reflectance peak was set to a depth of 0 µm. The following model was used to calculate depth for every image in the *z*-scan curve: depth of the current image = W MotPos of the interface minus W MotPos of the current image. All images in the *shaded areas* that corresponded to a negative calculated depth or were part of the third incomplete pass were discarded. (**B**) After alignment, image intensity data were plotted against depth. Because the specular reflection of the PMMA–coupling gel interface influenced the image intensity profile up to a 173-µm depth, all images below the 200-µm depth were discarded. In addition, all images above the 1200-µm depth were discarded, to create a standard 1000-µm depth range. After examining the PMMA slab in triplicate and the subsequent data processing, a smoothing interpolation was applied to the image intensity–depth plot (Fig. 3C).

4

Normative database for corneal backscatter analysis by in vivo confocal microscopy

Toine Hillenaar
Roger H. H. Cals
Paul H. C. Eilers
René J. Wubbels
Hugo van Cleynenbreugel
Lies Remeijer

Invest Ophthalmol Vis Sci. 2011;52:7274-7281

ABSTRACT

Purpose: To ascertain the sex and age relatedness, diurnal variation, and repeatability of backscatter measurement in the normal human cornea.

Methods: Seven corneal backscatter variants were measured by in vivo confocal microscopy (IVCM) in both normal eyes ($n = 314$) of 157 healthy subjects. These subjects were assigned to one or more of three groups. The sex and age relatedness of corneal backscatter were assessed in group 1 ($n = 300$), which comprised 75 men and 75 women evenly distributed over five age categories. To assess diurnal variation, eyes in group 2 ($n = 40$) were measured four times a day, at 3-hour intervals. The eyes in group 3 ($n = 50$) were examined four times a year to determine intersession repeatability. Intrasession repeatability was determined by performing all IVCM examinations in duplicate. Linear mixed models were used to assess the effects of sex, age, and time of measurement on corneal backscatter.

Results: Mean corneal backscatter was 3.5% higher in men ($P = 0.003$). From the age of 50 years, backscatter increased significantly in the anterior stroma ($P = 0.0003$). A small but statistically significant diurnal variation was found in all seven backscatter variants ($P < 0.01$). The test–retest coefficient of variation of mean corneal backscatter was 5.3%, comprising intra- and intersession repeatability.

Conclusions: Sex and time of measurement significantly affect corneal backscatter measured by IVCM, whereas age affects only backscatter in the anterior stroma. All three factors should be taken into account when conducting scientific research. For ophthalmic practice, the authors suggest ignoring these factors and propose a generalized normal range and minimum detectable change for each backscatter variant.

INTRODUCTION

In the past decade, the number of imaging techniques for in vivo assessment of the human cornea has burgeoned. Whereas imaging techniques such as Scheimpflug photography and anterior segment optical coherence tomography have been implemented in the ophthalmic clinic, in vivo confocal microscopy (IVCM) has never become common practice. Despite its great potential, the clinical use of IVCM remains confined to the diagnosis of rare corneal degenerations and dystrophies and the differentiation of uncommon pathogens in infectious keratitis.[1–5] Only recently has a wider clinical application been introduced that exploits the ability of IVCM to detect endothelial involvement in order to monitor disease activity in inflammatory corneal processes.[6] In addition to evaluating the corneal endothelium, disease status may also be assessed by another feature of IVCM, corneal backscatter. Although corneal backscatter has been studied in normal eyes using IVCM,[7,8] fundamental data about the effects of sex, age, and diurnal variation are still lacking. Knowledge of these effects and information on the repeatability of backscatter measurements are essential when studying disease progression in pathologic processes of the cornea or the outcome of corneal surgery. The purpose of this study was to ascertain the effects of sex, age, and time of measurement on corneal backscatter and to assess its repeatability as measured by IVCM.

METHODS

Subjects

For the present study, the eyes of 157 subjects (n = 314) were enrolled and categorized into three groups (Table 1). Several subjects were assigned to more than one group. Group 1 (n = 300) was designed to assess the sex- and age-related variation of corneal backscatter. Subjects in this group were evenly distributed over five age categories; 20 to 29, 30 to 39, 40 to 49, 50 to 59, and 60 to 79 years. Each category consisted of 15 men and 15 women. We also used group 1 to ascertain the morphologic aspects of aging in the normal cornea. Since the results on this topic are beyond the scope of the current paper, they are described in a separate paper. Diurnal variation in corneal backscatter was assessed in group 2 (n = 40). Subjects in group 2 were examined four times a day at 3-hour intervals. Group 3 comprised 25 subjects (n = 50) who were examined four times a year at 3-month intervals, to determine intersession repeatability. To assess intersession repeatability, we assumed that backscatter in a normal cornea remained stable over this 1-year period. All IVCM examinations were performed in duplicate to determine intrasession repeatability.

Table 1. Group characteristics

	Group 1 Sex, age relatedness	Group 2 Diurnal variation	Group 3 Intersession repeatability
Subjects, *n*	150	20	25
Mean age, *y*	45 (20-79)	38 (20-59)	44 (27-67)
Men, *n*	75	7	8
Eyes, *n*	300	40	50
Sessions, *n*	1	4	4
Time	9:00-12:00	9:00, 12:00, 15:00, 18:00	9:00-12:00
Month	0	0	0, 3, 6, 9
IVCM	+	+	+
US pachymetry	+	+	–
GAT IOP	+	+	–

US = ultrasound; GAT IOP = intraocular pressure measured with Goldmann applanation tonometry; + = performed; – = not performed

Subjects neither had a history of systemic disease, nor used any medication known to affect corneal transparency. Other exclusion criteria were previous inflammation, infection, or allergic reaction of the eye; ocular surgery or trauma; or a history of contact lens wear. Before enrollment subjects were examined by slit lamp biomicroscopy, to confirm an intact corneal epithelium, a clear corneal stroma, and absence of ocular inflammatory processes.

The protocol of this cross-sectional study was approved by our institutional review board and the local medical ethics committee and was performed in accordance with the Declaration of Helsinki. Informed consent was obtained from all subjects.

Corneal Backscatter Measurement

Corneal backscatter was measured by IVCM (Confoscan 4; Nidek Technologies, Padova, Italy), according to a previously described method.[6] Briefly, both subjects' eyes were given 1 drop of 0.4% oxybuprocaine (Ceban BV, Breda, The Netherlands) to ensure corneal anesthesia. An immersion gel (Vidisic; Dr. Mann Pharma, Berlin, Germany) was applied to the 40X objective lens. We used a *z*-ring adapter to enable backscatter measurement at different corneal depths and to reduce motion artifacts in the *z*-axis. After autoalignment, the central cornea was scanned in full-thickness mode with fixed device settings: 72% light intensity and a 6-µm scan step. With these settings, a scan contained three complete passes through the cornea.

Because corneal backscatter analysis by IVCM is subject to large interinstrument differences,[9] we standardized our measurements with a standard turbidity suspension (AMCO Clear; GFS Chemicals, Inc., Powell, OH), after which backscatter was expressed in scatter

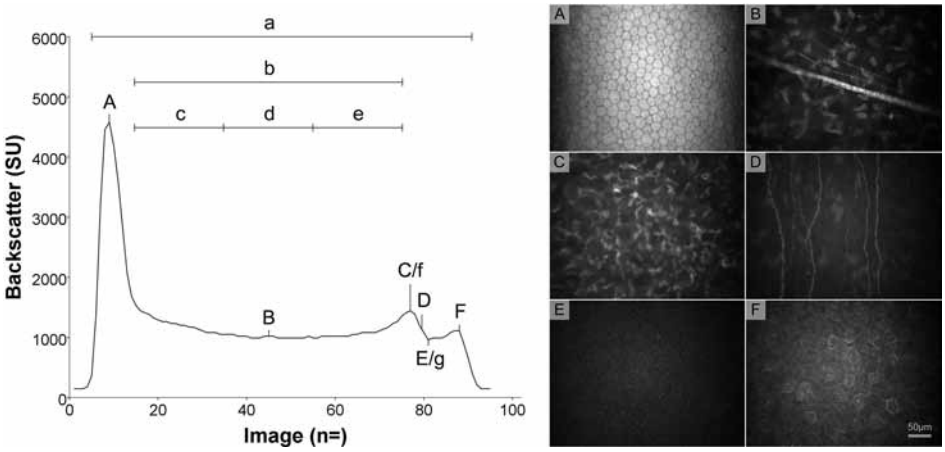

FIGURE 1. Backscatter measurements by IVCM. The IVCM images are 425 x 320 µm, with the bar representing 50 µm. Six characteristic layers of a normal human cornea and their position on the *z*-scan curve: (**A**) corneal endothelium; (**B**) corneal stroma showing a large straight nerve fiber; (**C**) the anterior stroma, characterized by a higher keratocyte density compared to middle and posterior thirds of the stroma.[10]; (**D**) subbasal nerve plexus; (**E**) basal epithelial cell layer; and (**F**) superficial epithelial cells. **(a–g)** Seven variants of corneal backscatter. For variants a to e, mean backscatter per image was calculated in three subsequent passes through the cornea.[9] Variants f and g represent mean peak values of the three subsequent passes in one scan. Backscatter of the **(a)** cornea, **(b)** stroma, **(c)** posterior third of the stroma, **(d)** middle third of the stroma, **(e)** anterior third of the stroma and of the **(f)** SP and **(g)** EV.

units (SU).[8,9] To test for light intensity variations of the confocal microscope over the day, we examined a solid piece of polymethylmethacrylate (PMMA; Opal 040 Perspex GS, Lucite International Ltd., Southampton, UK) on four occasions during a day. The same PMMA slab was used for a weekly reference scan to obtain long-term standardization of backscatter measurement. Once a year, opacity changes in the PMMA slab were verified (AMCO Clear; GFS Chemicals, Inc.). During the study, the ambient light in the room was kept constant.

For each measurement, seven variants of corneal backscatter were calculated (Fig. 1). Mean backscatter of the selected images of three passes through the cornea was used for backscatter values of the cornea, stroma, and the anterior, middle, and posterior thirds of the stroma. After determining the stromal boundaries (see the Appendix, Supplementary Material S1, http://www.iovs.org/lookup/suppl/doi:10.1167/iovs.11-7747/-/DCSupplemental), these values were computed semiautomatically with a purpose-made algorithm (see the algorithm, Supplementary Material S2, and the algorithm manual, Supplementary Material S3, http://www.iovs.org/lookup/suppl/doi:10.1167/iovs.11-7747/-/DCSupplemental). Manually determined mean peak values were used to express the epithelial valley (EV) and subepithelial peak (SP). Intra- and intersession repeatability were assessed for all seven variants of corneal backscatter.

Covariates

Because diurnal variation in central corneal thickness (CCT) and intraocular pressure (IOP) may correlate with corneal backscatter, these possible covariates were measured simultaneously with the IVCM examinations in groups 1 and 2. We recorded CCT as the mean of 10 readings with ultrasound (US) pachymetry (model SP-3000; Tomey Ltd., Tokyo, Japan). Intraocular pressure, measured with Goldmann applanation tonometry, was always performed after IVCM, to avoid interference of fluorescent staining of the tear film with the backscatter measurements. Both CCT and IOP were performed under topical anesthesia with oxybuprocaine 0.4%.

Statistical Analyses

P values were considered statistically significant when < 0.05 (SPSS for Windows, ver. 17.0; SPSS, Inc., Chicago, IL). To account for clustering of eyes within subjects, we used linear mixed models to assess sex and age relatedness (group 1) and diurnal variation of corneal backscatter (group 2). In the model for group 1, sex and eye were considered fixed factors, whereas age, CCT, and IOP were entered as covariates. The model for group 2 resembled the model for group 1 with the distinction that the covariate age was replaced with the fixed factor time. IOP was not included in the model for group 2, because it strongly correlated with time and caused collinearity of the statistical model.

Intra- and intersession repeatability were expressed in relative terms as coefficient of variation (COV) and in absolute terms as coefficient of repeatability (COR). The COV was defined as the within-subject SD (SD_W) divided by the mean backscatter and was expressed as a percentage, whereas the COR was defined as $1.96(\sqrt{2} \times SD_W)$.[11] Intrasession repeatability was calculated on the basis of 584 duplicate backscatter measurements. These duplicate measurements were also used to test whether subjects got accustomed to the IVCM examinations, which in turn may have resulted in better quality backscatter measurements. We analyzed this so-called "learning effect" by comparing all first measurements of each eye to the second measurements of that eye, using a paired Student's *t*-test. Furthermore, we used equation 1 to calculate the test–retest coefficient of variation (COV_T) for corneal backscatter on the basis of intrasession (COV_A) and intersession (COV_B) components:

$$COV_T = \sqrt{(COV_A^2 + COV_B^2)} \quad (1)$$

After considering the effects of sex, age, and time of measurement on corneal backscatter and assessing its repeatability, we constructed a generalized normal range for corneal backscatter. For this purpose, we applied a logarithmic transformation to acquire a

between-subject SD accounting for skewness of the data.[12] As normal range, we chose a 99% rather than a 95% reference interval because we expected our study population to comprise only supernormal corneas, as contact lens wearers and subjects who had undergone cataract surgery were not enrolled in the study. By taking the antilog, the normal range was transformed back to the original scale.

To identify clinically relevant change, the difference between two measurements within one subject should be larger than the difference explained by measurement error.[13] This minimum detectable change at the 95% confidence level ($MDC_{95\%}$) is defined by the COR. Because the COR varies with the amount of backscatter,[9] we expressed the $MDC_{95\%}$ as a percentage. By using equation 2 to compute the $MDC_{95\%}$, we also accounted for diurnal variation of corneal backscatter:

$$MDC_{95\%} = 3 \times COV_T \quad (2)$$

RESULTS

Mean corneal backscatter was 3.5% higher in the men than in the women (regression coefficient = 54.4 ± 36.3, $P = 0.003$; Table 2). Two outliers were seen at the higher end of the age spectrum (Fig. 2A, arrows). On closer inspection of these two outliers, the IVCM images showed abnormal depositions in the stroma of both corneas and epithelial deviations in one cornea. After exclusion of the outliers from statistical analysis, the influence of age on mean stromal backscatter was borderline significant ($P = 0.05$), because of strong age relatedness of backscatter in the anterior stroma ($P = 0.0003$; Table 3). Backscatter in the anterior stroma decreased slightly until 50 years of age, but increased significantly thereafter (Fig. 2B). The measured corneal backscatter correlated negatively with CCT, but was not correlated with IOP (Figs. 2C, 2D). We found no differences between right and left eyes.

Table 2. Sex relatedness of corneal backscatter measured by IVCM

	men	women	Δ_{SEX} (%)	*P*
Cornea	1248 ± 149	1206 ± 96	3.5	0.003
Stroma	1106 ± 181	1057 ± 108	4.6	0.005
Anterior stroma	1145 ± 177	1117 ± 125	2.5	NS
Mid stroma	962 ± 171	925 ± 106	4.1	0.02
Posterior stroma	1211 ± 232	1130 ± 135	7.2	0.001
Epithelial valley	1044 ± 103	1024 ± 99	1.9	NS
Subepithelial peak	1579 ± 252	1446 ± 177	9.2	0.0002

Data are expressed as mean SU ± SD. Δ_{SEX} = difference between men and women

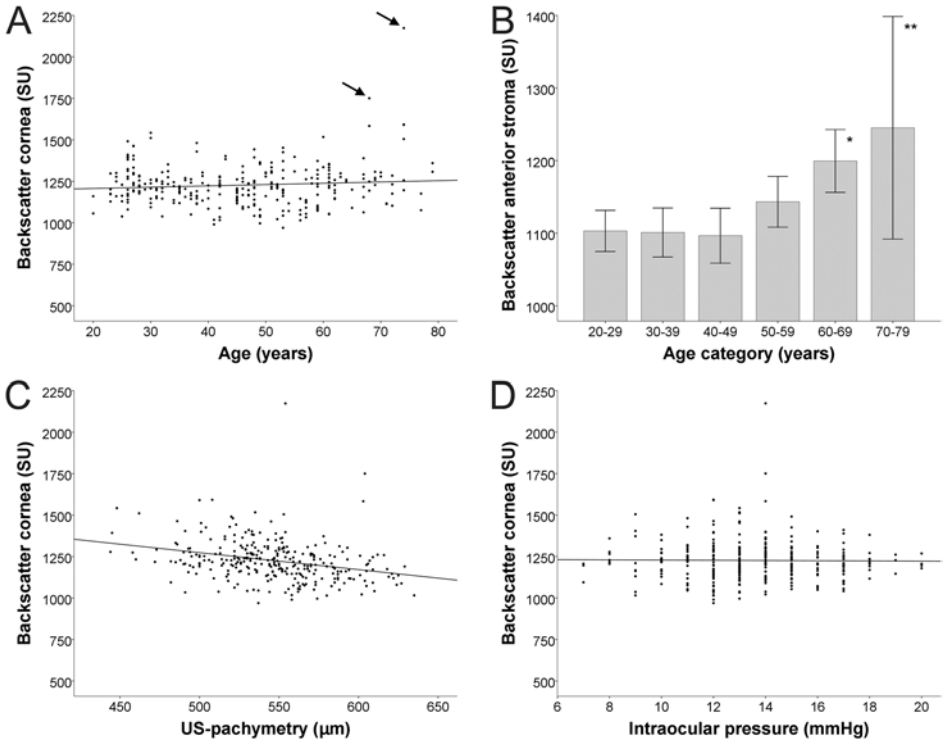

FIGURE 2. Age relatedness of corneal backscatter. (**A**) Mean corneal backscatter remained relatively stable with increasing age. Two outliers were seen at the higher end of the age spectrum (*arrows*). (**B**) Backscatter in the anterior third of the stroma per age category. After an initial decrease up to 50 years of age, backscatter in the anterior stroma showed an increase in the last two age categories. The last age category spanned 20 years instead of 10 years and was, for the purpose of this figure, divided into two decades, which comprised $n = 42$* and $n = 18$** eyes. Error bars represent 95% confidence intervals. (**C**) CCT correlated negatively with mean corneal backscatter (regression coefficient = –1.21 ± 0.25, $P < 0.0001$). (**D**) IOP did not correlate with mean corneal backscatter.

Table 3. Age-related changes of corneal backscatter measured by IVCM

	20-29 y	30-39 y	40-49 y	50-59 y	60-79 y	Max Δ_{AGE} (%)	*P*
Cornea	1245 ± 100	1217 ± 97	1187 ± 106	1204 ± 113	1257 ± 123	5.9	NS
Stroma	1091 ± 114	1068 ± 118	1039 ± 119	1066 ± 125	1114 ± 144	7.2	0.05
Anterior stroma	1103 ± 110	1101 ± 131	1097 ± 146	1143 ± 135	1190 ± 148	8.5	0.0003
Mid stroma	958 ± 115	939 ± 118	903 ± 110	928 ± 115	960 ± 139	6.3	NS
Posterior stroma	1212 ± 162	1165 ± 143	1117 ± 143	1126 ± 172	1193 ± 180	8.5	NS
Epithelial valley	1085 ± 119	1017 ± 97	1008 ± 91	1014 ± 77	1039 ± 85	7.6	NS
Subepithelial peak	1520 ± 221	1459 ± 166	1457 ± 227	1545 ± 191	1560 ± 254	7.1	NS

Data are expressed as mean SU ± SD. Max Δ_{AGE} = maximum difference between age categories.

Table 4. Diurnal variation of corneal backscatter measured by IVCM

	9 h	12 h	15 h	18 h	Max Δ_{DAY} (%)	*P*
Cornea	1220 ± 106	1238 ± 108	1253 ± 111	1250 ± 102	2.7%	0.002
Stroma	1058 ± 119	1073 ± 119	1088 ± 120	1088 ± 115	2.8%	0.0001
Anterior stroma	1085 ± 146	1108 ± 152	1122 ± 149	1114 ± 143	3.4%	0.001
Mid stroma	924 ± 106	933 ± 101	948 ± 107	949 ± 103	2.7%	0.0004
Posterior stroma	1165 ± 141	1179 ± 148	1194 ± 145	1200 ± 139	3.0%	0.001
Epithelial valley	1053 ± 103	1081 ± 124	1087 ± 112	1092 ± 105	3.7%	0.003
Subepithelial peak	1480 ± 211	1508 ± 218	1540 ± 231	1525 ± 210	4.1%	0.01

Data are expressed as mean SU ± SD. Max Δ_{DAY} = maximum diurnal variation

All seven variants of corneal backscatter showed a small (≤ 4%), but statistically significant diurnal variation (Table 4). CCT measured with ultrasound remained stable over the day, whereas IOP changed significantly (by up to 14%; Fig. 3). The diurnal variation in IOP was negatively correlated with the change in corneal backscatter (regression coefficient = –7.0 ± 5.0, $P = 0.006$).

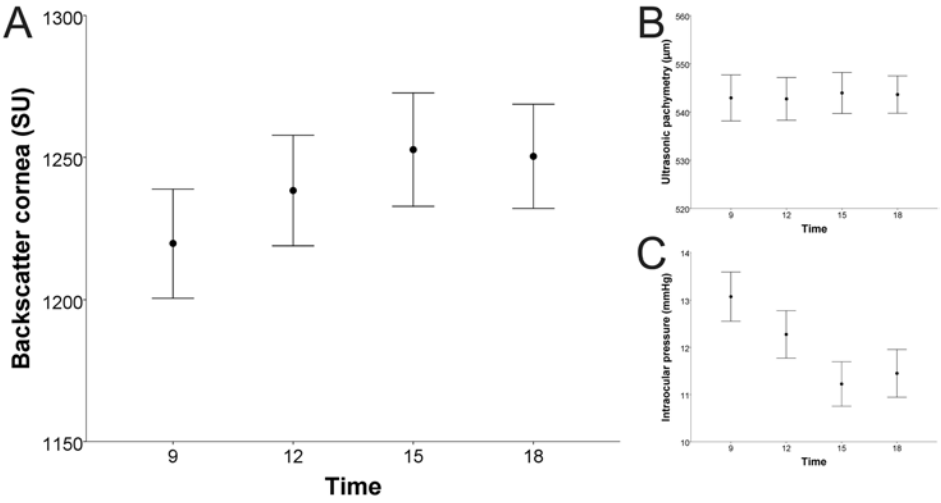

FIGURE 3. Diurnal variation of corneal backscatter. (**A**) Mean corneal backscatter varied significantly during the day: maximum variation 2.7%, $P = 0.002$. (**B**) CCT remained stable during the day. (**C**) Diurnal variation in IOP was exactly opposite to the change in corneal backscatter; maximum variation of IOP was 14.1%, $P < 0.0001$. Error bars represent 95% confidence intervals of the mean.

With test–retest COVs around 5%, all seven backscatter variants had a very good repeatability (Table 5). Only the backscatter measurement of the posterior third of the stroma had a slightly higher test–retest COV: 7%. We found no difference between intra- and intersession repeatability.

Table 5. Repeatability of backscatter measured by IVCM

	Intrasession		Intersession		
	COV (%)	COR	COV (%)	COR	COV_T (%)
Cornea	4.2	143	3.2	111	5.3
Stroma	3.8	114	3.2	98	5.0
Anterior stroma	4.0	127	3.5	111	5.3
Mid stroma	3.7	98	3.4	88	5.0
Posterior stroma	5.2	170	4.3	140	6.8
Epithelial valley	3.8	111	3.0	84	4.8
Subepithelial peak	4.0	169	3.6	155	5.4

Backscatter was expressed in SU.

When corneal backscatter is applied in ophthalmic practice, it is much more feasible to ignore the effects of sex, age, and time of measurement. Since these effects were relatively small, we constructed a generalized normal range and $MDC_{95\%}$ for all seven backscatter variants (Table 6).

Table 6. Generalized normal range and $MDC_{95\%}$ of corneal backscatter

	Mean	99% reference interval	$MDC_{95\%}$ (%)
Cornea	1222	966-1534	16
Stroma	1075	796-1435	15
Anterior stroma	1126	816-1531	16
Mid stroma	937	673-1285	15
Posterior stroma	1162	811-1635	20
Epithelial valley	1032	802-1316	15
Subepithelial peak	1508	1033-2156	16

Data are expressed in SU.

Our results were unaffected by change in light intensity of the confocal microscope over the day or during the study period. Also, we could not establish a "learning effect", as the first measurements were no different from the second measurements of the same eye.

DISCUSSION

The present study reports on corneal backscatter measurement in the largest normative IVCM database to date. Corneal backscatter in a normal population depended on the sex of the subject and time of measurement, whereas the influence of age was confined to backscatter in the anterior stroma. All three factors should be taken into account in the

design of a study that compares corneal backscatter measured by IVCM between patient groups. For detection and follow-up of corneal haze in individual patients, as is the case in ophthalmic practice, these factors have to be considered in another perspective. We suggest ignoring sex, age, and time of measurement when using corneal backscatter in ophthalmic practice, because the influence of these factors is much smaller than the variability of corneal backscatter between and within subjects.

Corneal backscatter has been reported to be sex independent.[14] In contrast with our study, these measurements were performed under nonspecular conditions. Under such conditions, scattering is elicited by the collagen fibrils in the stroma.[15] Because corneal backscatter is dominated by reflections from the cell nuclei when measured under specular conditions by IVCM, our results cannot be compared with Olsen's findings.[14] The reason for the small sex difference in corneal backscatter measured by IVCM, remains unclear. Sex difference in CCT, which might be influenced by hormones,[16] could not have interfered with our results, because CCT was a covariate in our linear mixed model. The keratocyte nuclei, a major source of corneal backscatter measured by IVCM, are also unlikely to have caused this difference between the sexes, as keratocyte density has been reported to be sex-independent.[10,17] Another explanation is a potential difference in the stromal extracellular matrix between men and women. This theory is supported by the higher incidence of corneal arcus in men.[18]

In the literature, there is no consensus on the age relatedness of corneal backscatter. In a study using blue light on a modified slit lamp, Olsen[14] found corneal backscatter to increase with age. This finding was disputed by other groups, who used Scheimpflug imaging[19] or white light on a modified slit lamp[20] and found corneal backscatter to be independent of age. Since different wavelengths and scattering angles were used in these studies and because corneal backscatter depends on these factors,[21,22] neither direct comparison of these studies nor comparison with our results is appropriate. The age-related backscatter pattern we found in the corneal stroma (Fig. 2B), can be explained by looking at the age-related morphologic changes. In young adults, backscatter in the stroma is largely composed of backscatter from the keratocyte nuclei. Because the number of keratocyte nuclei decreases with age,[10,17,23] stromal backscatter also decreases in the first five decades of life. In subjects aged 50 years and above, we found an increase in microdots, especially in the anterior third of the stroma (data not shown). This increase of small particles, which may represent dysgenic or apoptotic cellular remnants such as lipofuscin granules,[24,25] probably caused the increase in stromal backscatter.

In contrast with other studies,[14,20] we found corneal backscatter to correlate inversely with CCT. By using a confocal microscope instead of a slit lamp, we incorporated the specular reflection of the corneal endothelium into our backscatter measurements. The specular reflection induced a backscatter peak that slightly increased mean corneal backscatter. This effect of the specular reflection on mean corneal backscatter becomes

larger in a thinner cornea, because in a thinner cornea, backscatter is averaged over fewer images.

To our knowledge, diurnal variation of corneal backscatter has never been studied before. Other well-established cyclic factors such as CCT[26,27] and IOP[28] may have influenced our results. To minimize the effect of overnight swelling of the cornea, we started our measurements at least 2 hours after awakening. Having taken this precaution, in common with many other reports,[16] we found CCT to be stable during working hours. The characteristic diurnal variation of intraocular pressure we found is similar to that reported by others.[28,29] Because the diurnal variation of IOP was exactly opposite to the diurnal variation of corneal backscatter and because these two parameters were highly inversely correlated, it is possible that collinearity occurred. Even though collinearity suggests that the diurnal variation of IOP affected corneal backscatter, the two parameters may still be independent. After excluding light intensity variation and the so-called "learning effect" as confounding factors, a third potentially confounding factor remains. Repeated exposure of the cornea to preservatives in the anesthetic eye drop and the coupling gel may accelerate desquamation of the superficial epithelial cells, subsequently increasing epithelial backscatter.[9] Although we did not observe any such increase of bright superficial epithelial cells during the four measurement sessions, subtle effects of preservatives on corneal backscatter cannot be ruled out.

The repeatability of IVCM backscatter measurement depends on the homogeneity and degree of transparency of the specimen that is examined.[9] When examining a patient, however, the major limiting factor is the motion artifacts in the *z*-axis that occur during the 12 seconds of image acquisition. Consequently, low repeatability was reported for IVCM backscatter measurement in normal corneas: intrasession COR = 8.2 gray levels, intersession COR = 15.5 gray levels (Jalbert I, et al. *IOVS* 2002;43:ARVO E-Abstract 1713). Intersession repeatability was even worse for patients after excimer laser photorefractive keratectomy: COV = 35%.[30] The much higher intra- and intersession repeatability we found (Table 5) by using a *z*-ring adapter for stabilization of the image acquisition cannot be directly compared with the previous reports, as these reports did not calibrate their data sufficiently or examined corneas of different transparency. Our results can be compared with and are similar to calibrated slit lamp based backscatter measurement in normal corneas: COV = 3% to 7%.[14,20] Yet, these modified slit lamps are not commercially available and have a much lower axial and lateral resolution than IVCM. On the other hand, IVCM requires a specially trained optometrist or ophthalmologist to operate the confocal microscope and to assess the morphologic aspects of the corneal layers. Also, the quality of backscatter measurement by IVCM depends largely on the experience of the operator. To reduce interexaminer differences due to the subjective demarcation of the stromal boundaries, we protocolized the backscatter measurements (Appendix, Supplementary S1, http://www.iovs.org/lookup/suppl/doi:10.1167/iovs.11-7747/-/DCSupplemental). Us-

ing this protocol, we found that the posterior stroma was harder to demarcate than the anterior stroma. This resulted in a slightly higher COV for the posterior stroma than for the other backscatter variants.

Our findings imply that IVCM studies on corneal backscatter should account for the effects of sex, age, and time of measurement. For corneal backscatter to be used in ophthalmic practice, however, these effects on corneal backscatter should be contextualized. We suggest that the patient's sex and age be ignored, because their effects on the backscatter variants were smaller than the relative between-subject SDs. When the patient's sex and age are ignored, a generalized normal range for corneal backscatter may be used to detect corneal haze. The mean backscatter values of this normal range (Table 6) are somewhat higher than those reported by McLaren et al.[8] The origin of this disparity remains unclear and exemplifies the importance of a uniform calibration method as well as the need for a universal reference standard that is stable over time.[9]

Diurnal variation affects backscatter analysis only when corneal backscatter is monitored within a patient. Our finding that maximum diurnal variation for corneal backscatter was smaller than the test–retest COV (2.7% versus 5.3%) means that diurnal variation cannot reliably be observed in an individual patient. Nevertheless, diurnal variation should be taken into account when considering improvement or progression of corneal haze. By slightly overestimating the $MDC_{95\%}$, a clinically relevant change in corneal backscatter can still be detected when a follow-up visit is scheduled at a different time as the first visit.

Some issues should be considered before corneal backscatter is applied in ophthalmic practice. Because IVCM uses a magnification up to 500 times, only 0.14% of the corneal surface is imaged.[6] As a result, positional repeatability is low. In our opinion, corneal haze can be monitored with sufficient repeatability only if the central cornea is imaged and if the corneal haze is more or less homogeneous. When these conditions are met, corneal disorders may be monitored by mean corneal backscatter, whereas the other six backscatter variants may be used for specific purposes. For example, backscatter of the basal epithelial cell layer (EV) can be used to assess corneal hydration (Figs. 4A, 4B).[31] The EV may prove more sensitive than CCT in the detection of corneal edema, and therefore may be an important parameter in the evaluation of the cornea in Fuchs endothelial dystrophy, before cataract surgery. Likewise, subepithelial fibrosis in Fuchs endothelial dystrophy may be staged with the SP, to estimate the effect of Descemet stripping automated endothelial keratoplasty (DSAEK) on the postoperative best corrected visual acuity (Figs. 4C, 4D). Mean stromal backscatter and subdivision into anterior, middle, and posterior thirds may be used to monitor the inflammatory process in herpetic stromal keratitis (Figs. 4E, 4F). The powerful combination of corneal backscatter measurement with morphologic assessment of the corneal layers may improve treatment strategies in this complex chronic disease.

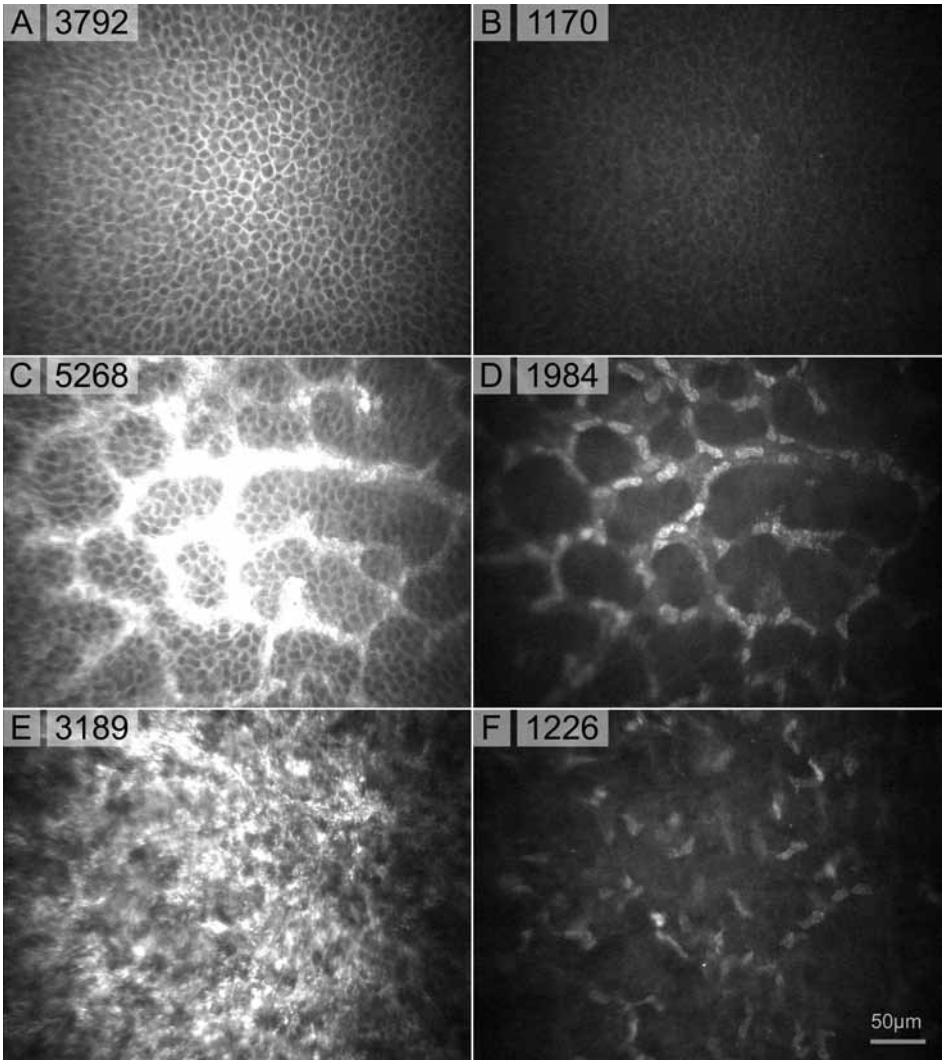

FIGURE 4. Future applications of corneal backscatter measurement. Images are 425 x 320 µm, with the bar representing 50 µm. (**A**, **B**) The EV can be used to objectively assess corneal hydration.[31] (**A**) The EV was 3792 SU in a patient with Fuchs endothelial dystrophy before DSAEK. (**B**) One month after DSAEK, corneal edema had diminished in the same patient: 1170 SU. (**C**, **D**) Subepithelial fibrosis may be assessed with the SP. (**C**) Characteristic reticular meshwork of subepithelial fibrosis in Fuchs endothelial dystrophy. (**D**) Exactly the same location was imaged in the same patient 6 months after DSAEK. The shape of the reticular meshwork had remained completely stable. Nevertheless, the SP declined from 5268 to 1984 SU. (**E**, **F**) Backscatter of the anterior, middle, and posterior parts of the stroma and their overall mean, may be used to monitor the inflammatory process in herpetic stromal keratitis. (**E**) During a recurrence, the stroma of this patient with herpes simplex keratitis showed an increase in backscatter: 3189 SU. (**F**) Mean stromal backscatter had returned to normal in the same patient 1 year after recurrence of the immune stromal keratitis: 1226 SU. All images (**A**–**F**) were acquired with fixed light intensity of 72%, after calibration of backscatter analysis.

In conclusion, this large, normative IVCM database enabled us to identify sex and time of measurement as significant factors in corneal backscatter measurement. Age is a less significant factor, as its influence is confined to backscatter in the anterior stroma. For research purposes, all three factors should be taken into account, whereas for use in ophthalmic practice, we suggest incorporating the effects of sex and age into the normal range for corneal backscatter and accounting for diurnal variation in the definition for improvement or progression of corneal haze. Such a generalized normal range and minimum detectable change for each backscatter variant is easily accessible in a clinical setting. However, before backscatter measurement can be used to detect and monitor pathologic processes in the cornea, further research is needed. Our normative database may serve as a reference for future studies on the clinical value of corneal backscatter measurement by IVCM.

Acknowledgments

The authors thank Sietske Huiskens and Elma Bras (Rotterdam Ophthalmic Institute) for excellent technical assistance, Netty Dorrestijn (Rotterdam Ophthalmic Institute) for organizing the referral of study subjects, and Tom van den Berg (Netherlands Institute for Neuroscience) for his helpful advice and suggestions in the preparation of this manuscript.

REFERENCES

1. Jalbert I, Stapleton F, Papas E, Sweeney DF, Coroneo M. In vivo confocal microscopy of the human cornea. *Br J Ophthalmol*. 2003;87:225–236.
2. Guthoff RF, Zhivov A, Stachs O. In vivo confocal microscopy, an inner vision of the cornea: a major review. *Clin Exp Ophthalmol*. 2009;37:100–117.
3. Niederer RL, McGhee CN. Clinical in vivo confocal microscopy of the human cornea in health and disease. *Prog Retin Eye Res*. 2010;29:30 –58.
4. Erie JC, McLaren JW, Patel SV. Confocal microscopy in ophthalmology. *Am J Ophthalmol*. 2009;148: 639–646.
5. Dhaliwal JS, Kaufman SC, Chiou AG. Current applications of clinical confocal microscopy. *Curr Opin Ophthalmol*. 2007;18:300–307.
6. Hillenaar T, Weenen C, Wubbels RJ, Remeijer L. Endothelial involvement in herpes simplex virus keratitis: an in vivo confocal microscopy study. *Ophthalmology*. 2009;116:2077–2086.
7. Patel SV, McLaren JW, Hodge DO, Bourne WM. Confocal microscopy in vivo in corneas of long-term contact lens wearers. *Invest Ophthalmol Vis Sci*. 2002;43:995–1003.
8. McLaren JW, Bourne WM, Patel SV. Standardization of corneal haze measurement in confocal microscopy. *Invest Ophthalmol Vis Sci*. 2010;51:5610–5616.
9. Hillenaar T, Sicam VA, Vermeer KA, et al. Wide-range calibration of corneal backscatter analysis by in vivo confocal microscopy. *Invest Ophthalmol Vis Sci*. 2011;52:2136–2146.
10. Patel S, McLaren J, Hodge D, Bourne W. Normal human keratocyte density and corneal thickness measurement by using confocal microscopy in vivo. *Invest Ophthalmol Vis Sci*. 2001;42:333–339.
11. Bland JM, Altman DG. Measurement error. *BMJ*. 1996;313:744.
12. Bland JM, Altman DG. Transforming data. *BMJ*. 1996;312:770.
13. Ravaud P, Giraudeau B, Auleley GR, et al. Assessing smallest detectable change over time in continuous structural outcome measures: application to radiological change in knee osteoarthritis. *J Clin Epidemiol*. 1999;52:1225–1230.
14. Olsen T. Light scattering from the human cornea. *Invest Ophthalmol Vis Sci*. 1982;23:81–86.
15. Freund DE, McCally RL, Farrell RA. Effects of fibril orientations on light scattering in the cornea. *J Opt Soc Am A*. 1986;3:1970–1982.
16. Doughty MJ, Zaman ML. Human corneal thickness and its impact on intraocular pressure measures: a review and meta-analysis approach. *Surv Ophthalmol*. 2000;44:367–408.
17. Hollingsworth J, Perez-Gomez I, Mutalib HA, Efron N. A population study of the normal cornea using an in vivo, slit-scanning confocal microscope. *Optom Vis Sci*. 2001;78:706–711.
18. Chua BE, Mitchell P, Wang JJ, Rochtchina E. Corneal arcus and hyperlipidemia: findings from an older population. *Am J Ophthalmol*. 2004;137:363–365.
19. Smith GT, Brown NA, Shun-Shin GA. Light scatter from the central human cornea. *Eye* (*Lond*). 1990;4:584 –588.
20. Patel SV, Winter EJ, McLaren JW, Bourne WM. Objective measurement of backscattered light from the anterior and posterior cornea in vivo. *Invest Ophthalmol Vis Sci*. 2007;48:166–172.
21. Feuk T. The wavelength dependence of scattered light intensity in rabbit corneas. *IEEE Trans Biomed Eng*. 1971;18:92–96.
22. Feuk T, McQueen D. The angular dependence of light scattered from rabbit corneas. *Invest Ophthalmol*. 1971;10:294–299.
23. Møller-Pedersen T. A comparative study of human corneal keratocyte and endothelial cell density during aging. *Cornea*. 1997;16: 333–338.

24. Efron N, Perez-Gomez I, Mutalib HA, Hollingsworth J. Confocal microscopy of the normal human cornea. *Cont Lens Anterior Eye*. 2001;24:16 –24.
25. Faragher RG, Mulholland B, Tuft SJ, Sandeman S, Khaw PT. Aging and the cornea. *Br J Ophthalmol*. 1997;81:814–817.
26. Mandell RB, Fatt I. Thinning of the human cornea on awakening. *Nature*. 1965;208:292–293.
27. Mertz GW. Overnight swelling of the living human cornea. *J Am Optom Assoc*. 1980;51:211–214.
28. de Venecia G, Davis MD. Diurnal variation of intraocular pressure in the normal eye. *Arch Ophthalmol*. 1963;69:752–757.
29. Kotecha A, Crabb DP, Spratt A, Garway-Heath DF. The relationship between diurnal variations in intraocular pressure measurements and central corneal thickness and corneal hysteresis. *Invest Ophthalmol Vis Sci*. 2009;50:4229–4236.
30. Møller-Pedersen T, Vogel M, Li HF, Petroll WM, Cavanagh HD, Jester JV. Quantification of stromal thinning, epithelial thickness, and corneal haze after photorefractive keratectomy using in vivo confocal microscopy. *Ophthalmology*. 1997;104:360–368.
31. Morishige N, Takahashi N, Chikamoto N, Nishida T. Quantitative evaluation of corneal epithelial oedema by confocal microscopy. *Clin Experiment Ophthalmol*. 2009;37:249–253.

Part II

Herpetic keratitis

5

Endothelial involvement in herpes simplex virus keratitis: an in vivo confocal microscopy study

Toine Hillenaar
Christien Weenen
René J. Wubbels
Lies Remeijer

Ophthalmology 2009;116:2077–2086

ABSTRACT

Purpose: To describe the appearance, frequency, and clinical consequences of corneal endothelial involvement in human herpes simplex virus (HSV) keratitis as seen by in vivo confocal microscopy (IVCM).

Design: Prospective observational case series.

Participants: A total of 285 patients with HSV keratitis who visited the cornea department of the Rotterdam Eye Hospital between May 2005 and May 2008. The control groups comprised the unaffected fellow eyes of patients with HSV keratitis, the eyes of 58 healthy volunteers, and the affected eyes of 62 patients with inflammatory corneal disorders other than HSV.

Methods: We examined the eyes of all participants by IVCM and slit-lamp examination. For IVCM, corneas were scanned with Confoscan 3 or 4 (Nidek Technologies, Albignasego, Padova, Italy).

Main outcome measures: All IVCM examinations were qualitatively reviewed for signs of endothelial deviations characteristic of endotheliitis. Endothelial cell density (ECD) was evaluated on the first and last visits of patients who were followed for more than 100 days. The differences in ECDs were calculated and converted to percent ECD change per year.

Results: Endothelial alterations characteristic of endotheliitis were detected by IVCM in 107 of 250 patients with HSV keratitis (43%). These deviations consisted of pseudoguttata, enlarged intercellular gaps, infiltration of inflammatory cells into the endothelial layer, loss of defined cell boundaries, spot-like holes, and endothelial denudation. All of these signs disappeared with appropriate antiviral and anti-inflammatory treatment. However, the endothelium in eyes with endotheliitis-characteristic alterations showed a significant decrease in ECD (10.3% per year) compared with healthy fellow eyes.

Conclusions: IVCM allows earlier detection of endothelial alterations in patients with HSV keratitis compared with slit-lamp examination. Although endotheliitis-specific alterations appear to resolve, the corneal endothelium can become irreversibly damaged.

INTRODUCTION

Herpes simplex virus (HSV) is the most common infectious cause of unilateral blindness in developed countries.[1] HSV keratitis is usually initiated by the cytopathic effect of the virus and may be followed by inflammatory responses, which can affect all layers of the cornea. The ocular sequelae of HSV infections are determined by the frequency and duration of disease recurrence and the immunologic response elicited.[2] The inflammatory response results in cellular infiltration, edema, neovascularization, and corneal scarring as a result of fibrosis and tissue destruction.

A classification scheme for HSV keratitis has been proposed: infectious epithelial keratitis (IEK), neurotrophic keratopathy, herpetic stromal keratitis (HSK), and endotheliitis.[3,4] These clinical manifestations are not mutually exclusive and form a continuum. Isolated corneal endotheliitis is relatively rare. Endotheliitis occurs more often in conjunction with HSK. Until now, slit-lamp examination has been the gold standard for detecting epithelial defects, stromal edema and infiltration, keratic precipitates (KPs), and iritis. However, endotheliitis might go undetected when visualization of the endothelium is hampered by accompanying stromal edema and infiltrates.

It is clinically important to identify endothelial involvement in an opaque or scarred cornea, because secondary neovascularization and scarring can occur as a result of persisting or untreated endothelial inflammation. Chronic endotheliitis can eventually lead to endothelial decompensation and the need for corneal transplantation.

Apart from the standard slit-lamp examination, human corneal endotheliitis can be appreciated by specular microscopy and in vivo confocal microscopy (IVCM). In specular microscopy, the affected endothelium is characterized by transient endothelial changes described as nonreflecting areas.[5,6] In vivo confocal microscopy has the advantage of greater magnification and visualization of the endothelial layer despite corneal opacification. Previously, only animal models were used to study HSV endotheliitis in detail. Subsequent electron microscopy analysis of the endothelium of endotheliitis-affected rabbit corneas revealed cellular edema, enlarged intercellular gaps, spot-like holes, loss of defined cell boundaries, peripheral endothelial denudation, and infiltration of inflammatory cells into the endothelial layer.[7–10] In vivo confocal microscopy allows us to evaluate the presence and variety of endotheliitis in human HSV keratitis. This study is the first to describe the appearance, frequency, and clinical consequences of corneal endothelial involvement in human HSV keratitis as seen by IVCM.

PATIENTS AND METHODS

Study population

We used slit-lamp examination and IVCM to examine both eyes of 285 patients with HSV keratitis, without previous corneal surgery, who visited the Cornea Service of the Rotterdam Eye Hospital between May 2005 and May 2008. Diagnosis of HSV keratitis was based on viral culture, polymerase chain reaction, or clinical history and slit-lamp examination. Thirty-five HSV-affected patients were excluded because of hindered visualization of the endothelium by IVCM (n = 19) and bilateral guttata as part of Fuchs' dystrophy (n = 6) or physiologic guttata (n = 10). The 250 patients who were included were categorized into a group with HSV-affected eyes (Group 1, n = 263) and an internal control group with nonaffected fellow eyes (Group 2, n = 214). In case of bilateral involvement (n = 17), both eyes were assigned to Group 1.

During the same period, the eyes of 58 healthy volunteers (of whom 2 were excluded because of the presence of physiologic guttata) and 62 patients with inflammatory corneal disorders other than HSV were examined by IVCM. The third group comprised both eyes (n = 112) of the 56 healthy volunteers. Group 4 consisted of the affected eyes (n = 68) of patients with inflammatory processes other than HSV. The affected eyes of patients with infectious keratitis (adenoviral, n = 8; bacterial, n = 13; fungal, n = 4; acanthamoeba keratitis, n = 17) and the affected eyes of patients with noninfectious corneal disease (contact lens overwear, n = 10; anterior uveitis, n = 10; corneal graft rejection after penetrating keratoplasty, n = 5; corneal graft rejection after lamellar

Table 1. Characteristics of 657 eyes from 368 subjects examined by in vivo confocal microscopy

	Group 1	**Group 2**	**Group 3**	**Group 4**
	HSV-affected eyes	Fellow eyes	Normal eyes	Other inflammatory disorders
No. of eyes after patient eligibility	267	233	112	68
No. of eyes without IVCM examination	4	19	0	0
No. of eyes included	263	214	112	68
Men, n	154	129	46	36
Women, n	109	85	66	32
Mean age in yrs (range)	51 (18-85)	52 (18-85)	40 (23-77)	40 (18-86)
Right eye, n	140	97	56	27
Left eye, n	123	117	56	41
HSV positive by culture or PCR, n	86	0	0	0

HSV = herpes simplex virus; IVCM = In vivo confocal microscopy; PCR = polymerase chain reaction.

keratoplasty, n = 1) completed this group. Table 1 displays the characteristics of the 4 study groups.

The protocol of this observational case series was approved by the local institutional review board and the medical ethical committee and was performed in accordance with the Declaration of Helsinki. Informed consent was obtained from all subjects.

Slit-lamp examination

All HSV-affected patients underwent a standardized clinical slit-lamp examination (Haag-Streit BQ 900, magnification 40X) by an experienced corneal specialist (LR). On each visit, the level of corneal involvement in HSV-affected eyes (Group 1) was scored according to the classification as proposed by Liesegang[3] and Holland and Schwartz.[4] On slit-lamp examination, the presence of KPs indicated the presence of endothelial involvement. Endothelium with pseudoguttata but without KPs was also scored positive for endothelial involvement.

In vivo confocal microscopy scanning procedure

All subjects were examined by 1 of our 2 medical researchers (TH and CW). The subjects' corneas were viewed by either Confoscan 3, from May 2005 to April 2006, or Confoscan 4, from April 2006 to May 2008 (Nidek Technologies, Albignasego, Padova, Italy). The white light source of both devices was derived from a 100- watt xenon lamp. The observed endothelial area was approximately 425x320 µm, with a 500X magnification and a lateral resolution of 0.6 µm/pixel. In all Confoscan 4 examinations, a *z*-ring and an internal fixation target were used for image stabilization. Before image acquisition, the cornea was anesthetized with 1 drop of 0.4% oxybuprocaine (Ceban BV, Breda, The Netherlands). A drop of Vidisic (Carbomer 2.0 mg/g, Dr. Mann Pharma, Berlin, Germany) on the 40X probe served as an immersion substance. The examination commenced when the central corneal endothelium was correctly aligned and focused. We used the full-thickness scanning mode with a 6-µm scan step during each examination. All examinations provided approximately 15 images of the endothelium. Because of uncontrolled subject movement during the 12 seconds of image acquisition, a single examination might show different endothelial areas of the central cornea.

In vivo confocal microscopy assessment of endothelial involvement

We considered pseudoguttata (cellular edema), enlarged intercellular gaps, spot-like holes, loss of defined cell boundaries, endothelial denudation, and infiltration of inflammatory cells into the endothelial layer, as previously described in animal models,[7–10]

characteristic of endothelial involvement in human HSV keratitis. We reviewed all IVCM examinations of the 4 groups for these signs of endothelial involvement and determined the prevalence of each. Any other features were identified and described.

Subjects were scored positive for endothelial involvement when at least 1 of all IVCM examinations performed contained 1 endothelial image that showed the anomalies mentioned above, with a minimum of 4 affected cell borders or 2 solitary lesions. Despite the presence of KPs, which were scored separately, the endothelium was scored negative for endothelial involvement when characteristic endothelial alterations were absent (Fig 1E, F).

Endothelial cell density measurement

The endothelial cell density (ECD) was determined in all eyes of patients in groups 1, 2, and 3, who were followed for more than 100 days. In our study, 2 different versions of the Confoscan were used. The Confoscan 3 and Confoscan 4 were not mutually calibrated. Therefore, we only analyzed ECD changes of eyes for which a single device was used for both the initial and final examinations. We used a manual counting method with polygonalarea selection to determine the ECD on the first and the last visits. The difference between these ECDs was calculated and converted to percent ECD change per year. A paired Student *t* test was performed for statistical analysis of the difference between the mean ECD of Groups 1 and 2. For statistical analysis of the ECD change, Group 1 was divided into 2 subgroups based on the presence (Group 1A) or absence (Group 1B) of endothelial involvement on IVCM. We used analysis of variance (ANOVA) with Tukey's post hoc test to evaluate differences between Groups 1A, 1B, 2, and 3. To compare the outcomes of slit-lamp examination and IVCM, we evaluated the ECD change when endothelial involvement was detected by either imaging method. Similar statistical analyses (ANOVA with Tukey's post hoc test) were performed.

RESULTS

Qualitative aspects of endothelial involvement in herpes simplex virus keratitis

The endothelial deviations, such as pseudoguttata (cellular edema), enlarged intercellular gaps, infiltration of inflammatory cells into the endothelial layer, loss of defined cell boundaries, spot-like holes, and endothelial denudation, which are considered characteristic of endothelial involvement in human HSV endotheliitis, are shown in Figure 1A to D. In HSV endotheliitis, pseudoguttata resemble true corneal guttata but

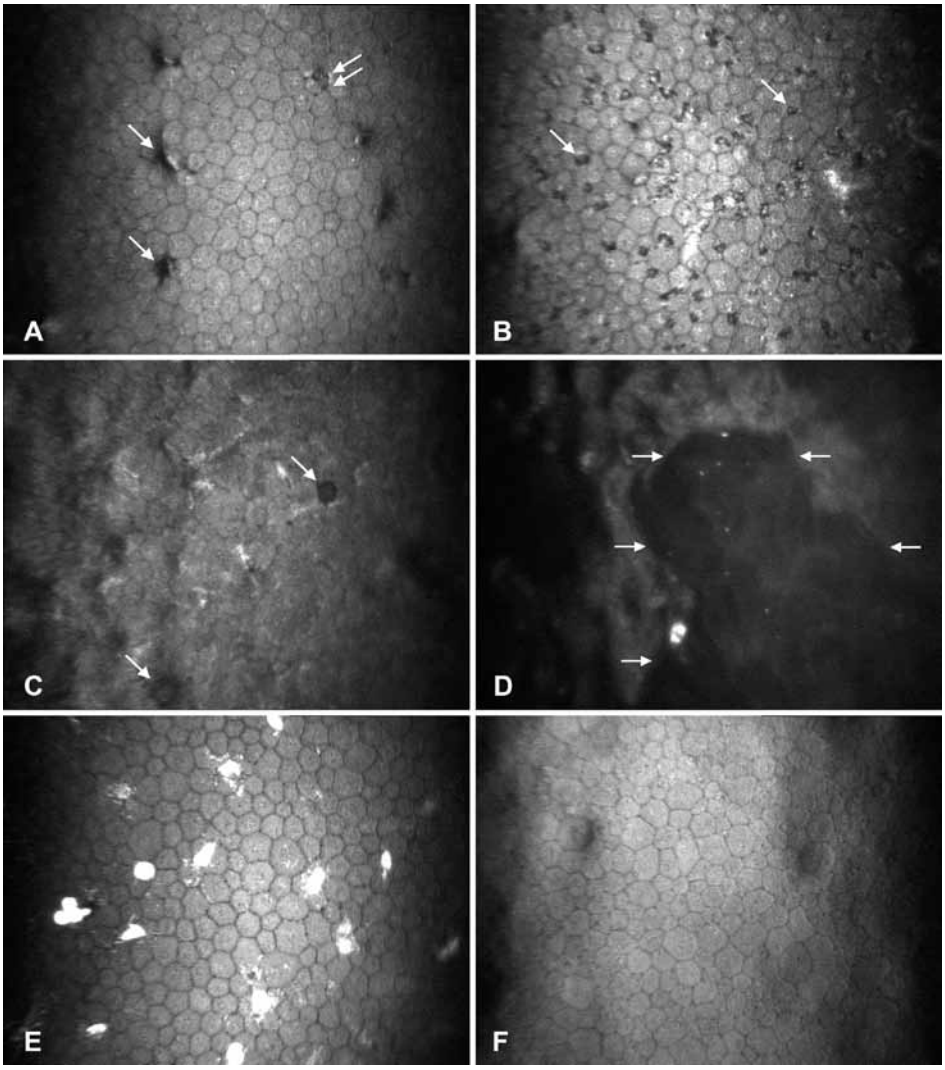

Figure 1. Various alterations characteristic of herpetic endotheliitis were identified using in vivo confocal microscopy (IVCM). **A–D**, Endothelial images scored positive for endotheliitis. **A**, Pseudoguttata (*single arrows*) and intercellular gaps (*double arrows*). **B**, Infiltration of inflammatory cells (*single arrows*). **C**, Pseudoguttata confluencing into a wave-like pattern, less visible cell borders, and spot-like holes (*single arrows*). **D**, Endothelial denudation (between *single arrows*). **E, F**, Endothelial images scored negative for endotheliitis. **E**, Normal endothelium with precipitated pigmented granules. **F**, Endothelium with increased polymegatism and pleomorphism.

are less regularly shaped. Instead of a round white dot in the center, they possess a line of increased reflection on the border of the elevated dark area. Intercellular gaps are characterized by small black dots at the vertices of endothelial cells and by pronounced intercellular borders. Infiltration of inflammatory cells into the endothelial layer was seen

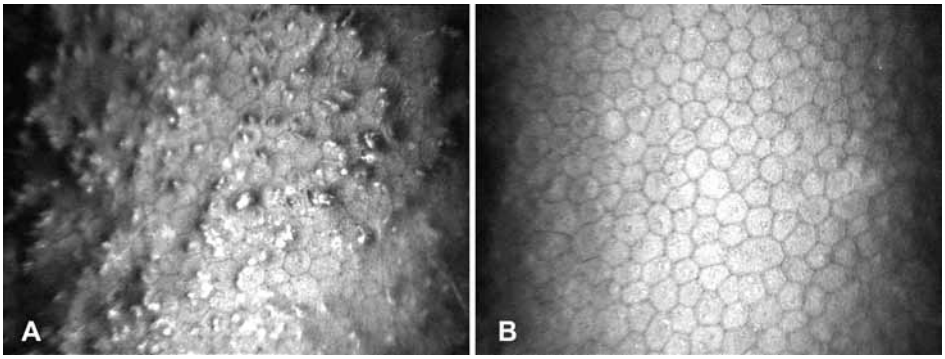

Figure 2. Endotheliitis is a transient phenomenon. **A**, Appearance of endothelial involvement during endotheliitis in a patient with culture-proven herpes simplex virus (HSV) keratitis. **B**, The same patient showed no signs of endotheliitis 3 weeks after initiation of treatment with appropriate antiviral and anti-inflammatory medication.

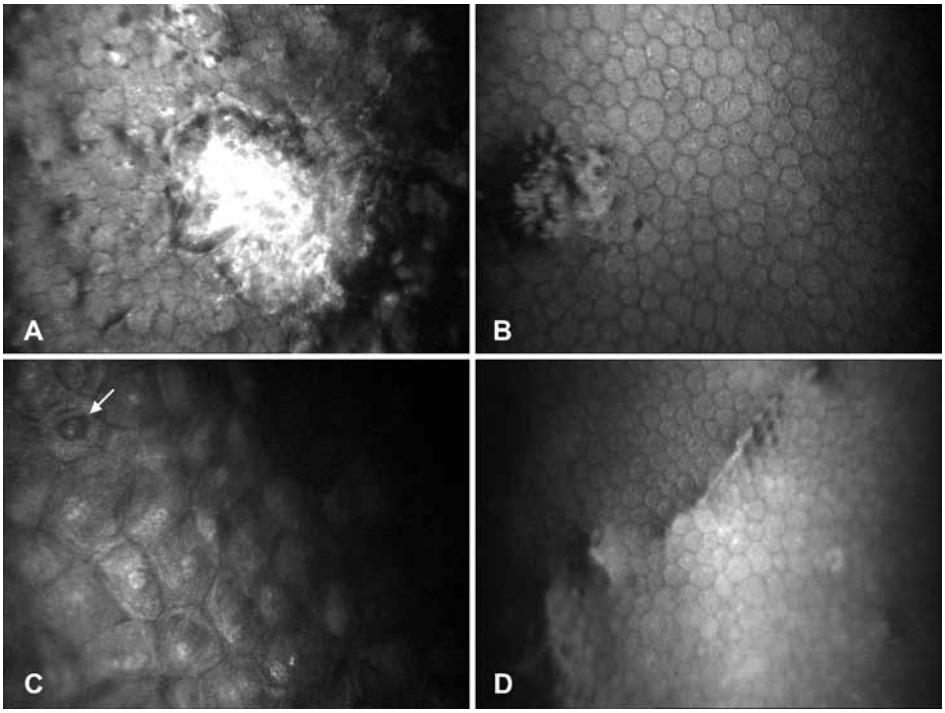

Figure 3. Uncommon endothelial deviations in herpes simplex virus (HSV)-affected eyes observed by in vivo confocal microscopy (IVCM). **A**, Focal rupture of Descemet's membrane with signs of endotheliitis surrounding the lesion. **B**, Cauliflower-shaped lesion. This lesion manifested several weeks after focal rupture of Descemet's membrane. **C**, Endothelial cell with owl's eye morphology (*single arrow*) in between large endothelial cells. **D**, Endothelial ridge.

mainly in patients with keratouveitis. These cells appeared as non-elevated grayish/black structures, approximately 13 µm in diameter. With few exceptions, these structures adhered to endothelial cell borders. Spot-like holes appeared as dark, round defects in the endothelial layer, with the diameter of 1 endothelial cell (~20 µm), whereas endothelial denudation consisted of larger areas (>50 µm) with similar dark appearance. Except for endothelial denudation, all of these characteristic alterations disappeared within 1 to 3 weeks on the condition that appropriate antiviral and anti-inflammatory treatments were prescribed (Fig 2).

In addition to these known alterations, other less common lesions were identified (Fig 3). Two patients presented with a focal rupture of Descemet's membrane with signs of endotheliitis surrounding the lesion. The focal rupture resulted in a cauliflowershaped lesion after several weeks. This deviation appeared as a glassy KP on slit-lamp examination. Endothelial cells with owl's eye morphology were observed in 1 patient. The cells appeared in between large endothelial cells, and these alterations were permanent by nature. Endothelial ridges were seen in 5 patients, mostly when stromal loss was present. The ridges were constant in position and shape during follow-up.

Quantitative aspects of endothelial involvement in herpes simplex virus keratitis

Presentation as determined by slit-lamp examination versus in vivo confocal microscopy

Endothelial involvement was detected by IVCM in 107 HSV-affected patients (43%). Neither the fellow eyes (Group 2) nor the eyes of healthy volunteers (Group 3) showed the characteristic endothelial deviations described previously.

Of all patients who showed endothelial involvement on IVCM, the most prevalent alteration was pseudoguttata (81%), followed by enlarged intercellular gaps (69%), infiltration of inflammatory cells into the endothelial layer (47%), loss of defined cell boundaries (29%), spot-like holes (6%), and endothelial denudation (6%). Combinations of these anomalies in a given patient did occur.

Table 2 summarizes slit-lamp and IVCM findings of all HSV-affected eyes (Group 1) during 846 visits. All clinical categories observed in HSV keratitis were accompanied by endothelial involvement in at least 21% of all visits. There was agreement between the findings of both imaging modalities in only 80 (33%) of 240 visits in which endothelial alterations were detected (Fig 4). In contrast, detection of KPs was equally balanced between both imaging methods.

Endothelial cell density

Mean ECDs were compared between HSV-affected eyes (Group 1) and fellow eyes (Group 2). Group 1 showed a mean ECD±standard deviation of 2404±601 cells/mm^2

Table 2. Clinical observations by slit-lamp examination and in vivo confocal microscopy of herpes simplex virus-affected eyes (Group1) per visit.

		Slit-lamp examination		In vivo confocal microscopy	
	Total visits	E+	KP	E+	KP
Category	n	n (%)	n (%)	n (%)	n (%)
No visible deviations	34	0 (0)	0 (0)	0 (0)	0 (0)
Infectious epithelial keratitis	31	0 (0)	0 (0)	8 (26)	4 (13)
Immune stromal keratitis	618	91 (15)	75 (12)	138 (22)	78 (13)
Necrotizing stromal keratitis	144	21 (15)	21 (15)	30 (21)	27 (19)
Isolated endotheliitis	3	3 (100)	2 (67)	2 (67)	2 (67)
Keratouveitis	16	12 (75)	13 (81)	15 (94)	8 (50)
Total	846	127 (15)	111 (13)	193 (23)	119 (14)

E+ = positive for endothelial involvement; KP = keratic precipitates; (%) = percentage of visits per category.

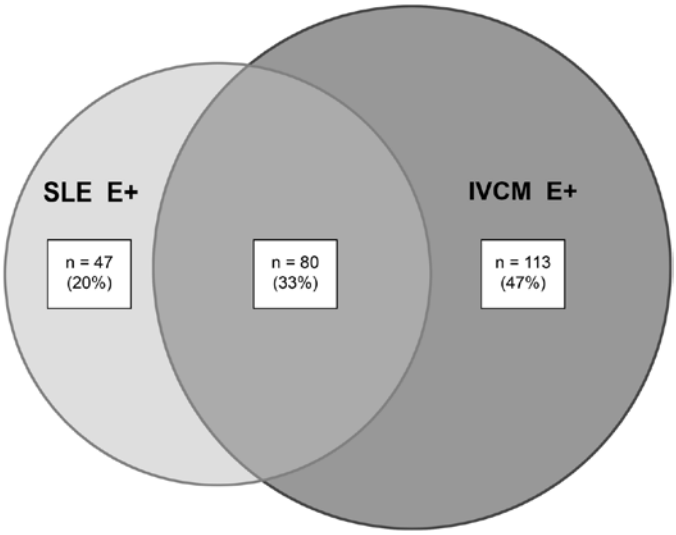

Figure 4. Distribution of 240 visits in which endothelial involvement was detected by slit-lamp examination or in vivo confocal microscopy (IVCM). IVCM E+ = endothelial involvement by in vivo confocal microscopy; n = number of visits; SLE E+ = endothelial involvement by slit-lamp examination.

versus 2694±410 cells/mm^2 in Group 2. The difference between these 2 groups was highly statistically significant ($P<10^{-9}$, paired Student *t* test). The characteristic endothelial changes present in Group 1A seemed to disappear completely, leaving no trace of endotheliitis. However, in this group, the ECD showed a mean decrease of 201±390 cells/mm^2 between the first and the last visits (Table 3). There was a highly statistically significant difference in ECD change when Group 1A was compared with the 3 other groups ($P<10^{-4}$, ANOVA with Tukey's post hoc test). In contrast, the ECD change in Group 1B did not differ significantly from that of the fellow eyes and the eyes of healthy volunteers.

Table 3. Effect of endothelial involvement on endothelial cell density as demonstrated by in vivo confocal microscopy

	Group 1A	Group 1B	Group 2	Group 3
	HSV+ / E+	HSV+ / E–	Fellow eyes	Normal eyes
Sample size, n	51	74	72	48
ECD_F (cells/mm^2)	2547 ± 531	2449 ± 542	2704 ± 384	2680 ± 329
ECD_L (cells/mm^2)	2346 ± 588	2411 ± 539	2685 ± 386	2645 ± 332
Datedif (d)	313 ± 164	326 ± 186	318 ± 150	281 ± 13
ΔECD (cells/mm^2)	–201[a] ± 390	–38 ± 181	–19 ± 149	–34 ± 132
%ΔECD/Y (%)	–10.3[b] ± 22.3	–1.2 ± 12.7	–0.9 ± 8.4	–1.5 ± 6.2

E+ = positive for endothelial involvement; E– = negative for endothelial involvement; n = number of eyes followed for >100 days, with the same IVCM device; ECD_F = ECD on first visit; ECD_L = ECD on last visit; datedif = difference between first and last visit; ΔECD = ECD change; %ΔECD/Y = percent ECD change per year; ECD = endothelial cell density; HSV+ = herpes simplex virus affected eyes; IVCM = in vivo confocal microscopy.

Values are mean ± standard deviation.

[a] $P < 0.0001$ (ANOVA, Tukey's post hoc test) compared to Groups 1B, 2, and 3.

[b] $P < 0.001$ (ANOVA, Tukey's post hoc test) compared to Groups 1B, 2, and 3.

When the ECD change was converted to percent ECD change per year, the difference between Group 1A and Group 1B remained statistically significant ($P<0.001$, ANOVA with Tukey's post hoc test). Again, the percent ECD change per year in HSV-affected eyes without endothelial involvement was statistically the same as that of the eyes in Groups 2 and 3.

The effect of endothelial involvement on the ECD was compared between the 2 imaging methods (Table 4). For ECD change and percent ECD change per year, varia-

Table 4. Effect of endothelial involvement on endothelial cell density in herpes simplex virus-affected eyes: slit-lamp examination versus in vivo confocal microscopy

	SLE E+ / IVCM E–	SLE E+ / IVCM E+	SLE E– / IVCM E+
Sample size, n	8	30	21
ECD_F (cells/mm^2)	2251 ± 319	2522 ± 597	2583 ± 431
ECD_L (cells/mm^2)	2280 ± 267	2281 ± 644	2439 ± 497
Datedif (d)	347 ± 269	332 ± 178	287 ± 142
ΔECD (cells/mm^2)	29 ± 116	–241 ± 483	–144 ± 190
%ΔECD/Y (%)	3.9 ± 8.2	–10.8 ± 25.8	–9.4 ± 16.9

E+ = positive for endothelial involvement; E– = negative for endothelial involvement; n = number of eyes followed for >100 days with the same IVCM device; ECD_F = ECD on first visit; ECD_L = ECD on last visit; Datedif = difference between first and last visit; ΔECD = ECD change between first and last visit; %ΔECD/Y = percent ECD change per year; ECD = endothelial cell density; IVCM = in vivo confocal microscopy; SLE = slit-lamp examination.

Values are mean ± standard deviation.

tion among the groups was statistically significant ($P = 0.01$ and $P<0.05$, respectively; ANOVA). However, Tukey's post hoc test did not show a clear separation between the groups.

Specificity of endothelial involvement

Pseudoguttata (cellular edema), enlarged intercellular gaps, and infiltration of inflammatory cells into the endothelial layer were also observed in patients with non-HSV infectious keratitis, including adenoviral, bacterial, fungal, and acanthamoeba keratitis (Fig 5, available at http://aaojournal.org) and in some noninfectious inflammatory processes, including anterior uveitis and corneal graft rejection in penetrating and lamellar keratoplasty (Fig 6, available at http://aaojournal.org). Except for adenoviral keratitis, which displayed a more reserved endothelial reaction, loss of defined cell boundaries was observed in all forms of infectious keratitis. Spot-like holes and endothelial denudation

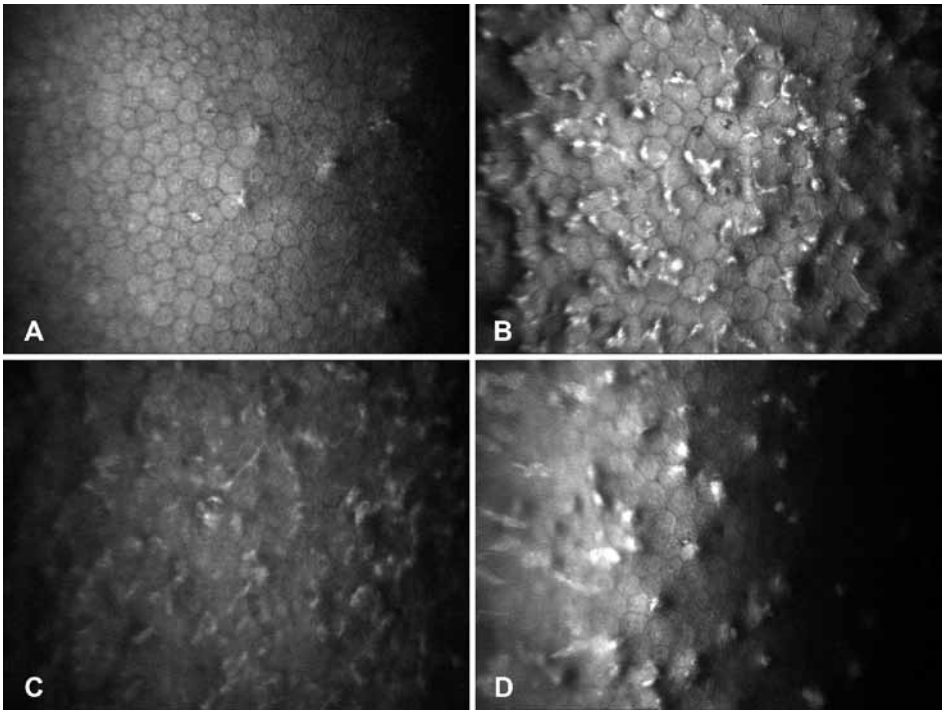

Figure 5. Endothelial involvement in different infectious corneal disorders, all of which were confirmed by culture. **A**, Pseudoguttata in a patient with adenoviral keratitis. **B**, Endothelial involvement in a patient with *Pseudomonas aeruginosa* keratitis. **C**, Endothelial involvement in a patient with *Aspergillus fumigatus* keratitis. **D**, Endothelial involvement in a patient with acanthamoeba keratitis. At the right side of this image, a few keratocyte nuclei are visible because of the slightly oblique cross-sectional view. Severe photophobia in these patients often hindered acquisition of clear perpendicular endothelial images.

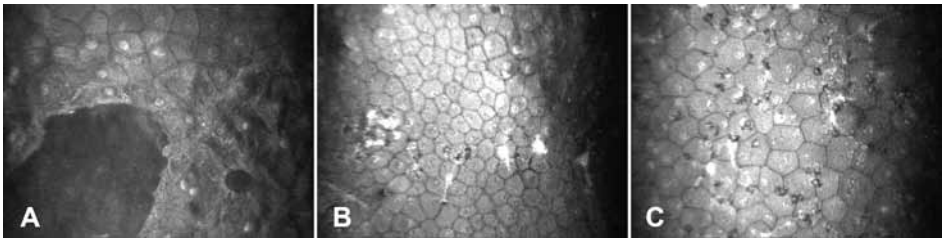

Figure 6. Endothelial involvement in noninfectious inflammatory corneal disorders. **A**, Endothelial involvement in a patient during corneal graft rejection. The endothelium showed a large, sharply demarcated area with endothelial denudation and a spot-like hole. **B**, Endothelial involvement in a posterior lamellar graft during the rejection process. Pseudoguttata, enlarged intercellular borders, and infiltration of inflammatory cells disappeared within 1 week of increased steroid therapy. **C**, Endothelial involvement in granulomatous uveitis secondary to sarcoidosis. Similar to herpes simplex virus (HSV) keratouveitis, infiltration of inflammatory cells was the most frequent alteration during endothelial involvement in patients with uveitis.

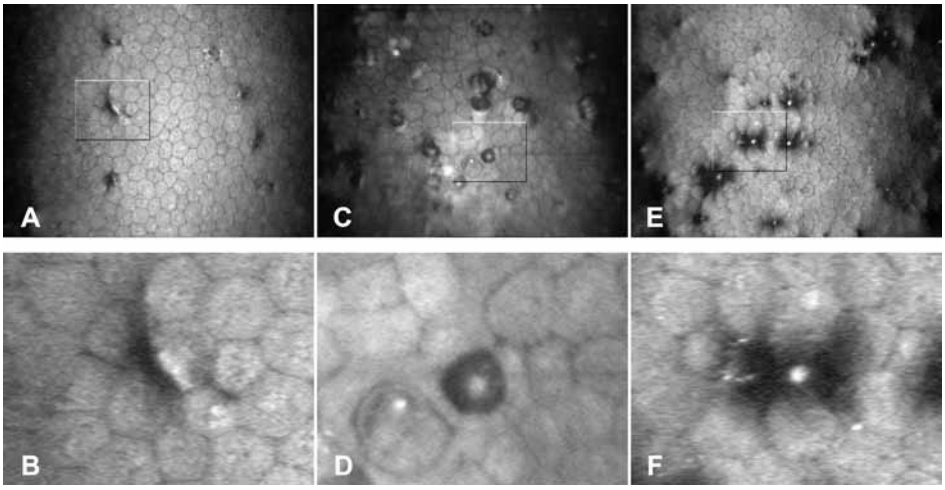

Figure 7. Differences between pseudoguttata in herpetic endotheliitis, endothelial blebs after contactlens overwear, and guttata as part of Fuchs' dystrophy. **A**, Pseudoguttata in herpetic endotheliitis. **B**, Enlarged image of the boxed pseudoguttae in Figure 7A. This deviation is characterized by an elevated dark area with a line of increased reflection on the border. **C**, Endothelial blebs after contactlens overwear. **D**, Enlarged image of the boxed endothelial bleb in Figure 7C. In contrast with pseudoguttata, this elevated dark area was sharply delineated with a round white dot in the center. **E**, Guttata as part of Fuchs' endothelial dystrophy. **F**, Enlarged image of the boxed guttate lesion in Figure 7E. Similar to pseudoguttata, this deviation consisted of an elevated dark area with a blurred border; however, this guttate lesion has a round white dot in the center. The differences are clearly visible in these sharp images; however, in practice, distinguishing between these 3 endothelial deviations is often impossible. Bilateralism and the resolution of the deviations within a few days or weeks are parameters that support the differentiation.

were only observed in patients with corneal graft rejection. Infiltration of inflammatory cells into the endothelial layer was the most distinct alteration of endothelial involvement in anterior uveitis. However, differentiation between infectious and noninfectious causes of endothelial involvement based on the appearance of the endothelium was not possible. Endothelial alterations due to contact lens overwear appeared different from all endothelial deviations described previously (Fig 7). These endothelial blebs disappeared within a few days without treatment.

DISCUSSION

This is the first study to describe in detail the endothelial deviations in human HSV-affected eyes as observed by IVCM. Until now, these types of deviations were only detectable by electron microscopy in ex vivo animal experiments.[7–10] We closely monitored the development and resolution of endotheliitis with high-resolution images in a large group of patients. Significant endothelial cell loss occurred not only when the endothelial changes were detectable by slit-lamp examination but also when they were visible only on IVCM. These findings influence both the perception of the inflammatory process and the therapy for patients with HSK.

As a result of the higher resolution (500X), IVCM enabled the detection of relatively common alterations, such as pseudoguttata, enlarged intercellular gaps, infiltration of inflammatory cells into the endothelial layer, loss of defined cell boundaries, spot-like holes, and endothelial denudation. Except for pseudoguttata, these alterations were undetectable by slit-lamp examination (40X). Different processes are responsible for the appearances of these endothelial alterations. Transient cellular edema causes endothelial cell bodies to swell, mimicking corneal guttata, thus the term "pseudoguttata."[11] Intra- and intercellular edema are also thought to cause less-pronounced cell borders and the opening up of intercellular junctions.[8,12] The appearance of a spot-like hole could be explained by the sloughing of a single endothelial cell. When a larger area lacked endothelial cells, we considered this endothelial denudation. The inflammatory cells that infiltrated the endothelial layer consisted of mononuclear leucocytes and to a lesser extent polymorphonuclear cells, as has been shown in animal experiments.[7,13,14] We consider these 6 common alterations characteristic of corneal endotheliitis.

In addition to these common alterations, some rare lesions were observed. In 2 patients, a breakthrough in Descemet's membrane, caused by a granulomatous reaction,[15,16] occurred. Endothelial cells with owl's eye morphology, considered to be pathognomonic for cytomegalovirus infection,[17–19] were seen in a patient with culture-proven HSV keratitis and in 3 patients with longstanding corneal grafts (Fig 8, available at http://aaojournal.org). These cells might occur as a result of a coinfection with cytomegalo-

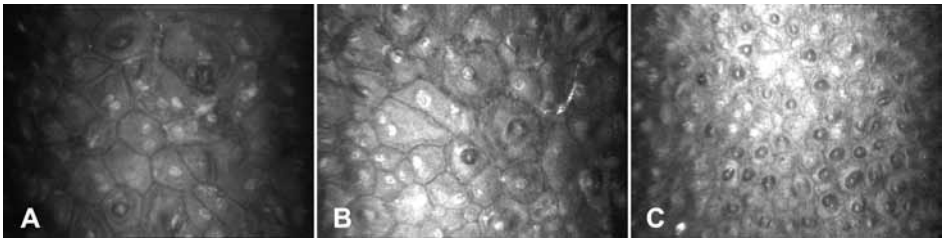

Figure 8. Endothelial cells with owl's eye morphology in 3 patients with penetrating corneal grafts, without known cytomegalovirus or herpes simplex virus (HSV) infection. **A**, Nine years after transplantation. **B**, Thirty-five years after transplantation. **C**, Multiple endothelial cells with owl's eye morphology in a corneal graft 37 years after surgery. This owl's eye appearance is probably caused by the shape of the endothelial cells. These cells were enlarged and possessed large nuclei that appeared to be raised above endothelial cell level. Because of the confocal technique, these "mounts" appeared as highly reflective dots in the center surrounded by a halo of low reflection. In contrast with guttata, pseudoguttata, and endothelial blebs, the "owl's eye" is always confined to a single endothelial cell.

virus or it could be that the diagnostic range in which these cells are seen needs to be extended. Endothelial ridges (n = 5) were seen in severely diseased corneas. We believe that fibrosis on the level of Descemet's membrane caused the endothelium to form these ridges. Because of the permanent nature of these 3 rare lesions, we consider these deviations part of the noninflammatory healing process of the cornea.

In the literature, different terminology is used to describe endothelial involvement in HSV keratitis. The term "disciform keratitis"[8,20] is used to describe a discus-like stromal infiltrate in HSK, with and without endothelial involvement, as well as for a centrally located endotheliitis with secondary corneal edema. Terms such as "herpetic endotheliitis,"[3,4,7] "transient endothelial changes,"[5,6] and "pseudoguttata"[11] are used to describe endothelial changes alone. With this in mind, the incidence of disciform keratitis, corneal endotheliitis, and pseudoguttata was reported to be 4% to 30% among patients with ocular HSV infection,[21,22] 3.4% in eyes with HSV keratitis,[23] and 1.1% in a general patient population.[24] In our study, the frequency of endothelial involvement determined by both slit-lamp and IVCM was much higher (28% and 43%, respectively). Pseudoguttata could be detected by IVCM in 35% of all HSV-affected patients. In addition to the confusing nomenclature and the differences among the patient groups, this higher frequency can be attributed to the increased sensitivity of IVCM compared with slit-lamp examination for detecting endothelial alterations.

All different clinical presentations observed in HSV keratitis were accompanied by endothelial involvement in at least 21% of all visits (Table 2). In the disease spectrum of an HSV infection, IEK is considered as isolated epithelial involvement,[3,4] and treatment is only directed at viral replication.[25] In our study, endothelial involvement was detected by IVCM in 26% of all visits with isolated IEK, whereas none of these eyes showed endothelial involvement by slit-lamp examination. To reduce endothelial cell loss in these cases,

one might consider application of topical corticosteroids. However, in our opinion, the increased risk of viral spread into the stroma[26] precludes this therapeutic intervention. New insights into the exact origin of these endothelial alterations might provide a solution for this dilemma.

Stromal disease is responsible for 30% to 49% of recurrent ocular HSV keratitis.[22,23,27–29] We found stromal involvement in 90% of all visits in patients with HSV keratitis. Two main factors may explain this difference: (1) All patients visited the Cornea Service in the Rotterdam Eye Hospital, which is a tertiary referral center; therefore, our study population was biased toward patients with more severely diseased corneas. (2) Accompanying subepithelial infiltration during IEK and "ghost scars" that remained after resolution of epithelial defects were scored as stromal involvement.

There was a large discrepancy in the detection of endothelial involvement between the 2 imaging methods. IVCM has the advantage of higher resolution and the ability to observe the endothelium in the presence of stromal opacification. With this increased sensitivity and because endothelial deviations often preceded KP formation, we were able to detect endothelial involvement by IVCM before endotheliitis became apparent by slit-lamp examination. The central cornea was involved in the majority of patients with HSV endotheliitis (80%). In less than 20%, a peripheral focal process occurred without central endothelial changes. Peripheral endothelial involvement will often be missed by IVCM because only 0.14% of the total corneal surface is examined. Therefore, although endothelial alterations can be detected earlier and more frequently by IVCM, slit-lamp examination remains fundamental for detecting endothelial involvement in the corneal periphery.

The central ECD in eyes with herpetic keratouveitis, measured by specular microscopy, is reported to be 12% to 19% lower than in healthy fellow eyes.[6,30,31] In eyes with disciform keratitis, a similar decrease in ECD is to be expected.[32] However, specular microscopy did not show a difference in ECD between eyes with disciform keratitis and healthy fellow eyes.[30] This latter finding contrasts with our finding of an 11% lower ECD in eyes with HSV keratitis. One of the major disadvantages of specular microscopy is that visualization of the endothelium is often difficult in the presence of stromal infiltrate or edema.[10] To avoid this problem, Hirose et al[30] photographed the areas adjacent to the opacification within a 3- to 4-mm diameter of the central cornea. This can confound the results when trying to measure the central ECD. The central ECD may be lower because of endothelial involvement behind the area of stromal infiltration or edema.

The follow-up period among subjects in our study was not consistent, and error could have been introduced when ECD change was converted to ECD change per year. Therefore, we first performed statistical analysis on the ECD change before analyzing the converted data. These nonsynchronized data showed strong statistical differences between HSV-affected eyes with endothelial alterations (Group 1A) and the other 3

groups (Groups 1B, 2, and 3), suggesting that differences in the follow-up period between groups did not confound the results. The decrease in ECD of normal corneas with increasing age varies from 0.2% to 2.8% per year,[33–35] which corresponds with our findings for HSV-affected eyes without endothelial involvement (Group 1B), non-affected fellow eyes (Group 2), and normal eyes of healthy volunteers (Group 3).

We compared both imaging methods with respect to the effect of endothelial involvement on the central ECD. Endothelial cell loss in HSV endotheliitis is not an unexpected finding. However, the trend that absolute and relative ECD change showed a stronger relationship with endothelial deviations detected by IVCM than by slit-lamp examination is remarkable (Table 4). The relatively small sample size and the large variance of the data prevent statistically significant statements in this regard; nevertheless, endothelial involvement as detected by IVCM contributed to endothelial cell loss, whereas these lesions often go undetected by slit-lamp examination.

Current treatment for patients with HSK consists of topical and oral antiviral treatment combined with topical corticosteroids.[36–38] The efficacy of topical corticosteroids was demonstrated by the Herpetic Eye Disease Study.[38] Delaying the initiation of corticosteroid treatment did not affect the eventual outcome of the disease at 6 months. However, the effects of treatment on ECD were not monitored in the Herpetic Eye Disease Study. Our data suggest that postponing instillation of steroids may have long-term detrimental effects on ECD.

As stromal edema and infiltration clear, the steroid dosage is tapered. However, inflammation can recur during this process. Monitoring endothelial involvement by IVCM could provide better guidance for phasing out corticosteroid therapy. Another important potential application of IVCM is screening for endothelial involvement in patients with presumed quiescent HSK before lamellar surgery. Postponing surgery until endothelial deviations subside might reduce the rapid recurrence of HSV infection in the lamellar graft.

The endothelial deviations as shown in Figure 1A to D proved to be nonspecific for HSV infection of the cornea. Other infectious and noninfectious inflammatory modalities, of which some have been described by the use of slit-lamp examination or specular microscopy,[24,39–41] showed similar alterations. Therefore, these endothelial changes cannot be seen as diagnostic for endothelial HSV infection. However, endothelial involvement as observed by IVCM may provide an excellent means for monitoring inflammatory activity in different kinds of keratitis.

In conclusion, we have demonstrated that in inflammatory processes the human corneal endothelium can be studied in high detail by IVCM. Our data show that IVCM allows early detection of treatable endothelial alterations in HSV keratitis that are not discernible by slit-lamp examination. Monitoring endothelial involvement and the consequent therapeutic adjustments might reduce the associated irreversible endothelial cell loss.

REFERENCES

1. Dawson CR, Togni B. Herpes simplex eye infections: clinical manifestations, pathogenesis and management. Surv Ophthalmol 1976;21:121–35.
2. Remeijer L, Osterhaus A, Verjans G. Human herpes simplex virus keratitis: the pathogenesis revisited. Ocul Immunol Inflamm 2004;12:255– 85.
3. Liesegang TJ. Classification of herpes simplex virus keratitis and anterior uveitis. Cornea 1999;18: 127– 43.
4. Holland EJ, Schwartz GS. Classification of herpes simplex virus keratitis. Cornea 1999;18:144 –54.
5. Vannas A, Ahonen R. Herpetic endothelial keratitis: a case report. Acta Ophthalmol (Copenh) 1981;59:296 –301.
6. Vannas A, Ahonen R, Makitie J. Corneal endothelium in herpetic keratouveitis. Arch Ophthalmol 1983;101:913–5.
7. Zheng X, Yamaguchi M, Goto T, et al. Experimental corneal endotheliitis in rabbit. Invest Ophthalmol Vis Sci 2000;41: 377–85.
8. Nagy RM, McFall RC, Sery TW, et al. Scanning electron microscope study of herpes simplex virus experimental disciform keratitis. Br J Ophthalmol 1978;62:838–42.
9. Oh JO. Endothelial lesions of rabbit cornea produced by herpes simplex virus. Invest Ophthalmol 1970;9:196 –205.
10. O'Brien WJ, Guy J, Taylor JL. Pathogenesis of corneal oedema associated with herpetic eye disease. Br J Ophthalmol 1990;74:723–30.
11. Krachmer JH, Schnitzer JI, Fratkin J. Cornea pseudoguttata: a clinical and histopathologic description of endothelial cell edema. Arch Ophthalmol 1981;99:1377– 81.
12. Slezak H, Grabner G, Stur M. Cornea pseudoguttata [in German]. Klin Monatsbl Augenheilkd 1983; 182:7–9.
13. Sery TW, Nagy RM. Cellular reaction in experimental herpetic disciform keratitis. Am J Ophthalmol 1977;84:675– 80.
14. Trinh L, Brignole-Baudouin F, Labbe A, et al. The corneal endothelium in an endotoxin-induced uveitis model: correlation between in vivo confocal microscopy and immunohistochemistry. Mol Vis [serial online] 2008;14:1149 –56. Available at: http://www.molvis.org/molvis/v14/a136/. Accessed March 13, 2009.
15. Holbach LM, Font RL, Naumann GO. Herpes simplex stromal and endothelial keratitis: granulomatous cell reactions at the level of Descemet's membrane, the stroma, and Bowman's layer. Ophthalmology 1990;97:722– 8.
16. Verjans GM, Remeijer L, Mooy CM, Osterhaus AD. Herpes simplex virus-specific T cells infiltrate the cornea of patients with herpetic stromal keratitis: no evidence for autoreactive T cells. Invest Ophthalmol Vis Sci 2000;41:2607–12.
17. Shiraishi A, Hara Y, Takahashi M, et al. Demonstration of "owl's eye" morphology by confocal microscopy in a patient with presumed cytomegalovirus corneal endotheliitis. Am J Ophthalmol 2007;143:715–7.
18. Koizumi N, Suzuki T, Uno T, et al. Cytomegalovirus as an etiologic factor in corneal endotheliitis. Ophthalmology 2008; 115:292–7.
19. Chee SP, Bacsal K, Jap A, et al. Corneal endotheliitis associated with evidence of cytomegalovirus infection. Ophthalmology 2007;114:798–803.

20. Sundmacher R, Neumann-Haefelin D. Herpes simplex virus isolations from the aqueous humor of patients suffering from focal iritis, endotheliitis, and prolonged disciform keratitis with glaucoma [in German]. Klin Monatsbl Augenheilkd 1979;175:488 –501.
21. Liesegang TJ. Epidemiology of ocular herpes simplex: natural history in Rochester, Minn, 1950 through 1982. Arch Ophthalmol 1989;107:1160 –5.
22. Hogan MJ, Kimura SJ, Thygeson P. Observations on herpetic keratitis and keratoconjunctivitis. AMA Arch Ophthalmol 1956;56:375– 88.
23. Uchio E, Hatano H, Mitsui K, et al. A retrospective study of herpes simplex keratitis over the last 30 years. Jpn J Ophthalmol 1994;38:196 –201.
24. Nakashima Y, Yoshitomi F, Oshika T. Clinical evaluation of cornea pseudoguttata. Br J Ophthalmol 2007;91:22–5.
25. Wilhelmus KR. Therapeutic interventions for herpes simplex virus epithelial keratitis. Cochrane Database Syst Rev 2008; (1):D002898.
26. Nasisse MP, Guy JS, Davidson MG, et al. Experimental ocular herpesvirus infection in the cat: sites of virus replication, clinical features and effects of corticosteroid administration. Invest Ophthalmol Vis Sci 1989;30:1758–68.
27. Norn MS. Dendritic (herpetic) keratitis. I. Incidence—seasonal variations—recurrence rate—visual impairment—therapy. Acta Ophthalmol (Copenh) 1970;48:91–107.
28. Whitcher JP, Dawson CR, Hoshiwara I, et al. Herpes simplex keratitis in a developing country: natural history and treatment of epithelial ulcers in Tunisia. Arch Ophthalmol 1976;94:587–92.
29. Labetoulle M, Auquier P, Conrad H, et al. Incidence of herpes simplex virus keratitis in France. Ophthalmology 2005;112: 888–95.
30. Hirose N, Shimomura Y, Matsuda M, et al. Corneal endothelial changes associated with herpetic stromal keratitis. Jpn J Ophthalmol 1988;32:14 –20.
31. Ahonen R, Vannas A. Clinical comparison between herpes simplex and herpes zoster ocular infections. In: Maudgal PC, Missotten L, eds. Herpetic Eye Diseases: Proceedings of the International Symposium at the Katholieke Universiteit Leuven. Dordrecht: Junk; 1985:389 –94. Documenta ophthalmologica. Proceedings series. vol. 44.
32. Sundmacher R. A clinico-virologic classification of herpetic anterior segment diseases with special reference to intraocular herpes. In: Sundmacher R, ed. Herpetische Augenerkrangen. München, Germany: JF Bergmann; 1981:202–10.
33. Bourne WM, Nelson LR, Hodge DO. Central corneal endothelial cell changes over a ten-year period. Invest Ophthalmol Vis Sci 1997;38:779–82.
34. Yee RW, Matsuda M, Schultz RO, Edelhauser HF. Changes in the normal corneal endothelial cellular pattern as a function of age. Curr Eye Res 1985;4:671– 8.
35. Doughty MJ, Muller A, Zaman ML. Assessment of the reliability of human corneal endothelial cell-density estimates using a noncontact specular microscope. Cornea 2000;19: 148–58.
36. Barron BA, Gee L, Hauck WW, et al. Herpetic Eye Disease Study: a controlled trial of oral acyclovir for herpes simplex stromal keratitis. Ophthalmology 1994;101:1871– 82.
37. Herpetic Eye Disease Study Group. Acyclovir for the prevention of recurrent herpes simplex virus eye disease. N Engl J Med 1998;339:300–6.
38. Wilhelmus KR, Gee L, Hauck WW, et al. Herpetic Eye Disease Study: a controlled trial of topical corticosteroids for herpes simplex stromal keratitis. Ophthalmology 1994;101: 1883–95.
39. Sundmacher R. Corneal endotheliitis: definition and clinical classification [in German]. Klin Monatsbl Augenheilkd 1984; 184:163–7.

40. Zantos SG, Holden BA. Transient endothelial changes soon after wearing soft contact lenses. Am J Optom Physiol Opt 1977;54:856–8.
41. Olsen T. Changes in the corneal endothelium after acute anterior uveitis as seen with the specular microscope. Acta Ophthalmol (Copenh) 1980;58:250–6.

6

Monitoring the inflammatory process in herpetic stromal keratitis: the role of in vivo confocal microscopy

Toine Hillenaar
Hugo van Cleynenbreugel
Georges M.G.M. Verjans
René J. Wubbels
Lies Remeijer

Ophthalmology 2012;119:1102-1110

ABSTRACT

Purpose: To investigate the role of in vivo confocal microscopy (IVCM) in the detection of inflammatory activity and follow-up of herpetic stromal keratitis (HSK).

Design: Prospective observational cohort study.

Participants: Thirty-eight patients with active HSK.

Methods: Within 7 days after diagnosis of active HSK, both eyes of each patient were examined by slit-lamp biomicroscopy and white-light IVCM (Confoscan 4; Nidek Technologies, Padova, Italy). The HSK-affected eyes were followed up at 1, 3, 6, and 12 months, whereas the unaffected fellow eyes were reexamined after 12 months. Three patients did not complete follow-up and were excluded for data analyses. All IVCM examinations were assessed for morphologic alterations characteristic of inflammatory activity and for corneal backscatter. As secondary outcome parameters, best-corrected visual activity (BCVA), central corneal thickness (CCT), intraocular pressure (IOP), and endothelial cell density (ECD) were determined at each study visit. We used repeated-measures analysis of variance to assess changes during the 12-month follow-up period and paired *t* tests to compare HSK-affected eyes with fellow eyes.

Main outcome measures: Presence of dendriform cells, pseudoguttae, and keratic precipitates, and follow-up of mean corneal backscatter.

Results: An increase of dendriform cells and pseudoguttae often accompanied stromal infiltration. Because these IVCM parameters were indiscernible or overlooked at slit-lamp examination, they proved to be excellent indicators of inflammatory activity. At 12 months' follow-up, mean corneal backscatter had decreased significantly by 36%, but still fell outside the normal range in 24 (69%) of the HSK-affected eyes. By using slit-lamp in conjunction with IVCM, we detected 17 recurrences in 14 of 35 patients (40%). Three of these recurrences were missed by slit-lamp, and 6 of these were missed by IVCM. At 12 months' follow-up, BCVA (–9 letters), CCT (–36 μm), and ECD (–313 cells/mm^2) were significantly lower, whereas IOP (1.8 mmHg) was significantly higher, in HSK-affected eyes compared with fellow eyes.

Conclusions: The data presented demonstrate that IVCM is complementary to slit-lamp examination in the follow-up of HSK, particularly because of its power to detect early signs of intracorneal inflammatory activity. Therapy guidance based on morphologic

assessment and corneal backscatter measurement by combined IVCM and slit-lamp examination may improve the outcome of HSK.

INTRODUCTION

Recurrent herpetic keratitis is a leading cause of infectious blindness in developed countries.[1] Herpes simplex virus (HSV) type 1 followed by varicella zoster virus are the most frequent causative agents.[2,3] Current knowledge of the cell types and inflammatory processes involved in initiation and perpetuation of the pathology of herpetic keratitis[4] offers new opportunities to improve the differential diagnosis of this recrudescent disease.[5,6] Herpetic stromal keratitis (HSK), representing a chronic corneal disease involving both a local viral cytopathic effect and a host immunologic and reparative response, is the most challenging HSV keratitis entity for an ophthalmologist. The accompanying loss of corneal sensation due to many recurrences leaves the patient with remarkably little discomfort, delaying medical consultation until blurring of vision occurs.[7] Even in the presence of this alarming symptom, ophthalmologists too often misinterpret active inflammation for quiescent scarring of the corneal stroma. In many large ophthalmic clinics, including ours, this phenomenon is enhanced by the many different ophthalmologists involved in the follow-up of patients with HSK. Because postponed treatment of unrecognized stromal inflammation promotes further scarring, neovascularization, thinning, and decompensation of the cornea, the inflammatory process in HSK is a major source of vision loss, which not uncommonly necessitates keratoplasty.[5] At present, slit-lamp biomicroscopy is the method of choice to assess HSK, despite ongoing advances of other imaging techniques, such as Scheimfplug photography, anterior segment optical coherence tomography (AS-OCT), and in vivo confocal microscopy (IVCM). Previously, IVCM has been used for in-depth imaging of the corneal layers in HSK.[8–12] These reports describe the morphologic aspects of HSK, yet do not comment on the course of these aspects during phases of activity and inactivity. Our group has recently introduced a more practical application of IVCM in the follow-up of HSK: assessment of inflammatory activity by detection of transient alterations of the corneal endothelium.[13] Analogous to detection of these endothelial changes, morphologic assessment of all corneal layers in conjunction with corneal backscatter analysis[14,15] may establish IVCM as an important clinical tool in the treatment of this recrudescent disease. The current study investigates the role of IVCM in the detection of inflammatory activity and long-term follow-up of HSK by assessing both morphologic aspects and corneal backscatter.

MATERIALS AND METHODS

Patients

Between February 2008 and October 2009, we enrolled 38 patients who visited the Cornea and External Disease Service of The Rotterdam Eye Hospital (Rotterdam, The Netherlands). The eligibility criteria included an age of 18 years or older, the presence of active HSK involving the central cornea, and the capability to undergo IVCM examination. Patients were excluded in case of bilateral involvement, a vision-deteriorating ocular disorder other than herpetic keratitis, or previous corneal surgery of the involved eye. Clinical diagnosis and evaluation were based on slit-lamp biomicroscopy by an experienced corneal surgeon (co-author LR). All patients were submitted to a standard treatment schedule (Table 1, available at http://aaojournal.org), unless a tailored approach was indicated when patients did not tolerate (n = 1) or were unresponsive to therapy (n = 4). After enrollment, the first study visit was scheduled within 7 days, followed by examinations at 1, 3, 6, and 12 months. Three patients did not complete follow-up and were excluded from data analyses. One patient with a severely diseased cornea showed further deterioration after the start of therapy and was submitted to keratoplasty after 4 months, whereas 2 patients refrained from follow-up after improvement of the stromal keratitis. The protocol of this prospective observational cohort study was approved by our institutional review board and the local medical ethical committee and adhered to the tenets of the Declaration of Helsinki. All patients gave their written, informed consent.

Table 1. Treatment schedule for patients with herpetic stromal keratitis

	Topical antiviral	**Systemic antiviral***		**Topical steroids**	
	Acyclovir 3% ointment (TD)	Acyclovir	Valacyclovir	Dexamethasone phosphate 0.1% (TD)	FML 0.1% (TD)
First visit	5	2000 mg	1500 mg	3	0
2 weeks**	3	1200 mg	1500 mg	3	0
1 month	0	800 mg	1000 mg	2	0
3 months	0	800 mg	1000 mg	1	0
6 months	0	800 mg	1000 mg	1	0
12 months	0	400 mg	500 mg	0	1
Recurrence***	5	2000 mg	1500 mg	3	0

* Acyclovir or Valacyclovir was prescribed; ** Clinical follow-up at 2 weeks was not a study visit;
*** Recurrence at slit-lamp examination; TD = times daily; FML = fluorometholone

Slit-Lamp Biomicroscopy

At each study visit, the patient was asked if he or she suspected a recurrence. Then the affected cornea was assessed for signs of active inflammation by slit-lamp biomicroscopy and IVCM. The fellow eye was examined only at the first and last visits. During slit-lamp examination, we assessed corneal epithelial defects, stromal infiltration, edema, thinning, and vascularization, pseudoguttae, keratic precipitates, and cells in the anterior chamber for their ability to indicate active corneal inflammation. A recurrence on slit-lamp examination was scored positive when any of these signs increased compared with the previous study visit, also considering possible intervening visits. The appearance at slit-lamp examination was assessed by a single observer (co-author LR), who was blinded to the IVCM results.

In Vivo Confocal Microscopy

We used a slit-scanning confocal microscope (Confoscan 4; Nidek Technologies, Padova, Italy) to study the cellular changes and to assess corneal backscatter in HSK. The microscope was equipped with a 40X objective lens, which required a coupling gel (Vidisic; Dr. Mann Pharma, Berlin, Germany) to image the corneal layers with 500X magnification. To minimize the effects of eye movements during the 12 seconds of image acquisition, we placed a *z*-ring adapter in front of the objective lens. Before examination, 1 drop of oxybuprocaine 0.4% (Ceban BV; Breda, The Netherlands) was instilled in the lower fornices of each eye. Then the microscope head was advanced, until the *z*-ring touched the central cornea. The different layers of the central cornea were imaged using fixed device settings: full-thickness mode, 72% light intensity, and a 6-µm scan step.

All IVCM examinations were reviewed for the presence of dendriform cells, pseudoguttae, and keratic precipitates, because of their potential to indicate inflammatory activity in HSK. Dendriform cells were scored positive when 5 or more of these cells were observed in a single frame, whereas for pseudoguttae and keratic precipitates a minimum of 2 was needed to acquire a positive score. The same morphologic features were scored in the fellow eyes. The IVCM observer (co-author TH) was blinded to the results at slit-lamp examination.

After calibration of the confocal microscope for corneal backscatter measurement,[16] we determined 5 backscatter variants expressed in scatter units (SUs). Mean backscatter of the cornea and anterior, middle, and posterior thirds of the stroma were computed semiautomatically using a purpose-made algorithm[15] (Fig 1). We considered backscatter at the basal epithelial cell layer as a measure for corneal edema (Fig 1F).[17] The epithelial valley (EV), which covered this measure, was calculated manually by averaging the indi-

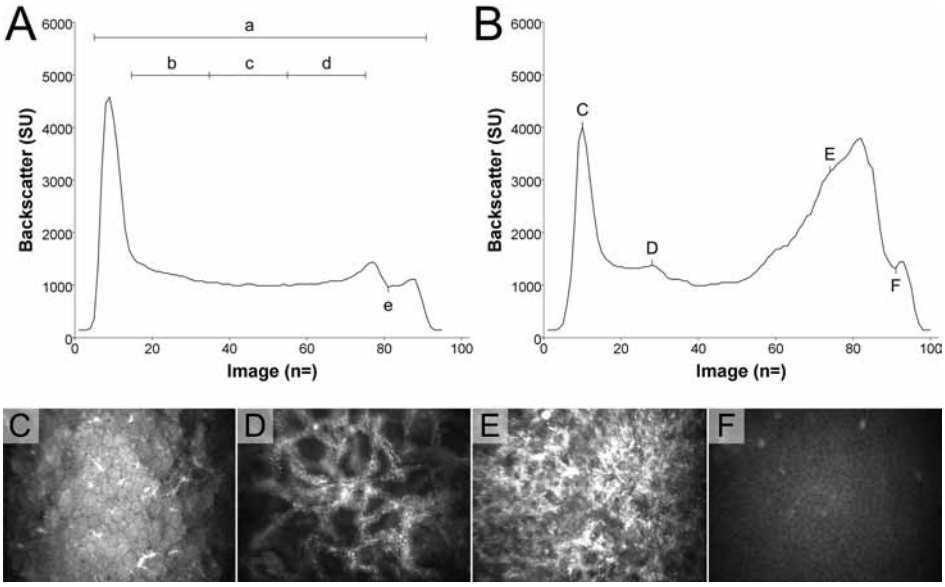

Figure 1. Backscatter measurements by in vivo confocal microscopy. **A**, *Z*-scan curve of a normal cornea. **B**, *Z*-scan curve of a cornea during an episode of herpetic stromal keratitis (HSK). Each position on the z-scan curve corresponds with a specific corneal layer. **C–F**, Morphologic changes of corneal layers in HSK influence corneal backscatter measurement. **C**, Endothelium with pseudoguttae and dendritiform keratic precipitates. **D**, Visible keratocyte cell processes in the posterior stroma. **E**, Increased backscatter in the anterior stroma. **F**, Corneal edema manifests as brightening of the intercellular spaces at the basal epithelial cell level. Backscatter at this level was considered as a measure for corneal edema; epithelial valley (EV). **a– e**, Five variants of corneal backscatter were determined in the HSK-affected eyes and the fellow eyes. **a**, Backscatter of the cornea. **b**, Backscatter of the posterior third of the stroma. **c**, Backscatter of the middle third of the stroma. **d**, Backscatter of the anterior third of the stroma. **e**, EV. n = frame number; SU = scatter unit.

vidual backscatter values corresponding with the basal epithelial cell layer of 3 passes in a single IVCM scan.

On IVCM, a recurrence was scored positive when 2 or more morphologic indicators of corneal inflammation had increased compared with the previous study visit or when mean corneal backscatter showed an increase >16% compared with the previous study visit. We considered an increase of >16% as a clinically relevant change because it exceeded the minimum detectable change for mean corneal backscatter.[15] Mean corneal backscatter was used for recurrence detection only after the first month, because this parameter was unreliable in the period right after disease activity.

Additional Examinations

In addition to slit-lamp and IVCM examinations, we assessed 4 other important parameters in the follow-up of HSK: best-corrected visual acuity (BCVA), central corneal thickness

(CCT), intraocular pressure (IOP), and endothelial cell density (ECD). By using manifest refraction, we measured the BCVA with Early Treatment of Diabetic Retinopathy Study charts at 4 m under standard illumination conditions.[18,19] The BCVA was scored letter by letter and expressed on the logarithm of the minimum angle of resolution (logMAR) scale.[20] The CCT was recorded as the mean of 10 readings with ultrasonic pachymetry (Tomey SP-3000; Tomey Ltd, Nagoya, Japan). The IOP was always measured after IVCM examination, using Goldmann applanation tonometry after staining of the tear film with a fluorescein strip. Both CCT and IOP were performed under topical anesthesia. We used images of the central endothelium acquired with IVCM to determine the ECD. A minimum of 75 cells were counted manually in a randomly selected polygonal area. Manufacturer's calibration for magnification was used after verification with a microgrid (Bürker counting chamber).

Statistical Analyses

To assess changes during the follow-up period in all backscatter variants, BCVA, CCT, IOP, and ECD, we used repeated-measures analysis of variance, preceded by Mauchly's sphericity test. When Mauchly's test indicated that the assumption of sphericity had been violated ($P<0.05$), a Greenhouse–Geisser correction was performed. In accordance with the results from our normative dataset,[15] age was entered as covariate and sex as grouping factor to analyze backscatter changes in the fellow eye. For the HSK-affected eye, age was substituted by the number of years since the first diagnosis of herpetic keratitis, because both covariates were significantly correlated and the latter was considered to influence corneal backscatter most. In a subgroup of patients who showed no recurrences on slit-lamp or IVCM examination and who showed improvement in mean corneal backscatter over the 12-month follow-up period, a Bonferroni correction was applied for multiple comparisons. Paired *t* tests were used to compare mean corneal backscatter, ECD, BCVA, CCT, and IOP of the HSK-affected eyes with their fellow eyes at the initial visit and after 12 months. All statistical analyses were performed using SPSS 17.0 (SPSS Inc., Chicago, IL). Tests were 2-sided, and $P<0.05$ was considered statistically significant.

RESULTS

Slit-Lamp Biomicroscopy

The baseline characteristics of the 35 included patients are shown in Table 2. Stromal infiltration was accompanied by multiple indicators of inflammatory activity (Table 3, available at http:// aaojournal.org), illustrating the heterogeneity of the clinical appear-

Table 2. Baseline characteristics

Subjects, n	35	
Mean age, yrs (range)	52	(18-85)
Men, n (%)	20	(57)
Ethnicity		
Caucasian, n (%)	33	(94)
Black, n (%)	2	(6)
HSV-1 positive by culture or PCR, n (%)	15	(43)
VZV positive by culture or PCR, n (%)	2	(6)
Mean history of herpetic keratitis, yrs (range)	8	(0-48)
Past episodes of herpetic keratitis, n (%)		
1	5	(14)
2-3	11	(31)
≥4	19	(54)
Episodes of herpetic keratitis last 2 yrs, n (%)		
1	14	(40)
2	12	(34)
≥3	9	(26)
Current systemic antiviral prophylaxis, n (%)	12	(34)
Current topical steroids, n (%)	15	(43)

HSV-1 = herpes simplex virus type 1; PCR = polymerase chain reaction; VZV = varicella zoster virus.

Table 3. Morphologic changes during one-year follow-up of herpetic stromal keratitis

Follow-up, months	0		1		3		6		12	
Slit-lamp biomicroscopy, n (%)	35	(100)	35	(100)	35	(100)	35	(100)	35	(100)
Punctate epithelial lesions, n (%)	6	(17)	2	(6)	7	(20)	7	(20)	9	(26)
Dendritic ulcer, n (%)	1	(3)	1	(3)	0	(0)	1	(3)	0	(0)
Geographic ulcer, n (%)	1	(3)	0	(0)	0	(0)	0	(0)	0	(0)
Neurotrophic ulcer, n (%)	1	(3)	1	(3)	0	(0)	0	(0)	0	(0)
Stromal infiltrate, n (%)	35	(100)	22	(63)	15	(43)	8	(23)	8	(23)
Stromal edema, n (%)	11	(31)	2	(6)	1	(3)	2	(6)	2	(6)
Stromal thinning, n (%)	7	(20)	9	(26)	7	(20)	7	(20)	6	(17)
Stromal vascularization, n (%)	5	(14)	4	(11)	4	(11)	4	(11)	2	(6)
Pseudoguttae, n (%)	7	(20)	0	(0)	0	(0)	1	(3)	3	(9)
Keratic precipitates, n (%)	15	(43)	7	(20)	8	(23)	6	(17)	5	(14)
Cells anterior chamber, n (%)	6	(17)	2	(6)	0	(0)	2	(6)	2	(6)
In vivo confocal microscopy, n (%)	35	(100)	35	(100)	35	(100)	35	(100)	35	(100)
Dendriform cells, n (%)	19	(54)	7	(20)	2	(6)	3	(9)	5	(14)
Pseudoguttae, n (%)	15	(43)	3	(9)	2	(6)	1	(3)	2	(6)
Keratic precipitates, n (%)	13	(37)	4	(11)	4	(11)	3	(9)	2	(6)

ance of HSK. On slit-lamp examination, a stromal infiltrate resolved within 6 months in 77% of all patients. After 12 months, however, stromal infiltration was still detected in 23% of the patients. Apart from stromal infiltration, a dendritic and geographic ulcer, stromal edema and vascularization, pseudoguttae, keratic precipitates, and cells in the anterior chamber were excellent indicators of corneal inflammatory activity showing an evident improvement over the follow-up period. Punctate epithelial lesions and stromal thinning remained stable during the course, and were therefore less suited to detect a recurrence using slit-lamp biomicroscopy.

In Vivo Confocal Microscopy

Two of the 245 IVCM examinations displayed too much stromal edema to assess the corneal endothelium. Of these 2 examinations, only the mean corneal backscatter and EV could be determined. All other IVCM examinations were of sufficient quality to determine all 5 backscatter variants.

On IVCM, disease activity was indicated by the presence of dendriform cells, pseudoguttae, and keratic precipitates (Table 3, available at http://aaojournal.org, Fig 2), which resolved after the start of therapy. Assessment of dendriform cells and pseudoguttae was of additive value to slit-lamp examination, because they could not be discerned or were overlooked by slit-lamp examination, and accompanied formation of a stromal infiltrate. During active inflammation, keratic precipitates were observed by IVCM, but were recognized more easily using slit-lamp biomicroscopy. The fellow eyes showed dendriform cells in 13% of all visits, whereas pseudoguttae and keratic precipitates were not observed in fellow eyes during follow-up.

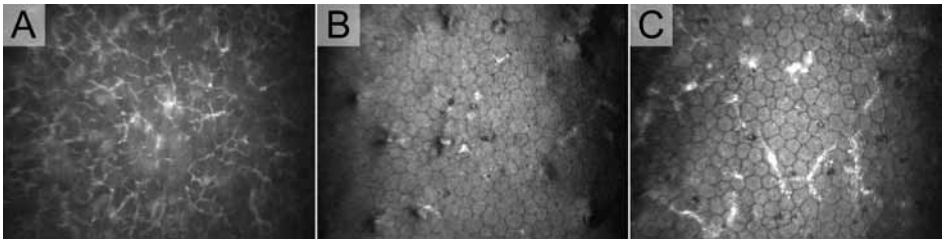

Figure 2. Morphologic alterations in active herpetic stromal keratitis (HSK) as observed by in vivo confocal microscopy (IVCM). **A**, Dendriform cells at the sub-basal nerve plexus level showed wire netting in this patient.[23] Under topical steroid treatment, the dendriform cells diminished in the central cornea but reappeared in 64% of all recurrences. **B**, Temporary alterations of the endothelial layer, such as pseudoguttae, intercellular gaps, and infiltration of inflammatory cells into the endothelial layer, preceded or accompanied a recurrence of HSK in 36% of all recurrences. **C**, Dendritiform keratic precipitates indicated disease activity in this patient with HSK. After resolution of these keratic precipitates, round pigmented deposits remained.

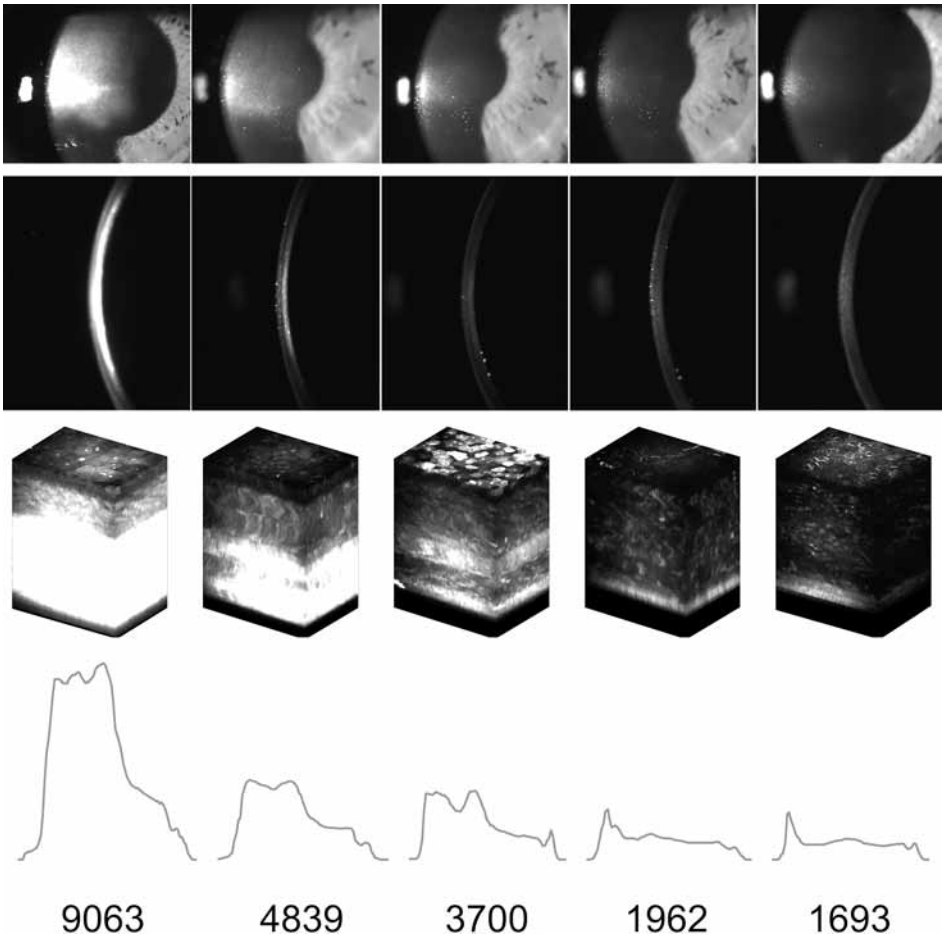

Figure 3. Illustrative case: 1-year follow-up of herpetic stromal keratitis (HSK) using slit-lamp biomicroscopy and in vivo confocal microscopy (IVCM). At the moment of the first slit-lamp photograph, this 26-year-old woman used 800 mg oral acyclovir and topical 0.1% dexamethasone once daily and visited our clinic for a regular follow-up after a 3-year history of recurring HSK. A few days before the visit, she experienced slight blurring of vision, but noticed that she was able to read again without glasses. Slit-lamp examination revealed opacification of the middle and posterior third of the stroma, which was already described 3 months before. Other signs of inflammation seemed absent. Although slit-lamp appearance was inconclusive for a stromal recurrence, her best-corrected visual acuity had declined from 20/30 to 20/40 since her last visit. Therefore, she was enrolled in the current study, subjected to our standard therapy regimen for stromal recurrences (Table 1), and monitored by slit-lamp and IVCM. Despite dense opacification in the posterior part of the stroma, IVCM did reveal pseudoguttae at the first study visit, clearly indicating disease activity. Follow-up by slit-lamp showed a great improvement in the first 3 months, resulting in an optically clear cornea, which remained clear thereafter. However, IVCM showed mean corneal backscatter continued to decrease, also after 3 months. This was completely overlooked by slit-lamp biomicroscopy. Furthermore, corneal thickness at slit-lamp biomicroscopy seemed normal at each study visit. Nevertheless, ultrasonic pachymetry showed marked corneal thinning of the HSK-affected eye compared with the fellow eye, which became increasingly evident during the course. Columns: first study visit, 1-, 3-, 6-, 12-month(s) follow-up. Rows: slit-lamp photography: broad beam, optical section; IVCM: stack of images, *z*-scan curve with corneal backscatter in scatter units. (*See also Color figures, p. 207.*)

Similar to morphologic assessment at a cellular level, objective corneal backscatter measurement by IVCM was of additive value to monitor disease activity in long-term follow-up of HSK. The additional role of IVCM is illustrated by a representative case (Fig 3), which emphasizes the inability of slit-lamp biomicroscopy to detect subtle changes in corneal opacity.

At the first study visit, mean corneal backscatter was 2185 SU (174%) higher in HSK-affected eyes than in fellow eyes (Table 4) and fell outside the normal range in 33 of the 35 HSK-affected eyes (94%). After 12 months, mean corneal backscatter in HSK-affected eyes had reduced significantly by 1235 SU (36%; $P = 0.0002$), but remained 958 SU (77%) higher than in fellow eyes. At the last study visit, still 24 of 35 HSK-affected eyes (69%) fell outside the normal backscatter range. We distinguished 3 different backscatter patterns over the follow-up period: recurrence, stable, and improvement (Fig 4, available at http://aaojournal.org). In patients without a recurrence (n = 16), who showed a clinically relevant decrease in mean corneal backscatter over the 12-month follow-up period (Fig 4C, available at http://aaojournal.org), backscatter decreased significantly from 1 to 3 months ($P = 0.001$), from 3 to 6 months ($P = 0.003$), and from 6 to 12 months ($P = 0.004$). Backscatter did not change significantly from the first visit to 1 month.

In the different parts of the stroma, backscatter was highest in the anterior third in 69% of all visits, in the middle third in 6% of all visits, and in the posterior third in 25% of all visits. Over the follow-up period, backscatter declined significantly in all 3 parts of the stroma. The EV, as an indicator for corneal edema, also reduced significantly. This

Table 4. Corneal backscatter during one-year follow-up of herpetic stromal keratitis measured by in vivo confocal microscopy

Follow-up, months	0	1	3	6	12	Δ_{YEAR}	*P*
HSK							
Cornea	3441 ± 1880	2888 ± 1264	2472 ± 1147	2164 ± 1128	2206 ± 1134	-36%	0.0002
Anterior stroma	5091 ± 3502	3919 ± 2701	3132 ± 2357	2627 ± 2213	2766 ± 2026	-46%	0.0009
Mid stroma	3271 ± 2456	2742 ± 1699	2330 ± 1609	1943 ± 1451	2059 ± 1576	-37%	0.0008
Posterior stroma	3129 ± 2841	2702 ± 1582	2417 ± 1348	2120 ± 1279	2136 ± 1403	-32%	0.01
Epithelial valley	2523 ± 1342	1787 ± 854	1469 ± 355	1350 ± 289	1413 ± 473	-44%	0.0004
FE							
Cornea	1256 ± 157	ND	ND	ND	1248 ± 170	-1%	NS
Anterior stroma	1183 ± 192	ND	ND	ND	1173 ± 203	-1%	NS
Mid stroma	984 ± 183	ND	ND	ND	989 ± 196	0%	NS
Posterior stroma	1192 ± 238	ND	ND	ND	1208 ± 235	1%	NS
Epithelial valley	1062 ± 90	ND	ND	ND	1026 ± 93	3%	NS

Δ_{YEAR} = 1-year change of backscatter in percentage; HSK = herpetic stromal keratitis affected eye; FE = fellow eye; ND = not done; NS = not significant.

Data are expressed as mean ± standard deviation backscatter in scatter units. SU ± standard deviation.

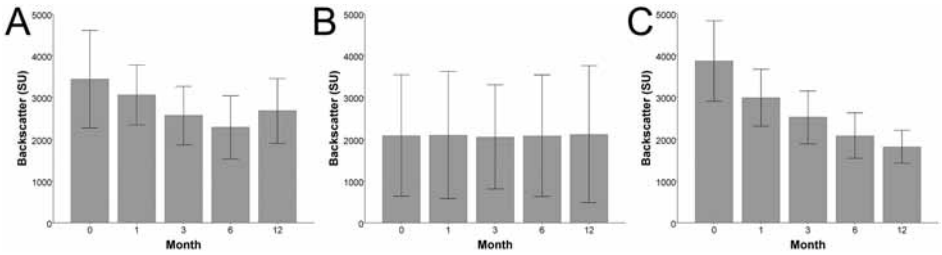

Figure 4. One-year follow-up of mean corneal backscatter in herpetic stromal keratitis. Three backscatter patterns were distinguished. **A,** Recurrence; patients with a recurrence on slit-lamp examination or *in vivo* confocal microscopy (n=14). **B,** Stable; patients without a clinically relevant change during follow-up (n=5). **C,** Improvement; patients with a clinically relevant decrease (>16%)[14] from start to end of follow-up (n=16). SU = scatter units; Error bars represent 95% confidence intervals of the mean.

EV, however, was influenced by backscatter of the underlying anterior stroma. Corneal edema was reliably quantified by the EV only when the anterior stroma was unaffected (n = 4).

In 131 of 140 follow-up visits (94%), slit-lamp and IVCM examinations agreed on recurrence detection. By using slit-lamp examination in conjunction with IVCM, we detected 17 recurrences in 14 of 35 patients (40%). Three patients showed 2 recurrences during the 12-month follow-up period. The overlap of the 2 imaging modalities on recurrence detection is shown in Figure 5 (available at http://aaojournal.org). Among the 6 recur-

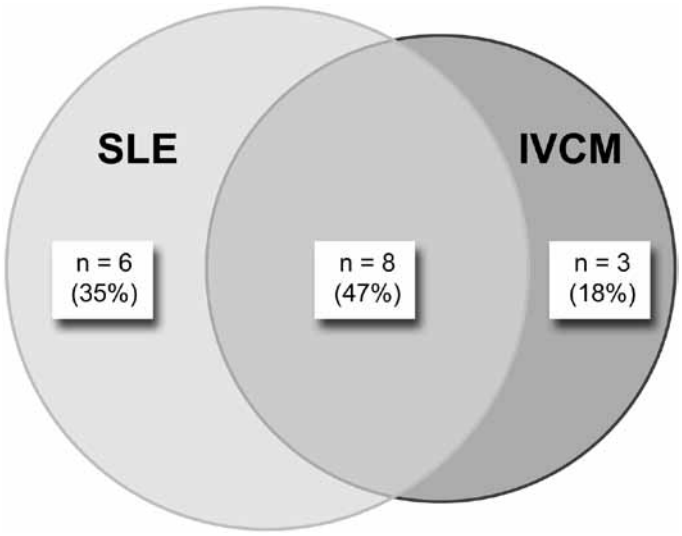

Figure 5. Detection of recurrences in herpetic stromal keratitis by slit-lamp examination (SLE) versus *in vivo* confocal microscopy (IVCM). Fourteen recurrences were detected in twelve patients with slit-lamp examination. On IVCM, eleven recurrences were seen in ten patients. Overlap between the two imaging modalities was found in 47% of all cases.

rences detected solely by slit-lamp examination, 1 was a peripherally localized epithelial recurrence, 2 were small subepithelial infiltrates, and 1 was an off-centered immune stromal recurrence. The 2 remaining recurrences were doubtful and may represent passed subclinical recurrences in between the study visits. Recurrences on IVCM were indicated by a clinically relevant change of mean corneal backscatter in 10 of the 11 cases (91%). When a recurrence was detected on IVCM, dendriform cells were observed in 64% of examinations, pseudoguttae were observed in 36% of examinations, and keratic precipitates in 18% of examinations.

The patient's experience was a poor predictor for inflammatory activity in HSK. In only 5 of 17 recurrences detected by slit-lamp or IVCM did the patient report a recurrence. Moreover, on 8 occasions the patient reported a recurrence, which could not be confirmed by slit-lamp or IVCM. On 3 of these occasions the IOP was increased to 30 mmHg.

Additional Examinations

At the end of the 12-month follow-up period, BCVA of the HSK-affected eyes had improved from 0.30 to 0.09 logMAR (–0.21 logMAR; $P<0.0001$), the CCT had decreased from 527 to 504 µm (–23 µm; $P = 0.039$), and the ECD had declined from 2498 to 2441 cells/mm^2 (–57 cells/mm^2; $P = 0.010$) (Fig 6, available at http://aaojournal.org). The IOP did not change significantly, although 3 patients showed an increase to >30 mmHg. When comparing HSK-affected eyes with fellow eyes at the end of follow-up, the BCVA (–9 letters; $P = 0.0002$), CCT (–36 µm; $P<0.0001$), and ECD (–313 cells/mm^2; $P<0.0001$) were significantly lower, whereas the IOP was significantly higher in HSK-affected eyes (1.8 mmHg; $P = 0.027$).

DISCUSSION

The current study reports on the role of IVCM in the clinical assessment of HSK. For evaluation of the inflammatory process in HSK, slit-lamp biomicroscopy remains the gold standard. However, using IVCM in addition to slit-lamp examination has 2 main advantages. First, IVCM allows early detection of a recurrence based on the device's ability to assess the appearance of dendriform cells and pseudoguttae. These indicators of inflammatory activity herald formation of stromal infiltration and dissipate early with improvement of HSK. Second, corneal opacification in HSK is objectively quantified by IVCM backscatter analysis at a level that is beyond the detection limits of the slit-lamp biomicroscope. Measurement of corneal backscatter enables long-term monitoring of the inflammatory process in HSK and facilitates objective detection of stromal recurrences. Below, we discuss the usefulness of clinical parameters in the

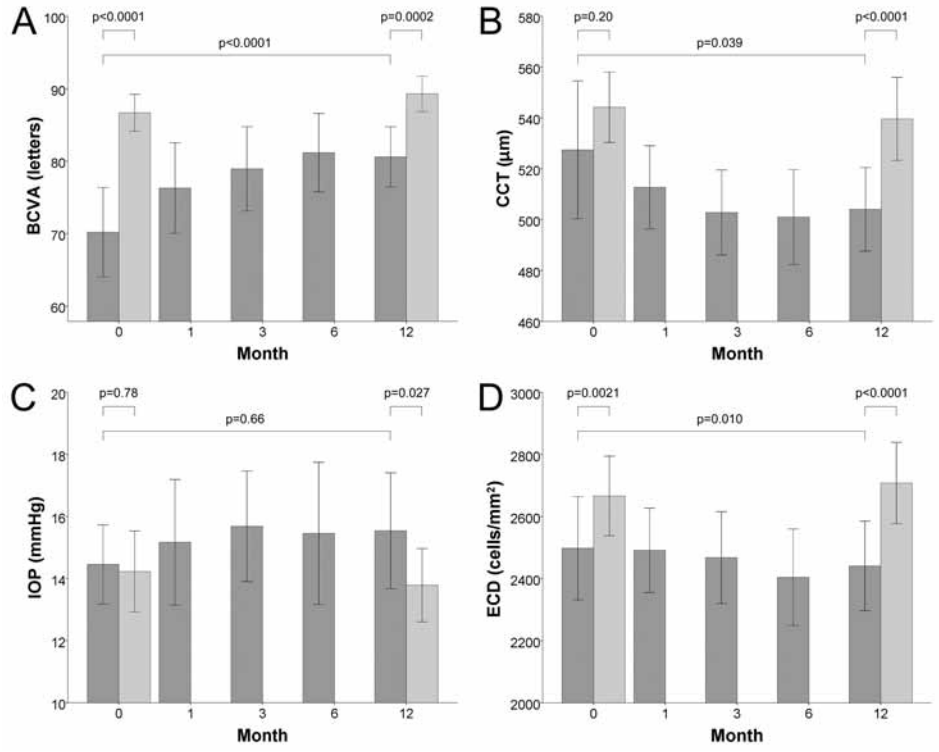

Figure 6. Additional examinations during one-year follow-up of herpetic stromal keratitis (HSK). **A,** Best corrected visual acuity (BCVA). **B,** Central corneal thickness (CCT). **C,** Intraocular pressure (IOP). **D,** Endothelial cell density (ECD). Dark grey bars represent HSK-affected eyes. Light gray bars represent fellow eyes. Error bars represent 95% confidence intervals of the mean.

follow-up of HSK, acquired with slit-lamp biomicroscopy, IVCM, and other additional examinations.

Slit-Lamp Biomicroscopy

To improve interobserver communication and to facilitate management of herpetic keratitis, this disease entity is classified into 4 main categories: infectious epithelial keratitis, neurotrophic keratopathy, HSK, and endotheliitis.[5,6] The broad spectrum of inflammatory activity indicators identified in HSK underline the vast overlap among these categories and emphasize the multifactorial characteristics of HSK. For therapy evaluation and recurrence detection in HSK, each indicator needs to be assessed at every follow-up visit. This armamentarium for recurrence detection is completed by blepharitis, conjunctivitis, and iritis,[5,6] which were not systematically scored in our study because we focused on the corneal alterations. Even with these many indicators, slit-

lamp detection of inflammatory activity in HSK remains a diagnostic challenge because patients with HSK often have an extensive history of recurrences leading to undefined stromal opacification.

We found punctate epithelial lesions unsuited for recurrence detection in HSK-affected eyes because they persisted during follow-up. This persistence may partially be explained by the toxic effect of acyclovir ointment.[5] The punctate epithelial keratopathy, however, persisted even after discontinuation of the topical antiviral agent. Therefore, corneal surface irregularities due to a damaged epithelial basement membrane,[5] together with corneal hypesthesia of the HSK-affected eye and concomitant bilateral dry eye,[21] seem a better explanation for the persistent punctate epithelial lesions. Early identification and subsequent management of concomitant dry eye symptoms may, in its turn, lower the number of recurrences in HSK and prevent neurotrophic keratopathy from developing.

In Vivo Confocal Microscopy

Contrary to previous IVCM reports that documented the morphologic appearance of different corneal layers in HSV keratitis without following up on the patients,[8–12] we focused on the changes in morphology and corneal backscatter in active HSK over a 1-year period. This study design enabled us to identify IVCM parameters that are complementary to slit-lamp appearance. Table 5 (available at http://aaojournal.org) summarizes the additional value of these IVCM parameters and documents their timing in the follow-up of HSK.

Table 5. Additional value of in vivo confocal microscopy parameters in the follow-up of herpetic stromal keratitis

Follow-up, months	0	≤1	>1
Morphology			
Dendriform cells	++	++	++
Pseudoguttae	++	++	++
Keratic precipitates	+	+	+
Backscatter			
Cornea	–	–	++
Anterior stroma	–	–	+
Mid stroma	–	–	+
Posterior stroma	–	–	+
Epithelial valley*	–	+	+

– = no additional value; + = minor additional value; ++ = major additional value

* only of additional value when the anterior stroma is unaffected

Dendriform cells, which appear at the level of the basal epithelial cells and between the fibers of the sub-basal nerve plexus,[22,23] have been postulated to represent dendritic cells.[24] These cells, initiating and controlling the transition of local innate to adaptive immune responses,[25] are present in higher numbers at the border compared with the center of normal corneas.[22] During trauma, including viral infections, the cornea-resident dendritic cells migrate to the site of tissue damage.[24] In accordance with our data, this influx of dendritic cells heralds the immune stromal response during reactivation of herpetic keratitis in experimental HSK animal models.[26] With clinical improvement of the stromal infiltration, we found the dendriform cells to dissipate and even to disappear completely in nearly all patients within 3 months. Because they reappeared in 64% of all recurrences, dendriform cells were excellent indicators of inflammatory activity.

In a previous report, we have shown the morphologic alterations characteristic of corneal endotheliitis.[13] Of these endothelial alterations, pseudoguttae are the most prevalent and have been observed only during the active phase in herpetic keratitis. They are caused by transient cellular edema,[27] which also constitutes other inflammatory modalities of the cornea.[13] Like true corneal guttae, pseudoguttae can also be assessed by viewing the endothelial specular reflex by slit-lamp biomicroscopy. In HSK-affected eyes, however, opacification of the stroma due to edema, infiltration, and scarring often hindered a clear view of the endothelium.

Although keratic precipitates were indicative of a recurrence, they were not complementary to slit-lamp biomicroscopy. Their appearance was similar to the dendritiform keratic precipitates that have been documented in various subtypes of uveitis.[28–30] These studies have independently shown that dendritiform keratic precipitates are suggestive of an infectious cause of the uveitis. Likewise, herpetic endotheliitis may be caused by the direct cytopathic effect of the virus. Indirect effects due to the local host response, however, remain an alternative cause.

Except for HSV-affected eyes, also unaffected fellow eyes have shown a significant reduction of the sub-basal nerve plexus on IVCM.[12] Whereas these alterations of the sub-basal nerve plexus suggest subclinical bilateral involvement, we did not find any evidence of inflammation in the fellow eyes. The prevalence of dendriform cells equaled that in normal eyes,[14] pseudoguttae and keratic precipitates were not found, and all 5 backscatter variants in the fellow eyes remained stable during follow-up and fell within normal range.[15] Therefore, causative factors other than subclinical inflammation, such as central neural downregulation,[12] or concurrent bilateral dry eye[21] may explain the reduction of the sub-basal nerve plexus in unaffected fellow eyes.

In addition to the above-described morphologic changes, IVCM of HSV-affected corneas has also shown hyperreflective basal epithelial cells,[9] abnormal extracellular stromal matrix,[8] and hyperreflective activated keratocytes.[9,10] These morphologic changes add up to a slit-lamp detectable haze, which can be graded according to a system reported

by Fantes et al.[31] An alternative for this coarse grading system is digital slit-lamp photography and computer-assisted image analysis, which has been used to evaluate density of HSK in the course of the Herpetic Eye Disease Study.[32,33] This study has shown that the density of HSK corneas acquired by image analysis correlates with clinical haze grading. However, calibration of image analysis for use in a clinical setting seems rather difficult and time-consuming, because slit-lamp photography depends on many settings that influence haze measurement, including slit height, length, and angle; filters; magnification; and voltage. Furthermore, other factors, such as light reflections from the tear film and iris color,[32] variations of the light source or camera sensitivity over time,[34] and image saturation,[16] should be taken into account for optimal slit-lamp photography.

In case of IVCM, long-term standardization of corneal backscatter analysis in transparent and opaque corneas has recently been validated.[16] By using these calibration methods and minimum detectable changes for corneal backscatter measurement,[15] we were able to detect objectively 8 of the 14 HSK recurrences (57%) that were indicated by an experienced corneal surgeon (co-author LR) at slit-lamp examination. The 3 additional recurrences that were detected solely by IVCM emphasize the diagnostic difficulty and subjective nature of recognizing an HSK recurrence at slit-lamp examination. A disadvantage of IVCM, however, is the limited field of view. Because only 0.14% of total corneal surface was imaged, paracentral or peripheral recurrences that did not involve the visual axis could not be detected by IVCM.

Corneal edema, which is often present in active HSK, had a dampening effect on backscatter in the stroma. In 12 of 35 patients with HSK resolution of corneal edema led to a paradoxical increase of backscatter in the first month, arguing to exclude this parameter during the first month after-recurrence (Table 5, available at http://aaojournal.org). This was confirmed by a subgroup analysis of 16 of 35 patients with HSK, who improved from start to end of follow-up (Fig 4C, available at http://aaojournal.org). Although mean corneal backscatter in this subgroup decreased by 23% in the first month, this decrease was not significant. The same subgroup demonstrated that clearance of the cornea after active HSK was a continuing process. This process may represent the clearance of viral DNA and antigen and resolution of the immune response after an episode of HSK.[35] Alternatively, the continuing decrease in backscatter may be due to recovery of the corneal crystallin concentration. These specific water-soluble proteins in the cytoplasm of corneal keratocytes may contribute to the transparency of corneal tissue by minimizing the fluctuations in refractive indices within keratocytes, and between keratocytes and the surrounding collagen fibers.[36] Corneal crystallin expression is markedly reduced in migrating fibroblasts and myofibroblasts, which represent the reparative response in the HSK cornea. When the reparative response extinguishes and fibroblasts differentiate back to keratocytes, the concentration of corneal crystallins increases, resulting in clearance of the cornea. Irrespective of the

origin, continuing clearance emphasizes the importance of early recurrence detection and treatment in HSK.

Whereas corneal edema tempered the increase of stromal backscatter due to infiltration, it increased backscatter at the intercellular spaces of the basal epithelial cells, as indicated by the EV. Unfortunately, because the depth of field of this confocal microscope is 26 µm,[37] the EV was often outshined by increased backscatter at the anterior stroma. Therefore, the EV can only reliably be used to indicate corneal edema in a minority of patients with HSK with a clear anterior stroma.

Additional Examinations

In HSV disciform keratitis, corneal thickness at the midpoint of the inflamed area has been found to decrease by 15% with resolution of the inflammation.[38] The same study has also reported that CCT in eyes with HSV disciform keratitis is thicker than in fellow eyes. Our study confirmed the decline of CCT with resolution of corneal edema (5% in 3 months). However, in contrast with the results of Wilhelmus et al,[38] we found CCT in HSK-affected eyes to be thinner than in fellow eyes even at the first study visit (Fig 6B, available at http://aaojournal.org). This corneal thinning in HSK-affected eyes was largely overlooked by slit-lamp examination and emphasizes the continuum between immune stromal keratitis and necrotizing stromal keratitis.

Stromal edema, elicited by a recurrence, may return the cornea to its original shape before corneal thinning. This may lead to paradoxical refractive changes, as shown by our illustrated case (Fig 3). These continuing refractive changes along with a decrease in corneal sensibility probably impaired the ability of patients to indicate a recurrence. Disease deterioration according to the patient's perception correlated with an increase of IOP >30 mmHg in 3 cases. Therefore, regular check-up of IOP in patients with HSK is recommended, also because steroid treatment may lead to secondary glaucoma.[39]

Concordant with our previous study,[13] ECD decreased significantly after a recurrence. This irreversible endothelial cell loss was confirmed by a significantly lower ECD in the HSK-affected eyes compared with the fellow eyes.

Clinical Implications and Future Developments

We recently started a trial at our hospital to integrate IVCM in the standard clinical evaluation of HSK. In addition to slit-lamp biomicroscopy, BCVA, and IOP, we now systematically assess dendriform cells, pseudoguttae, and mean corneal backscatter by IVCM to enhance recurrence detection in HSK. Earlier detection and treatment of inflammatory activity are likely to improve the outcome of HSK. Nevertheless, IVCM-guided therapy adjustment in HSK requires careful evaluation, because complications of overtreatment

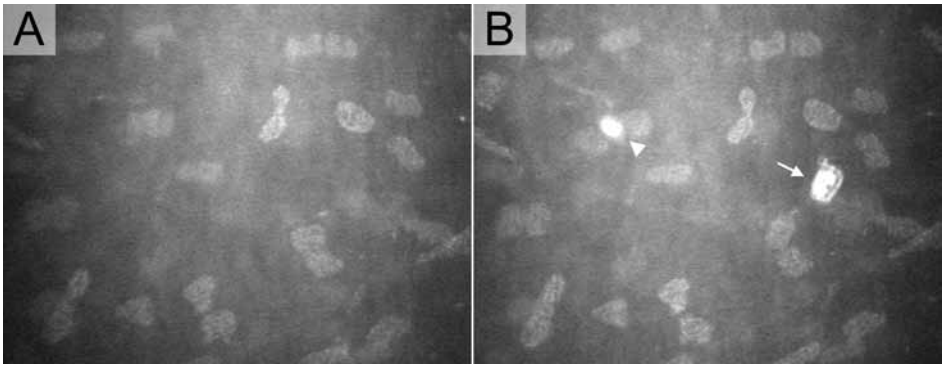

Figure 7. Topographic repeatability. Due to patient movement, a limited field of view, and the lack of an eye tracking system topographic repeatability of in vivo confocal microscopy is fairly low. In our experience only the central cornea can be imaged with sufficient repeatability. With some luck, the same area can be imaged twice. **A**, Posterior stroma of one of the herpetic stromal keratitis patients at 3 months follow-up. **B,** At twelve months follow-up the same area was imaged. For nine months, the position of the keratocyte nuclei had remained stable. However, two "activated keratocytes" were visible; one located between two quiet keratocyte nuclei (arrowhead) and one solitary (arrow). Instead of activated keratocytes these cells may represent inflammatory cells, as they seemed in contact with keratocytes (arrowhead) or had a horseshoe-shaped nucleus (arrow), and could not be discerned nine months earlier.

and resistance to antiviral medications may increase.[40] When IVCM is used in a clinical setting, 3 conditions need to be recognized. First, because of its limited field of view and moderate topographic repeatability (Fig 7, available at http://aaojournal.org), this expensive technique cannot be used without slit-lamp examination. Second, extensive knowledge of normal corneal morphology and its variants is needed to identify pathologic changes.[14,41] Third, for reliable corneal backscatter measurement, IVCM requires calibration, an experienced operator, and a certain degree of homogeneity of the corneal opacification.[16] These conditions may limit the use of IVCM to large ophthalmic centers, which have referred high numbers of patients with HSK and have sufficient experience with IVCM.

A promising alternative for assessment of cellular morphology and corneal backscatter measurement is AS-OCT. This user-friendly noncontact device has the advantages of imaging a larger area, higher depth penetration, and shorter image acquisition time compared with IVCM. However, the lateral resolution of AS-OCT is still insufficient for identification of dendriform cells and differentiation of pseudoguttae from true corneal guttae. Also, for backscatter measurement in opaque corneas, as is the case in HSK, AS-OCT requires the ability to adjust light intensity when image saturation occurs.[16] Until these limitations are solved, IVCM is preferable to AS-OCT in the follow-up of HSK.

In conclusion, our study demonstrates the multifactorial characteristics and accompanying diagnostic difficulties of HSK. For recurrence detection and long-term follow-up of this chronic disease, slit-lamp biomicroscopy remains the gold standard. However,

supplementary IVCM examination enhances early detection of inflammatory activity by combining morphologic assessment at a cellular level and objective corneal backscatter measurement. Therapy adjustment based on these IVCM parameters may improve the outcome of HSK.

REFERENCES

1. Liesegang TJ. Herpes simplex virus epidemiology and ocular importance. Cornea 2001;20:1–13.
2. Young RC, Hodge DO, Liesegang TJ, Baratz KH. Incidence, recurrence, and outcomes of herpes simplex virus eye disease in Olmsted County, Minnesota, 1976–2007: the effect of oral antiviral prophylaxis. Arch Ophthalmol 2010;128:1178–83.
3. Ragozzino MW, Melton LJ III, Kurland LT, et al. Populationbased study of herpes zoster and its sequelae. Medicine (Baltimore) 1982;61:310–6.
4. Remeijer L, Osterhaus A, Verjans G. Human herpes simplex virus keratitis: the pathogenesis revisited. Ocul Immunol Inflamm 2004;12:255–85.
5. Liesegang TJ. Classification of herpes simplex virus keratitis and anterior uveitis. Cornea 1999;18: 127–43.
6. Holland EJ, Schwartz GS. Classification of herpes simplex virus keratitis. Cornea 1999;18:144–54.
7. Dawson CR, Togni B. Herpes simplex eye infections: clinical manifestations, pathogenesis and management. Surv Ophthalmol 1976;21:121–35.
8. Rosenberg ME, Tervo TM, Muller LJ, et al. In vivo confocal microscopy after herpes keratitis. Cornea 2002;21:265–9.
9. Gabison EE, Alfonsi N, Doan S, et al. Archipelago keratitis: a clinical variant of recurrent herpetic keratitis? Ophthalmology 2007;114:2000–5.
10. Martone G, Alegente M, Balestrazzi A, et al. In vivo confocal microscopy in bilateral herpetic keratitis: a case report. Eur J Ophthalmol 2008;18:994–7.
11. Patel DV, McGhee CN. Laser scanning in vivo confocal microscopy demonstrating significant alteration of human corneal nerves following herpes zoster ophthalmicus. Arch Neurol 2010;67: 640–1.
12. Hamrah P, Cruzat A, Dastjerdi MH, et al. Corneal sensation and subbasal nerve alterations in patients with herpes simplex keratitis: an in vivo confocal microscopy study. Ophthalmology 2010; 117:1930–6.
13. Hillenaar T, Weenen C, Wubbels RJ, Remeijer L. Endothelial involvement in herpes simplex virus keratitis: an in vivo confocal microscopy study. Ophthalmology 2009;116:2077–86.
14. Hillenaar T, van Cleynenbreugel H, Remeijer L. How normal is the transparent cornea? Effects of aging on corneal morphology. Ophthalmology 2012;119:241–8.
15. Hillenaar T, Cals RH, Eilers PH, et al. Normative database for corneal backscatter analysis by in vivo confocal microscopy. Invest Ophthalmol Vis Sci 2011;52:7274–81.
16. Hillenaar T, Sicam VA, Vermeer KA, et al. Wide-range calibration of corneal backscatter analysis by in vivo confocal microscopy. Invest Ophthalmol Vis Sci 2011;52:2136–46.
17. Morishige N, Takahashi N, Chikamoto N, Nishida T. Quantitative evaluation of corneal epithelial oedema by confocal microscopy. Clin Experiment Ophthalmol 2009;37:249–53.
18. Ferris FL III, Kassoff A, Bresnick GH, Bailey I. Newvisual acuity charts for clinical research. Am J Ophthalmol 1982;94:91–6.
19. Ferris FL III, Sperduto RD. Standardized illumination for visual acuity testing in clinical research. Am J Ophthalmol 1982;94:97–8.
20. Bailey IL, Bullimore MA, Raasch TW, Taylor HR. Clinical grading and the effects of scaling. Invest Ophthalmol Vis Sci 1991;32:422–32.
21. Keijser S, van Best JA, van der Lelij A, Jager MJ. Reflex and steady state tears in patients with latent stromal herpetic keratitis. Invest Ophthalmol Vis Sci 2002;43:87–91.

22. Zhivov A, Stave J, Vollmar B, Guthoff R. In vivo confocal microscopic evaluation of Langerhans cell density and distribution in the normal human corneal epithelium. Graefes Arch Clin Exp Ophthalmol 2005;243:1056–61.
23. Guthoff RF, Zhivov A, Stachs O. In vivo confocal microscopy, an inner vision of the cornea - a major review. Clin Experiment Ophthalmol 2009;37:100–17.
24. Mastropasqua L, Nubile M, Lanzini M, et al. Epithelial dendritic cell distribution in normal and inflamed human cornea: in vivo confocal microscopy study. Am J Ophthalmol 2006;142:736–44.
25. Banchereau J, Steinman RM. Dendritic cells and the control of immunity. Nature 1998;392:245–52.
26. Miller JK, Laycock KA, Nash MM, Pepose JS. Corneal Langerhans cell dynamics after herpes simplex virus reactivation. Invest Ophthalmol Vis Sci 1993;34:2282–90.
27. Krachmer JH, Schnitzer JI, Fratkin J. Cornea pseudoguttata: a clinical and histopathologic description of endothelial cell edema. Arch Ophthalmol 1981;99:1377–81.
28. Wertheim MS, Mathers WD, Planck SJ, et al. In vivo confocal microscopy of keratic precipitates. Arch Ophthalmol 2004;122:1773–81.
29. Mahendradas P, Shetty R, Narayana KM, Shetty BK. In vivo confocal microscopy of keratic precipitates in infectious versus noninfectious uveitis. Ophthalmology 2010;117:373–80.
30. Kanavi MR, Soheilian M, Naghshgar N. Confocal scan of keratic precipitates in uveitic eyes of various etiologies. Cornea 2010;29:650–4.
31. Fantes FE, Hanna KD, Waring GO III, et al. Wound healing after excimer laser keratomileusis (photorefractive keratectomy) in monkeys. Arch Ophthalmol 1990;108:665–75.
32. Wilhelmus KR, Mitchell BM, Dawson CR, et al, Herpetic Eye Disease Study Group. Slitlamp biomicroscopy and photographic image analysis of herpes simplex virus stromal keratitis. Arch Ophthalmol 2009;127:161–6.
33. Wilhelmus KR, Mitchell BM, Jones DB, Herpetic Eye Disease Study Group. Photographic monitoring of herpes simplex virus keratitis during anti-inflammatory treatment. Arch Ophthalmol 2011; 129:252–3.
34. Patel SV, Winter EJ, McLaren JW, Bourne WM. Objective measurement of backscattered light from the anterior and posterior cornea in vivo. Invest Ophthalmol Vis Sci 2007;48:166–72.
35. Kaye SB, Baker K, Bonshek R, et al. Human herpesviruses in the cornea. Br J Ophthalmol 2000;84: 563–71.
36. Jester JV. Corneal crystallins and the development of cellular transparency. Semin Cell Dev Biol 2008;19:82–93.
37. McLaren JW, Nau CB, Kitzmann AS, Bourne WM. Keratocyte density: comparison of two confocal microscopes. Eye Contact Lens 2005;31:28–33.
38. Wilhelmus KR, Sugar J, Hyndiuk RA, Stulting RD. Corneal thickness changes during herpes simplex virus disciform keratitis. Cornea 2004;23:154–7.
39. Carnahan MC, Goldstein DA. Ocular complications of topical, peri-ocular, and systemic corticosteroids. Curr Opin Ophthalmol 2000;11:478–83.
40. Duan R, de Vries RD, Osterhaus AD, et al. Acyclovir-resistant corneal HSV-1 isolates from patients with herpetic keratitis. J Infect Dis 2008;198:659–63.
41. Niederer RL, McGhee CN. Clinical in vivo confocal microscopy of the human cornea in health and disease. Prog Retin Eye Res 2010;29:30–58.

7

Zipper cell endotheliopathy: a new subset of idiopathic corneal edema

Toine Hillenaar
Cornelia M. Mooy
Georges M.G.M. Verjans
Lies Remeijer

Ophthalmology 2010;117:2255–2262

ABSTRACT

Purpose: To report the clinical and histologic findings of a new subset of idiopathic corneal edema: zipper cell endotheliopathy.

Design: Observational case report.

Participant: A 55-year-old woman with unilateral bullous keratopathy.

Methods: Clinical observation consisted of slit-lamp examination and in vivo confocal microscopy (IVCM). Aqueous humor samples and the excised corneal button were analyzed for the presence of herpes viruses. The excised cornea was subjected to detailed immunohistochemistry (IHC) and scanning and transmission electron microscopy.

Main outcome measures: Clinical and pathologic characteristics of zipper cell endotheliopathy.

Results: In vivo confocal microscopy revealed unique morphologic alterations of the corneal endothelial layer. Focal areas of denudation were surrounded by endothelial cells with zipper-like cell borders and intercellular structures. Besides central corneal edema, no other signs of corneal inflammation were detected. A herpes virus origin for the bullous keratopathy was excluded. The IHC analysis disclosed positive staining for cytokeratin (CK) 7, CK8/18, and CK19, suggesting epithelial metaplasia of the endothelial cells. Ultrastructural examination confirmed the IVCM findings by showing large areas of endothelial denudation and vacuolated endothelial cells with large, broad-based extensions that partially overlapped neighboring cells. Despite extensive complementary research and review of the literature, the endothelial alterations could not be attributed to any known corneal disorder.

Conclusions: To the authors' knowledge, zipper cell endotheliopathy is a new subset of idiopathic corneal edema. The case report presented illustrates the potential use of IVCM to differentiate the spectrum of corneal disorders and to discover new corneal diseases.

INTRODUCTION

Corneal transparency is largely attributable to a strict fluid and electrolyte balance within the different layers of the cornea. Bullous keratopathy occurs when excessive fluid accumulates in the corneal stroma and becomes trapped beneath an intact epithelial barrier.[1] Two main pathophysiologic mechanisms give rise to this corneal edema: endothelial malfunction and increased intraocular pressure.[2] Congenital hereditary endothelial dystrophy, Fuchs' endothelial dystrophy, posterior polymorphous corneal dystrophy (PPCD), and iridocorneal endothelial (ICE) syndrome are primary causes of endothelial failure. Secondary causes include trauma and corneal inflammation. In clinical practice, differentiation between these entities often is possible. However, herpetic endotheliitis, PPCD, and ICE syndrome can present with overlapping features, obfuscating the diagnosis and application of subsequent appropriate therapeutic intervention.[3–6] This article reports a case with unilateral bullous keratopathy, which displayed a zipper-like arrangement of the endothelial cell borders on in vivo confocal microscopy (IVCM). To the authors' knowledge, this is the first case report describing the detailed in vivo and ex vivo histopathologic features of these novel endothelial changes, referred to as *zipper cell endotheliopathy*.

CASE REPORT

A 55-year-old woman was referred to the Cornea and External Disease Service at the Rotterdam Eye Hospital (Rotterdam, The Netherlands) in February 2006. She had a 14-year history of presumed herpetic disciform keratitis in the left eye for which she had received oral acyclovir, acyclovir ointment, and topical prednisolone treatments during multiple disease recurrences. Three months before the first examination at the clinic, she experienced another episode of blurred vision, redness, and pain in her left eye. On examination, her best-corrected visual acuity (BCVA) was 20/20 in the right eye and 20/100 in the left eye. The intraocular pressures were 15 mmHg in the right eye and 12 mmHg in the left eye. Results of slit-lamp examination of her right eye were normal. Her left eye revealed a focal bullous aspect of the central cornea (Fig 1A). In specular view, the clear corneal periphery displayed an undulating aspect of the endothelial layer without typical guttata, pseudoguttata, or a finely hammered silver appearance. No vesicles or band formations within the endothelial layer were observed. The left eye showed no signs of inflammation such as stromal infiltration, keratic precipitates, or iritis. Under the working diagnosis of presumed herpetic disciform keratitis, her treatment was changed to 500 mg oral valacyclovir twice daily and topical 0.1% dexamethasone twice daily.

Two months later, the BCVA in the left eye had improved to 20/25 and the central corneal edema had subsided (Fig 1B). The patient's corneas were subjected to IVCM

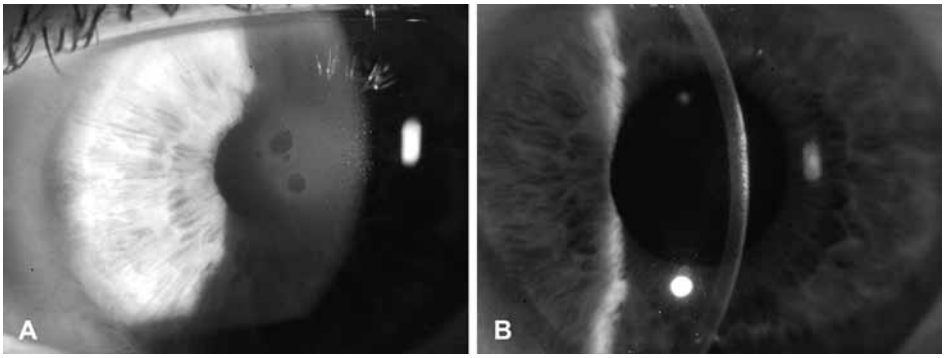

Figure 1. Photographs showing results of slit-lamp examination. **A**, At first presentation, the central cornea showed a focal, gradually demarcated area with stromal edema and several epithelial bullae. **B**, Two months later, with reduction of the corneal edema, the epithelial bullae had resolved; however, the reflectivity of the anterior stroma was increased. (*See also Color figures, p. 208.*)

analyses, using both the Confoscan 3 and 4 (Nidek Technologies, Padova, Italy), according to a previously described method.[7] On IVCM, the central endothelium showed prominent zipper-like interdigitations of the cell margins (Fig 2A). Minor stromal edema was still detectable, whereas other inflammatory parameters such as dendritic cells at the sub-basal plexus level or keratic precipitates were absent.

The condition of her left cornea remained stable over the next 10 months. However, with phasing out of medications, the corneal edema recurred. The intraocular pressure increased to 28 mmHg in the left eye with an open anterior chamber angle on gonioscopic examination. The IVCM analyses showed several areas of endothelial denudation located underneath the central stromal edema (Fig 2B). The paracentral endothelium disclosed meandering cell borders. However, in contrast with previous visits, the interdigitations seemed to be ligated from the endothelial cells, creating small intercellular structures (Fig 2C). During the next 9 months, IVCM analyses showed declining areas of bare Descemet's membrane with acyclovir ointment administered 5 times daily, topical dexamethasone (0.1%) administered 3 times daily, 500 mg oral valacyclovir administered 3 times daily, and topical timolol twice daily. Nevertheless, her vision deteriorated further after this second period of recovery. The stromal edema recurred over the central one third of the cornea without other signs of inflammation. Afterward, the central endothelium could not be visualized by IVCM. After 23 months, all therapy was ceased, and 1 month later an aqueous humor (AH) tap was performed for diagnostic purposes.

Finally, 29 months after the initial presentation, she underwent top hat mushroom penetrating keratoplasty. Her BCVA at that time was 20/400. During surgery, a second AH sample was collected for analogous herpes virus diagnostic analyses. The postoperative course was uncomplicated. Fourteen months after surgery, her BCVA was 20/40 and she had a clear corneal graft without recurrence of the endotheliopathy.

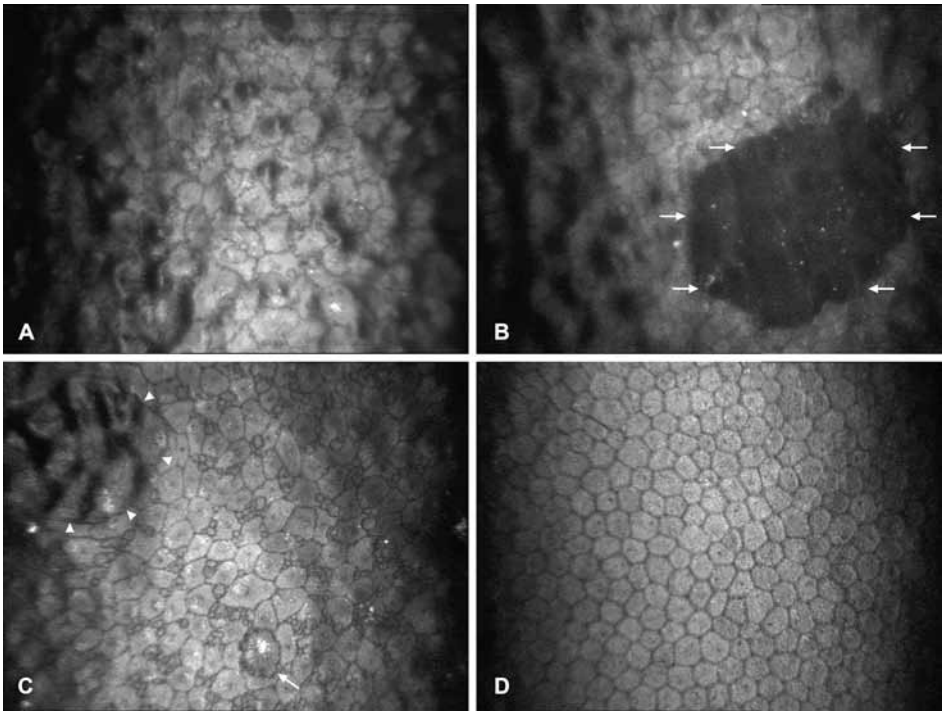

Figure 2. In vivo confocal microscopy. **A**, Intercellular margins of the endothelial cells of the central cornea display a highly meandering aspect. The endothelial layer has an irregular, undulating aspect without typical guttata, pseudoguttata, or a light–dark reversal of the cells. **B**, With recurrence of the corneal edema, the central endothelium displays an area of bare Descemet's (between the opposing arrows). **C**, At a paracentral location at the 9-o'clock position, the interdigitations of the cell borders seem to be ligated from the endothelial cell bodies, creating small, solitary, intercellular structures. Other morphologic features were a nummular area with a diameter of approximately 150 µm (arrowheads), and the presence of a darkened endothelial cell with a bright central reflection (arrow), presumably in apoptosis. **D**, Normal endothelium in the patient's normal right eye. Endothelial cell density, 2179 cells/mm^2.

The protocol, which included this observational case report, was approved by the local institutional review board and the medical ethical committee and was performed in accordance with the Declaration of Helsinki. Informed consent was obtained from the subject.

METHODS

Herpes Virus Diagnostic Analyses

Analyses of the AH samples were performed as described previously[8,9] for DNA or evidence of local antibody production specific for the following herpes viruses: herpes simplex virus types 1 and 2, varicella zoster virus, cytomegalovirus, or Epstein-Barr virus.

The corneal button, with a diameter of 7.0 mm on the epithelial side and 9.0 mm on the endothelial side, was divided through its center into 2 equal parts. Subsequently, one half of the cornea was divided into 2 quarters. One quarter of the corneal tissue was triturated and DNA was isolated using the MagnaPure DNA tissue kit II (Roche Diagnostics, Almere, The Netherlands) combined with the MagnaPure LC isolation station (Roche Diagnostics), according to the manufacturer's instructions. The presence of intracorneal deposition of viral DNA of the herpes simplex virus, varicella zoster virus, cytomegalovirus, and Epstein-Barr virus was assayed with real-time polymerase chain reaction, essentially as described previously.[8] The sensitivity of the real-time polymerase chain reaction assays used was approximately 200 virus genome copies/ml.[8]

In Situ Analyses of the Corneal Button

To determine the histopathologic features of the corneal lesions, the excised corneal button was subjected to detailed in situ analyses including immunohistochemistry (IHC), scanning electron microscopy (SEM), and transmission electron microscopy (TEM).

For IHC, one half of the cornea was formalin fixed, embedded in paraffin, and stained with hematoxylin–eosin. Subsequently, tissue sections were incubated with the following primary monoclonal antibodies to determine the expression of the following cytokeratins (CKs): CK5/6 (clone D5/16 B4; DakoCytomation, Heverlee, Belgium) dilution 1:50; CK7 (OV-TL 12/30; DakoCytomation) dilution 1:1000; CK8/18 (5D3; Biogenex, San Ramon, CA) dilution 1:1000; CK19 (RCK 108; DakoCytomation) dilution 1:25; and CK 34BE12 (34BE12; DakoCytomation) dilution 1:50. Sections were developed with EnVision horseradish peroxidase (DakoCytomation) using diaminobenzidine as substrate (DakoCytomation), which resulted in a brown color in CK-expressing cells. All tissue sections were counterstained with hematoxylin, resulting in blue nuclei. Both a negative control (i.e., omission of primary antibody) and positive control (i.e., human tissue expressing the respective cytokeratin) were included on every slide.

One quarter of the cornea was fixed in 1.5% glutaraldehyde and was submitted for SEM and TEM. For SEM, half of the specimen was buffered in 0.1 M Na-cacodylate for 1 hour at room temperature, followed by dehydration in a series of graduated ethanol solutions up to 100%. After critical point drying, the specimen was mounted on stubs and sputter-coated with gold palladium. Subsequently, the endothelial surface was examined with a JSM 6700F scanning electron microscope (JEOL, Tokyo, Japan).

The remaining half of the glutaraldehyde-fixed specimen was postfixed in a 1:1 mixture of 2% osmium tetroxide and 2% potassium ferrocyanide and was dehydrated in ascending alcohol concentrations. The tissue was treated with propylene oxide and embedded in epon. First, 1-µm thick sections were stained with toluidine blue. A representative slice subsequently was sectioned into 100- to 120-nm slices and was stained with uranyl ac-

etate and lead citrate. These ultra-thin sections were examined with a Philips Morgagni 268D transmission electron microscope (Philips, Eindhoven, The Netherlands).

RESULTS

Analyses of both AH samples and the corneal button showed no evidence of a herpes virus origin (data not shown). Light microscopy showed bullous keratopathy and microcystic map-dot-fingerprint dystrophy. No signs of stromal inflammation were detected. The Descemet's membrane was slightly irregular with focally double-layered endothelium with oval nuclei (Fig 3A). The IHC analyses revealed that the endothelial cells stained strongly positive for CK8/18, positive for CK19, and focally positive for CK7 (Fig 3B–D). The endothelial cells were negative for CK5/6 and 34BE12 (data not shown).

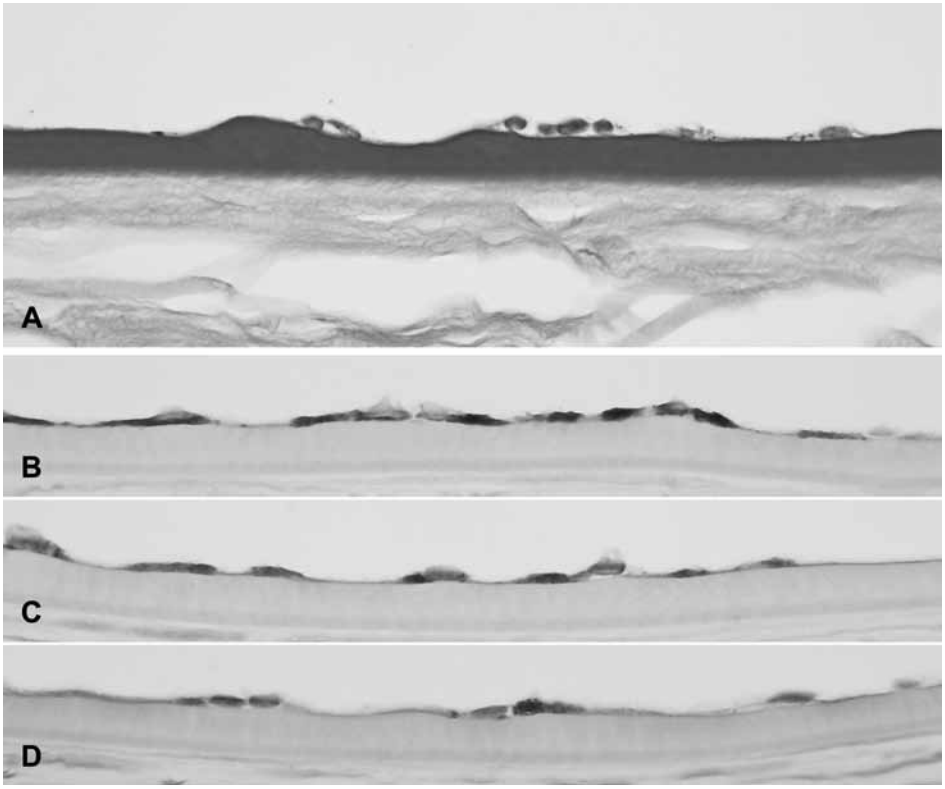

Figure 3. Photomicrographs showing light microscopy and immunohistochemical analysis results. **A**, Light microscopy showing a slightly irregular Descemet's membrane with a focally double-layered endothelium with oval nuclei. **B**, Immunohistochemically, the cytoplasm of the endothelial cells stained strongly positive for cytokeratin 8/18. **C**, Positive staining for cytokeratin 19. **D**, Focal positive staining for cytokeratin 7. (*See also Color figures, p. 209.*)

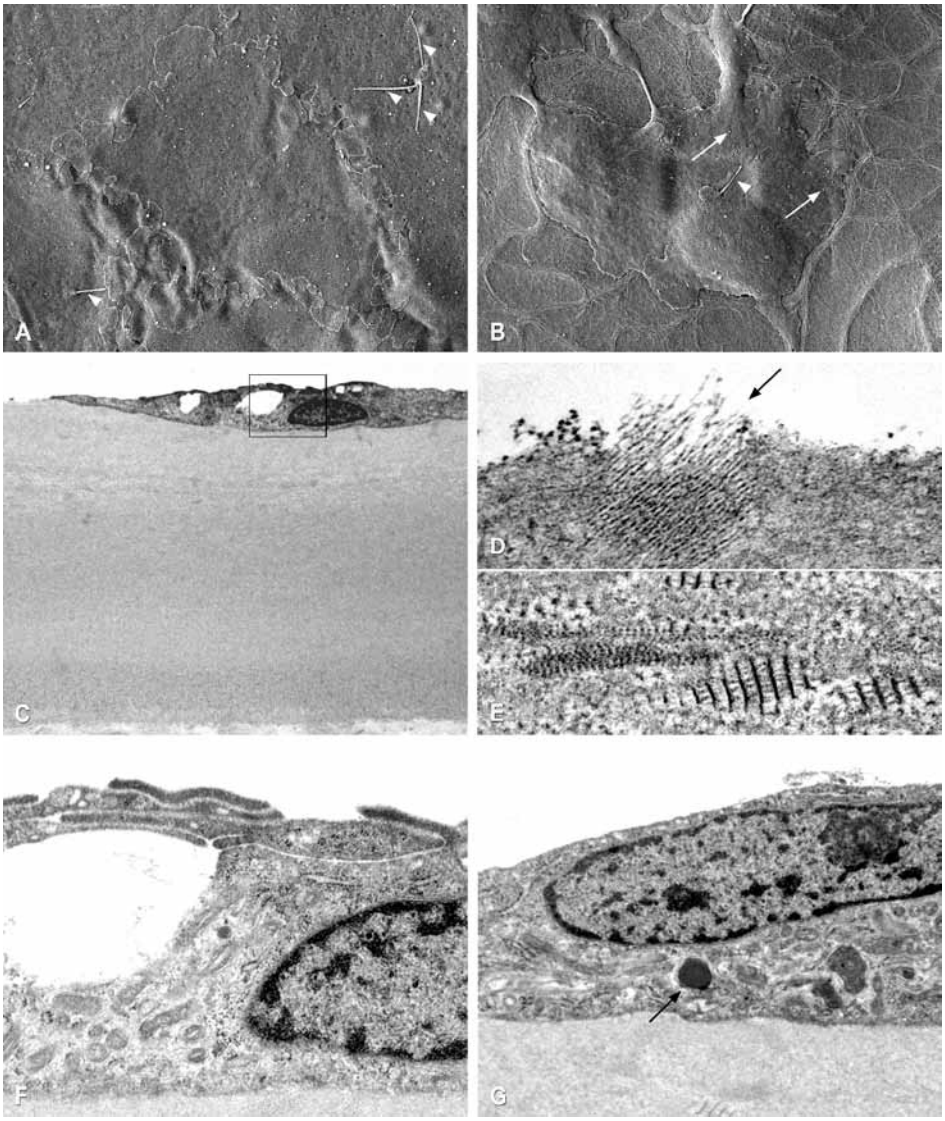

Ultrastructural examination of the corneal endothelial surface revealed a variety of abnormalities (Fig 4). Endothelial cells were decreased in number and displayed increased polymegathism and pleomorphism. The endothelial apical surface was smooth and contained few microvilli (10–15 per cell). Additionally, most endothelial cells possessed 1 or more cilia. The most prominent deviation, however, was the appearance of the apical intercellular borders that disclosed large, broad-based interlocking processes. These zipper-like cell margins partially overlapped with the neighboring cells. A few cell borders had opened up and revealed small intercellular areas of bare Descemet's mem-

Figure 4. Scanning electron microscopy (SEM) and transmission electron microscopy results. **A**, Appearance of a so-called zipper cell on SEM. The cell margins show large, broad-based interdigitations that overlapped neighboring cells. Most zipper cells contained 1 or more cilia (arrowheads). **B**, Migrating endothelial cell appears to bridge a large denuded area. The cell maintains contact with the leading edge through filipodial cytoplasmic projections. Other features of the apical cell surface were small sheets of extending plasma membrane, a flat bulge representing a large oval nucleus, few microvilli (arrows), cellular pits, and a central cilium (arrowhead). The denuded parts of Descemet's membrane show a reticular pattern of collagen fibrils. **C**, Transmission electron microscopy revealing an irregularly thickened Descemet's membrane, only partially covered by vacuolated endothelial cells with oval nuclei. Besides abnormal lamination, Descemet's membrane displayed a posterior collagenous layer (PCL). **D**, This PCL shows irregularly arranged wide-spaced collagen with areas devoid of endothelial cells and with fibrillar extensions into the anterior chamber (arrow). **E**, Wide-spaced collagen showing a striated fusiform configuration, with an internode distance of approximately 100 nm. **F**, Higher magnification of the boxed area in Figure 4C showing an intercellular border without junctions that terminates in a large vacuole. Consequently, the vacuole seems to communicate directly with the anterior chamber. **G**, In addition to mitochondria and endoplasmic reticulum, several endothelial cells contained electron-dense lysosomal-like structures (arrow). The endothelial surface was smooth without prominent microvilli.

brane. Other parts of the posterior corneal surface showed larger areas of endothelial denudation, exhibiting thin criss-cross–orientated collagen fibers. No necrotic cells or signs of inflammation could be identified.

On TEM (Fig 4C–G), the Descemet's membrane displayed irregular intumescences and a disorganized fiber structure of its posterior portion, consistent with a posterior collagenous layer. Although the enlarged endothelial cells had overlapping cell margins, squamous differentiation was absent. A few endothelial cells possessed a small, dark nucleus with little cytoplasm, whereas others displayed prominent cytoplasm with vacuolization, scattered organelles, and few lysosomal-like structures. The lateral borders showed few intermediate junctions. No inflammatory component was found.

DISCUSSION

This report describes a new subset of idiopathic corneal edema referred to as *zipper cell endotheliopathy*. This condition is described in a patient with unilateral bullous keratopathy and is characterized by alterations of the endothelial layer, showing zipper-like cell borders and intercellular structures. In vivo confocal microscopy enabled high-resolution images of the endothelial layer in an obscured cornea to be obtained. To the authors' knowledge, this report is the first to describe these unique morphologic changes in human corneal endothelium in vivo.

Zipper cell endotheliopathy may represent an aberrant wound healing response to chronic endothelial damage provoked by any kind of stimulus (trauma, toxic injury, increased intraocular pressure, inflammation, or degenerative processes). Characteristic zipper-like cell borders were demonstrated during endothelial wound repair in ex vivo

animal models.[10] Intercellular structures can result after endothelial wound closure, as was demonstrated in human corneal flat mounts preserved in organ culture medium.[11]

In humans, endothelial cell division is only a minor component of the reparative response.[12] A continuous monolayer of cells is reestablished in denuded areas mainly by reorganization, enlargement, and migration.[10] During migration, most endothelial cells stay in contact with the leading edge of the wound.[11] This feature was observed by SEM in the patient (Fig 4B). Migration of endothelial cells from the peripheral to paracentral regions of the cornea may cause an increase in cilia, as seen in the corneal button in the patient, whereas cilia normally are found in a zone 1.25 to 0.75 mm from the trabecular meshwork and are sparse in the central and paracentral regions of the endothelium.[13] Another element of the endothelial repair process is the production of a posterior collagenous layer with guttata-like excrescences.[10,12] In the current case, this may explain the permanent undulating aspect of the endothelium in specular view by slit-lamp examination.

Based on medical history and clinical findings, congenital hereditary endothelial dystrophy, Fuchs' endothelial dystrophy, increased intraocular pressure, and trauma were ruled out. Appendix 1 (available at http://aaojournal.org) summarizes the 3 remaining options in the differential diagnosis of unilateral corneal edema with endothelial changes: herpetic endotheliitis, posterior polymorphous corneal dystrophy, and the iridocorneal endothelial syndrome.

Herpetic Endotheliitis

The patient had a recrudescent course of blurred vision, ocular redness, and pain at presentation. This intermittent pattern of symptoms and unilateral involvement is characteristic of herpetic endotheliitis.[14] Also, the undulating aspect of the endothelium in specular view may fit with herpetic endotheliitis. Pseudoguttata, which are responsible for this wave-like appearance, can be observed in all kinds of inflammatory disorders during the active phase. With appropriate treatment, the cellular edema disappears within several weeks and the endothelium returns to its flattened state, showing a golden reflection in specular view.[7] In this case, however, the undulating aspect persisted during follow-up. Furthermore, both IVCM and in situ analyses of the excised cornea did not reveal characteristic inflammatory signs that commonly accompany herpetic endotheliitis. Stromal infiltration, keratic precipitates, and iritis[15,16] were not observed during the complete course.

Besides endothelial denudation, IVCM images of the patient showed no endothelial alterations, which are characteristic of herpetic endotheliitis (Fig 5A). Vice-versa, zipper-like cell borders or intercellular structures were not observed in a large IVCM study of endothelial alterations in herpes simplex virus keratitis.[7] Finally, the viral diagnostic

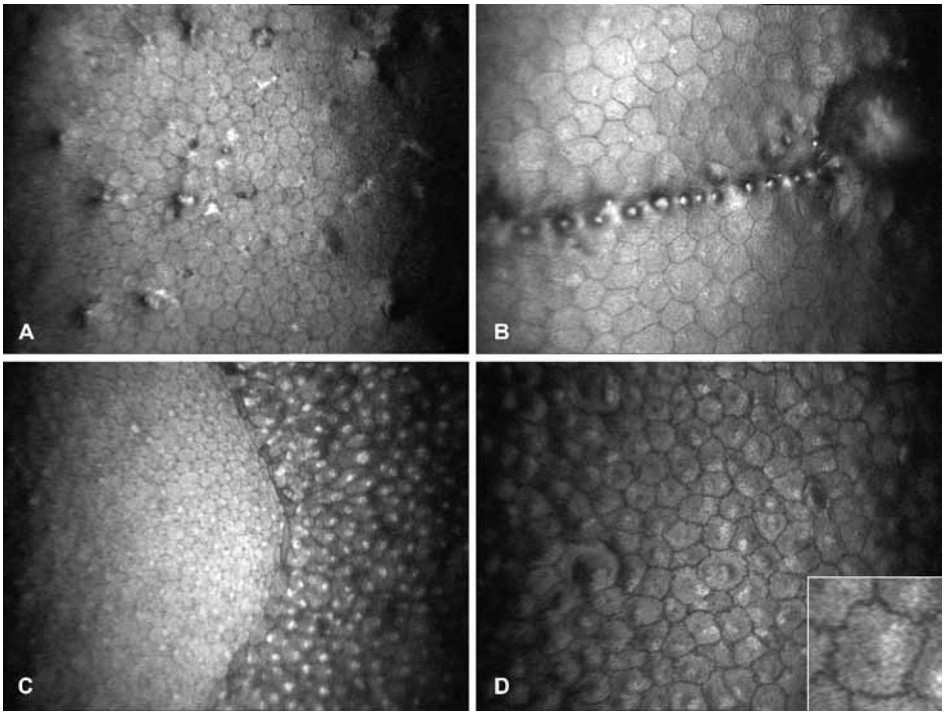

Figure 5. In vivo confocal microscopy images of patients with herpetic endotheliitis, posterior polymorphous corneal dystrophy (PPCD), and iridocorneal endothelial (ICE) syndrome showing the differential diagnosis of zipper cell endotheliopathy. **A**, Pseudoguttata, intercellular gaps, and infiltration of inflammatory cells in a patient with herpetic endotheliitis. Endothelial cell density (ECD), 3254 cells/mm^2. **B**, Band formation and a vesicle in the endothelial layer of a patient with PPCD. ECD, 1268 cells/mm^2. **C**, Endothelium in a patient with ICE syndrome. A borderline is detected with, on the right side, affected ICE cells that show characteristic light–dark reversal and, on the left side, normal endothelial cells: subtotal, ICE (+).[31] ECD (left side), 7684 cells/mm^2. **D**, Endothelium in another patient with ICE syndrome. The entire posterior corneal surface was covered with ICE tissue: total ICE.[31] ECD, 1380 cells/mm^2. Bottom right inset shows enlargement of 1 ICE cell with zipper-like cell borders.

analyses on the sequential AH samples and the excised cornea did not provide evidence for a herpes virus origin of disease.

Posterior Polymorphous Corneal Dystrophy

Posterior polymorphous corneal dystrophy is considered a hereditary bilateral disorder with, in some cases, considerable asymmetry.[17] Although the current patient had no known relatives with corneal disorders, unilateralism can still fit with PPCD. Nonetheless, most patients with PPCD remain asymptomatic and only a few cases show a slow progressive course.[18,19] An intermittent course, as seen in the current patient, has never been documented for PPCD. In addition, endothelial alterations characteristic of PPCD,

such as vesicles or band formations[20] (Fig 5B), were not observed by slit-lamp or IVCM examination.

Many cases of PPCD have peripheral anterior synechiae at presentation.[3] These iridocorneal adhesions are correlated with a higher incidence and severity of glaucoma and with worse visual outcome after keratoplasty.[20] On gonioscopic examination, the current patient had an open angle without iridocorneal adhesions.

Double-layered endothelial cells with an irregularly thickened Descemet's membrane, as displayed by light microscopy, are suggestive of PPCD;[21] however, the relatively low resolution of light microscopy limits the ability to differentiate between partially overlapping and true double layering of endothelial cells. Eventually, double layering was excluded by TEM, which showed only overlapping endothelial cells.

Expression of CK7, CK8/18, and CK19 was found in the endothelial cells of the patient. This CK expression pattern is consistent with PPCD[19,22,23] and is probably related to a metaplastic process in the endothelial layer.[23] However, expression of epithelial CKs also has been reported for congenital hereditary endothelial dystrophy,[22] Fuchs' endothelial dystrophy,[24] and ICE syndrome.[25–27] Hence, epithelial metaplasia may represent a nonspecific response of distressed endothelial cells. In the authors' opinion, differentiation between corneal disorders based on IHC is impossible at present.

Iridocorneal Endothelial Syndrome

As in the current patient, ICE syndrome is characterized by unilateral involvement. An intermittent pattern of symptoms, although uncommon, is documented for ICE syndrome.[28] However, iridocorneal adhesions, one of the main findings in ICE syndrome,[29] were not observed in the current patient.

Diagnosis of ICE syndrome by specular microscopy or IVCM is based on the detection of ICE cells[30] (Fig 5C). These epithelial-like endothelial cells can display meandering cell borders, as we observed in another patient diagnosed with ICE syndrome (Fig 5D). Despite this similarity, the IVCM images of the endothelial alterations in the current patient showed manifest differences compared with these ICE cells. There was no regular cobblestone appearance of the endothelial layer, as can be seen in ICE-affected tissue, the endothelial cells lacked hyperreflective nuclei or light–dark reversal, the zipper-like interdigitations of the cell margins were more prominent, and intercellular structures were detected. Ultrastructural examination, as well as IVCM, has shown zipper-like arrangements of the cell borders in ICE cells.[32] The large, broad-based extensions of endothelial cells like those seen in the current patient, however, showed manifest differences compared with the complex interlocking projections that account for the zipper-like configurations in ICE syndrome. The broad-based extensions in the current case may have created the aspect of intercellular structures when viewed by IVCM.

Expression of cilia at the apical surface of endothelial cells in the central cornea, as seen in the current patient, also is reported for ICE patients.[33] In contrast to this report, several endothelial cells in the current patient possessed up to 3 cilia (Fig 4A). Besides cilia, the apical surface of ICE cells displays increased microvilli expression and formation of endothelial blebs.[33] The lateral intercellular borders of these epithelial-like endothelial cells were found to contain numerous desmosomes.[34] In contrast, the endothelial cells in the current patient showed a normal distribution of microvilli, lacked endothelial blebs, and exhibited intermediate junctions consistent with normal endothelium.[35] No evidence was found for the presence of a low-grade chronic inflammatory process like those observed in ICE syndrome.[32]

Epithelial metaplasia of the endothelial layer is described for ICE syndrome.[25–27] Isolated expression was observed only for CK3[27] and CK19.[26] Furthermore, there are conflicting reports about the expression of CK8/18.[23] Based on the staining pattern observed in the patient, ICE syndrome could neither be diagnosed nor ruled out.

In conclusion, extensive complementary research and review of the literature could not provide a cause for the endothelial changes in the patient. Zipper cell endotheliopathy is a new subset of idiopathic corneal edema characterized by unique morphologic alterations that may represent an aberrant wound-healing response to chronic endothelial damage. Long-term follow-up of the patient and reports of similar cases are needed to provide further insight in the incidence, cause, and treatment options of zipper cell endotheliopathy. Furthermore, this case is an excellent illustration of the possible use of IVCM to study cellular changes in an obscured cornea. This technique can be used for further differentiation of the spectrum of known corneal disorders and can lead to the discovery of new corneal diseases.

REFERENCES

1. Feiz V. Corneal edema. In: Krachmer JH, Mannis MJ, Holland EJ, eds. Cornea. 2nd ed. vol. 1. London: Elsevier Mosby; 2005:359–63.
2. Levenson JE. Corneal edema: cause and treatment. Surv Ophthalmol 1975;20:190–204.
3. Cibis GW, Krachmer JH, Phelps CD, Weingeist TA. Iridocorneal adhesions in posterior polymorphous dystrophy. Trans Sect Ophthalmol Am Acad Ophthalmol Otolaryngol 1976;81: 770–7.
4. Anderson NJ, Badawi DY, Grossniklaus HE, Stulting RD. Posterior polymorphous membranous dystrophy with overlapping features of iridocorneal endothelial syndrome. Arch Ophthalmol 2001;119:624–5.
5. Alvarado JA, Underwood JL, Green WR, et al. Detection of herpes simplex viral DNA in the iridocorneal endothelial syndrome. Arch Ophthalmol 1994;112:1601–9.
6. Grupcheva CN, Craig JP, Sherwin T, McGhee CN. Differential diagnosis of corneal oedema assisted by in vivo confocal microscopy. Clin Experiment Ophthalmol 2001;29:133–7.
7. Hillenaar T, Weenen C, Wubbels RJ, Remeijer L. Endothelial involvement in herpes simplex virus keratitis: an in vivo confocal microscopy study. Ophthalmology 2009;116: 2077–86.
8. Remeijer L, Duan R, van Dun JM, et al. Prevalence and clinical consequences of herpes simplex virus type 1 DNA in human cornea tissues. J Infect Dis 2009;200:11–9.
9. Milikan JC, Kuijpers RW, Baarsma GS, et al. Characterization of the varicella zoster virus (VZV)-specific intra-ocular T-cell response in patients with VZV-induced uveitis. Exp Eye Res 2006;83: 69–75.
10. Van Horn DL, Sendele DD, Seideman S, Buco PJ. Regenerative capacity of the corneal endothelium in rabbit and cat. Invest Ophthalmol Vis Sci 1977;16:597–613.
11. Hoppenreijs VP, Pels E, Vrensen GF, et al. Effects of human epidermal growth factor on endothelial wound healing of human corneas. Invest Ophthalmol Vis Sci 1992;33:1946–57.
12. Waring GO III, Bourne WM, Edelhauser HF, Kenyon KR. The corneal endothelium: normal and pathologic structure and function. Ophthalmology 1982;89:531–90.
13. Svedbergh B, Bill A. Scanning electron microscopic studies of the corneal endothelium in man and monkeys. Acta Ophthalmol (Copenh) 1972;50:321–36.
14. Sundmacher R, Muller O. The corneal endothelium in ophthalmic zoster [in German]. Klin Monbl Augenheilkd 1982; 180:271–4.
15. Liesegang TJ. Classification of herpes simplex virus keratitis and anterior uveitis. Cornea 1999;18: 127–43.
16. Holland EJ, Schwartz GS. Classification of herpes simplex virus keratitis. Cornea 1999;18:144–54.
17. Waring GO III, Rodrigues MM, Laibson PR. Corneal dystrophies. II. Endothelial dystrophies. Surv Ophthalmol 1978;23:147–68.
18. Cibis GW, Krachmer JA, Phelps CD, Weingeist TA. The clinical spectrum of posterior polymorphous dystrophy. Arch Ophthalmol 1977;95:1529–37.
19. Moroi SE, Gokhale PA, Schteingart MT, et al. Clinicopathologic correlation and genetic analysis in a case of posterior polymorphous corneal dystrophy. Am J Ophthalmol 2003; 135:461–70.
20. Patel DV, Grupcheva CN, McGhee CN. In vivo confocal microscopy of posterior polymorphous dystrophy. Cornea 2005;24:550–4.
21. Krachmer JH. Posterior polymorphous corneal dystrophy: a disease characterized by epithelial-like endothelial cells which influence management and prognosis. Trans Am Ophthalmol Soc 1985;83:413–75.

22. Cockerham GC, Laver NV, Hidayat AA, McCoy DL. An immunohistochemical analysis and comparison of posterior polymorphous dystrophy with congenital hereditary endothelial dystrophy. Cornea 2002;21:787–91.
23. Jirsova K, Merjava S, Martincova R, et al. Immunohistochemical characterization of cytokeratins in the abnormal corneal endothelium of posterior polymorphous corneal dystrophy patients. Exp Eye Res 2007;84:680–6.
24. Hidayat AA, Cockerham GC. Epithelial metaplasia of the corneal endothelium in Fuchs endothelial dystrophy. Cornea 2006;25:956–9.
25. Kramer TR, Grossniklaus HE, Vigneswaran N, et al. Cytokeratin expression in corneal endothelium in the iridocorneal endothelial syndrome. Invest Ophthalmol Vis Sci 1992;33: 3581–5.
26. Levy SG, McCartney AC, Baghai MH, et al. Pathology of the iridocorneal-endothelial syndrome: the ICE-cell. Invest Ophthalmol Vis Sci 1995;36:2592–601.
27. Hirst LW, Bancroft J, Yamauchi K, Green WR. Immunohistochemical pathology of the corneal endothelium in iridocorneal endothelial syndrome. Invest Ophthalmol Vis Sci 1995;36:820–7.
28. Patel A, Kenyon KR, Hirst LW, et al. Clinicopathologic features of Chandler's syndrome. Surv Ophthalmol 1983;27: 327–44.
29. Shields MB. Progressive essential iris atrophy, Chandler's syndrome, and the iris nevus (Cogan-Reese) syndrome: a spectrum of disease. Surv Ophthalmol 1979;24:3–20.
30. Laganowski HC, Sherrard ES, Muir MG, Buckley RJ. Distinguishing features of the iridocorneal endothelial syndrome and posterior polymorphous dystrophy: value of endothelial specular microscopy. Br J Ophthalmol 1991;75:212–6.
31. Sherrard ES, Frangoulis MA, Muir MG, Buckley RJ. The posterior surface of the cornea in the iridocorneal endothelial syndrome: a specular microscopical study. Trans Ophthalmol Soc U K 1985; 104(Pt 7):766–74.
32. Alvarado JA, Murphy CG, Maglio M, Hetherington J. Pathogenesis of Chandler's syndrome, essential iris atrophy and the Cogan-Reese syndrome. I. Alterations of the corneal endothelium. Invest Ophthalmol Vis Sci 1986;27:853–72.
33. Sherrard ES, Frangoulis MA, Muir MG. On the morphology of cells of posterior cornea in the iridocorneal endothelial syndrome. Cornea 1991;10:233–43.
34. Levy SG, Kirkness CM, Moss J, et al. The histopathology of the iridocorneal-endothelial syndrome. Cornea 1996;15: 46–54.
35. Barry PA, Petroll WM, Andrews PM, et al. The spatial organization of corneal endothelial cytoskeletal proteins and their relationship to the apical junctional complex. Invest Ophthalmol Vis Sci 1995;36:1115–24.

APPENDIX 1.

Differential diagnosis of zipper cell endotheliopathy

A. Herpetic endotheliitis

Clinical features	– Recurrent episodes of blurred vision – Ocular pain/discomfort – Mild photophobia – Limbal injection	+ 1; 2
Slit-lamp examination	– 3 forms of herpetic endotheliitis: disciform, diffuse, and linear – Keratic precipitates, corneal edema, iritis – Severe cases may show corneal scarring, neovascularisation and decompensation – Increased intraocular pressure – Vast majority of cases unilateral	+/– 1; 2; 9
Specular microscopy / In vivo confocal microscopy (Fig 6)	– Pseudoguttata – Intercellular gaps – Infiltration of inflammatory cells – Loss of defined cell borders – Spot-like holes – Endothelial denudation	– 14; 15
Viral associations	– HSV-1 antigen, HSV DNA, and HSV particles have been demonstrated in endothelial cells, aqueous humor, and trabeculae – Varicella-zoster virus particles were found by transmission electron microscopy in endothelial cells – Cytomegalovirus DNA was detected by PCR in aqueous humor	– 24-31
Light microscopy	– Edema, degeneration, or absence of endothelial cells – Regular or thinned Descemet's membrane – Some cases disclosed granulomatous cell reactions at the level of Descemet's membrane	– 27; 35; 36
Immunohistochemical analysis	– No documented cytokeratin expression pattern	x
Scanning electron microscopy	– Cellular edema, with concomitant opening-up of intercellular junctions – Loss of defined cell boundaries – Increased number and length of microvilli – Giant cell formation – Spot-like holes – Peripheral endothelial denudation – Infiltration of inflammatory cells	– 46-48
Transmission electron microscopy	– 2 cell types: normal and degenerating endothelial cells – Incorporation of inflammatory cells into the endothelial layer – Posterior collagenous layer – Granulomatous cell reactions at the level of Descemet's membrane – Retrocorneal ridges	+/– 47; 48; 55-57
Genetic analysis	– Not applicable	x

Symbols in the gray box at the top left corner of each section are an indication of the level of conformity with zipper cell endotheliopathy; + = supportive; +/– = indifferent; – = unsupportive; x = not known / not applicable; HSV = herpes simplex virus; PCR = polymerase chain reaction; CK = cytokeratin

B. Posterior polymorphous corneal dystrophy

Clinical features	– Most cases asymptomatic. – Slow, painless, visual loss due to corneal decompensation or intercurrent glaucoma	– 3-5
Slit-lamp examination	– 3 forms of endothelial alterations: vesicles, band formations, and diffuse alterations – Thickening of Descemet's membrane – Corneal decompensation – Broad iridocorneal adhesions, corectopia – Increased intraocular pressure – Most cases bilateral, often asymmetric	+/– 3; 4; 10
Specular microscopy / In vivo confocal microscopy (Fig 6)	– Vesicular and curvilinear abnormalities – Guttata – Polymegathism, pleomorphism – Hyperreflectivity around the lesions at the level of Descemet's membrane	– 16-19
Viral associations	– No evidence for association with viral infections	+
Light microscopy	– Multilayering of endothelial cells – Polygonal cells with round nuclei and large cytoplasm – Irregular thickening of Descemet's membrane	+ 4; 37
Immunohistochemical analysis	– Positive staining: CK7, CK8, CK18, CK19, pan-cytokeratin (=AE1/AE3) – Weak staining: CK1, CK3/12, CK4, CK5/6, CK10, CK10/13, CK14, CK16, CK17 – Negative: CK2e, CK9, CK15, CK20	+ 39-42
Scanning electron microscopy	– 2 endothelial cell populations: endothelial-like and epithelial-like cells – Increased number of microvilli – Areas of bare Descemet – Nest of abnormal cells	– 4; 49-52
Transmission electron microscopy	– 4 cell types: normal, epithelial-like, fibroblast-like, and degenerating endothelial cells – Epithelial-like cells: multilayering, desmosomes, microvilli, scant mitochondria, and cytokeratin intermediate filaments – Descemet's membrane: irregular thicknening, normal anterior banded and abnormal posterior non-banded zone, and a posterior collagenous layer	+/– 4; 37; 49-52; 58
Genetic analysis	– Autosomal dominant inheritance – Mutations found in COL8A2, VSX1, and TCF8 genes	x 3; 60-62

Symbols in the gray box at the top left corner of each section are an indication of the level of conformity with zipper cell endotheliopathy; + = supportive; +/– = indifferent; – = unsupportive; x = not known / not applicable; HSV = herpes simplex virus; PCR = polymerase chain reaction; CK = cytokeratin

C. Iridocorneal endothelial syndrome

Clinical features	– Pupillary distortion – Progressive, sometimes intermittent, visual loss, as result of corneal edema or secondary glaucoma – Occasionally ocular pain	+/– 6-8
Slit-lamp examination	– Finely hammered silver appearance of endothelium (Chandler's syndrome) – Diffuse corneal edema – Peripheral anterior synechiae, distortion of the pupil, iris atrophy (essential iris atrophy) – Small nodules on iris surface (Cogan-Reese syndrome) – Increased intraocular pressure – Vast majority of cases unilateral	+/– 6; 7; 11-13
Specular microscopy / In vivo confocal microscopy (Fig 6)	– ICE-cells: epithelial-like endothelial cells with bright nuclei, showing "light-dark reversal" – Polymegathism, pleomorphism – Some cases displayed a demarcation line between ICE-cells and normal endothelial cells: "subtotal-ICE"	– 20-23
Viral associations	– HSV DNA has been demonstrated by PCR in aqueous humor and corneal specimens – Some cases showed elevated levels of serum antibodies to Epstein-Barr virus	+/– 32-34
Light microscopy	– Multilayering of endothelial cells – Attenuated endothelial cells with flattened nuclei – Diffuse thickening of Descemet's membrane	+/– 8; 38
Immunohistochemical analysis	– Positive staining: CK3 (=AE5), CK5/8, CK19, CK8/18/19 (=Pkk1), pan-cytokeratin (=AE1+AE3, CK-BS, 34BE12, KL1) – Negative: CK8/18, CK13 (=AE8)	+/– 43-45
Scanning electron microscopy	– 3 endothelial cell populations: healthy cells, cells with surface modifications, and necrotic cells – Increased number of microvilli, filipodia, blebs, central cilium – Zipper-like intercellular borders – Areas of endothelial denudation	+/– 38; 53; 54
Transmission electron microscopy	– 4 cell types: normal, epithelial-like, fibroblast-like, and necrotic endothelial cells – Epithelial-like cells: multilayering, desmosomes, microvilli, conspicuous tono- and intermediate filaments, absent marginal fold, and increased tortuosity of intercellular borders – Low grade inflammation with infiltration of inflammatory cells – Descemet's membrane: uniform thickening, normal anterior banded and abnormal posterior non-banded zone, and a posterior collagenous layer	+/– 8; 38; 54; 59
Genetic analysis	– No documented inheritance pattern – Only few familial cases reported	x 6

Symbols in the gray box at the top left corner of each section are an indication of the level of conformity with zipper cell endotheliopathy; + = supportive; +/– = indifferent; – = unsupportive; x = not known / not applicable; HSV = herpes simplex virus; PCR = polymerase chain reaction; CK = cytokeratin

REFERENCES

1. Liesegang TJ. Classification of herpes simplex virus keratitis and anterior uveitis. Cornea 1999;18: 127-43.
2. Holland EJ, Schwartz GS. Classification of herpes simplex virus keratitis. Cornea 1999;18:144-54.
3. Cibis GW, Krachmer JA, Phelps CD, Weingeist TA. The clinical spectrum of posterior polymorphous dystrophy. Arch Ophthalmol 1977;95:1529-37.
4. Krachmer JH. Posterior polymorphous corneal dystrophy: a disease characterized by epithelial-like endothelial cells which influence management and prognosis. Trans Am Ophthalmol Soc 1985;83:413-75.
5. Waring GO, III, Bourne WM, Edelhauser HF, Kenyon KR. The corneal endothelium: normal and pathologic structure and function. Ophthalmology 1982;89:531-90.
6. Shields MB. Progressive essential iris atrophy, Chandler's syndrome, and the iris nevus (Cogan-Reese) syndrome: a spectrum of disease. Surv Ophthalmol 1979;24:3-20.
7. Wilson MC, Shields MB. A comparison of the clinical variations of the iridocorneal endothelial syndrome. Arch Ophthalmol 1989;107:1465-8.
8. Patel A, Kenyon KR, Hirst LW, et al. Clinicopathologic features of Chandler's syndrome. Surv Ophthalmol 1983;27:327-44.
9. Sundmacher R. A clinico-virologic classification of herpetic anterior segment diseases with special reference to intraocular herpes. In: Sundmacher R, ed. Herpetische Augenerkrangen. München, Germany: JF Bergmann; 1981:202-10.
10. Waring GO, III, Rodrigues MM, Laibson PR. Corneal dystrophies. II. Endothelial dystrophies. Surv Ophthalmol 1978;23:147-68.
11. Chandler PA. Atrophy of the stroma of the iris; endothelial dystrophy, corneal edema, and glaucoma. Am J Ophthalmol 1956;41:607-15.
12. Cogan DG, Reese AB. A syndrome of iris nodules, ectopic Descemet's membrane, and unilateral glaucoma. Doc Ophthalmol 1969;26:424-33.
13. Yanoff M. Iridocorneal endothelial syndrome: unification of a disease spectrum. Surv Ophthalmol 1979;24:1-2.
14. Vannas A, Ahonen R, Makitie J. Corneal endothelium in herpetic keratouveitis. Arch Ophthalmol 1983;101:913-5.
15. Hillenaar T, Weenen C, Wubbels RJ, Remeijer L. Endothelial involvement in herpes simplex virus keratitis: an in vivo confocal microscopy study. Ophthalmology 2009;116:2077-86.e1-2.
16. Hirst LW, Waring GO, III. Clinical specular microscopy of posterior polymorphous endothelial dystrophy. Am J Ophthalmol 1983;95:143-55.
17. Laganowski HC, Sherrard ES, Muir MG. The posterior corneal surface in posterior polymorphous dystrophy: a specular microscopical study. Cornea 1991;10:224-32.
18. Patel DV, Grupcheva CN, McGhee CN. In vivo confocal microscopy of posterior polymorphous dystrophy. Cornea 2005;24:550-4.
19. Cheng LL, Young AL, Wong AK, et al. Confocal microscopy of posterior polymorphous endothelial dystrophy. Cornea 2005;24:599-602.
20. Hirst LW, Quigley HA, Stark WJ, Shields MB. Specular microscopy of iridocorneal endothelia syndrome. Am J Ophthalmol 1980;89:11-21.
21. Grupcheva CN, McGhee CN, Dean S, Craig JP. In vivo confocal microscopic characteristics of iridocorneal endothelial syndrome. Clin Experiment Ophthalmol 2004;32:275-83.

22. Sherrard ES, Frangoulis MA, Muir MG, Buckley RJ. The posterior surface of the cornea in the iridocorneal endothelial syndrome: a specular microscopical study. Trans Ophthalmol Soc U K 1985; 104 (Pt 7):766-74.
23. Chiou AG, Kaufman SC, Beuerman RW, et al. Confocal microscopy in the iridocorneal endothelial syndrome. Br J Ophthalmol 1999;83:697-702.
24. Ohashi Y, Yamamoto S, Nishida K, et al. Demonstration of herpes simplex virus DNA in idiopathic corneal endotheliopathy. Am J Ophthalmol 1991;112:419-23.
25. Sundmacher R, Neumann-Haefelin D. Herpes simplex virus isolations from the aqueous humor of patients suffering from focal iritis, endotheliitis, and prolonged disciform keratitis with glaucoma [in German]. Klin Monatsbl Augenheilkd 1979;175:488-501.
26. Holbach LM, Asano N, Naumann GO. Infection of the corneal endothelium in herpes simplex keratitis. Am J Ophthalmol 1998;126:592-4.
27. Holbach LM, Font RL, Naumann GO. Herpes simplex stromal and endothelial keratitis: granulomatous cell reactions at the level of Descemet's membrane, the stroma, and Bowman's layer. Ophthalmology 1990;97:722-8.
28. Robin JB, Steigner JB, Kaufman HE. Progressive herpetic corneal endotheliitis. Am J Ophthalmol 1985;100:336-7.
29. Koizumi N, Suzuki T, Uno T, et al. Cytomegalovirus as an etiologic factor in corneal endotheliitis. Ophthalmology 2008;115:292-7.
30. Maudgal PC, Missotten L, De Clercq E, Descamps J. Varicella-zoster virus in the human corneal endothelium: a case report. Bull Soc Belge Ophtalmol 1980;190:71-86.
31. Amano S, Oshika T, Kaji Y, et al. Herpes simplex virus in the trabeculum of an eye with corneal endotheliitis. Am J Ophthalmol 1999;127:721-2.
32. Alvarado JA, Underwood JL, Green WR, et al. Detection of herpes simplex viral DNA in the iridocorneal endothelial syndrome. Arch Ophthalmol 1994;112:1601-9.
33. Groh MJ, Seitz B, Schumacher S, Naumann GO. Detection of herpes simplex virus in aqueous humor in iridocorneal endothelial (ICE) syndrome. Cornea 1999;18:359-60.
34. Tsai CS, Ritch R, Straus SE, et al. Antibodies to Epstein-Barr virus in iridocorneal endothelial syndrome. Arch Ophthalmol 1990;108:1572-6.
35. Green WR, Zimmerman LE. Granulomatous reaction to Descemet's membrane. Am J Ophthalmol 1967;64:Suppl: 555-8.
36. Hogan MJ, Kimura SJ, Thygeson P. Pathology of Herpes Simplex Kerato-Iritis. Trans Am Ophthalmol Soc 1963;61:75-99.
37. Sekundo W, Lee WR, Kirkness CM, et al. An ultrastructural investigation of an early manifestation of the posterior polymorphous dystrophy of the cornea. Ophthalmology 1994;101:1422-31.
38. Alvarado JA, Murphy CG, Maglio M, Hetherington J. Pathogenesis of Chandler's syndrome, essential iris atrophy and the Cogan-Reese syndrome. I. Alterations of the corneal endothelium. Invest Ophthalmol Vis Sci 1986;27:853-72.
39. Ross JR, Foulks GN, Sanfilippo FP, Howell DN. Immunohistochemical analysis of the pathogenesis of posterior polymorphous dystrophy. Arch Ophthalmol 1995;113:340-5.
40. Jirsova K, Merjava S, Martincova R, et al. Immunohistochemical characterization of cytokeratins in the abnormal corneal endothelium of posterior polymorphous corneal dystrophy patients. Exp Eye Res 2007;84:680-6.
41. Moroi SE, Gokhale PA, Schteingart MT, et al. Clinicopathologic correlation and genetic analysis in a case of posterior polymorphous corneal dystrophy. Am J Ophthalmol 2003;135:461-70.
42. Cockerham GC, Laver NV, Hidayat AA, McCoy DL. An immunohistochemical analysis and comparison of posterior polymorphous dystrophy with congenital hereditary endothelial dystrophy. Cornea 2002;21:787-91.

43. Levy SG, McCartney AC, Baghai MH, et al. Pathology of the iridocorneal-endothelial syndrome: the ICE-cell. Invest Ophthalmol Vis Sci 1995;36:2592-601.
44. Hirst LW, Bancroft J, Yamauchi K, Green WR. Immunohistochemical pathology of the corneal endothelium in iridocorneal endothelial syndrome. Invest Ophthalmol Vis Sci 1995;36:820-7.
45. Kramer TR, Grossniklaus HE, Vigneswaran N, et al. Cytokeratin expression in corneal endothelium in the iridocorneal endothelial syndrome. Invest Ophthalmol Vis Sci 1992;33:3581-5.
46. Nagy RM, McFall RC, Sery TW, et al. Scanning electron microscope study of herpes simplex virus experimental disciform keratitis. Br J Ophthalmol 1978;62:838-42.
47. Zheng X, Yamaguchi M, Goto T, et al. Experimental corneal endotheliitis in rabbit. Invest Ophthalmol Vis Sci 2000;41:377-85.
48. O'Brien WJ, Guy J, Taylor JL. Pathogenesis of corneal oedema associated with herpetic eye disease. Br J Ophthalmol 1990;74:723-30.
49. Levy SG, Moss J, Noble BA, McCartney AC. Early-onset posterior polymorphous dystrophy. Arch Ophthalmol 1996;114:1265-8.
50. Threlkeld AB, Green WR, Quigley HA, et al. A clinicopathologic study of posterior polymorphous dystrophy: implications for pathogenetic mechanism of the associated glaucoma. Trans Am Ophthalmol Soc 1994;92:133-65.
51. Henriquez AS, Kenyon KR, Dohlman CH, et al. Morphologic characteristics of posterior polymorphous dystrophy: a study of nine corneas and review of the literature. Surv Ophthalmol 1984;29: 139-47.
52. Rodrigues MM, Sun TT, Krachmer J, Newsome D. Epithelialization of the corneal endothelium in posterior polymorphous dystrophy. Invest Ophthalmol Vis Sci 1980;19:832-5.
53. Sherrard ES, Frangoulis MA, Muir MG. On the morphology of cells of posterior cornea in the iridocorneal endothelial syndrome. Cornea 1991;10:233-43.
54. Levy SG, Kirkness CM, Moss J, et al. The histopathology of the iridocorneal-endothelial syndrome. Cornea 1996;15:46-54.
55. Dawson C, Togni B, Moore TE, Jr. Structural changes in chronic herpetic keratitis: studied by light and electron microscopy. Arch Ophthalmol 1968;79:740-7.
56. Ahonen R, Vannas A, Makitie J. Virus particles and leukocytes in herpes simplex keratitis. Cornea 1984;3:43-50.
57. Lass JH, Krishnan N, Velasco ME, Plotkin J. Human Herpes Simplex Stromal Keratitis: an Immunoperoxidase and Electron Microscopic Study. Cornea 1983;2:147-58.
58. Boruchoff SA, Kuwabara T. Electron microscopy of posterior polymorphous degeneration. Am J Ophthalmol 1971;72:879-87.
59. Alvarado JA, Murphy CG, Juster RP, Hetherington J. Pathogenesis of Chandler's syndrome, essential iris atrophy and the Cogan-Reese syndrome. II. Estimated age at disease onset. Invest Ophthalmol Vis Sci 1986;27:873-82.
60. Biswas S, Munier FL, Yardley J, et al. Missense mutations in COL8A2, the gene encoding the alpha2 chain of type VIII collagen, cause two forms of corneal endothelial dystrophy. Hum Mol Genet 2001;10:2415-23.
61. Heon E, Greenberg A, Kopp KK, et al. VSX1: a gene for posterior polymorphous dystrophy and keratoconus. Hum Mol Genet 2002;11:1029-36.
62. Krafchak CM, Pawar H, Moroi SE, et al. Mutations in TCF8 cause posterior polymorphous corneal dystrophy and ectopic expression of COL4A3 by corneal endothelial cells. Am J Hum Genet 2005; 77:694-708.

8

General discussion

GENERAL DISCUSSION

8.1 STRENGTHS AND LIMITATIONS OF *IN VIVO* CONFOCAL MICROSCOPY

To gain inside in the role of *in vivo* confocal microscopy (IVCM) in corneal practice one should evaluate both strengths and limitations of the technique. The pros and cons of IVCM are perfectly illustrated by a promising clinical application that is introduced in this thesis: monitoring herpetic stromal keratitis (HSK).[1] Because of its principle, confocal microscopy has unequalled transverse and axial resolutions, which allow optical sectioning of the cornea at a cellular level without the use of vital dyes. To date, confocal microscopy is the only imaging modality that has been able to detect antigen presenting dendriform cells in the living human cornea. These dendriform cells may constitute an essential part of the local immune response in HSK[2] and can be monitored by IVCM to follow the effects of antiviral and anti-inflammatory therapy. The superior magnification attained by IVCM, however, comes at certain costs. Because only one-thousandth of the total corneal surface is imaged, IVCM is strongly affected by local changes in corneal cell populations. For example, scanning a small subepithelial infiltrate will show numerous dendriform cells at subbasal nerve plexus level, whereas, the cornea may show a normal aspect only few hundreds of microns away from the infiltrate. Within a complete IVCM scan, such displacements in image location often occur due to involuntary patient movements caused by respiration, pulse, and other external factors during the twelve seconds of image acquisition. One can imagine that examining a photophobic patient with HSK renders images from many different locations, if the IVCM scan succeeds at all. Even when a skilled operator uses the *z*-ring adapter for image stabilization, it is virtually impossible to image the same area twice. This low topographic repeatability, in addition to the small contamination hazard of this contact imaging method, and the high level of training required to produce good quality scans and to detect pathological processes in the cornea, are probably the main reasons that IVCM has not yet become common practice in the assessment of microbial keratitis.

The use of IVCM in a clinical setting is likely to increase when several adjustments to the current technique are made. Topographic repeatability would improve, when the image acquisition time is reduced, which may well be possible with the ongoing technological advances. Moreover, topographic repeatability would be further enhanced, when an external fixation target is displayed in front of the fellow eye instead of a continuously moving internal fixation target in front of the eye that is examined. When an eye tracking system would be developed and implemented, it may even be possible to image the same area over time. Also, certain software adaptations would surely add to the popularity of the current IVCM devices. Custom-made software is already available to (semi)automatically quantify the subbasal nerve fiber density,[3] compose large overview

maps of the different corneal layers,[4] and measure corneal backscatter.[5] Additionally, the software for endothelial cell assessment needs to be updated, because the current automatic software has been shown to produce unreliable results on cell density, polymegathism, and pleomorphism.[6] Nevertheless, even without these improvements IVCM is currently the only technique that enables simultaneous measurement of (sublayer) pachymetry, subbasal nerve fiber density, endothelial cell density, and corneal backscatter, but IVCM is also unique in combining these quantitative analyses with *in vivo* morphologic assessment of corneal cell populations.

8.2 ALTERNATIVE IMAGING TECHNIQUES

An ideal device for *in vivo* corneal imaging would combine an overview of the total cornea with magnification of the region of interest up to a cellular level. Such a device would allow pachymetry, keratometry, and backscatter to be quantified as well as morphologic cellular changes to be assessed at each location in the cornea. Until such a multifunctional instrument is available, corneal imaging devices can be divided on the basis of a wide or a small field of view. Using the small field of view of IVCM, we have demonstrated that backscatter measurement allows objective quantification of corneal opacification and therefore offers great potential in the detection and follow-up of corneal pathology. However, because of the minute field of view and the inability to image the same area twice, backscatter measurement by IVCM is limited to corneas with a homogenous distribution of the opacification. By expanding the field of view and applying an eye tracking system, corneal backscatter measurement can also be used for long-term follow-up of inhomogeneous opacities. Currently, two popular wide-field non-contact imaging techniques are capable of measuring corneal backscatter: rotating Scheimpflug imaging[7] and anterior segment optical coherence tomography (AS-OCT).[8] These techniques have the potential to surpass IVCM on its ability to quantify corneal backscatter. Small-field imaging techniques on the other hand, such as multiphoton microscopy, may provide additional insights in the cellular morphology of the unstained cornea, especially when these nonlinear microscopic techniques are combined with IVCM.[9]

Scheimpflug photography

The Scheimpflug principle, introduced in 1906 by Theodor Scheimpflug, was developed for military purposes to enhance the accuracy of photo maps by aerial photography.[10] In ophthalmology, Scheimpflug photography allows documentation of curved structures, such as the cornea and the lens, with enhanced depth of focus and minimal image distortion.[11] Using 470-475 nm blue light and a rotating CCD camera, the currently

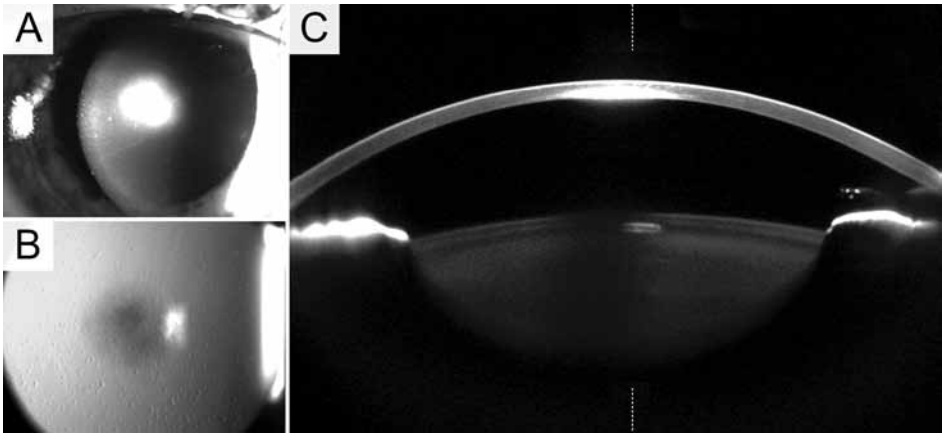

Figure 1. Scheimpflug photography in herpetic stromal keratitis. **A.** Slit-lamp image of herpetic disciform keratitis. **B.** Retro-illumination of the same cornea revealed that pseudoguttae extended far beyond the disciform inflammation. **C.** Scheimpflug imaging showed the disciform inflammatory process affected the posterior three quarters of the stroma. Densitometry of these Scheimpflug images may be used to monitor the inflammatory process in herpetic keratitis. (*See also Color figures, p. 210.*)

available Scheimpflug imaging devices acquire multiple radial cross-sections of the anterior segment within 2 seconds (Figure 1).[12] Their primary goal is to measure corneal topography, but they also provide measurements of pachymetry, wavefront aberrations, anterior chamber depth, and densitometry of the cornea and lens.

Recently, Scheimpflug photography has been used to establish normal values of corneal density in healthy subjects and to monitor the healing process in bacterial keratitis.[7] Otri et al.[7] found corneal density to be independent of age and showed light scattering declined significantly during the 4 weeks of follow-up. They concluded that Scheimpflug densitometry can be used to quantify the corneal response to infection and monitor the effects of therapy. This study however, ignored several conditions that complicate studies on corneal backscatter. Before reporting on normal values of corneal densitometry measured by Scheimpflug photography, calibration is essential. In this thesis we have shown that interinstument difference is an important factor, but also variations in the light source intensity during a follow-up period need to be verified.[13] Without calibration the data is dimensionless and cannot be reproduced by other researchers. Moreover, adequate age distribution as well as the choice of the right statistical test is prerequisite when studying the effect of aging on corneal backscatter. After meticulous calibration, balancing our study population for age and accounting for clustering of eyes within subjects by using a linear mixed model, we found age did affect corneal backscatter, but in the anterior stroma only.[5] Furthermore, the current Scheimpflug imaging devices have a fixed light intensity that cannot be adjusted when image saturation occurs in opaque corneas. Conversely, IVCM can prevent image saturation by manually reducing

light intensity and adjust for this reduction with predetermined algorithms.[13] Despite the inability to account for image saturation, Scheimpflug photography has the advantages of recording a much greater imaging surface, the non-contact method, and user friendliness compared to IVCM. Therefore, with proper calibration, Scheimpflug photography may prove a good alternative for monitoring corneal backscatter in diseased corneas.

AS-OCT

The other wide-field corneal imaging technique, AS-OCT, is an evolution of the retinal OCT which has been introduced in 1991 by David Huang and co-workers.[14] Optical coherence tomography is based on low-coherence interferometry which measures the echo time delay and magnitude of backscattered or reflected light.[15] The principle of OCT is analogous to that of ultrasound imaging with the exception that light is emitted and reflected instead of sound.[16] In 1994, Izatt et al. were the first to report on OCT imaging of the cornea and anterior segment.[17] Since then, the technique has evolved rapidly mainly because of the transition from time-domain to spectral-domain OCT.[18] With this paradigm shift, the scanning speed increased and axial resolution has improved from 18 µm (time-domain OCT, Visante AS–OCT, Carl Zeiss Meditec, Inc., Dublin, CA) to 4 µm (spectral-domain OCT, Spectralis OCT®, Heidelberg Engineering GmbH, Heidelberg, Germany). AS-OCT has similar advantages to IVCM as Scheimpflug photography. The main difference between the two wide-field imaging techniques is that Scheimpflug photography captures an optical section as a single image, whereas AS-OCT acquires thousands of A-scans to compose a cross-sectional tomogram.[19] Because the tomogram is a composition, the OCT technique may not be as accurate as Scheimpflug photography in assessing corneal topography.[19] On the other hand, the axial resolution and depth penetration of AS-OCT are much better than Scheimpflug photography. Because of these qualities AS-OCT is in a clinical setting often used to map corneal thickness and depth of corneal opacities. These pachymetry maps allow corneal surgeons to more accurately plan refractive or lamellar surgery (Figure 2),[18] but can also be used to quantify corneal inflammation and monitor the treatment response.[20]

Monitoring of microbial keratitis would be even further enhanced when AS-OCT is calibrated for objective corneal backscatter measurement. Nevertheless, only two reports are available that document corneal backscatter measurement by AS-OCT.[8,21] Using time-domain AS-OCT, corneal pachymetry and backscatter were measured during swelling and deswelling of the cornea induced by patching of the eye during 3 hours of contact lens wear.[8] During the deswelling period after contact lens removal, the change in corneal thickness was highly correlated with the change in backscatter. This finding strengthens the hypothesis that backscatter measurement can be used to quantify corneal edema.[5,22] The same group also studied corneal backscatter before and after refrac-

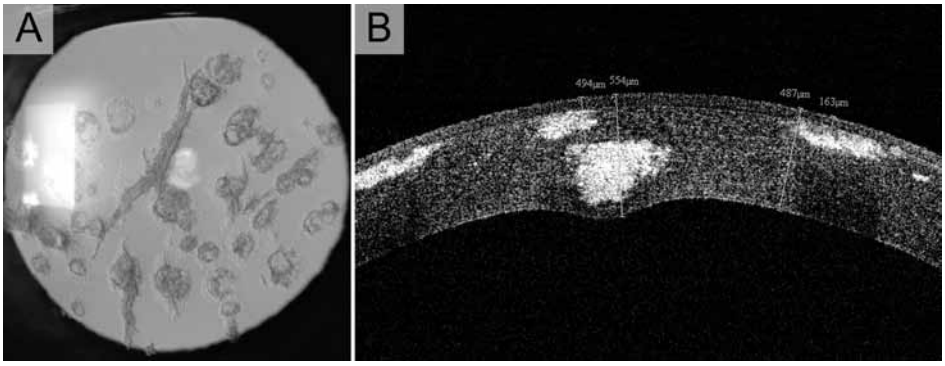

Figure 2. Anterior segment optical coherence tomography (AS-OCT) in Avellino dystrophy **A.** Retro-illumination showing both lattice and granular depositions. **B.** AS-OCT was used to choose the type of keratoplasty. Because one of the opacities clearly indented the corneal endothelium, we accepted incomplete excision of the opacities using deep lamellar keratoplasty. (*See also Color figures, p. 210.*)

tive surgery. Wang et al.[21] found an increase of corneal backscatter after photoablation, but more importantly, they demonstrated that corneal backscatter can objectively be quantified by AS-OCT. These reports, however, used normalized instead of calibrated absolute backscatter values. Therefore, this wide-field corneal imaging technique also, requires calibration and validation before corneal backscatter measurement can be used in a clinical setting. In such context, it should be noticed that AS-OCT, Scheimpflug photography, and IVCM cannot be mutually compared, because these techniques use different wavelengths and measurement angles, and backscatter analysis depends on these factors.[23,24]

Because AS-OCT collects multiple cross-sectional tomographic images with high axial resolution in reduced acquisition time, this technique can also be used to create en face images. Moreover, with the appropriate equipment and accurate settings, AS-OCT should be able to provide en face images that go beyond the diffraction limit of IVCM.[25] Grieve et al. have used an ultrahigh-resolution, full-field OCT with an incoherent halogen light source to acquire such en face images of corneal epithelial cells and keratocytes.[26] Because their first design was unsuitable for clinical use, they further reduced the image acquisition time. The higher speed, enabled full-field OCT to image a rat cornea *in vivo*, but at the expense of detection sensitivity.[25] Therefore, en face AS-OCT images, although they may represent the future, are still surpassed by the quality and resolution of IVCM images. Comparable or even higher resolutions, however, are attained by small-field, optical sectioning techniques that use nonlinear excitation of fluorescent molecules or harmonic generation: multiphoton microscopy.[27]

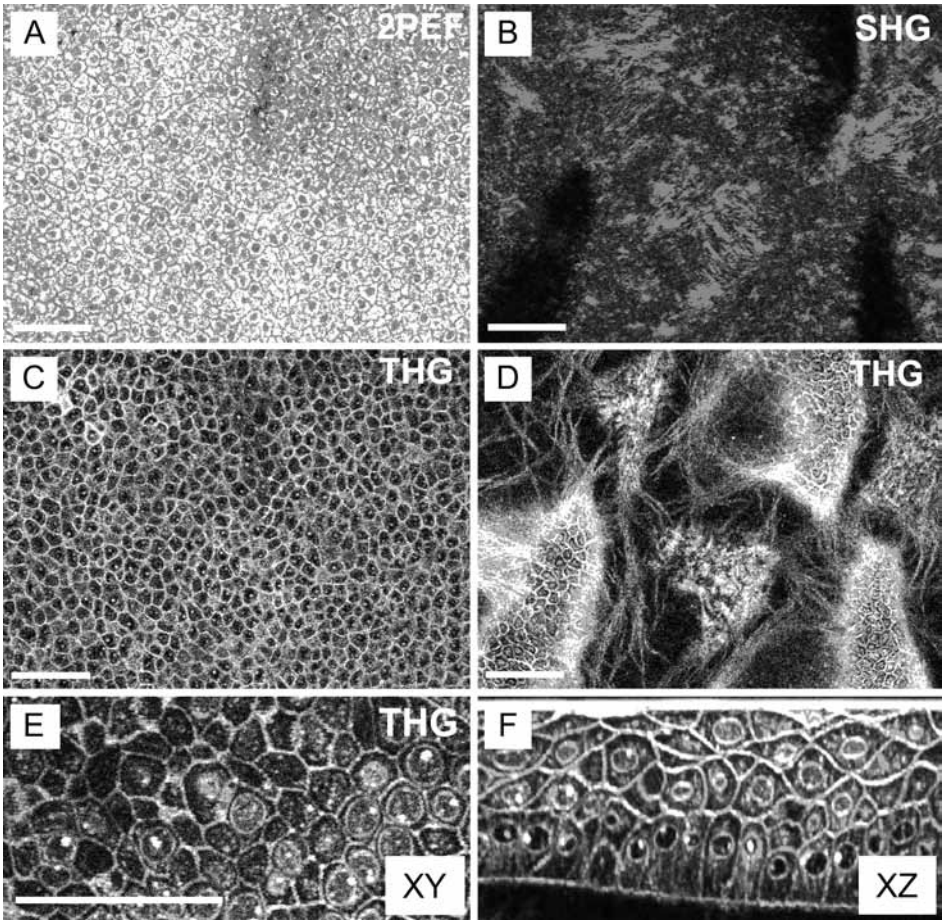

Figure 3. Multiphoton microscopy of an excised unstained human cornea. **A**. Two-photon excited fluorescence (2PEF) imaging revealed the cytoplasm of the basal epithelial cells **B**. Second-harmonic generation (SHG) imaging of the epithelium-stromal junction. **C**. Third-harmonic generation (THG) imaging showed the cell borders of the basal epithelial cells. **D**. Comparison of SHG (Figure 3B) and THG signals from the epithelium-stromal junction demonstrates that SHG images the stromal collagen lamellae, but not the epithelial cells. **E**. THG image of epithelial wing cells in XY directions composed from a Z-stack. **F**. Representative XZ reprojection from the same data. This figure is adapted from Aptel, 2010[28] and reprinted with permission from the Association for Research in Vision and Ophthalmology.
(*See also Color figures, p. 211.*)

Multiphoton microscopy

Multiphoton microscopy (Figure 3), which includes two-photon excited fluorescence (TPEF), and second- (SHG), and third-harmonic generation (THG) imaging, has the advantage that fluorescent and harmonic images can be acquired contemporarily, as these three imaging techniques use the same excitation source, typically a femtosecond

laser.[28] By using separate detectors, different sources of contrast provide structural and biochemical information on a single optical section.

In TPEF imaging, tissue is excited with pulsed 700 to 900 nm coherent light. Shorter-wavelength signals emitted by intrinsic chromophores such as nicotinamide adenine dinucleotide (phosphate) NAD(P)H, flavins, retinoids, lipofuscin, elastin, and others[29] are then captured by highly sensitive detectors. These signals are mainly derived from NAD(P)H positive cytoplasmic organelles, which allow corneal resident cells, but also migrating inflammatory cells to be visualized.[30,31] Recently, TPEF imaging was used to study the migratory patterns of immune cells in an *in vivo* mouse model of suture induced corneal neovascularisation.[32] By using exogenous fluorophores to stain lymphatic vessel walls, Steven et al.[32] showed for the first time the intravital real-time transmigration of immune cells into lymphatic vessels. This study demonstrates the great potential of TPEF imaging to broaden our knowledge on the mechanisms involved in ocular immunology.

In SHG, noncentrosymmetric structures such as collagen are excited by longer-wavelength photons, and emit second harmonic signals at exactly half the excitation wavelength.[9,28] Cornea wide, 3-D reconstructions of SHG image stacks have shown that the anterior stroma consists of highly intertwined sutural collagen lamellae that insert into Bowman's layer.[33] Based upon these findings, sutural lamellae, which make up the anterior corneal mosaic[34] and correspond with K-structures observed by IVCM,[35] are suggested to be responsible for maintaining corneal rigidity and shape.[33,36] This would explain the finding that regions of corneal thinning and ectasia in keratoconus are apparently devoid of these sutural collagen fibers.[37]

Analogous to SHG, THG signals are mainly detected in the forward direction, but unlike SHG, they do not require molecular asymmetry and therefore can be produced in any medium.[28] For THG, pulsed 1100-1200 nm light is used to reveal heterogeneities of only a few 100 nm,[38] such as nonaqueous cytoplasmic organelles, interfaces, fibrillar structures, and cell processes.[28] In a recent study, THG imaging revealed the morphology of the corneal epithelial cells, but also the insertion of the sutural lamellae in Bowman's layer in high quality en face and longitudinal cross-sections.[28] The same study also provided support for the existence of a posterior corneal mosaic, which we suspected based on the enhanced visibility of reproducible posterior stromal folds with applanation or aging of the cornea.[39] Using THG, these folds or cracks were observed throughout the stroma and appeared to be a continuation of the sutural lamellae.[28] Aptel et al.[28] also detected a hexagonal array of fibrous patches at the level of Descemet's membrane that seemed to connect the endothelial cells to the stroma. We have shown, using IVCM, that this hexagonal lattice structure of Descemet's membrane became increasingly visible with aging of the cornea.[39]

Before multiphoton microscopy can be used for *in vivo* imaging of the human cornea, the main disadvantages of these nonlinear microscopic techniques have to be addressed. For TPEF imaging, which has the disadvantage of depositing energy into tissue, much research is required to develop a strategy to prevent photodamage.[9] Although SHG and THG are absorption-free and can be used without photobleaching effects, harmonic imaging has another disadvantage that currently impedes its use in ophthalmic practice. Harmonic signals are emitted predominantly in the forward direction, with only very weak signals in the backscattered path.[9] This backscattered signal may be enhanced using an absorbing dye,[40] but also new optical techniques such as wavefront aberration optimization and adaptive optics, may be the key for future *in vivo* applications.[41] Until these restrictions of multiphoton microscopy are eliminated, IVCM remains exclusive in the assessment of cellular morphology in the living human cornea.

8.3 FUTURE RESEARCH DIRECTIONS

IVCM in herpetic stromal keratitis

In chapters 3.1 and 3.2 we have shown that morphologic assessment and corneal backscatter analysis by IVCM complementary to slit-lamp biomicroscopy enable early detection of inflammatory activity in herpetic keratitis.[1,42] Dendriform cells and pseudoguttae are often detected by IVCM before stromal infiltration occurs. In recurring immune stromal keratitis, however, the subsequent inflammatory process is very hard to distinguish from quiescent scarring. By monitoring corneal backscatter, IVCM allows quantification of the amount of haze, and facilitates objective detection of stromal recurrences. We postulated that therapy guidance based on these new IVCM inflammatory activity indicators, in addition to slit-lamp examination, may improve the outcome of herpetic stromal keratitis. To investigate this postulate, a succeeding study will soon be initiated, which compares the outcomes of two patient groups with HSK. In one group therapeutic decisions will be based on slit-lamp examination in conjunction with IVCM, whereas in the other group decisions will be based on slit-lamp examination solely. A key point in this future study is the choice of the observer. When a corneal specialist with extensive experience in the treatment of HSK will perform slit-lamp examination in these patients, the difference in outcome between the two patient groups is expected to be small. Conversely, this difference is likely to be enhanced when a final-year ophthalmology resident is responsible for slit-lamp examination. The latter option seems a better reflection of the ophthalmic practice. Another important study feature is the choice of additional measurements. As mentioned above, Scheimpflug

photography and AS-OCT may offer a better alternative to IVCM in the quantification of corneal backscatter. This future study provides a great opportunity to compare the three imaging modalities. However, the additional measurements may endanger the study feasibility, because they require careful planning and will take extra time, which is enhanced with each additional follow-up visit.

Quantification of edema in Fuchs' endothelial dystrophy

Although backscatter of the basal epithelial cell layer, the so-called epithelial valley (EV), can be used to assess corneal hydration,[5,22] we could not confirm this finding in patients with HSK.[1] In these patients, the EV was generally outshined by the underlying hyperreflective anterior stroma. Yet, in patients with Fuchs' endothelial dystrophy, who usually display a relatively clear anterior stroma, the EV may accurately reflect the amount of corneal edema. To test this hypothesis, we have studied the predictive factors for corneal decompensation in patients with Fuchs' endothelial dystrophy.[43] Eighty-nine patients with Fuchs' endothelial dystrophy were carefully examined prior to cataract surgery assessing 29 parameters including best corrected visual acuity, contrast sensitivity, corneal topography, cataract density, intraocular straylight, ultrasonic pachymetry, and corneal backscatter among others. Postoperatively, measurements were repeated at 1, 2, and 12 months. After twelve months follow-up, 35 (39.3%) of 89 patients showed corneal decompensation which required endothelial keratoplasty. Multivariate logistic regression analysis of 34 pre- and intra-operative parameters indicated ultrasonic pachymetry and corneal backscatter analysis were predictive of corneal decompensation. Compared with ultrasonic pachymetry, the EV showed superior sensitivity and specificity in predicting progression of the corneal edema, necessitating endothelial keratoplasty. Furthermore, the EV can be measured with high repeatability because the corneal edema tends to distribute evenly across the basal epithelial cells. Therefore the measurement location has little effect on the backscatter of the basal epithelial cells (EV). These results support a role of IVCM in the assessment of the decompensation risk in Fuchs' endothelial dystrophy patients before cataract surgery. A detailed report of the latter study is currently in preparation.

Pathogen-specific inflammatory response in infectious keratitis

Unlike *Acanthamoeba* and fungal species, viruses (20-300 nm) and most bacteria (0.5-5 µm) lie beyond the detection limit of IVCM. Nevertheless, it may be possible to distinguish these pathogens as causative agents of microbial keratitis. In general, viruses and bacteria differ in their mechanisms to damage the corneal resident cells. Viruses damage the host cells by entering the cells and replicating at the host's expense, whereas bacterial damage depends on their ability adhere or enters the host cells or deliver

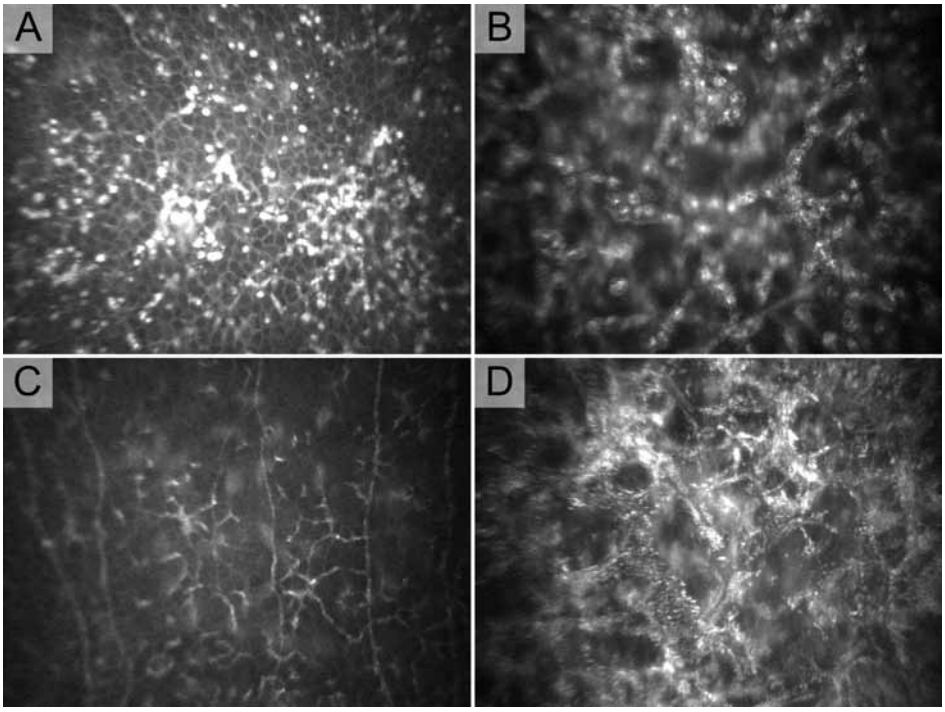

Figure 4. Differentiation of pathogen-specific inflammatory response in bacterial and viral keratitis. *In vivo* confocal microscopy of keratitis elicited by culture-proven (**A-B**) *Pseudomonas aeruginosa* and (**C-D**) herpes simplex virus. **A.** In *Pseudomonas aeruginosa* keratitis, small hyperreflective structures (2-6 µm) were observed at subbasal nerve plexus level. **B**. The stroma displayed a coarse granular reaction. **C**. In herpes simplex keratitis, large dendriform cells (up to 100 µm) showed wire netting with the subbasal nerve plexus. **D.** The stroma showed a fine granular reaction.

toxins.[44] In reaction to the different mechanisms involved in tissue injury, the host inflammatory response differs between viruses and bacteria. Although these inflammatory responses are certainly not mutually exclusive, a viral infection induces a relatively slow mononuclear and cytopathic-cytoproliferative inflammation, whereas a bacterial infection typically causes an acute suppurative polymorphonuclear reaction.[45] These host responses may, on its turn, lead to different morphological changes as observed by IVCM. In our experience, there are indeed differences in morphologic appearance between viral and bacterial keratitis, which are more pronounced in the early phase of the infection and at the boundaries of the involved tissue. The dendriform cells at subbasal nerve plexus level are smaller in bacterial keratitis and display long processes in viral keratitis (Figure 4A+C). These morphologic differences may reflect the maturation status of the dendriform cells.[46] Another morphological difference is observed in the corneal stroma. A virus induces a highly reflective fine granular reaction, whereas the

granular reaction to a bacterium is coarser and less hyperreflective (Figure 4B+D). These pathogen-specific morphologic changes will be addressed in a future study.

Correlative microscopy

Although most bacteria are too small to detect, the lateral resolution of 0.6 µm/pixel implies that some bacterial pathogens lie within the detection limits of IVCM. Moreover, Pseudomonas *aeruginosa*, one of the most common causative organisms of bacterial keratitis, should theoretically be detectable on IVCM. Still, IVCM images of this Gram-negative rod measuring 0.5 to 0.8 µm by 1.5 to 3.0 µm[47] have, to the author's knowledge, never been reported. The lack of reports on this subject may be explained by the concurrent inflammatory reaction that hinders bacteria to be distinguished from cellular debris.[48] To date, only *Streptococcus viridans* and *Staphylococcus werneri*,[49] *Borrelia burgdorferi*,[50] and *Nocardia asteroides*[51] have been observed in humans using IVCM. But how do we know that the small white dots in these IVCM images represent bacteria? In a clinical setting, the lack of histological evidence remains a common problem interpreting IVCM observations. For research purposes, an increasingly popular solution is the use of correlative microscopy, which is based on the use of different optical techniques to study the same specimen.[9] Of the micro-organisms mentioned above, only the appearance of *Nocardia asteroides* was verified by IVCM scanning of the corresponding blood agar culture plate, showing thin and short beaded filamentous structures. Similar acid-fast filamentous organisms were demonstrated using light microscopy after staining the corneal scrapings by the modified Ziehl-Nielsen technique.[51] Because *in vivo* findings are verified against *ex vivo* analyses, correlative microscopy has greatly improved our understanding of IVCM observations. Whereas early IVCM reports described the morphological appearances of many, often rare, corneal diseases without validating the results histologically, the current trend is to critically review these interpretations by means of correlative microscopy complemented by other analyses such as polymerase chain reaction, immunohistochemistry, and genetic assays.[52–54]

Nature of dendriform cells

The need to histologically validate IVCM observations is also clear from our consecutive publications on herpetic keratitis. For many years, the branching structures at subbasal nerve plexus level that emanate during herpetic keratitis were described as Langerhans cells.[1,55] Langerhans cells, however, are specialized antigen presenting cells that are identified by the electron microscopic appearance of Birbeck granules,[56] which comprise the langerin/CD207 molecule.[57] Because IVCM is incapable of identifying Birbeck granules, it was suggested to substitute the term Langerhans cells by dendritic cells.[58] Eventually, a

more descriptive term such as dendriform cells[1] seems more appropriate as, in addition to dendritic cells, these structures may also account for monocytes and macrophages.[59] Nomenclature can only be specified, when the exact nature of these dendriform cells is ascertained. Confocal microscopy is the method designated to provide a bridge between *in vivo* imaging and *ex vivo* histopathology and may help us to unravel the nature of dendriform cells.

8.4 CONCLUSIONS

In this thesis we have broadened the scope of IVCM by validating corneal backscatter measurement and demonstrating its additional value in the follow-up of HSK. When validation is extended to wide-field imaging techniques such as Scheimpflug photography and AS-OCT, corneal backscatter will provide an easy-accessible objective parameter to monitor corneal diseases. Therefore it seems only a matter of time before corneal backscatter measurement belongs to the standard armamentarium of the corneal specialist. The powerful combination of corneal backscatter measurement with morphologic assessment at a cellular level, however, is exclusive to IVCM. Despite the growing interest for this technique, the use of IVCM in ophthalmic practice remains limited to a minority of the corneal disease services in developed countries. The clinical application of this high-end imaging device will surely expand when its practicability is improved up to a level that a trained technician is able to acquire high quality scans of the same location over time. To attain these essential improvements, efforts should be made to lower the image acquisition time and to develop an eye-tracking system. Until then, IVCM is the domain of enthusiastic corneal specialists who are willing to spend their precious time on the interpretation of static black and white images. Nonetheless, when they compare these IVCM images with slit-lamp observations and validate their interpretations by means of correlative microscopy, their reward is a unique insight in the degenerative and pathologic processes of the cornea. It is through such invaluable knowledge of cellular morphology in unfixed tissue and the inexorable technological advances that a revolutionary ophthalmic discipline will evolve in the coming years: histopathology of the living eye. *In vivo* confocal microscopy will undoubtedly provide the basis for this new exciting discipline.

REFERENCES

1. Hillenaar T, van Cleynenbreugel H, Verjans GM, et al. Monitoring the inflammatory process in herpetic stromal keratitis: the role of in vivo confocal microscopy. Ophthalmology 2012;119: 1102-1110.
2. Polcicova K, Biswas PS, Banerjee K, et al. Herpes keratitis in the absence of anterograde transport of virus from sensory ganglia to the cornea. Proc Natl Acad Sci U S A 2005;102:11462-7.
3. Meijering E, Jacob M, Sarria JC, et al. Design and validation of a tool for neurite tracing and analysis in fluorescence microscopy images. Cytometry A 2004;58:167-76.
4. Zhivov A, Guthoff R, Stachs O. [On-line mapping of corneal structures with in vivo laser scanning microscopy]. Klin Monbl Augenheilkd 2009;226:980-3.
5. Hillenaar T, Cals RH, Eilers PH, et al. Normative database for corneal backscatter analysis by in vivo confocal microscopy. Invest Ophthalmol Vis Sci 2011;52:7274-81.
6. Kitzmann AS, Winter EJ, Nau CB, et al. Comparison of corneal endothelial cell images from a noncontact specular microscope and a scanning confocal microscope. Cornea 2005;24:980-4.
7. Otri AM, Fares U, Al Aqaba MA, Dua HS. Corneal Densitometry as an Indicator of Corneal Health. Ophthalmology 2011.
8. Wang J, Simpson TL, Fonn D. Objective measurements of corneal light-backscatter during corneal swelling, by optical coherence tomography. Invest Ophthalmol Vis Sci 2004;45:3493-8.
9. Masters BR. Correlation of histology and linear and nonlinear microscopy of the living human cornea. J Biophotonics 2009;2:127-39.
10. Scheimpflug T. Der photoperspektrograph und seine anwendung. Photogr Korr 1906;43:516-31.
11. Wegener A, Laser-Junga H. Photography of the anterior eye segment according to Scheimpflug's principle: options and limitations - a review. Clin Experiment Ophthalmol 2009;37:144-54.
12. Oliveira CM, Ribeiro C, Franco S. Corneal imaging with slit-scanning and Scheimpflug imaging techniques. Clin Exp Optom 2011;94:33-42.
13. Hillenaar T, Sicam VA, Vermeer KA, et al. Wide-range calibration of corneal backscatter analysis by in vivo confocal microscopy. Invest Ophthalmol Vis Sci 2011;52:2136-46.
14. Huang D, Swanson EA, Lin CP, et al. Optical coherence tomography. Science 1991;254:1178-81.
15. Pircher M, Hitzenberger CK, Schmidt-Erfurth U. Polarization sensitive optical coherence tomography in the human eye. Prog Retin Eye Res 2011;30:431-51.
16. Konstantopoulos A, Hossain P, Anderson DF. Recent advances in ophthalmic anterior segment imaging: a new era for ophthalmic diagnosis? Br J Ophthalmol 2007;91:551-7.
17. Izatt JA, Hee MR, Swanson EA, et al. Micrometer-scale resolution imaging of the anterior eye in vivo with optical coherence tomography. Arch Ophthalmol 1994;112:1584-9.
18. Ramos JL, Li Y, Huang D. Clinical and research applications of anterior segment optical coherence tomography - a review. Clin Experiment Ophthalmol 2009;37:81-9.
19. Belin MW, Khachikian SS, McGhee CN, Patel D. New technology in corneal imaging. Int Ophthalmol Clin 2010;50:177-89.
20. Konstantopoulos A, Yadegarfar G, Fievez M, et al. In vivo quantification of bacterial keratitis with optical coherence tomography. Invest Ophthalmol Vis Sci 2011;52:1093-7.
21. Wang J, Thomas J, Cox I. Corneal light backscatter measured by optical coherence tomography after LASIK. J Refract Surg 2006;22:604-10.
22. Morishige N, Takahashi N, Chikamoto N, Nishida T. Quantitative evaluation of corneal epithelial oedema by confocal microscopy. Clin Experiment Ophthalmol 2009;37:249-53.

23. Feuk T. The wavelength dependence of scattered light intensity in rabbit corneas. IEEE Trans Biomed Eng 1971;18:92-6.
24. Feuk T, McQueen D. The angular dependence of light scattered from rabbit corneas. Invest Ophthalmol 1971;10:294-9.
25. Grieve K, Dubois A, Simonutti M, et al. In vivo anterior segment imaging in the rat eye with high speed white light full-field optical coherence tomography. Opt Express 2005;13:6286-95.
26. Grieve K, Paques M, Dubois A, et al. Ocular tissue imaging using ultrahigh-resolution, full-field optical coherence tomography. Invest Ophthalmol Vis Sci 2004;45:4126-31.
27. Zipfel WR, Williams RM, Webb WW. Nonlinear magic: multiphoton microscopy in the biosciences. Nat Biotechnol 2003;21:1369-77.
28. Aptel F, Olivier N, Deniset-Besseau A, et al. Multimodal nonlinear imaging of the human cornea. Invest Ophthalmol Vis Sci 2010;51:2459-65.
29. Zipfel WR, Williams RM, Christie R, et al. Live tissue intrinsic emission microscopy using multiphoton-excited native fluorescence and second harmonic generation. Proc Natl Acad Sci U S A 2003; 100:7075-80.
30. Piston DW, Masters BR, Webb WW. Three-dimensionally resolved NAD(P)H cellular metabolic redox imaging of the in situ cornea with two-photon excitation laser scanning microscopy. J Microsc 1995;178:20-7.
31. Wang BG, Koenig K, Riemann I, et al. Intraocular multiphoton microscopy with subcellular spatial resolution by infrared femtosecond lasers. Histochem Cell Biol 2006;126:507-15.
32. Steven P, Bock F, Huttmann G, Cursiefen C. Intravital two-photon microscopy of immune cell dynamics in corneal lymphatic vessels. PLoS One 2011;6:e26253.
33. Jester JV, Winkler M, Jester BE, et al. Evaluating corneal collagen organization using high-resolution nonlinear optical macroscopy. Eye Contact Lens 2010;36:260-4.
34. Bron AJ. Anterior corneal mosaic. Br J Ophthalmol 1968;52:659-69.
35. Kobayashi A, Yokogawa H, Sugiyama K. In vivo laser confocal microscopy of Bowman's layer of the cornea. Ophthalmology 2006;113:2203-8.
36. Morishige N, Takagi Y, Chikama T, et al. Three-dimensional analysis of collagen lamellae in the anterior stroma of the human cornea visualized by second harmonic generation imaging microscopy. Invest Ophthalmol Vis Sci 2011;52:911-5.
37. Morishige N, Wahlert AJ, Kenney MC, et al. Second-harmonic imaging microscopy of normal human and keratoconus cornea. Invest Ophthalmol Vis Sci 2007;48:1087-94.
38. Debarre D, Beaurepaire E. Quantitative characterization of biological liquids for third-harmonic generation microscopy. Biophys J 2007;92:603-12.
39. Hillenaar T, van Cleynenbreugel H, Remeijer L. How normal is the transparent cornea? Effects of aging on corneal morphology. Ophthalmology 2012;119:241-8.
40. Yu CH, Tai SP, Kung CT, et al. Molecular third-harmonic-generation microscopy through resonance enhancement with absorbing dye. Opt Lett 2008;33:387-9.
41. Bueno JM, Gualda EJ, Artal P. Analysis of corneal stroma organization with wavefront optimized nonlinear microscopy. Cornea 2011;30:692-701.
42. Hillenaar T, Weenen C, Wubbels RJ, Remeijer L. Endothelial involvement in herpes simplex virus keratitis: an in vivo confocal microscopy study. Ophthalmology 2009;116:2077-86.
43. van Cleynenbreugel H, Remeijer L, van Rooij J, et al. Cataractchirurgie in ogen met Fuchs' endothelial dystrophy. vergadering Nederlands Oogheelkundig Gezelschap . 2011. Abstract
44. Samuelson J. General pathology of infectious diseases. In: Kumar V, Cotran RS, Robbins SL, eds. Basic pathology, 6th ed. Philadelphia: Saunders, 2012; chap. 9.

45. Srinivasan M, Mascarenhas J, Prashanth CN. Distinguishing infective versus noninfective keratitis. Indian J Ophthalmol 2008;56:203-7.
46. Zhivov A, Stachs O, Kraak R, et al. In vivo confocal microscopy of the ocular surface. Ocul Surf 2006;4:81-93.
47. Todar K. Todar's online textbook of bacteriology: Pseudomonas aeruginosa. http://www.textbookofbacteriology.net/pseudomonas.html . 2012. Electronic Citation
48. Kanavi MR, Javadi M, Yazdani S, Mirdehghanm S. Sensitivity and specificity of confocal scan in the diagnosis of infectious keratitis. Cornea 2007;26:782-6.
49. Kaufman SC, Laird JA, Cooper R, Beuerman RW. Diagnosis of bacterial contact lens related keratitis with the white-light confocal microscope. CLAO J 1996;22:274-7.
50. Linna T, Mikkila H, Karma A, et al. In vivo confocal microscopy: a new possibility to confirm the diagnosis of Borrelia keratitis? Cornea 1996;15:639-40.
51. Vaddavalli PK, Garg P, Sharma S, et al. Confocal microscopy for Nocardia keratitis. Ophthalmology 2006;113:1645-50.
52. Hillenaar T, Mooy CM, Verjans GM, Remeijer L. Zipper cell endotheliopathy: a new subset of idiopathic corneal edema. Ophthalmology 2010;117:2255-62.
53. Jing Y, Liu C, Wang L. A novel TACSTD2 mutation identified in two Chinese brothers with gelatinous drop-like corneal dystrophy. Mol Vis 2009;15:1580-8.
54. Vincent AL, Niederer RL, Richards A, et al. Phenotypic characterisation and ZEB1 mutational analysis in posterior polymorphous corneal dystrophy in a New Zealand population. Mol Vis 2009; 15:2544-53.
55. Rosenberg ME, Tervo TM, Muller LJ, et al. In vivo confocal microscopy after herpes keratitis. Cornea 2002;21:265-9.
56. Birbeck MS, Breathnach AS, Everall JD. An electron microscopic study of basal melanocytes and high level clear cells (Langerhans cell) in vitiligo. J Invest Dermatol 1961;37:51-64.
57. Valladeau J, Ravel O, Dezutter-Dambuyant C, et al. Langerin, a novel C-type lectin specific to Langerhans cells, is an endocytic receptor that induces the formation of Birbeck granules. Immunity 2000;12:71-81.
58. Mastropasqua L, Nubile M, Lanzini M, et al. Epithelial dendritic cell distribution in normal and inflamed human cornea: in vivo confocal microscopy study. Am J Ophthalmol 2006;142:736-44.
59. Cruzat A, Witkin D, Baniasadi N, et al. Inflammation and the nervous system: the connection in the cornea in patients with infectious keratitis. Invest Ophthalmol Vis Sci 2011;52:5136-43.

9

Summary / Samenvatting
Dankwoord
Curriculum vitae
List of publications
Color figures

SUMMARY

In vivo confocal microscopy (IVCM) allows the living human cornea to be studied on a cellular level. This thesis describes new IVCM applications that fully exploit the abilities of this multi-purpose imaging technique. Our major objective was to investigate the clinical value of IVCM for the corneal specialist. **Chapter 1** is a general introduction in the field of confocal microscopy. The technological advances that preceded the invention of the confocal microscope are described and its main principle of a common focal point of the illumination and observation pathways is discussed. In the last two decades the use of confocal microscopy has clearly made the transition from basic research into ophthalmic practice. Also, the annual number of articles on IVCM shows that interest in the technique has increased exponentially over the last 20 years. Nevertheless, IVCM is not widely used in a clinical setting. Its scope remains confined to diagnosing *Acanthamoeba* or filamentous fungal keratitis, early detection of corneal dystrophies and degenerations, assessing the endothelial cell density (ECD) in opacified corneas, and measuring the depth of these opacities. The scope of IVCM, however, may greatly be enhanced when corneal backscatter analysis, another feature of IVCM, is validated for clinical use. We performed three basic studies to enable morphologic cellular assessment to be combined with corneal backscatter analysis, before this powerful combination was studied in herpetic keratitis.

In **Part I**, which covers the basic studies in this thesis, we examined 300 transparent corneas of 150 healthy volunteers using IVCM. This normative study population was evenly distributed over 5 age categories ranging from 20 to 79 years and comprised 75 women and 75 men. Based on this study population, **Chapter 2** describes the morphologic diversity of the normal cornea and discusses the changes that appear with aging. We found microdots in the anterior stroma, folds in the posterior stroma, opacification of Descemet's membrane, and corneal guttae to increase significantly with age. To further illustrate the morphologic diversity of the transparent cornea, we introduced a novel phenotypic variant of corneal endothelium: "salt and pepper endothelium". Because the morphologic diversity of the cornea is enhanced with aging, we conclude that knowledge of the common morphologic variants and of the effects of aging is essential to detect degenerative disorders or pathologic processes in the cornea.

Chapter 3 reports on two calibration methods for IVCM that allow backscatter in normal and opaque corneas to be measured over time and with different machines. Corneal backscatter is expressed in absolute scatter units (SU) after standardization with a commercially available turbidity suspension. Because this turbidity standard is impractical for daily use and garanteed for only 1 year, we proposed a solid reference standard made of polymethylmethacrylate to enable long-term calibration of corneal backscatter measurement. After expressing backscatter in SU, we found a difference of

18% between two similar confocal microscopes, measured with equal light intensities. This finding indicates the necessity to calibrate corneal backscatter measurement in order to compare study results across laboratories.

In **Chapter 4**, we investigated the effects of sex, age, and diurnal variation on seven corneal backscatter variants measured by IVCM. In addition, we determined the inter- and intrasession repeatability for each of these backscatter variants based on the same normative study population that indicated the morphologic corneal diversity in Chapter 2. Corneal backscatter was 3.5% higher in men, increased significantly in the anterior stroma from the age of 50 years, and showed a small, but significant diurnal variation. The influence of sex, age, and time of measurement, however, was smaller than the variability between and within subjects. Therefore, we accounted for these effects in a generalized normal range and minimum detectable change for each backscatter variant.

Part II comprises the IVCM studies on herpetic keratitis. The characteristics, frequency, and clinical consequences of endothelial involvement in herpes simplex virus (HSV) keratitis are described in **Chapter 5**. Over a 3-year period we examined the affected and fellow eyes of 285 patients with HSV keratitis. Endothelial involvement was found not only in isolated endotheliitis, but also in >20% of the visits covering other manifestations of HSV keratitis such as infectious epithelial keratitis, stromal keratitis, and keratouveitis. Using IVCM we detected similar endothelial alterations as were previously described in *ex vivo* animal models. Pseudoguttae were the most common alteration, followed by enlarged intercellular gaps, spot-like holes, loss of defined cell boundaries, endothelial denudation, and infiltration of inflammatory cells into the endothelial layer. These alterations often preceded formation of keratic precipitates and disappeared with appropriate antiviral and anti-inflammatory treatment. However, HSV-affected eyes with endothelial involvement showed a significant decrease in ECD (10% per year) compared with healthy fellow eyes.

In **Chapter 6,** we applied the previously acquired knowledge on corneal morphology and backscatter to investigate the role of IVCM in the detection of inflammatory activity and long-term follow-up of herpetic stromal keratitis (HSK). Thirty-eight patients with active HSK were followed regularly over a 12-month period using slit-lamp biomicroscopy and IVCM. Dendriform cells and pseudoguttae proved to be excellent indicators of inflammatory activity as they heralded formation of stromal infiltration and dissipated early with improvement of the HSK. Of the 14 recurrences identified by an experienced corneal specialist at slit-lamp examination, 8 (57%) were objectively confirmed by IVCM analysis of corneal backscatter. Additionally, IVCM detected 3 recurrences that were missed at slit-lamp examination. These results unambiguously demonstrate the added value of IVCM. However, because of IVCM's limited field of view, slit-lamp biomicroscopy remains the gold standard in the follow-up of HSK. Therefore, therapy guidance based

on combined IVCM and slit-lamp examination seems the best option to improve the outcome of HSK.

Chapter 7 reports on the clinical and histological findings of another novel phenotype of corneal endothelium: "Zipper cell endotheliopathy". The unique zipper-like interdigitations of the endothelial cell borders were identified by IVCM and underlied idiopathic corneal edema in a 55-year-old woman with unilateral bullous keratopathy. Despite a 14-year history of presumed herpetic keratitis, a herpes virus origin for the bullous keratopathy could not be confirmed after meticulous analysis of two aqueous humor samples and the excised corneal button. Using immunohistochemical analysis, we did find evidence for epithelial metaplasia of the endothelial cells, whereas the zipper-like appearance was characterized by overlapping cells with broad-based extentions at electron microscopy. The *in vivo* and *ex vivo* findings in zipper cell endotheliopathy do not fit any known corneal disorder, but may represent an aberrant wound-healing response to endothelial damage of undetermined source. This case-report illustrates the potential of IVCM to further differentiate the spectrum of corneal disorders and to discover new corneal diseases.

The discussion of this thesis in **Chapter 8** summarizes the strengths and limitations of IVCM, upon which several soft- and hardware improvements to the current technique are proposed. In the future, corneal backscatter measurement by IVCM is likely to be replaced by techniques that provide an overview of the total cornea, such as Scheimpflug photography and anterior segment optical coherence tomography. Also, morphologic assessment of the corneal cells layers may be substituted or enhanced by two-photon excitated fluorescence imaging combined with second- and third-harmonic generation imaging. However, before these non-linear microscopic techniques can be used for *in vivo* imaging of the human cornea several important restrictions have to be eliminated. Until that day, IVCM remains the only imaging modality that allows living cells in the human cornea to be studied morphologically. Such IVCM studies have greatly enhanced our knowledge of degenerative and pathologic processes in the cornea and will provide the basis for the emergence of a new ophthalmic discipline: histopathology of the living eye.

SAMENVATTING

Met *in vivo* confocale microscopie (IVCM) kan het hoornvlies van levende mensen op celniveau beoordeeld worden. Dit proefschrift beschrijft nieuwe toepassingen voor IVCM die de mogelijkheden van deze multifunctionele beeldvormende techniek ten volle benutten. Onze belangrijkste doelstelling was het bepalen van de praktische waarde van IVCM voor de corneaspecialist. **Hoofdstuk 1** is een algemene inleiding op het gebied van confocale microscopie. In dit hoofdstuk komen de technologische ontwikkelingen aan de orde die voorafgingen aan de uitvinding van de confocale microscoop. Ook wordt het belangrijkste principe van confocale microscopie besproken: een gemeenschappelijk brandpunt van de belichtings- en de observatiearm. In de laatste twee decennia heeft er een duidelijke vertaalslag plaatsgevonden van basaal wetenschappelijk onderzoek naar de oogheelkundige praktijk. Daarnaast laat het jaarlijks aantal artikelen over IVCM zien dat de interesse voor deze techniek in de afgelopen 20 jaar exponentieel is toegenomen. Desondanks wordt IVCM niet vaak in de oogheelkundige praktijk gebruikt. Het toepassingsgebied van IVCM blijft hierbij beperkt tot het diagnosticeren van *Acanthamoeba* of draadvormende schimmels als oorzaak van keratitis, vroege opsporing van corneale dystrofieën en degeneraties, bepaling van de endotheelceldensiteit (ECD) in troebele cornea's en het meten van de diepte van deze vertroebelingen. Het toepassingsgebied van IVCM zou echter fors uitgebreid kunnen worden als analyse van backscatter (hoeveelheid troebeling) in de cornea voor gebruik in de praktijk gevalideerd wordt. Wij hebben drie basisstudies verricht om het beoordelen van de celmorfologie te kunnen combineren met het meten van corneale backscatter. Daarna hebben wet we deze unieke combinatie bestudeerd in patiënten met herpetische keratitis.

Voor **Deel I**, dat de basisstudies in dit proefschrift beslaat, hebben we 300 heldere cornea's van 150 gezonde mensen onderzocht met IVCM. Deze normatieve studiepopulatie bestond uit 75 vrouwen en 75 mannen in de leeftijd van 20 tot en met 79 jaar, gelijkmatig verdeeld over 5 leeftijdscategorieën. Op basis van deze studiepopulatie wordt in **Hoofdstuk 2** de morfologische diversiteit van de normale cornea beschreven en komen de veranderingen die optreden door veroudering aan de orde. Wij vonden dat microdeposities in het anterieure stroma, plooien in het posterieure stroma, vertroebeling van het membraan van Descemet en corneale guttata significant toenamen met de leeftijd. Om de morfologische diversiteit van de heldere cornea te benadrukken, beschrijven we ook een nieuwe fenotypische variant van cornea endotheel: "salt and pepper endothelium". Doordat de morfologische diversiteit van de cornea verder toeneemt met de leeftijd concluderen wij dat kennis van de veelvoorkomende morfologische varianten en van de verouderingsprocessen essentieel is om degeneratieve of pathologische processen in de cornea te kunnen detecteren.

Hoofdstuk 3 behandelt twee kalibratiemethodes voor IVCM waarmee backscatter in normale en troebele cornea's gemeten en vervolgd kan worden met verschillende apparaten. Corneale backscatter wordt uitgedrukt in absolute scatter units (SU) na kalibratie met een commercieel beschikbare turbiditeitssuspensie. Omdat deze turbiditeitsstandaard niet praktisch is in het dagelijks gebruik en slechts voor één jaar gegarandeerd wordt, stellen wij voor om een vaste stof als referentiestandaard te gebruiken. Deze referentiestandaard bestaat uit polymethylmethacrylaat en maakt kalibratie van corneale backscatter over een langere periode mogelijk. Met het uitdrukken van backscatter in SU vonden wij dat twee gelijke apparaten, ingesteld met dezelfde lichtintensiteit, een verschil van 18% vertoonden. Deze bevinding benadrukt de noodzaak om corneale backscatter metingen te kalibreren. Alleen zo kunnen de resultaten van verschillende apparaten en studies met elkaar vergeleken worden.

In **Hoofdstuk 4**, hebben we gekeken naar de invloed van geslacht, leeftijd en dagschommeling op zeven varianten van corneale backscatter, zoals gemeten met IVCM. Daarnaast hebben we voor elk van deze varianten de inter- en intrasessie herhaalbaarheid bepaald met behulp van dezelfde normatieve studiepopulatie die in Hoofdstuk 2 gebruikt werd om de morfologische diversiteit van de cornea aan te tonen. We vonden dat corneale backscatter 3,5% hoger was in mannen, significant toenam in het anterieure stroma na het 50e levensjaar en een beperkte, maar significante dagschommeling vertoonde. De invloed van geslacht, leeftijd en tijdstip van de meting was echter kleiner dan de variabiliteit tussen en binnen proefpersonen. Hier hebben wij rekening mee gehouden bij het opstellen van algemeen toepasbare normaalwaardes en minimum detecteerbare veranderingen voor elke backscatter variant.

Deel II omvat de IVCM studies naar herpetische keratitis. De kenmerken, frequentie en klinische consequenties van betrokkenheid van het endotheel bij herpes simplex virus (HSV) keratitis worden beschreven in **Hoofdstuk 5**. Gedurende een periode van 3 jaar hebben we de aangedane en contralaterale ogen van 285 patiënten met HSV keratitis onderzocht. Betrokkenheid van het endotheel werd niet alleen bij een geïsoleerde endotheliitis gezien, maar ook in >20% van alle bezoeken van patiënten met andere manifestaties van HSV keratitis zoals infectieuze epitheliale keratitis, stromale keratitis en keratouveitis. Met IVCM vonden wij dezelfde endotheliale veranderingen die eerder zijn aangetoond in *ex vivo* diermodellen. Pseudoguttata waren de meest voorkomende verandering, gevolgd door vergroting van de intercellulaire ruimtes, ronde gaten in het endotheel, vervaging van de celgrenzen, endotheliale denudatie en infiltratie van ontstekingscellen in de endotheliale cellaag. Deze veranderingen gingen vaak vooraf aan de vorming van endotheelbeslag en verdwenen schijnbaar volledig met het instellen van adequate antivirale en anti-inflammatoire therapie. De HSV-aangedane ogen vertoonden echter een significante daling van de ECD (10% per jaar) ten opzichte van de gezonde contralaterale ogen.

In **Hoofdstuk 6**, hebben we de eerder verworven kennis van de corneale morfologie en backscatter gebruikt om de rol van IVCM bij de detectie van ontstekingsactiviteit en lange termijn follow-up van herpetische stromale keratitis (HSK) te onderzoeken. Achtendertig patiënten met actieve HSK werden 12 maanden structureel vervolgd met de spleetlamp en IVCM. Dendriforme cellen en pseudoguttata bleken uitstekende indicatoren van ontstekingsactiviteit, omdat ze voorafgingen aan stromale infiltratie en snel verdwenen met het verbeteren van de HSK. Van de 14 recidieven die door een ervaren corneaspecialist met de spleetlamp werden geïdentificeerd, werden er 8 (57%) objectief bevestigd met IVCM analyse van de corneale backscatter. Bovendien detecteerde IVCM 3 recidieven die bij spleetlamponderzoek gemist werden. Deze resultaten bevestigen onmiskenbaar de toegevoegde waarde van IVCM. Maar vanwege het beperkte blikveld van IVCM blijft spleetlamp onderzoek de gouden standaard bij het vervolgen van HSK. Al met al lijkt therapiekeuze gebaseerd op de combinatie van IVCM en spleetlamp de beste manier om de uitkomst van HSK te verbeteren.

Hoofdstuk 7 beschrijft de klinische en histologische bevindingen van een ander nieuw fenotype van het cornea endotheel: "Zipper cell endotheliopathy". De unieke meanderende celgrenzen van het endotheel werden ontdekt met IVCM en waren geassocieerd met idiopathisch cornea oedeem in een 55 jarige vrouw met unilaterale bulleuze keratopathie. Ondanks dat zij al 14 jaar bekend was met een veronderstelde herpetische keratitis, kon dit niet bevestigd worden na uitgebreide analyse van twee monsters uit voorste oogkamer en de geëxcideerde corneale button. Met behulp van immunohistochemische analyse vonden we wel aanwijzingen voor epitheliale metaplasie van de endotheel cellen. De meanderende vorm van de celgrenzen werd gekenmerkt door overlappende cellen met brede uitlopers bij elektronenmicroscopie. De *in vivo* en *ex vivo* bevindingen van Zipper cell endotheliopathy passen bij geen enkele tot nu toe bekende corneale aandoening. Mogelijk vertegenwoordigen ze een aberrante wondhelingsreactie na endotheliale schade van onbekende origine. Dit case report illustreert de potentie van IVCM om het spectrum van bekende corneale aandoeningen verder te differentiëren en nieuwe corneale ziektes te ontdekken.

In de discussie van dit proefschrift in **Hoofdstuk 8** worden de sterke en zwakke punten van IVCM samengevat, waarna er verscheidene suggesties ter verbetering van de soft- en hardware van de huidige techniek worden gedaan. In de toekomst zal corneale backscatter analyse door IVCM waarschijnlijk vervangen worden door technieken die een overzicht geven van de totale cornea zoals Scheimpflug fotografie en voorsegment optische coherentie tomografie. Ook de morfologische beoordeling van corneale celpopulaties wordt mogelijk vervangen of verbeterd door twee-fotonen excitatie en fluorescentie beeldvorming gecombineerd met tweede en derde harmonische generatie afbeeldingstechnieken. Voordat deze non-lineaire microscopische technieken gebruikt kunnen worden voor *in vivo* beeldvorming van de menselijke cornea zullen er

nog enkele essentiële beperkingen overwonnen moeten worden. Tot het zover is, blijft IVCM de enige beeldvormende techniek die het mogelijk maakt om de morfologie van levende cellen in de cornea te bestuderen. Dit soort IVCM studies zullen onze kennis van degeneratieve en pathologische processen in de cornea enorm vergroten en zullen de basis leggen voor de totstandkoming van een nieuwe oogheelkundige discipline: histopathologie van het levende oog.

DANKWOORD

Het is alweer zes jaar geleden dat ik bij Lies Remeijer op sollicitatiegesprek mocht komen. Via Marijke Wefers-Bettink had ik gehoord van deze onderzoeksplek in Het Oogziekenhuis Rotterdam (OZR) en zij had me bij haar zus aanbevolen. Deze kans was een prachtige opstap om in opleiding tot oogarts te komen en ik wilde dan ook, in mijn onwetendheid, niet langer dan een jaar in het onderzoek blijven hangen. Het liep anders.

Na vier dagen inwerken door mijn voorgangster Christien Weenen, begon mijn proefperiode van drie maanden waarin vooral een introductie in de wereld van de corneaspecialist en het inventariseren van de mogelijkheden van confocale microscopie op de voorgrond stonden. Het evaluatiegesprek met Lies na deze proefperiode zal ik nooit meer vergeten. Met haar uitzonderlijke talent om mensen te doorgronden, had ze natuurlijk mijn ambivalente houding ten opzichte van het onderzoek opgemerkt. Al voordat de vorderingen van ons onderzoek ter sprake kwamen, raadde ze mij aan m'n gevoel te volgen en snel in de kliniek aan de slag te gaan. Ik was het met haar eens, maar door de verzamelde gegevens was ik inmiddels danig in verwarring gebracht. Een uur later had deze verwarring plaats gemaakt voor een groeiend enthousiasme. De gegevens bleken zoveel potentie te hebben dat we ze wel samen moesten uitwerken. Het enige logische gevolg was een promotieonderzoek. Het resultaat is gebundeld in dit proefschrift, maar zal nog jaren doorwerken in vele ideeën voor nieuwe onderzoekslijnen die nog uitgewerkt kunnen worden.
Lies, ik kan je niet genoeg bedanken voor al je opofferingen tijdens deze fantastische periode in mijn leven. Je hebt me gemotiveerd, geïnspireerd, je bent een voorbeeld in vele facetten van het leven, maar je hebt me bovenal de kans gegeven om mijn droom, om topsporter te worden, waar te maken. Want promoveren is topsport! En ik hoop nog jaren, samen, op het hoogste niveau actief te blijven.

Maar promoveren is bovenal een teamsport. Een topsporter kan niet presteren zonder de enorme organisatie achter hem, waarin ieder radertje onmisbaar is. Allereerst wil ik alle vrijwilligers en alle patiënten die aan onze onderzoeken hebben meegewerkt, ontzettend bedanken voor hun motivatie om, vaak meerdere malen en soms jaren achtereen, achter de Confoscan plaats te nemen. Ik ben er bijzonder trots op dat ook vele collega's van het OZR, tot de directie aan toe, aan het onderzoek hebben bijgedragen.

Promoveren is zonder twijfel ook een jurysport. Een artikel wordt alleen beter door de vakmensen die ieder woord onder een vergrootglas leggen. Ik ben veel dank verschuldigd aan mijn promotor en opleider prof. dr. J.C. van Meurs. Beste Jan, dank voor het vertrouwen om de opleiding te mogen combineren met de laatste fase van het promo-

tieonderzoek. Ook de andere leden van de leescommissie prof. dr. G. van Rij, prof. dr. A.D.M.E. Osterhaus en dr. R.M.M.A. Nuijts hartelijk dank voor de vlotte beoordeling van mijn proefschrift.

Natuurlijk wil ik ook alle co-auteurs, waaronder enkele in het bijzonder, bedanken voor hun waardevolle inbreng. George Verjans, jouw enthousiasme voor het vak is besmettelijk. Telkens na de onderlinge gesprekken kraakten mijn hersenen van de vele ideeën die zich ondertussen hadden gevormd. Deze ideeën hebben mede vorm gegeven aan dit proefschrift. Daarnaast zijn meerdere artikelen naar een hoger niveau getrokken door jouw inbreng. Ik vind het ontzettend leuk en voel me vereerd dat je in de promotiecommissie plaats wilt nemen.

Beste Neeltje Mooy, hartelijk dank voor de mogelijkheid om de *in vivo* corneale morfologie te kunnen staven aan *ex vivo* histopathologie. Door deze unieke aanpak hebben we Ophthalmology zover gekregen dat ze een case-report hebben geaccepteerd. En dan liggen er nog een aantal mooie case-reports op de plank.

Arni Sicam, without you I was still struggeling with the standardization of the backscatter measurements. I'm sure, with your help we'll soon finish our article on corneal aberrations in HSV patients. I wish you every success with the promotion of your latest invention, the superior corneal topographer: CASSINI.

Drs. ir. Roger Cals, als oudste co-assistent werd je aan mij gekoppeld om een deel van de onderzoeksgegevens te verwerken. Hoeveel geluk hebben Lies en ik gehad met jouw kennis van programmeren, opgedaan bij de studie werktuigbouwkunde op de T.U. Delft. Met jouw hulp bleek het ineens mogelijk om de gegevens automatisch te verwerken en daarnaast heb je ook nog een onmisbare inbreng gehad in het ontwikkelen van de kalibratiemethode. Heel veel dank!

Een topsporter heeft ook de middelen en een omgeving nodig om te kunnen werken aan zijn vaardigheden. Deze omgeving is mij altijd geboden door het cornea-team. Allereerst, Hugo van Cleynenbreugel, wat vind ik het nog steeds jammer dat je er voor gekozen hebt om het nationale cornea-team van onze zuiderburen te versterken. Bedankt dat je altijd klaar stond om je kennis te delen. Oh, en dan moeten we nog het grootste Confoscan project tot een goed einde zien te brengen. Dank voor je vooruitziende blik bij het schrijven van het protocol en natuurlijk voor het motiveren van de patiënten om met de Fuchs studie mee te doen. Het zou zomaar kunnen dat juist dit project de grootste impact zal hebben.

Annette Geerards en Jeroen van Rooij, jullie hebben een enorme bijdrage geleverd aan het vergroten van de Confoscan database door iedere bijzondere casus door te sturen. Juist deze aanvulling is voor mij van grote waarde geweest, niet alleen omdat mijn kennis van de cornea werd vergroot, waardoor de confocale beelden beter geïnterpreteerd konden worden, maar ook omdat het mijn enthousiasme voor het vak heeft aangewakkerd. Daarnaast stonden jullie altijd klaar om mijn vragen te beantwoorden en hebben jullie veel studiepatiënten aangeleverd. Heel veel dank voor jullie inzet om dit project tot een succes te maken.

Sietske Huiskens en Elma Bras, dit project was nooit geslaagd zonder jullie hulp. Ik vond het heel gezellig om met jullie samen te werken en ik mis de relaxte sfeer waarin we de beslommeringen in het OZR, Focuskliniek en ROI konden doornemen. Sietske, wat ben ik blij dat je de Confoscan traditie in ere houdt. En Elma, ook dit jaar hebben we weer in de Bourgogne kunnen genieten van jullie "De Waard" tent. Hopelijk kunnen we hem voor volgend jaar alweer reserveren? Dank jullie beiden voor de fijne periode.

Dan Ans Hoogendam en Dorry Vavier, jullie zagen me alweer aankomen met de meest onmogelijke verzoeken om afspraken met elkaar te combineren en om weer even een studiepatiënt tijdens een compleet overboekt spreekuur in te plannen. Maar altijd weer, zelfs buiten werktijd, werd er aan deze verzoeken voldaan. Deze twee dames verdienen een standbeeld!

In de eerste 3 jaren van het promotieonderzoek had ik, zonder het zelf te beseffen, een uitzonderingspositie in het OZR. Waar ik ongestoord kon werken in een eigen kamer met raam op de 1e etage, moesten mijn collega-onderzoekers opereren vanuit een gedeelde, donkere kamer in de kelder. Beste The-Ahn, Leonieke en Esther, jullie doorzettingsvermogen is een voorbeeld voor mij geweest. Dank voor de fijne samenwerking.

Dat er behalve kennis, doorzettingsvermogen en geduld, ook flexibiliteit nodig is om een promotieonderzoek tot een succes te maken, werd duidelijk met de komst van het Rotterdams Oogheelkundig Instituut (ROI). Vanaf begin 2009, moesten alle onderzoeken, inclusief de apparatuur, verplaatst worden naar het gebouw aan de overkant. Ineens was er de GCP cursus en vele lastige regels waaraan alle metingen moesten voldoen. Er kwamen steeds meer onderzoekers bij, waardoor we onderzoekskamers moesten delen en er zelfs per kamer een planning gemaakt moest worden. Ja, het begin was wat stroef. Gelukkig heb je dan je nieuwe roomies. Lieve Myrthe en Eva, jullie hebben ervoor gezorgd dat ik me, vanaf het begin, thuis heb gevoeld in het ROI. Doordat we onze ervaringen konden delen, maakten de frustraties al snel plaats voor het besef dat een

opstartfase altijd met tegenslagen gepaard gaat en dat er juist nieuwe mogelijkheden lagen. Veel dank voor dat inzicht en voor de vele gezellige momenten samen.

Die nieuwe mogelijkheden ontstonden mede doordat in het ROI verschillende disciplines onder 1 dak kwamen te werken. Zo konden er ineens grote projecten snel en zorgvullig gepland en uitgevoerd worden. Vooral in de laatste fase van de dataverzameling en bij het ontwikkelen van de kalibratiemethode was de hulp van mijn ROI collega's onmisbaar. Annemiek, Boy, Caroline, Dirk, Ellen, Elsbeth, Jetty, Johannes, Koen, Linda, Marja, Mieke en Sankha dank voor jullie inzet en prettige samenwerking. Rene Wubbels, dank dat je deur altijd open stond om lastige statistische vraagstukken te kunnen bespreken. Beste Netty Dorrestijn en Seerp Baarsma, jullie hebben in een kort tijdsbestek gezorgd voor een fijne werkomgeving, waarin alle voorwaarden aanwezig zijn om op hoog niveau onderzoek te verrichten. Er staat nu een organisatie om trots op te zijn! Dank voor jullie interesse in mijn onderzoek en voor alle mogelijkheden die mij werden geboden.

Je bent je er niet altijd van bewust, maar als je onderzoek doet naar een nieuwe beeldvormende techniek ben je volledig afhankelijk van kwetsbare apparatuur. Ik vond het eigenlijk maar onzin om iedere week een back-up van de onderzoeksgegevens te maken. Totdat de computer crashte. Radjin Koelin, bedankt dat je me vanaf het begin duidelijk hebt gemaakt dat een goede back-up noodzaak is, maar ook voor de vele extra uren/dagen die je hebt besteed aan het herstellen en stabilizeren van onze database.

Moreover, when an imaging device is pushed to its limits, it's just a matter of time before it starts to resist. In such case you need good contacts with the manufacturer. Dear Mauro Campigotto, thank you and your team of NIDEK Technologies for the support, when our Confoscan stopped functioning. I really appreciate the professional relationship we built up over the past few years.

Ook de jongens van de MID bedankt. Marcel Goedhart, Andre Mooi en Pieter Westerhof dank voor het creëren van de perfecte werkomgeving waarin de patiënten in een korte tijd meerdere apparaten konden afwerken. Maar ook voor het fabriceren van die inventieve houder die het kalibreren van de backscatter metingen mogelijk heeft gemaakt.

Bart van Dooren, alleen doordat ik bij jou in het Amphia Ziekenhuis van een tweede Confoscan gebruik mocht maken, kon de kalibratiemethode voor het meten van backscatter gevalideerd worden. Ontzettend bedankt voor je gastvrijheid, maar ook voor je hulp tijdens mijn beginperiode in het OZR, waarin je me de kunst van het onderzoeken hebt bijgebracht.

Beste Tom van den Berg, hartelijk dank voor alle gedachtenwisselingen over scatter in de cornea, waardoor onze onderzoeksresultaten beter in perspectief geplaatst konden worden. Ik ben vereerd dat u in de promotiecommissie plaats wilt nemen.

Beste Ton de Jong, Jos Onderwater en Peter Neeskens, jullie prachtige foto's hebben dit proefschrift van een extra dimensie voorzien. Veel dank voor de introductie in de wondere wereld van de elektronen microscopie.

Sjoerd de Faber, Amir Naseri en Nidal Cossack dank voor jullie inzet bij die eindeloze dataverwerking.

Dan wat dichter bij huis. Annette Moll, heel veel dank dat je tijdens de co-schappen, op het moment dat de twijfel het grootst was, me hebt geïnteresseerd voor de oogheelkunde. Het is fijn om te weten dat ik altijd voor een goed gesprek kan aankloppen. Tot snel in Ouddorp!

De laatste anderhalf jaar van mijn promotieonderzoek waren zonder twijfel het zwaarst. Vooral het mentale deel om 's avonds en in het weekend weer achter de computer te kruipen. Dan is het heel fijn om met plezier naar je werk te gaan. Hiervoor wil ik mijn (ex-)collega AIOS'en bedanken. Benny, Birte, Christien, Chantal, Danny, Erik, Esther, Fleur, Gertjan, Josine, Kristel, Leigh, Maartje, Mariëlle, Niels, Peter, Renoe, Ronald, Rudolf, Sharmila, Tanya, Tom, Thomas en Yashna, veel dank voor jullie interesse en steun tijdens deze lastige laatste fase van mijn promotietraject.

Net zo belangrijk voor die goede werksfeer zijn de stafleden in het OZR. Al kreeg ik heel regelmatig de vraag wanneer het boekje nu eindelijk af was. Wat ben ik blij dat ik daar geen antwoord meer op hoef te geven. Ontzettend bedankt voor jullie interesse, maar vooral voor alle inspanningen om jullie kennis en kunde te delen.

Mijn paranimfen Karin Littink en Marc den Heijer, het is een eer om jullie naast me te hebben. Karin, al vanaf onze eerste ontmoeting in Fort Lauderdale bewonder ik je wetenschappelijke drive. Ik ben er van overtuigd dat je het daarmee nog ver gaat brengen. Het is heel fijn om de promotie- en stage-ervaringen met jou te kunnen delen. Marc, mijn oude huisgenoot op de Abraham Kuyperlaan 9b, we vieren alweer het 20e jaar van onze vriendschap. Dank dat je er altijd voor me bent.

Lieve vrienden, Jopie & Lies, Peet & Carmen, Tim & Manon, Jette, Bello, Lex, Paulus, Esther, Mirjam & Martijn, Marcel & Monique, Reinier & Marloes, wat ben ik trots, blij en dankbaar

dat ondanks de drukte van de afgelopen periode onze vriendschap nog steeds heel hecht is. Het proefschrift is af, eindelijk kan ik jullie weer vaker zien.

Net als een topsporter kan een promovendus alleen het allerhoogste niveau bereiken als er een stabiel thuisfront is, waarop je altijd kan terugvallen. Lieve Riny en Kees Sinke, het is fantastisch om te zien hoe jullie met je kleinzoon omgaan. De onvoorwaardelijke liefde die daar vanaf straalt, maakt het dat we Jord met een gerust hart bij jullie kunnen achterlaten. Dank voor jullie inzet, goede zorgen en het meeleven gedurende mijn onderzoek. Adriaan Sinke, beste zwager, met jouw droge humor wist je mijn promotieonderzoek altijd weer in het juiste perspectief te plaatsen. Dank voor je interesse in mijn onderzoek, maar natuurlijk nog veel meer voor het bieden van een toevluchtsoord in de mooiste stad van Europa.

Lieve pap en mam, wat moet ik zeggen… Jullie hebben ervoor gezorgd dat alle voorwaarden aanwezig waren om onbezorgd de schooltijd en studententijd te doorlopen. En zelfs nu Ouddorp niet meer thuis is, zorgen jullie ervoor dat het wel zo voelt. Ik heb het aan jullie te danken dat ik vandaag als eerste promovendus binnen onze familie mijn proefschrift mag verdedigen.

Allerliefste Sas, van iedere dag samen met jou en onze Jordje geniet ik. Met meer dan bewondering kijk ik naar hoe je je carrière combineert met het moederschap. En daarnaast heb je, schijnbaar moeiteloos, mij altijd de kans gegeven om deze promotie tot een goed einde te brengen. Hiervoor zal ik je altijd dankbaar blijven. Vanaf volgend jaar begint jouw grote avontuur. Hopelijk kunnen we daar met z'n viertjes..? net zo'n succes van maken.

CURRICULUM VITAE

Toine Hillenaar was born on September 27th 1980 in Dirksland, the Netherlands. He graduated from secondary school at the Jacob van Liesveldt College in Hellevoetsluis, the Netherlands in 1998. In the same year he started his medical studies at the Erasmus University Rotterdam. From his second year he joined a medical student team to support the nursing staff at the department of surgical oncology and abdominal surgery of the University Hospital Rotterdam Dijkzigt. After two years he became the student team leader until he commenced his clinical rotations. In 2002 he travelled to Pretoria, South Africa, to follow a clinical internship at the emergency department of the Pretoria Academic Hospital. Before he obtained his medical degree in 2006 he conducted a retrospective study on the management of vitreous hemorrhage at the emergency unit of The Rotterdam Eye Hospital.

After this positive experience with scientific research, he started the work described in this thesis under supervision of Dr. Lies Remeijer at The Rotterdam Eye Hospital (Prof. Dr. Jan van Meurs), in January 2007. His first publication as first author was in 2009 in the November issue of Ophthalmology, after which several other publications in the same journal followed. He presented his work at many national and international meetings and in 2010 he received an ARVO International Travel Grant. In the same year he was invited as speaker at the EVER congress in Crete, Greece. In April 2011, he started his residency in Ophthalmology at The Rotterdam Eye Hospital (Prof. Dr. Jan van Meurs), which he will complete in 2015.

LIST OF PUBLICATIONS

Hillenaar T, Cossack NZ, Braaf B, Remeijer L, Sicam VA.
Corneal aberrations in herpetic stromal keratitis.
Manuscript in preparation.

Van Cleynenbreugel H, Remeijer L, **Hillenaar T.**
Cataract surgery in patients with Fuchs' endothelial dystrophy: epithelial backscatter predicts corneal decompensation.
Manuscript in preparation.

Cossack NZ, **Hillenaar T,** Remeijer L.
In vivo confocal microscopy of self-limiting corneal edema with multiple parallel lines on the endothelium (SCEMPLE).
Article submitted for publication.

Hillenaar T, van Cleynenbreugel H, Verjans GM, Wubbels RJ, Remeijer L.
Monitoring the inflammatory process in herpetic stromal keratitis: the role of in vivo confocal microscopy.
Ophthalmology 2012 Jun;119(6):1102-1110.

Hillenaar T, van Cleynenbreugel H, Remeijer L.
How normal Is the transparent cornea? Effects of aging on corneal morphology.
Ophthalmology 2012 Feb;119(2):241-248.

Van Cleynenbreugel H, Remeijer L, **Hillenaar T**.
Descemet stripping automated endothelial keratoplasty: effect of intraoperative lenticule thickness on visual outcome and endothelial cell density.
Cornea 2011 Nov;30(11):1195-1200.

Hillenaar T, Cals RH, Eilers PH, Wubbels RJ, van Cleynenbreugel H, Remeijer L.
Normative database for corneal backscatter analysis by in vivo confocal microscopy.
Investigative Ophthalmology and Visual Science 2011 Sep 21;52(10):7274-7281.

Saelens IE, Bleyen I, **Hillenaar T,** Thiadens AA, Beekhuis WH, Remeijer L, Van Rij G.
Long-term follow-up of hydrogel intracorneal lenses in 2 aphakic eyes.
Journal of Cataract and Refractive Surgery 2010 Dec;36(12):2200-2203.

Hillenaar T, Sicam VA, Vermeer KA, Braaf B, Remeijer L, Cals RH, de Boer JF.
Wide-range calibration of corneal backscatter analysis by in vivo confocal microscopy.
Investigative Ophthalmology and Visual Science 2011 Apr 5;52(5):2136-2146.

Hillenaar T, Mooy CM, Verjans GM, Remeijer L.
Zipper cell endotheliopathy: a new subset of idiopathic corneal edema.
Ophthalmology 2010 Dec;117(12):2255-2262.

Hillenaar T, Weenen C, Wubbels RJ, Remeijer L.
Endothelial involvement in herpes simplex virus keratitis: an in vivo confocal microscopy study.
Ophthalmology 2009 Nov;116(11):2077-2086.e1-2.

Van Cleynenbreugel H, **Hillenaar T,** Remeijer L.
Graft insertion during Descemet-stripping automated endothelial keratoplasty: pulling the graft inward.
Journal of Cataract and Refractive Surgery 2008 Apr;34(4):534-536.

Color figures

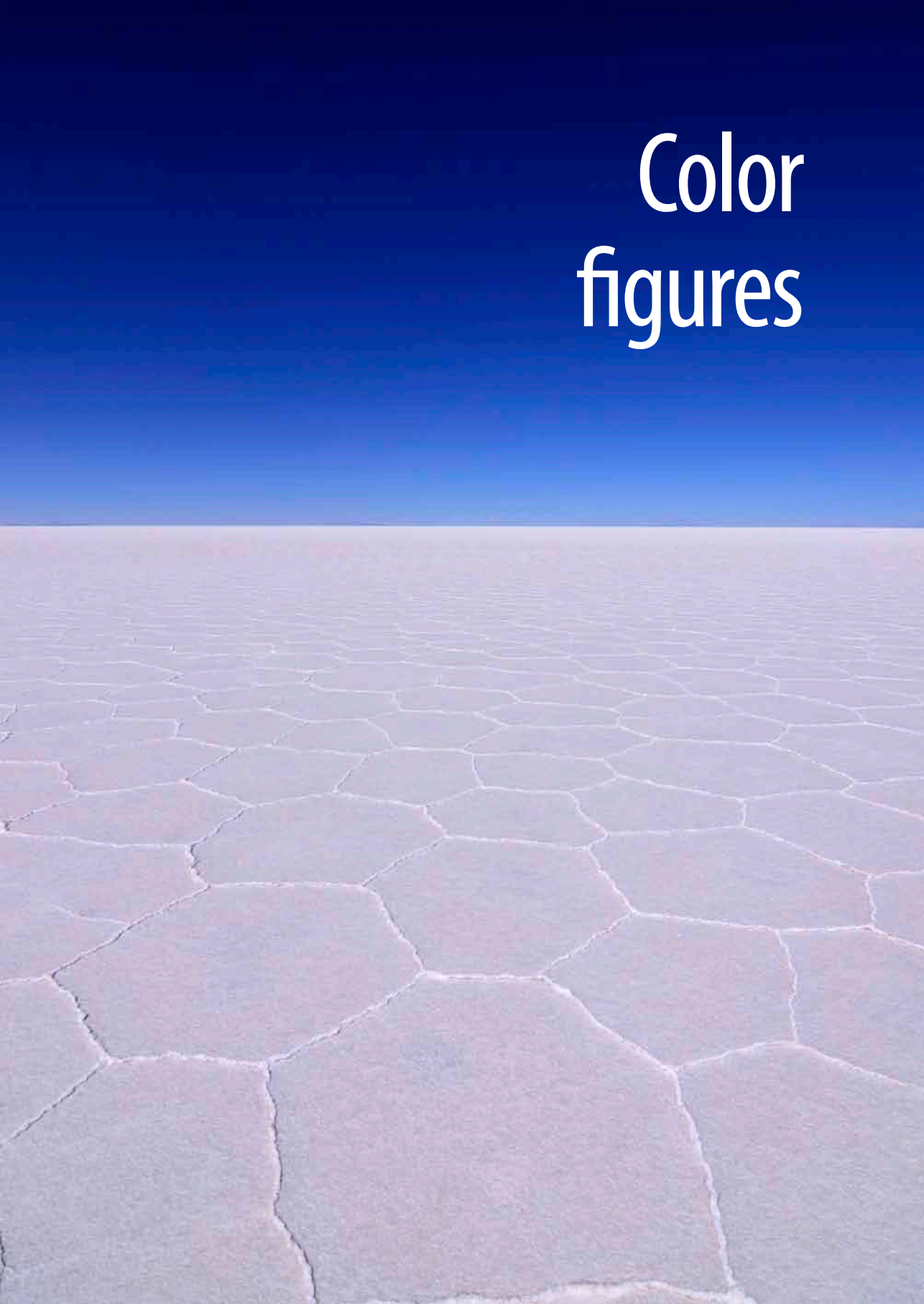

CHAPTER 1

Figure 2. For the studies presented in this thesis, we used a slit scanning confocal microscope (Confoscan 4, NIDEK Technologies, Albignasego, Padova, Italy; reprinted with permission) equipped with a 100 watt halogen light source. Using a 40X Zeiss Acroplan objective lens with a high numerical aperture of 0.75, this instrument achieves a lateral resolution of 0.6 µm[1] and an axial resolution of 10 to 26 µm.[34,35] An optical coupling agent is applied to the objective lens to provide high-resolution images of 425x320 µm, after reducing the blink reflex with topical anesthetics. A *z*-ring adapter can be used to further reduce the motion artifacts induced by involuntary eye movements, pulse, and respiration during the 12 seconds of image acquisition.

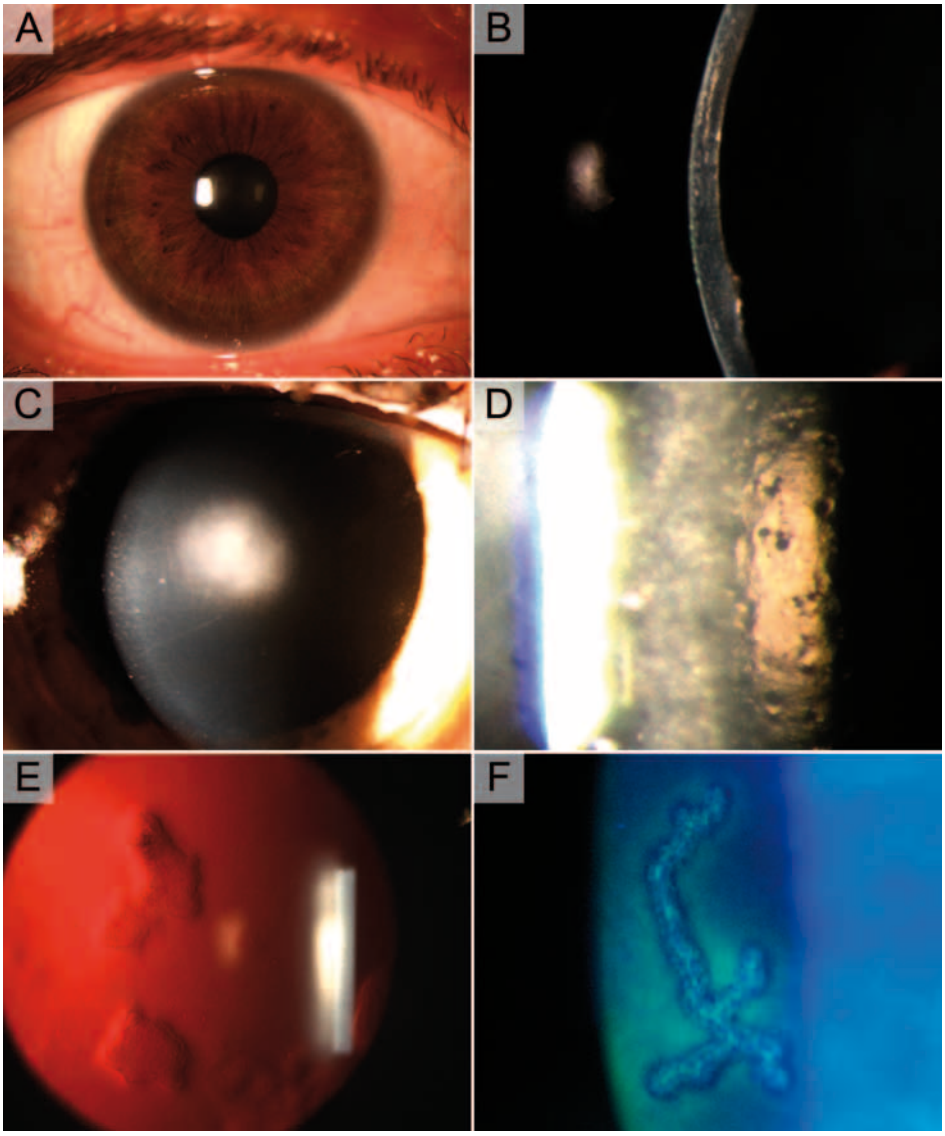

Figure 4. Standard observation techniques for clinical slit-lamp biomicroscopy illustrated by photography of different manifestations of HSV keratitis. **A.** Direct diffuse illumination showing conjunctival hyperemia. **B.** Optical section showing sheet-like corneal opacifications, stromal edema, and keratic precipitates in herpetic endotheliitis. **C.** Scattering sclero-corneal illumination showing spherical immune stromal keratitis. **D.** Specular illumination showing pseudoguttae. **E.** Retro-illumination showing thinned corneal areas after necrotizing stromal keratitis. **F.** Fluorescence illumination showing dendritic ulceration of the corneal epithelium.

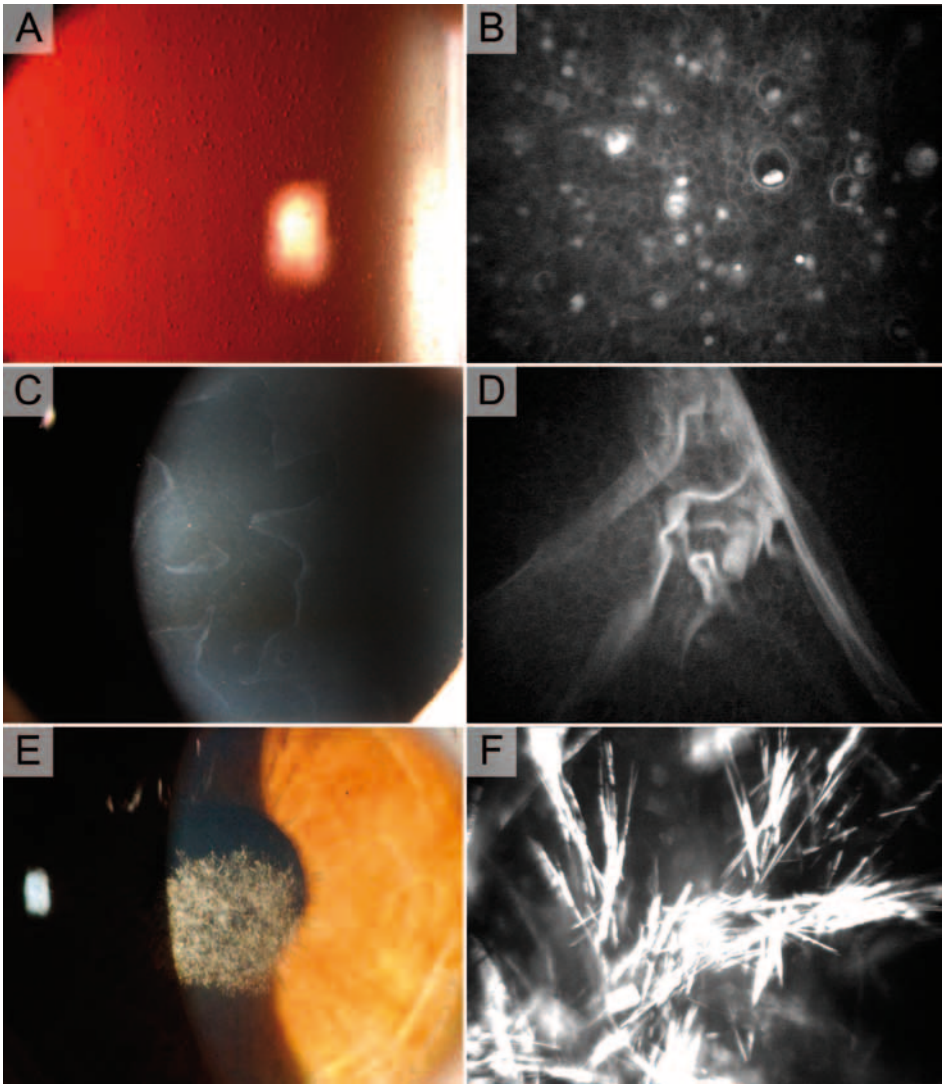

Figure 9. *In vivo* confocal microscopy (IVCM) allows early detection of corneal dystrophies and degenerations. **A.** Meesmann corneal dystrophy. **B.** Confocal microscopy showed intraepithelial cysts filled with peculiar substance. **C.** Epithelial basement membrane dystrophy (EBMD). Unlike the term suggests, EBMD is generally regarded an age-related corneal degeneration. **D.** Confocal microscopy showed extensive folding of Bowman's layer. **E.** Schnyder crystalline corneal dystrophy. **F.** Confocal microscopy showed crystalline deposits in the anterior stroma.

CHAPTER 2

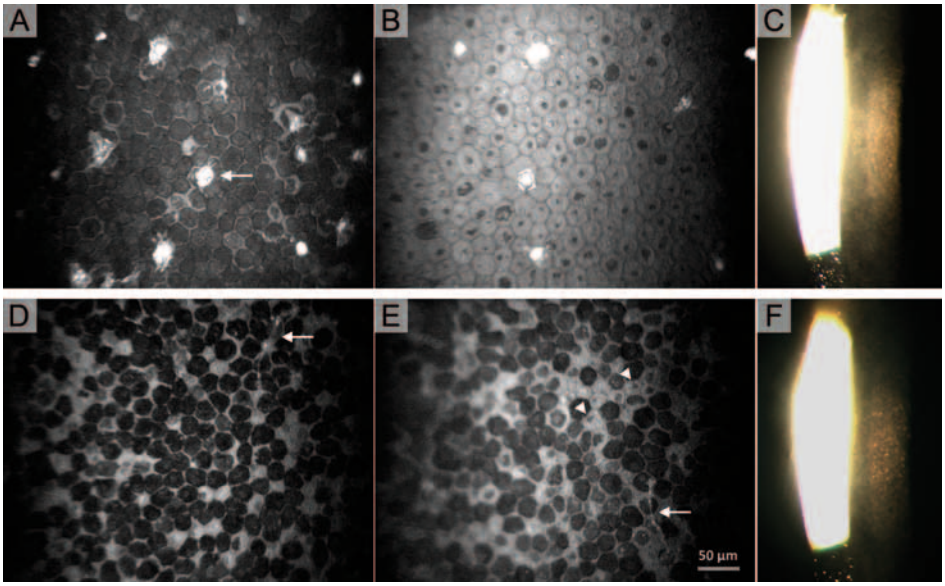

Figure 2. Salt and pepper endothelium. Two subjects with transparent corneas showed unique morphologic alterations of the corneal endothelial cells. The IVCM images are 425x320 µm. **A–C**, The first subject was a 70-year-old man. **A**, His right eye showed a dark-light reversal of the endothelial cells and precipitated granules (*arrow*) on a flat endothelial layer. Endothelial cell density (ECD): 2373 cells/mm^2. **B**, The left eye showed an early stage of the same endothelial alterations. The center of nearly all endothelial cells showed a variable-sized black discoloration. This eye also showed pigmented material on the endothelium. ECD: 2054 cells/mm^2. **C**, At slit-lamp examination, the endothelial specular reflection had a somewhat grayish aspect in the right eye, whereas the left eye displayed no evident alterations in specular view (not shown). **D–F**, The second subject was a 57-year-old man. **D**, Salt and pepper endothelium (black and white cell bodies) was seen in the right eye. A small dendritiform structure was precipitated on the endothelial layer (*arrow*). ECD: 2442 cells/mm^2. **E**, The left eye also showed salt and pepper endothelium. Some of the endothelial cells displayed early-stage alterations, as were seen in the left eye of the first subject (*arrowheads*). Again, a dendritiform precipitate (*arrow*) was observed. ECD: 2529 cells/mm^2. **F**, Endothelium in specular view with the slit-lamp showed a gravel tile aspect in both eyes. IVCM = in vivo confocal microscopy.

CHAPTER 6

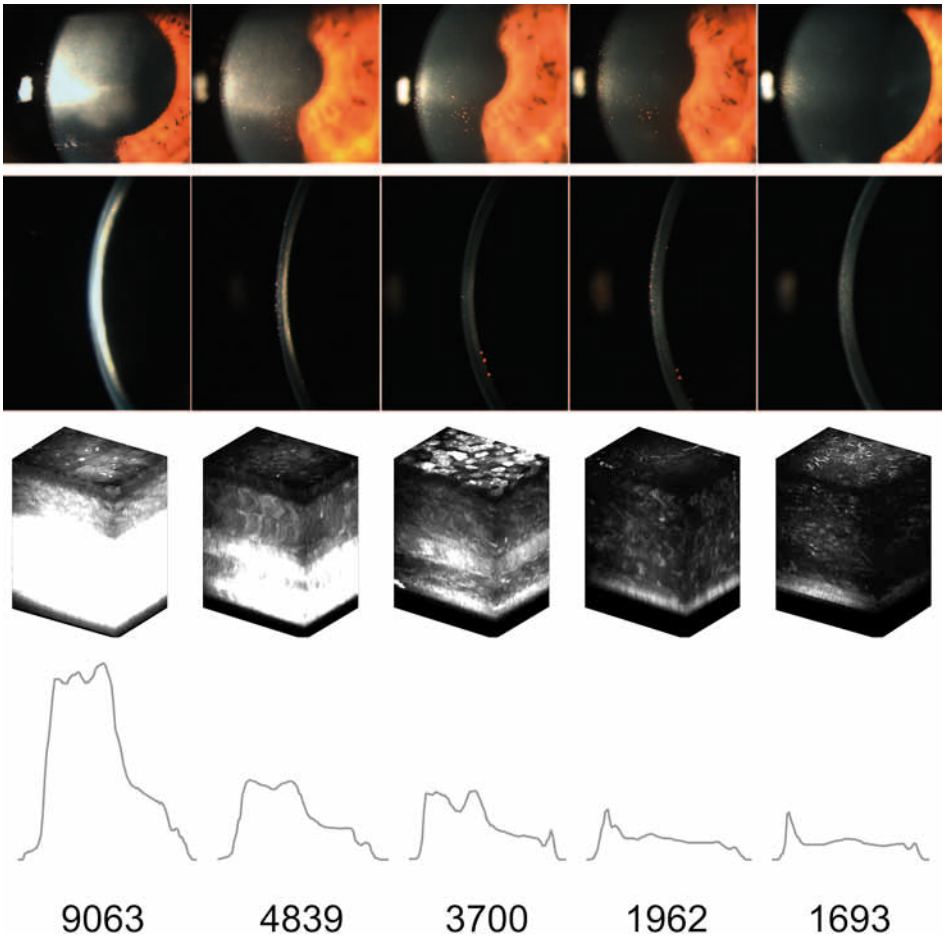

Figure 3. Illustrative case: 1-year follow-up of herpetic stromal keratitis (HSK) using slit-lamp biomicroscopy and in vivo confocal microscopy (IVCM). At the moment of the first slit-lamp photograph, this 26-year-old woman used 800 mg oral acyclovir and topical 0.1% dexamethasone once daily and visited our clinic for a regular follow-up after a 3-year history of recurring HSK. A few days before the visit, she experienced slight blurring of vision, but noticed that she was able to read again without glasses. Slit-lamp examination revealed opacification of the middle and posterior third of the stroma, which was already described 3 months before. Other signs of inflammation seemed absent. Although slit-lamp appearance was inconclusive for a stromal recurrence, her best-corrected visual acuity had declined from 20/30 to 20/40 since her last visit. Therefore, she was enrolled in the current study, subjected to our standard therapy regimen for stromal recurrences (Table 1), and monitored by slit-lamp and IVCM. Despite dense opacification in the posterior part of the stroma, IVCM did reveal pseudoguttae at the first study visit, clearly indicating disease activity. Follow-up by slit-lamp showed a great improvement in the first 3 months, resulting in an optically clear cornea, which remained clear thereafter. However, IVCM showed mean corneal backscatter continued to decrease, also after 3 months. This was completely overlooked by slit-lamp biomicroscopy. Furthermore, corneal thickness at slit-lamp biomicroscopy seemed normal at each study visit. Nevertheless, ultrasonic pachymetry showed marked corneal thinning of the HSK-affected eye compared with the fellow eye, which became increasingly evident during the course. Columns: first study visit, 1-, 3-, 6-, 12-month(s) follow-up. Rows: slit-lamp photography: broad beam, optical section; IVCM: stack of images, *z*-scan curve with corneal backscatter in scatter units.

CHAPTER 7

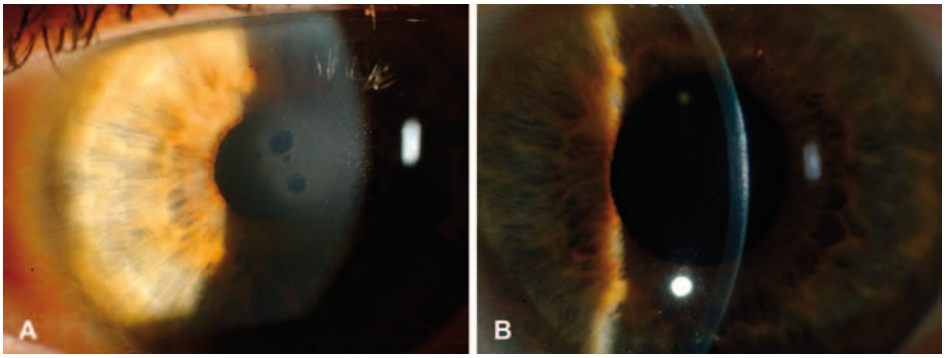

Figure 1. Photographs showing results of slit-lamp examination. **A**, At first presentation, the central cornea showed a focal, gradually demarcated area with stromal edema and several epithelial bullae. **B**, Two months later, with reduction of the corneal edema, the epithelial bullae had resolved; however, the reflectivity of the anterior stroma was increased.

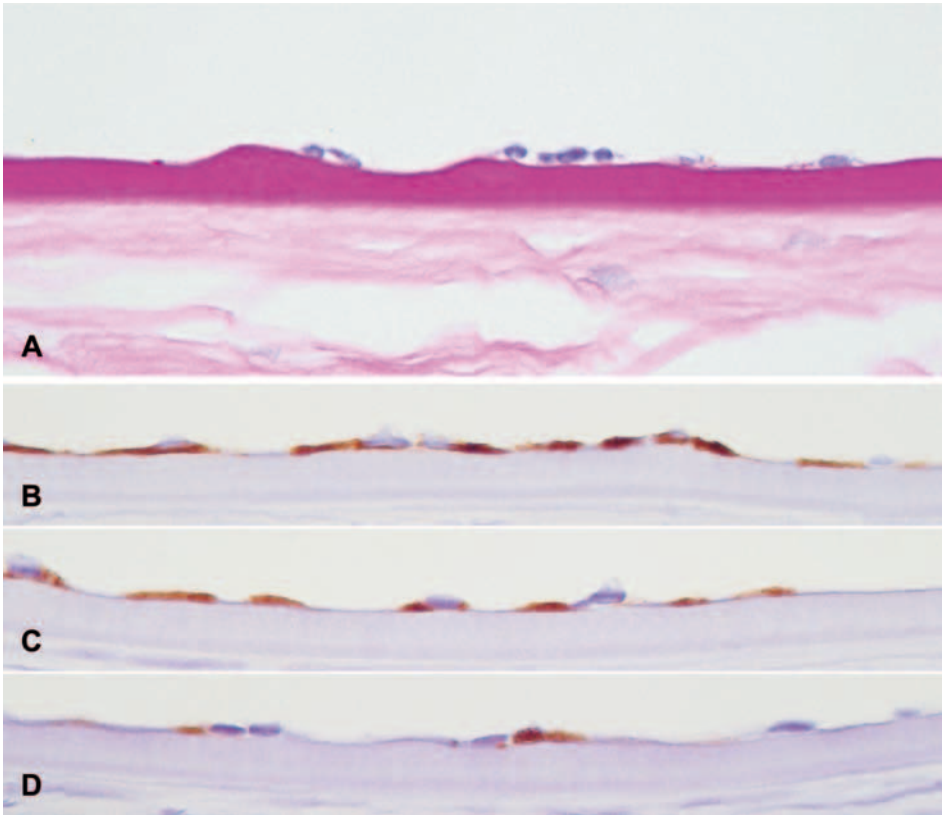

Figure 3. Photomicrographs showing light microscopy and immunohistochemical analysis results. **A**, Light microscopy showing a slightly irregular Descemet's membrane with a focally double-layered endothelium with oval nuclei. **B**, Immunohistochemically, the cytoplasm of the endothelial cells stained strongly positive for cytokeratin 8/18. **C**, Positive staining for cytokeratin 19. **D**, Focal positive staining for cytokeratin 7.

CHAPTER 8

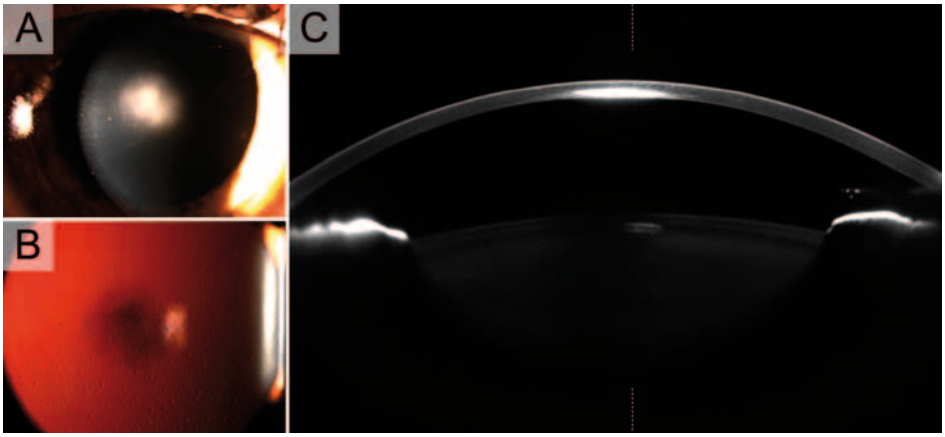

Figure 1. Scheimpflug photography in herpetic stromal keratitis. **A.** Slit-lamp image of herpetic disciform keratitis. **B.** Retro-illumination of the same cornea revealed pseudoguttae extending far beyond the disciform inflammation. **C.** Scheimpflug imaging showed the disciform inflammatory process affected the posterior three quarters of the stroma. Densitometry of these Scheimpflug images may be used to monitor the inflammatory process in herpetic keratitis.

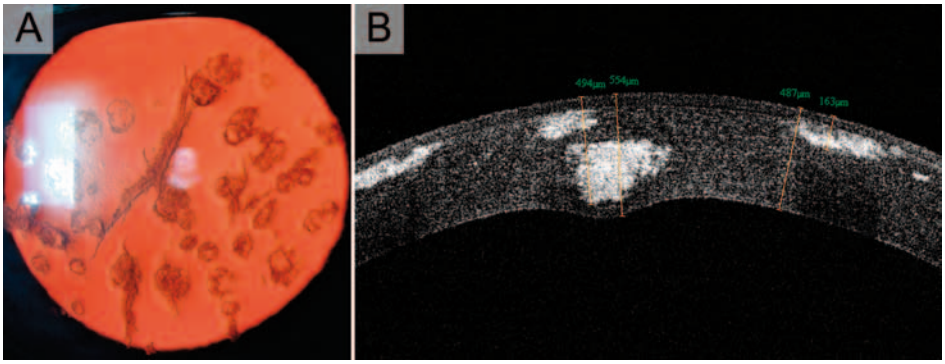

Figure 2. Anterior segment optical coherence tomography (AS-OCT) in Avellino dystrophy **A.** Retro-illumination showing both lattice and granular depositions. **B.** AS-OCT was used to choose the type of keratoplasty. Because one of the opacities clearly indented the corneal endothelium, we accepted incomplete excision of the opacities using deep lamellar keratoplasty.

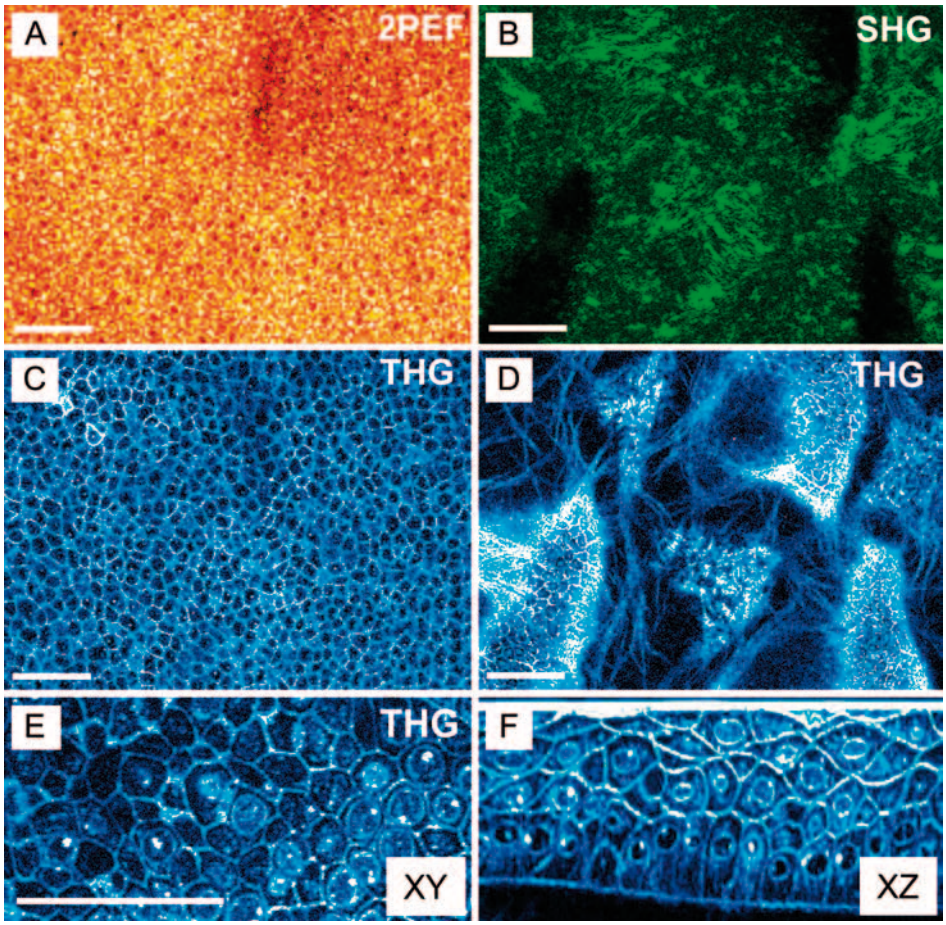

Figure 3. Multiphoton microscopy of an excised unstained human cornea. **A**. Two-photon excited fluorescence (2PEF) imaging revealed the cytoplasm of the basal epithelial cells **B**. Second-harmonic generation (SHG) imaging of the epithelium-stromal junction. **C**. Third-harmonic generation (THG) imaging showed the cell borders of the basal epithelial cells. **D**. Comparison of SHG (Figure 3B) and THG signals from the epithelium-stromal junction demonstrates that SHG images the stromal collagen lamellae, but not the epithelial cells. **E**. THG image of epithelial wing cells in XY directions composed from a Z-stack. **F**. Representative XZ reprojection from the same data. This figure is adapted from Aptel, 2010[28] and reprinted with permission from the Association for Research in Vision and Ophthalmology.